A COUPLED DEM/CFD ANALYSIS OF DIE FILLING PROCESS

YU GUO

BSc, MSc

A thesis submitted to The University of Birmingham

for the degree of

DOCTOR OF PHILOSOPHY

Department of Chemical Engineering

The University of Birmingham

January 2010

ABSTRACT

This thesis reports numerical analyses of powder flow, mixing and segregation behavior during die filling in a vacuum and in air using an Eulerian-Lagrangian model, which employs a Discrete Element Method (DEM) for the particles and Computational Fluid Dynamics (CFD) for the air with a two-way air-particle interaction coupling term.

The effects of air and particle properties (size, density, size distribution, cohesion etc.) on powder flow are explored. The results are in a good agreement with experimental observations. Powder flow is characterized in terms of a dimensionless mass flow rate and a critical filling velocity. When air is present, the powder flow characteristics depend on the particle size and density and can be classified into an air-sensitive regime and an air-inert regime.

It is found that the difference in particle size and/or density can cause segregation during die filling. Therefore, parametric studies are undertaken to examine the effects of some factors, such as particle size or density ratio, shoe speed, initial mass fraction of fine particles, initial height of powder bed and cohesion.

Suction filling with a movable punch is also simulated. It has been shown that the utilization of suction can significantly improve the powder flow rate and reduce the density-induced segregation.

KEY WORDS: Discrete Element Method, Computational Fluid Dynamics, air effect, powder flow, segregation, suction, die filling

ACKNOWLEDGEMENTS

I owe my deepest gratitude to my supervisors Dr. Charley Wu and Dr. Colin Thornton for mentoring me throughout the course of my PhD study. Without their unreserved support and encouragement, this project would not have been seen completion. Moreover, their broad knowledge and their logical way of thinking have been of great value for me.

I am heartily thankful to Dr. David Kafui for his patient help with the code and computer problems. I also wish to thank Prof. Jonathan Seville and Dr. Andy Ingram for their constructive comments on this project. In addition, I also benefited from discussions with Prof. Alan Cocks at the beginning of my PhD study.

Special thanks go to EPSRC and the School of Chemical Engineering in the University of Birmingham for providing me with a 3-year fully-funded PhD studentship.

Finally, I would like to thank my parents and my sister for their permanent love and support.

TABLE OF CONTENTS

LIST OF FIGURES

LIST OF TABLES

NOMENCLATURE

Ar	Archimedes number
$C_{\mathrm{D}i}$	Fluid drag coefficient for particle *i*
D_0	Diameter of the circular orifice
D_c	Concentration deviation
E_i	Young's modulus of particle *i*
E^*	Effective Young's modulus
F_c	Pull-off force
F_n	Normal force
F_nd	Normal damping force
F_t	Tangential force
F_td	Tangential damping force
$F_\mathrm{t}^\mathrm{peel}$	Critical tangential force below which peeling occurs
$F_\mathrm{t}^\mathrm{slide}$	Tangential force when sliding occurs
F_n^H	Effective Hertzian force
G_i	Shear modulus of particle *i*
G^*	Effective shear modulus
H	Initial height of powder bed in the shoe
I_i	Moment of inertia of particle *i*
K_n	Normal stiffness
K_t	Tangential stiffness
L	Width of shoe
M	Mass flow rate
M_f	Average molar mass of air
M_V	Volumetric flow rate

$\overline{M}$	Average mass flow rate
M^*	Dimensionless mass flow rate
P	Air pressure
P_0	Standard atmospheric pressure (1.01325×10^5 Pa)
R_i	Radius of particle i
Re_{pi}	Reynolds number of particle i
R^*	Effective radius
T	Elapsed time from the start of die filling
$\overline{T}$	Duration of die filling
T^*	Temperature of air
V	Cumulative solid volume of particles deposited into the die
V_i	Total solid volume of the mixture in cell i
V_{pi}	Volume of particle i
V_{bed}	Total solid volume of the powder bed
V_{total}	Total solid volume of the particles eventually discharged into the die
$\tilde{V}_i$	Solid volume of the light particles in cell i
a	Radius of the contact area
b_0	Width of the orifice or die opening
c_i	Volume concentration of light particles in cell i
c_m	Mean volume concentration of light particles in the initial system
d_c	Diameter of coarse particles
d_f	Diameter of fine particles
d_p	Mean particle diameter
d_p^*	A dimensionless term defined by $d_p^* = d_p/b_0$
g	Gravitational acceleration

h	Height of die
l	Thickness of powder system in planar flow
m	Cumulative mass of particles deposited into the die
m_{f}	Mass of particles in a fully filled die
m_i	Mass of particle i
m_{s}	Mass of a single fine particle
m_{total}	Total mass of particles eventually deposited into the die
p	Fluid pressure
t	Thickness of die
u_{y}	Vertical air velocity
v_{c}	Critical filling velocity
v_{p}	Punch velocity
v_{s}	Shoe velocity
w	Width of die
x	x-coordinate of the cells
$\mathrm{x_f}$	Initial average fines mass fraction
$\mathrm{x_i}$	Fines mass fraction in cell i
$\mathrm{x^d}$	Transient fines mass fraction in the die
$\mathrm{x_f^L}$	Limiting fines mass fraction
$\mathrm{x_i^s}$	Fines mass fraction in a given sample discharged from the shoe
y	y-coordinate of the cells
z	z-coordinate of the cells

Greeks:

ΔF_{n}	Normal incremental force
ΔF_{t}	Tangential incremental force

ΔV_c	The volume of a fluid cell
Δm_i	Mass of a given sample discharged from the shoe
Δt	Time step
$\Delta \delta_n$	Relative normal incremental displacement
$\Delta \delta_t$	Relative tangential incremental surface displacement
Φ_ρ	Ratio of solid particle density to air density
α	Power in the equation $\delta = (v_c / v_s)^\alpha$
β	Damping coefficient
γ	Surface energy
δ	Fill ratio
δ_n	Relative normal displacement
ε	Void fraction
ζ	Air sensitivity index
ζ_l	Air sensitivity index of light particles
ζ_h	Air sensitivity index of heavy particles
η	Air viscosity
η^*	A dimensionless term defined by $\eta^* = \eta / (\rho_b g^{1/2} b_0^{3/2})$
κ	Half-angle of the flowing zone
κ_h	Hopper half-angle
μ_b	Bulk viscosity of a fluid
μ_p	Friction coefficient between particles
μ_{pw}	Friction coefficient between a particle and a wall
μ_s	Shear viscosity of a fluid
ν_i	Poisson's ratio of particle *i*
ξ	A dimensionless parameter to characterize the sensitivity of particles to the air

ξ_c	A critical value of ξ
ρ_{a}	Air density
ρ_{b}	Bulk density of a powder
ρ_{f}	Fluid density
ρ_{h}	Density of heavy particles
ρ_{l}	Density of light particles
ρ_{s}	Solid particle density
ϕ	A term defined by $\phi = \rho_{\mathrm{b}} g^{1/2} l b_0^{3/2} \left[1 - k\left(d_{\mathrm{p}}/b_0\right)\right]^{3/2}$

Vectors and tensors:

$\mathbf{F}_{\mathrm{c}i}$	Particle-particle contact force acting on particle i
$\mathbf{F}_{\mathrm{d}i}$	Drag force acting on particle i
$\mathbf{F}_{\mathrm{fp}i}$	Fluid-particle interaction force acting on particle i
$\mathbf{F}^*_{\mathrm{fp}}$	Fluid-particle interaction force per unit volume
$\mathbf{T}_i$	Torque acting on particle i
$\mathbf{g}$	Gravitational acceleration vector
$\mathbf{u}$	Fluid velocity
$\mathbf{v}_i$	Translational velocity of particle i
$\mathbf{x}_i$	Coordinates of particle i
$\boldsymbol{\delta}$	Identity tensor
$\boldsymbol{\theta}_i$	Angular rotational displacement of particle i
$\boldsymbol{\xi}_{\mathrm{f}}$	Local average stress tensor in a fluid
$\boldsymbol{\tau}_{\mathrm{f}}$	Viscous stress tensor
$\boldsymbol{\omega}_i$	Angular velocity of particle i

CHAPTER 1: INTRODUCTION

1.1. Background

Die compaction is a typical processing route for powders and has been employed to manufacture a wide range of products, such as pharmaceutical tablets, powder metallurgy (PM) parts, ceramics, detergent tablets, and foodstuffs. The process of die compaction generally consists of three stages (Wu and Cocks, 2004): die filling, compaction and ejection. In the die filling stage, the powder is delivered from a reservoir hopper through a hose into a movable container (i.e., feed shoe), and then the shoe moves over a confined cavity (i.e., a die) thereby depositing the powder into it. After die filling, the deposited powder is compressed by the punches to form a coherent compact. Finally, the compact is ejected from the die. In the PM and ceramic industries, the die compaction could be followed by further processes, e.g., sintering and/or sizing.

In general, a consistent and uniform die filling process is always desirable. Heterogeneity during die filling can propagate through the subsequent processes and finally lead to serious product defects, such as cracking, low strength, distortion and shrinkage (Xie and Puri, 2006). On the other hand, a fast filling process is preferable in order to improve the productivity. Understanding the die filling process can provide essential guidelines to optimise materials, equipment and processes in terms of uniformity and productivity (Sinka and Cocks, 2009). This has motivated increasing interest in the study of die filling.

Since Cocks et al. (2001) identified the scientific issues involved in die filling, his co-workers have undertaken a series of experimental studies and the effects of powder characteristics, apparatus features and some operating conditions on the powder flow behaviour during die filling have been explored (Wu et al., 2003a and c; Schneider et al., 2005; Schneider et al., 2007). In their experiments, a high speed camera was used to visualize the macroscopic powder flow patterns.

For a better understanding of die filling, a Discrete Element Method (DEM) has also been used to model this process and the results seem very promising (Wu and Cocks, 2006; Wu, 2008; Guo et al., 2009a and b; Bierwisch et al., 2009). DEM modelling can provide some micro-dynamic information, e.g. individual particle trajectories and transient interaction forces, which is usually impossible to obtain in the physical experiments (Zhu et al., 2007; 2008). Such micro-dynamic information is essential to understand the underlying physics of granular matter. Compared to experimental investigations, it is much easier to undertake the parametric study in the DEM modelling because the system parameters (particle properties, die geometry, shoe speed etc.) can be prescribed freely.

As observed in die filling experiments (Wu et al., 2003c; Wu and Cocks, 2006), the presence of air has a significant impact on the powder flow during die filling, especially with small and light particles. In order to model the interaction between air and particles during die filling in air, we employ a coupled Discrete Element Method (DEM) and Computational Fluid Dynamics (CFD) approach. In the coupled DEM/CFD approach, the particle dynamics is modelled using DEM while the flow of air is modelled using CFD; and a two-way coupling of air and particles is

incorporated. Therefore, the effect of air can be examined thoroughly. In addition, mixing and segregation behaviour during the die filling can also be investigated.

1.2. Objectives

The objectives of this study are summarized as follows:

- To examine the effect of air on powder flow, mixing and segregation behaviours during die filling.
- To explore the powder flow behaviour during die filling and examine the effects of particle properties (size, density, size distribution, cohesion etc.) on powder flowability.
- To investigate the density-induced segregation and examine the effects of density ratio and shoe velocity on the segregation tendency.
- To simulate suction filling and examine the effect of suction on the powder flowability and density-induced segregation.
- To explore the size-induced segregation and examine the effects of size ratio, initial fines mass fraction, shoe velocity, cohesion and powder level in the shoe.

1.3. Layout of this thesis

In Chapter 2, the published literature on die filling and DEM modelling is reviewed, and the coupled DEM/CFD approach used in this study is presented.

In Chapter 3, the die filling processes in a vacuum and in air are simulated and the effect of air on the powder flow behaviour during die filling is examined. The effects of particle size, density, size distribution and cohesion are also investigated.

In Chapter 4, a bi-column mixture and a bi-layer mixture used in die filling are considered. The competing flow of particles of different densities, and therefore different air sensitivities, is explored. The effect of air on the competing flows is also discussed.

In Chapter 5, density-induced segregation during die filling is investigated using binary mixtures of identical sized particles but of different densities. The evolution of component concentration in the die region during die filling is analyzed, and the effects of shoe velocity and particle density ratio on the segregation behaviour are also investigated.

In Chapter 6, suction filling in the presence of air is simulated. The effect of suction on the powder flow behaviour and density-induced segregation is examined by comparing suction filling with conventional gravity filling.

In Chapters 3-6, only two dimensional (2D) simulations are performed. However, the die filling system in reality is normally three dimensional (3D). Therefore, in Chapter 7, 3D simulations are performed and compared with 2D simulations so that the difference between 2D and 3D simulations can be evaluated.

In Chapter 8, segregation during die filling due to the particle size difference is analysed, and a parametric study is undertaken to explore the effects of shoe velocity, particle size ratio, initial fines mass fraction, cohesion and initial height of powder bed on the segregation tendency.

In Chapter 9, the conclusions of this study are summarized and some recommendations for optimising die filling are made. Finally, the limitations of this research are discussed and some possible future work is proposed.

CHAPTER 2: LITERATURE REVIEW

2.1. Introduction

In this chapter, the progress in the research of die filling is reviewed first, and then the theoretical development and major applications of DEM modelling are discussed. Finally, the methodology used in this study, i.e., a coupled DEM/CFD approach, is presented.

2.2. Die filling

The previous studies on die filling can be categorized into three subject areas: powder flow from a shoe, powder packing inside a die and segregation during die filling. These three areas will be discussed, respectively, in the following sections.

2.2.1. Powder flow from a shoe

The powder flow behaviour during die filling is governed by a combination of a number of factors: powder characteristics (particle size, size distribution, density, shape and surface properties), apparatus features (shoe and die design) and operating conditions (shoe kinematics, the absence or presence of air, suction, vibration, agitation, aeration, humidity and temperature). Understanding the effects of these factors is crucial for the selection of operating parameters and the control of the filling process.

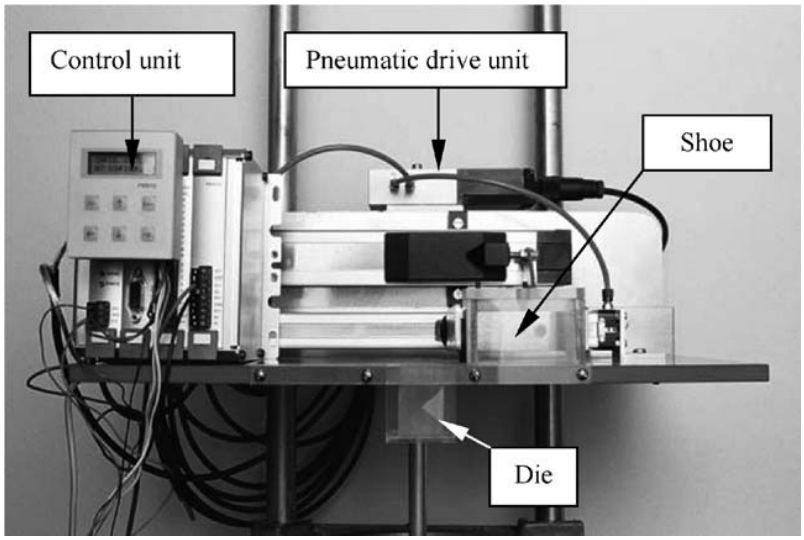

Figure 2.1 A model die filling system (Wu et al., 2003c).

2.2.1.1. Types of flow

Wu et al. (2003c) developed a model die filling system in order to investigate the powder flow behaviour during die filling, as shown in Figure 2.1. The system consists of a transparent die and a transparent shoe which allow the die filling process to be observed and recorded by using a high-speed video system. The size and shape of the die cavity are adjustable. The shoe is driven by a pneumatic drive unit which is controlled by a microprocessor, so that the shoe can move at a range of velocities and accelerations which are representative of industrial processing. The entire system is enclosed in a vacuum chamber with glass walls, within which a vacuum of less than 1 Torr (i.e., 133.3 Pa) can be achieved. Therefore, die filling in a vacuum can also be conducted.

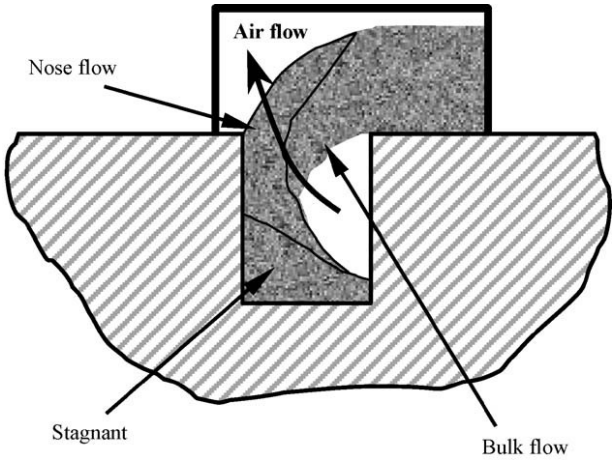

Figure 2.2 Illustration of powder flow patterns in die filling (Wu et al., 2003c).

By adopting the model die filling system (Figure 2.1), systematic studies on powder flow behaviour during die filling were conducted (Wu et al., 2003a and c; Wu and Cocks, 2004; Wu and Cocks, 2006; Schneider et al., 2005; Schneider et al., 2007; Jackson et al., 2007; Sinka et al., 2009; Sinka and Cocks, 2009). Wu et al. (2003c) identified two types of powder flow: nose flow and bulk flow, as illustrated in Figure 2.2. When the shoe with a fixed mass of powder translates over the die, the initial acceleration of the shoe and friction between the bottom of the powder mass and the base plate forces the powder towards the back of the shoe, forming a nose shaped profile. The powder from the top region of the shoe can then be delivered into the die by cascading down the upper surface of the nose. This type of flow is referred to as nose flow. As the tip of the nose moves across the die opening, the powder is delivered into the die by detaching from the bottom surface of the powder mass. This type of flow is referred to as bulk flow. Wu et al. (2003c) found that nose flow promotes fast air evacuation and rapid free surface flow so that a high flow rate can be achieved. While the powder detaching rate in bulk flow is low due to the combined effects of the entrapped air and interlocking of the particles. Nose flow and bulk flow are two primary flow patterns during die filling with free-flowing powders. Moreover,

for cohesive powders, such as most pharmaceutical powders, Sinka et al. (2004) and Schneider et al. (2007) observed a third flow mechanism: intermittent flow, in which the powder is deposited into the die in the form of a discrete release of large chunks of agglomerated powder.

2.2.1.2. Characterisation of powder flow in die filling

As argued by Sinka et al. (2004) and Wu and Cocks (2004), a lot of experimental techniques can be used to characterize the flow properties of powders. However, different measurement techniques can produce a different rank order of flowability for a given powder. It is therefore important that the flow characterisation is carried out using a device that captures the physical phenomena involved in the process under consideration. Thus, from the die filling point of view, the characterisation of powder flow requires a facility which can mimic the real industrial die filling process, such as the model die filling system shown in Figure 2.1. When the shoe moves over the die at a low velocity, the die cavity can be completely filled. As the shoe velocity increases, the die cavity is just partially filled due to the reduction of filling time and the increase in the interlocking of particles at the acceleration stage. Therefore, there exists a maximum shoe velocity at which the die is completely filled. This maximum velocity is referred to as critical filling velocity (Wu et al., 2003c). The higher the critical filling velocity, the better the powder flows. Therefore, the critical filling velocity can be used to quantify the flowability of powders in die filling.

2.2.1.3. Influence of particle properties

A range of metallic powders (Cocks et al., 2001; Wu et al., 2003c; Schneider et al., 2005) and pharmaceutical powders (Sinka et al., 2004; Schneider et al.,2007) were

investigated using the model die filling system (Figure 2.1). It was observed that small irregular shaped particles have a low flow rate and a low critical filling velocity due to the strong interaction and interlocking of the particles (Wu et al., 2003c; Schneider et al., 2005). Lubricants added to the powders result in a reduction of powder flow rate due to the increased interaction and a higher shear resistance between the particles as they flow into the die (Schneider et al., 2005). The influences of the inter-particle friction and particle shape were investigated using DEM modelling by Wu and Cocks (2006) and Wu (2008). A higher critical filling velocity was obtained for a powder with a lower inter-particle friction. This is due to the fact that the particles with the lower inter-particle friction can slide past each other more easily and therefore have better flowability. It was also found that the particles with shapes that can tessellate (e.g., rectangle and hexagon) have a lower critical filling velocity than those with shapes that can not tessellate (e.g., pentagon, nonagon, dodecagon and circle). For particles which can tessellate, strong interlocking of particles which exists in some parts of the randomly packed powder bed inhibits the flow of particles into the die, resulting in a low net filling rate. The DEM study of die filling by Wu (2008) also showed that a polydisperse system has a higher filling rate and a higher critical filling velocity than a mono-disperse system, which has a particle diameter identical to the average particle diameter of the poly-disperse system. It is noted that the particle properties are generally combined with other factors (e.g., the presence of air, die geometry etc.) to influence the powder flow behaviour in die filling. This will be discussed subsequently.

2.2.1.4. Influence of air

The influence of air on the filling process was evaluated by comparing the results from the physical tests in air and in a vacuum for all the aforementioned powders (Cocks et al., 2001; Wu et al., 2003c; Sinka et al., 2004; Schneider et al., 2005; Schneider et al.,2007). The powder generally flows smoothly and rapidly in a vacuum, except for some cohesive pharmaceutical powders for which intermittent flow occurs (Schneider et al., 2007). When air is present the powder flow process can become chaotic due to the interaction between powder and air flow. The air can be momentarily entrapped inside the die. As the powder flows into the die, the built up pressure of the entrapped air increases, opposing the flow of powder into the die. Therefore, for a given powder, a lower flow rate and a lower critical filling velocity are obtained in air compared to in a vacuum. The difference between the flow rates in air and in a vacuum is more pronounced for particles of small sizes and low densities, implying that the air has a more significant impact on the flow of small and light particles (Wu et al., 2003c). Wu et al. (2003c) suggested that the air may have four major effects on the flow process in die filling: i) adverse air pressure gradient caused by the expansion of the powder as it falls opposes the particle motion; ii) pressure built up by air trapped in the die also opposes the flow of powder; iii) drag force exerted by air slows down the powder flow; iv) air flowing between the particles provides a lubricating effect by facilitating the particles to effectively slide past each other more easily. The first three effects are negative to the effective filling, while the last effect could improve powder flowability. The development of an efficient filling requires a balance between suppression of the negative effects and promotion of the positive effects.

2.2.1.5. Influence of shoe kinematics

The shoe kinematics also has a significant effect on powder flow behaviour in die filling (Wu et al., 2003c). For die filling at a low shoe velocity, nose flow dominates. Nose flow can promote rapid powder delivery and fast air evacuation. However, the net die filling rate is counterbalanced by the fact that powder flows into the die just through a small portion of the die opening in nose flow. When the shoe moves at a high velocity, the tip of the nose moves across the die quickly and then bulk flow dominates. For this case, the net filling rate decreases as shoe velocity increases. This is because the increase of shoe velocity reduces the time for particles to build up the vertical speed above the die opening and also enhances the interlocking of particles (Wu et al., 2003c). Sawayama and Seki (1999) allowed the shoe to shake above the die for a moment in their die filling experiments and found that the shaking motion of the shoe improved the filling rate especially for narrow die cavities. This is because the shaking facilitates the flow of powders by breaking up the interlocking and arching of particles.

2.2.1.6. Influence of shoe design

In order to improve the flow of powders during die filling, several types of shoes have been designed with special features. As discussed above, the air entrapped inside the die can significantly prevent the flow of powders into the die. Therefore, how to reduce the effect of the entrapped air is crucial to improve the filling rate. To facilitate the rapid evacuation of air from the die, an air-replacement shoe was developed by Sawayama and Seki (1999) and an agitated shoe by Hashimoto et al. (2002). The air-replacement shoe was constructed by dividing an ordinary feed shoe in half by a pipe at the bottom so that the air can escape through the pipe. Experimental results showed

that the fill rate was improved considerably by using an air-replacement shoe. The agitated shoe involved an agitator which was made up of a rotational device bearing stirring rods and was located inside the shoe. Stirring the powder in the shoe can increase the air permeability of the powder bed and then allow the air to be released more easily from the die cavity, so that the powder can flow into the die more easily. It was reported that using an agitating device, the filling rate increased between 20% and 80% (Hashimoto et al., 2002).

The nose flow, as previously discussed, is faster than bulk flow. Therefore, promotion of nose flow can probably lead to a more efficient filling process. With this consideration, Cocks et al.(2001) and Wu et al.(2003c) employed a shoe comprising of several compartments separated with transversal walls so that nose flow was expected to occur in each compartment. Experimental results showed that the filling rate and critical shoe velocity were increased by using the shoes containing two or three compartments, and this improvement becomes more significant for powders with small and irregular particles. However, further increasing the number of the compartments or reducing the width of each compartment results in no additional increase in filling rate due to the creation of deep narrow channels of powder which inhibits the formation of the noses.

Although the presence of air generally resists the flow of powders, it can provide a lubricating effect to facilitate particles to slide past each other more easily. By taking advantage of this, Kondoh et al. (1998) and Urata et al.(1998) proposed an aeration powder filling system and Zahrah et al. (2001) developed a die filling system with a fluidized shoe. In both systems, a gas is blown into the shoe at a low rate to ‘coat’

particles and separate them, thereby reducing interparticle friction and increasing powder flow rate. The adoption of aerated or fluidized shoes can considerably improve flowability, especially of powders with poor flow properties. Despite the advantages of the above specially designed shoes, there is concern that the processes of agitation, free surface flow and fluidization can cause segregation of powder blends. Therefore, great care must be taken when using these shoes to deliver the powders of different particle properties.

2.2.1.7. Influence of powder level in the shoe

The filling rate is also dependent on the initial powder level in the shoe. During die filling with a low powder bed in the shoe, the powder from the top free surface of the powder bed can fall rapidly into the die, creating a nose shaped profile. With the formation of the nose, a gap is created between the flow stream and the front wall of the shoe, which can facilitate the evacuation of air from the die. As a result, it was observed that the filling rate increased with decreasing powder level in the shoe (Sawayama and Seki, 1999). However, the beneficial effect of the rapid nose flow can be counterbalanced by the fact that the powder is delivered into the die through a small portion of die opening. Thus, a low net filling rate can be obtained if the powder bed in the shoe is too low (Schneider et al., 2005). The experimental results from Schneider et al. (2005) also showed that at higher shoe velocities, when the bulk flow dominates, there was a critical powder level in the shoe, above which the filling rate was independent of the height of powder bed in the shoe, and a cohesive powder had a greater critical powder level than a smooth easily-flowing powder.

2.2.1.8. Influences of die geometry and die orientation

The die geometry (size and shape) also influences the powder flow pattern and flow rate in die filling (Wu et al., 2003c; Schneider et al., 2005). Wu et al. (2003c) demonstrated that the Beverloo equation (Beverloo, 1961), which was proposed to evaluate the mass discharge rate of granular materials from a hopper, can also be used to determine the net flow rate into a die from a shoe delivery system, and furthermore, they proposed that the critical shoe velocity can be expressed as a function of the hydraulic diameter of the die opening and the die height. Schneider et al. (2005) argued that the constant parameter in the Beverloo equation depends on the shoe velocity, and using dimensional analysis they developed a critical filling velocity model, which implies that the critical filling velocity increases as the hydraulic diameter of die opening increases and/or the die height decreases. Wu et al. (2003c) examined complex shaped dies (i.e., stepped dies) in their die filling experiments and observed that the powder flow pattern depended on the shoe kinematics, the location of the step with respect to the direction of shoe motion and whether the die filling is conducted in air or vacuum. When using dies with rectangular cross-sections, Wu and Cocks (2004) and Sinka et al. (2009) observed an effect of die orientation: by aligning the longer axis of the rectangle with the direction of shoe motion higher filling rates were obtained for dies with high ratio of height to hydraulic diameter. In this case the nose flow dominates for a longer time and air escapes easily therefore leading to a fast filling process.

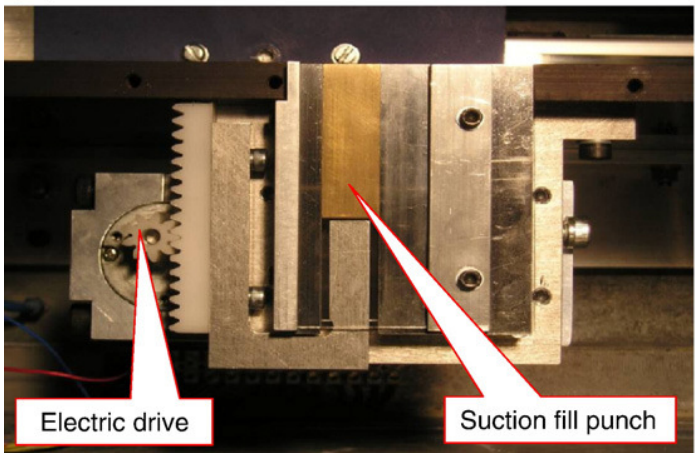

Figure 2.3 A suction filling system (Sinka et al., 2009).

2.2.1.9. Influence of suction

Conventionally, the flow of powder into a die is driven by gravity when the shoe moves over the die. This die filling method is referred to as gravity filling. However, in a rotary tablet press, the effect of suction becomes a key element of the die filling process (Jackson et al., 2007). In this process, the die cavity is initially occupied by a movable punch and this punch moves downwards when the shoe moves across the die opening. The motion of the punch 'sucks' the powder into the die by creating a partial vacuum below the powder. This die filling method is referred to as suction filling. In suction filling, air is not entrapped to hinder the flow of powder into the die. On the other hand, the formation of the vacuum below the powder induces a high pressure difference between the top and bottom of powder bed, and this pressure difference forces the powder into the die. As a result, a high filling rate is expected under the influence of suction. Based on the model die filling system (Wu et al., 2003c), Jackson et al. (2007) incorporated a suction device, which consists of a punch inserted into the die and a weight connected to the punch. When the shoe moves over the die, the weight is released to drag the punch down. An upgraded suction filling

mechanism, as shown in Figure 2.3, was developed by Sinka et al. (2009) with an electric drive to allow detailed studies of the effect of a wider range of suction filling conditions. Jackson et al. (2007) found that suction filling led to an increase in the critical filling velocity by a factor of approximately 2.5. When the shoe velocity exceeded the critical velocity, a larger amount of powder was fed into the die after suction filling and the amount of powder fed into the die decreases less abruptly with the increase of shoe velocity during suction filling compared to gravity filling (Sinka et al., 2009).

2.2.2. Powder packing inside a die

A uniform fill density distribution and a consistent filling outcome are desirable to achieve high product quality. Many studies have been conducted to evaluate the effects of a number of factors on powder packing behaviour inside a die cavity, which determines the fill uniformity and consistency.

2.2.2.1. Influences of die geometry and die orientation

Experimental work by Bocchini (1987) using rectangular dies of various widths showed that sparse boundary layers were present at the die walls and across these boundary layers the apparent density increases from a low value to the bulk value in the middle of the die cavity. Due to the presence of the boundary layers, the fill density decreased as die width decreased. When the die width was sufficiently large, the fill density tended to be constant as the boundary effect became negligible. These results are consistent with the previous experimental observations using a set of circular dies of different diameters by Rice and Tengzelius (1986), who found that the fill density decreased with decreasing die diameter and it remained constant when the

die diameter was sufficiently large. A simple theory was proposed by Bocchini (1987) to describe the fill density as a function of the hydraulic radius of the die opening and the thickness of the boundary layer for different die geometries; and the theoretical predictions were in good agreement with the experimental results.

Die orientation with respect to the direction of shoe motion also has an impact on the fill density. For die filling with a long-narrow die opening, a higher fill density is obtained when the shoe moves in the direction orthogonal to the long axis of the die compared to in the direction parallel to the long axis of the die (Bocchini, 1987; Wu and Cocks, 2004). Bocchini (1987) argued that this is because filling orthogonal to the long die axis produces more frequent particle rebounds from wall to wall as the powder flows into the die and this leads to a densification due to the particle rearrangement. Haskins and Jandeska (1998) used computed tomography to examine the spatial powder distribution and found that the powder density distribution depends on the die shape and the orientation of the die with respect to the direction of shoe motion. The powder density appeared to be higher near the concave die surfaces than near the convex die surfaces in die filling with a core rod inside the die cavity. For a die with slots, teeth and other geometric discontinuities, higher powder densities were obtained in the regions oriented along the axis of the shoe motion than in the regions off the axis. When filling a ring shaped die, Hjortsberg and Bergquist (2002) observed that the powder density was generally higher in the sections parallel to the direction of shoe motion.

2.2.2.2. Influence of shoe kinematics

The kinematics of the shoe has a significant impact on powder flow during the die filling process, and consequently it also has an influence on the powder packing behaviour inside the die. A systematic experimental study was conducted by Hjortsberg and Bergquist (2002) to investigate the effect of shoe motion on density variations after die filling with a ring shaped die. They found that the powder density increased as the shoe speed increased. During die filling, the kinetic energy of moving particles can be partially transferred into the die cavity, in which it causes rearrangement of the particles and compaction. The increase of shoe speed results in an increase of kinetic energy of particles and hence in an increased densification in the die.

In the experiments of Hjortsberg and Bergquist (2002), the shoe was allowed to stay above the die for several seconds before returning to its starting position, which provided enough time for the particles to be deposited into the die cavity under the pressure from the powder mass above, thereby resulting in a higher packing density in the die compared to without settling. After one passage of the shoe over the die, the shoe was also allowed to move over the already filled die for several more times, and the packing density in the die was found to increase with the number of shoe passages until a limit was reached. This is a result of the denser packing rearrangement of particles in the die cavity due to the interactions of the moving particles in the shoe and the stationary particles in the die when the shoe moves over the die. Rice and Tengzelius (1986) indicated that it is most significant for the fill density to increase with the number of shoe passages when the shoe speed is high, suggesting the importance of the dwell time over the die.

A pressure deposition tester (PDT) was developed by Xie and Puri (2007a; 2007b; 2008) to analyze the uniformity in die deposition. This device is based on the principle that an anisotropic fill density distribution would result in an uneven particulate vertical pressure distribution on the bottom surface of the die (Xie and Puri, 2007a). As a result, the uniformity of the packed power in the die can be evaluated by measuring the pressure distribution at the bottom of the die. Using the PDT, Xie and Puri (2007a; 2007b) tested die depositions with various feed shoe speeds and with dies of different shapes. They found that feed shoe speed did have an effect on pressure distribution and therefore on uniformity. However, this effect depended on the die shape, for instance, the highest feed shoe speed considered in their studies led to the most uniform pressure distribution for the cylindrical dies (Xie and Puri, 2007a), but led to the most non-uniform pressure distribution for the toroidal dies (Xie and Puri, 2007b). Higher momentum possessed by particles at higher shoe speed was expected to contribute to relatively uniform filling by minimizing arching and allowing rearrangement of particles. However, due to the presence of the central pole in a toroidal die, the particle packing behaviour could be affected by the interaction of particles and the central pole (Xie and Puri, 2007b).

2.2.2.3. Influence of shoe features

Some of the aforementioned shoes with special features also have a good capability to improve the uniformity as well as the flowabililty. When using an air-replacement shoe, weight variations of compacts were significantly improved (Sawayama and Seki, 1999). Using an agitated shoe, Hashimoto et al. (2002) reported weight variation can be reduced by up to 30% compared with the performance of a conventional feed shoe.

The improvement in the weight variation was found to depend on the rotating speed of the agitator and the optimum agitation speed, at which the minimum weight variation was obtained, varied according to the powder properties, shoe velocity and die geometry. An aerated shoe was developed to fill the thin and complex-shaped cavities quickly and uniformly (Kondoh et al., 1998; Urata et al., 1998). The experimental results showed that using such an aerated shoe the weight scattering, the maximum value of density variation and the maximum value of height variation of the compacts were significantly reduced, especially in fast filling. Zahrah et al. (2001) developed a fluidised shoe and they found that the weight variation could be improved by a factor of 3 to 4 using such a fluidised shoe.

2.2.2.4. Influence of other operating parameters

Other important operating parameters, such as filling method, powder level in the shoe, lubrication and vibration, have also been examined in the previous studies. Demetry et al. (1998) developed tactile sensors as a tool to evaluate the density uniformity of the packed powders in dies prior to compaction. In this method, non-uniform mass distribution in the die was detected as gradients in the transmitted pressure by a tactile sensor located at the bottom of the die. By filling the die in different ways, they found that pouring the powder immediately above the die opening rather than from the side of the die results in a more uniform density distribution.

The height of the powder bed in the shoe is also a potential factor which can influence the fill density. Sawayama and Seki (1999) reported that the filling density increased as the powder level in the shoe increased when the die was completely filled.

However, there should be a limit for this and the experimental results of Hjortsberg and Bergquist (2002) confirmed the existence of this limit by indicating that powder density is insensitive to the amount of powder in the shoe when the powder level is above a critical value.

Adding lubricants to the powder can increase the fill density, as pointed out by Rice and Tengzelius (1986). This is because the presence of lubricants can make the particles slide past each other more easily and reduce the chance to form arches and bridges, thereby leading to a denser packing of particles. It was found that the extent of this increase in fill density depended on the amount and type of lubricant used.

Using a vibrator attached to the die, the effect of vibration at different frequencies was investigated by Rice and Tengzelius (1986). In general, a higher fill density was obtained with vibration compared to that without vibration and the fill density increased with the vibration frequency. However, vibrating at too high a frequency appeared to result in fluidization and hence in low densities in certain dies, especially of small sizes.

2.2.3. Segregation during die filling

During die filling, powder blends consisting of particles of different physical properties such as density, size and/or shape are commonly used. The difference in particle properties can cause segregation, which is referred to as a homogeneous powder blend becoming spatially non-uniform in such a manner that the particles having the same properties congregate in one part of the mixture during handling and processing (Rhodes, 1998). Segregation in die filling may influence product quality

by causing variations in filling density and compound concentration from compact to compact. Therefore, segregation is a typical problem and needs to be minimized.

Thirteen segregation mechanisms of granular mixtures were identified by de Silva et al. (2000) as follows: trajectory, air current, rolling, sieving (or sifting), impact, embedding, angle of repose, push-away, displacement, percolation, fluidization, agglomeration, and concentration-driven displacement. By combining similar mechanisms (such as sifting and displacement being special cases of percolation) and dismissing some infrequently-occurred mechanisms (such as embedding or push-away), these thirteen mechanisms have been subsequently condensed to four primary mechanisms (Ketterhagen et al., 2008):

1) percolation, or sifting, segregation whereby smaller particles pass through a matrix of larger particles in the direction of gravitational acceleration, and this is enhanced by local shear stain,
2) angle of repose segregation whereby particles with a smaller angle of repose flow over particles with a larger angle of repose during, for example, filling of a bin or silo,
3) trajectory segregation whereby smaller or more angular particles move at a lower velocity due to stronger frictional effects when a thin layer of granular mixture flows down a chute, which results in different trajectories upon discharge from the chute, and
4) fluidization, or elutriation, segregation whereby differences in drag forces on particles in a mixture tend to fluidize or entrain the fine and/or light particles causing them to segregate.

During die filling, all these four types of segregation may occur. When a mixture of different sized particles is used, segregation with an excess of fines at the bottom can occur due to the percolation of fines through the void space in the structure of coarse particles. The segregation due to different angles of repose may also occur when particles of different shapes are packing inside the die cavity. When the powder is delivered into the die cavity along a free surface, for instance, in nose flow, the large particles tend to flow over the top of small ones on the top surface and then cascade into the die. Under this condition, segregation occurs due to the different trajectories of large and small particles upon the free surface flow. When air is present during die filling, the air flow can influence the distribution of small and/or light particles by entraining them.

To some extent, the powder delivering process during die filling is analogous to the powder flow during the discharge from a hopper or a bin. The segregation in hopper flow has attracted an increasing interest. Standish (1985a, b) experimentally investigated size-induced segregation in emptying a hopper, and found that the concentration of fine particles in the discharge stream was high at the initial stage and low at the final stage due to the percolation of fines through the voids in the matrix of coarse particles. Similar behaviour was also observed by Arteaga and Tüzün (1990) for the discharge of powder mixtures from a mass-flow hopper. Furthermore, they also found that there was a large excess of fine particles immediately before the completion of discharge in funnel flow (Arteaga and Tüzün, 1990; Tüzün and Arteaga, 1992). It was observed that segregation almost did not occur when the fines fraction was high enough in the mixture. Thus, a model was proposed to predict the feasibility of segregation by assuming that the segregation of a mixture would stop when the

surface area of all the large particles was completely covered by small particles. Ketterhagen et al. (2007; 2008) performed three-dimensional DEM simulations to explore the segregation during powder flow from a hopper. In their work, the effects of various factors, such as particle properties, hopper geometries and initial fill method, were systemically investigated. The results showed that the extent of segregation in hopper discharge was determined by the particle size ratio, hopper wall angle and hopper fill method, whereas it was only slightly affected by hopper dimensions and the particle density ratio.

As the powder flows into the die during die filling, the development of a heap with free surface flows can be observed (Wu et al., 2003a and 2003c; Guo et al., 2009). During the formation of a heap by pouring a powder mixture, the larger and/or lighter particles flow down along the free surface and accumulate at the base, whereas smaller and/or heavier particles sink into the core of the heap close to the pouring point (Drahun and Bridgwater, 1983; Khakhar et al., 1999; Meakin, 1990). A mathematical model was proposed by Prigozhin (1993) to quantitatively examine this free surface segregation in the heap formation with binary systems, and the predicted concentration distributions of segregating components in the granular bed were in good agreement with the experimental results obtained by Drahun and Bridgwater (1983). Following on from this, Pudasaini and Mohring (2002) developed a model for the free surface size segregation with polydisperse granular systems composed of multiple components. Furthermore, spontaneous stratification with alternating layers of small and large particles was also observed in a quasi-two-dimensional heap formation when large particles had larger angle of repose than small ones (Makse et al., 1997), and even when large and small particles have the identical angle of repose

under the condition that a low powder feed rate was applied (Baxter et al., 1998). Cizeau et al. (1999) developed a cellular automaton model and a continuum model to analyze this spontaneous stratification. They found that spontaneous stratification occurred when the repose angle of large particles (θ_{22}) was larger than the repose angle of small particles (θ_{11}), and that stratification could also be obtained when θ_{22} was slightly smaller than θ_{11} as long as the flowing layer of particles was thin and all the rolling particles were in contact with the surface of the sandpile. When θ_{22} was much smaller than θ_{11}, only segregation, but no stratification, occurred. These predicted results were consistent with the previous experimental observations (Makse et al., 1997; Baxter et al., 1998).

Segregation during die filling was investigated by Lawrence and Beddow (1968a, b) and their experimental results showed that the size-induced segregation occurred with a higher concentration of fine particles at the bottom of the die and a higher concentration of coarse particles in the periphery of the die cavity, due to the filtration of fines through the flowing powder mass. However, the difference in particle densities was not found to have a significant impact on segregation (Lawrence and Beddow, 1968a). By using a vibrating die (Lawrence and Beddow, 1968b), the radial segregation was reduced, because the inner mound of fines tended to be levelled off; while the vertical segregation was found to depend on the amplitude and frequency of the vibration. When the die was oscillated at low or high amplitude, the powder mass was quiescent or bouncing and the vertical segregation was minimized; when the die was oscillated at intermediate amplitude and high frequency, the churning of powder mass occurred and the vertical segregation was increased. In the above experimental

studies of the segregation in die filling, the particle densities and sizes were so large that the effect of air was negligible.

2.3. Discrete Element Method

The Discrete Element Method (DEM) is a numerical method for computing the dynamics of an assembly of discrete particles. Since it was first applied to problems in rock and soil mechanics by Cundall and Strack (1979), DEM has developed rapidly with the dramatic increase in computing capability. In this section, the theoretical developments and some major applications of DEM are briefly discussed.

2.3.1. Theoretical developments

In DEM, the individual particle trajectories are tracked in such a manner that the translational and rotational displacements of each particle are incremented at fixed time steps by integrating the equations of motion which are governed by Newton's second law. The particles are normally accelerated by interparticle and gravitational forces. If the particles are handled in the presence of a fluid, the fluid-particle interaction force can also have a significant impact on the motion of particles. Two types of DEM have been proposed: the hard-sphere and the soft-sphere approaches. In a hard-sphere simulation, collisions are assumed to be binary and instantaneous, the particle velocities after a collision are related to the velocities before the collision and depend on the coefficients of restitution and friction (Li and Kuipers, 2002, 2003). The deformation of, and the forces between, particles are not explicitly considered. Thus, the hard-sphere method is typically applicable to rapid particle flow. By contrast, in the soft-sphere simulation, the deformation of particles in contact are modelled, and the interparticle forces can be calculated from the deformations based

on the given force models. As indicated in previous work (Zhu et al., 2007), the soft-sphere method is capable of handling multiple particle contacts which is crucial in the simulations of quasi-static systems. Therefore, the soft-sphere method is believed to be superior to the hard-sphere method and has been extensively used to study various particle handling processes. The development of various force models for soft-sphere DEM is discussed below.

2.3.1.1. Interparticle forces

The majority of DEM researchers use a simple linear spring-dashpot model to describe the contact interaction between two spherical particles, in which both the normal force-displacement relationship and tangential force-displacement relationship were assumed to be linear. To account for the viscous dissipation, a damping term that is proportional to the relative velocity was involved in both normal and tangential forces. More detailed and physically sound contact force models were developed for the frictional elastic contact between two spheres in the normal direction by Hertz (1882) and in the tangential direction by Mindlin and Deresiewicz (1953). Based on Hertz theory (see also Johnson, 1985), the normal force follows a non-linear relationship with the normal displacement. Unfortunately, as demonstrated by Mindlin and Deresiewicz (1953), due to the tangential slip between the contacting surfaces, the tangential force-displacement relationship depends on the whole loading history and the instantaneous rate of change of the normal and tangential force or displacement. Therefore, a direct tangential force-displacement relationship is impossible to be obtained and an incremental procedure is required to determine the force law in the tangential direction. The application of the classic contact mechanics-based theories of Hertz (1982) and Mindlin and Deresiewicz (1953) enables the evolution of contacts

to be determined using physically realistic particle properties, such as Young's modulus and Poisson's ratio, compared to the spring-dashpot type contact models in which artificial contact stiffnesses are used and the link with the physical properties of the particles is obscure.

Di Renzo and Di Maio (2004) studied the influence of different contact-force models on the accuracy of the simulated collision process, and they compared three models: a linear model, based on a Hooke-type relationship; a non-linear model, based on the Hertz theory (1882) for the normal force-displacement relationship and the no-slip solution of the Mindlin and Deresiewicz theory (1953) for the tangential force-displacement relationship; a non-linear model with hysteresis, based on the complete theories of Hertz and Mindlin and Deresiewicz. They indicated that it is important to account for the non-linearity in the contact model and micro-slip effects in order to obtain the correct time evolution of the forces, velocities and displacements during collision, and therefore the complete theories of Hertz and Mindlin and Deresiewicz should be addressed to perform deeper analyses on granular materials in motion.

As an approximation of the complex Mindlin and Deresiewicz model (1953), Walton and Braun (1986) and Walton (1993) proposed a simplified expression of tangential stiffness for the case of constant normal force. This simplification improves the efficiency in calculation; however, this model is shown to be not accurate for a number of cases (Vu-Quoc et al., 2000). Therefore, an improved and more accurate tangential force-displacement model was proposed by incorporating into the Walton and Braun tangential model (1986) the four cases of varying normal and tangential forces from the Mindlin and Deresiewicz (1953) theory (Vu-Quoc and Zhang, 1999).

Langston et al. (1994; 1995) ignored the effect of loading history and assumed that the tangential force can be explicitly expressed as a function of tangential displacement and normal force. This model is much simpler and less time demanding in DEM simulations compared to the complete Mindlin and Deresiewicz model, so that it has also been used by Zhou et al. (1999) to simulate sandpile formation with rolling friction. More realistic models that incorporate the effects of plastic deformation were developed by Thornton (1997) and Vu-Quoc et al. (2001).

When fine particles are involved, the surface effect on the packing and flow behaviour of particles due to van der Waals forces may become significant. This phenomenon is normally referred to as auto-adhesion (Yin, 1992). For the normal loading of elastic spheres in the presence of adhesion, JKR theory (Johnson et al., 1971) and DMT theory (Derjaguin et al., 1975) were developed based on the Hertz model to take into account the surface energy. The JKR theory predicts a larger contact area than that predicted by Hertz theory. Within the contact area, compressive stress acts in the inner circular region following a Hertzian-type distribution and the outer annulus experiences tensile stresses which are infinite at the perimeter. By contrast, the DMT theory assumes that the shape of the particles is not affected by the surface forces and hence the contact area experiences a compressive stress distribution as predicted by Hertz theory and, outside the contact area, there is a tensile stress which decreases with surface separation. However, as pointed out by Thornton and Yin (1991), both JKR and DMT theories are approximations to the general solution that must account for the surface force acting outside the contact area and the controlling principles of the deformations within the contact area. By adopting the JKR theory for normal loading, Thornton (1991) developed a model combining the theories of Savkoor and

Briggs (1977) and Mindlin and Deresiewicz (1953) to describe the tangential force-displacement relationship for two adhered elastic spheres. In the theory of Thornton (1991), a smooth transition from peeling to sliding was assumed, and after peeling, the tangential loading was proposed to follow the Mindlin and Deresiewicz model (1953) in terms of an effective normal force until sliding occurs. Furthermore, Thornton and Ning (1998) proposed a more complex model for the elastic-perfectly plastic contact with adhesion in the normal direction.

2.3.1.2. Fluid-particle interaction forces

When particle systems include the presence of a fluid (a gas or liquid), the movement of particles can be resisted or promoted by the interaction between the fluid and the particles. Therefore, the fluid-particle interaction force must be properly considered in DEM to model a fluid-particle flow process. As suggested by Anderson and Jackson (1967), this force can be decomposed into (i) a component due to macroscopic variations in the fluid stress tensor, and (ii) a component representing the effect of detailed variations of the point stress tensor as the fluid flows around a particle. The first component comprises the forces due to the fluid pressure gradient and the viscous stress tensor. The second component, which includes skin friction and drag contributions, was believed to comprise of a drag force and a virtual or added mass force (Anderson and Jackson , 1967; Kafui et al., 2002).

The drag force describes the force due to the relative motion between fluid and particle, which leads to an unbalanced pressure distribution as well as shear stresses on the particle surface (Johnson, 1998). The drag force acts on the particle in a direction opposite to the motion of the particle through the fluid and its magnitude

depends on the relative velocity between particle and fluid. In general, the drag force can be determined by experimentally based correlations (Ergun, 1952; Wen and Yu, 1966; Richardson, 1971; Di Felice, 1994) or numerical simulations (Choi and Joseph, 2001; Zhang et al., 1999). These correlations possess similar predictive capability, although their accuracy may differ (Li and Kuipers, 2003). The virtual mass force, accounting for the resistance of the surrounding fluid mass that is accelerated by the particle, is a function of the acceleration of the relative velocity between a particle and the surrounding fluid (Li et al., 1999; Potic et al., 2005).

Together with the above forces, there also exist some other fluid-particle interaction forces including the Basset force (Li et al., 1999) and lift forces (Yuu et al., 2000; Xiong et al., 2005). The Basset force, which is also known as the history force or memory force, describes the force due to the lagging boundary development with changing relative velocity (acceleration) of the particle moving through a fluid (Crowe et al., 1998). It takes into account the viscous effect and addresses the temporal delay in boundary layer development caused by the acceleration of the particle. The effects of the virtual mass force and the Basset force may become negligible when the density ratio of fluid to solid particle is small. However, they can be significantly large when a dense gas or a liquid is present and/or the particle is accelerated at a high rate (Johnson, 1998). The lift forces, including the Saffman lift force and the Magnus lift force, are perpendicular to the direction of the relative velocity between particle and fluid. The Saffman lift force is caused by the fluid shearing motion due to the velocity gradient around the particle (Xiong et al., 2005; Johnson, 1998). According to Johnson (1998), this lift force is negligible at very small shear rates or very low (particle) Reynolds number. The Magnus lift force is due to

the particle rotation which causes a fluid velocity differential on the surface of the particle by entraining the surrounding fluid (Xiong et al., 2005; Zhu et al., 2007).

2.3.1.3. Modelling of fluid-particle two-phase flow

The existing approaches to model fluid-particle flow can be classified into three categories: continuum-continuum approach, discrete-discrete approach and continuum-discrete approach.

In the continuum-continuum approach, both fluid and solid particle phases are treated as interpenetrating continua. The representative of this approach is two fluid modelling (TFM), which has dominated fluid-particle fluidization modelling for decades (Gidaspow, 1994; Kuipers and van Swaaij, 1997; Arastoopour, 2001). However, as argued by Yu and Xu (2003), the effective application of this model depends heavily on the constitutive relations for the solid particle phase and the momentum exchange between phases, which are impossible to obtain within its framework. This becomes particularly true when dealing with different types of particles that should be treated as different phases.

In the discrete-discrete model, the fluid phase is discretised as a limited number of fluid particles using the Lattice-Boltzmann (LB) method or pseudo-particle method (PPM). By simulating the interaction of these fluid particles, the fluid flow behaviour emerges automatically from the intrinsic particle streaming and collision processes. For the solid particle phase, DEM is normally employed to model the interaction and motion of solid particles. For the discrete-discrete approach, two models were proposed, namely a coupled LB/DEM model (Cook et al., 2004) and a coupled

PPM/DEM model (Ge and Li, 2001, 2003). Using these models the detailed interaction of fluid and solid particles can be obtained. However, the numerical analysis with a discrete-discrete approach can be computationally expensive due to the particle-like discretization of the fluid phase, so a massively parallel implementation of the model is extremely demanded.

In the continuum-discrete approach, the flow of fluid, which is treated as a continuum medium, is modelled by solving the Navier-Stokes equations and the motion of discrete particles by solving Newton's second law of motion applied to individual particles. A direct numerical simulation (DNS) and a coupled CFD/DEM method have been proposed. In DNS (Hu, 1996; Pan et al., 2002), a combined weak formulation is developed to implicitly describe the fluid-particle coupling system. The fluid phase is resolved by meshing the field with the computational cells which are much smaller than particle size and the void size among the particles, and the surfaces of particles are treated as moving boundaries of the fluid field. Therefore, the detailed information on fluid flow around a single particle and hydrodynamic interactions between fluid and particles can be obtained. The major drawback of DNS is its capacity to model particle collisions. In previous work, an artificial repulsive force was introduced to keep the particles apart (Glowinski et al., 2000; Pan et al., 2002). As a result, so far, the DNS model has been mainly applied to the hydrodynamic interaction-dominant flow of fluid and particles, and this limits its applicability to the fluid-particle flow where particle-particle interactions (collisions) are significant (Zhu et al., 2007).

The coupled CFD/DEM approach was first proposed by Tsuji et al. (1993), and then widely applied to the simulation of multiphase flow in chemical and process engineering applications. In this approach, the motion of particles is modelled using DEM, in which both fluid-particle and particle-particle interactions have been incorporated; while the fluid flow is determined using the traditional CFD based on the Navier-Stokes equations in terms of local average variables (Anderson and Jackson, 1967). The computational domain is partitioned by the fluid cells that are larger than the particle size but still very small compared to the whole domain. Void fraction is introduced into the governing equations for the fluid in order to consider the effect of the presence of particles in the fluid cells. As indicated by Yu and Xu (2003) and Zhu et al. (2007), the CFD/DEM is believed to be the most popular and attractive approach to model the fluid-particle two-phase flow due to its lower computational cost compared to LB/DEM and DNS, and better capability to capture the particle physics as compared to TFM

2.3.2. Applications of DEM

As pointed out by Zhu et al. (2007; 2008), DEM simulations can provide some micro-dynamic information, e.g. individual particle trajectories and transient interaction forces, which is extremely difficult, if not impossible, to be obtained in the physical experiments with small and many particles. Such micro-dynamic information is essential to understand the underlying physics of particulate matter. As a result, DEM or DEM-based simulations have been widely employed to investigate many powder handling processes, including heap formation (Luding, 1997; Baxter et al., 1997; Matuttis et al., 2000; Smith et al., 2001; Zhou et al., 2003; Tüzün et al., 2004; Fazekas et al., 2005), particle packing (Hong, 1998; Yang et al., 2000, 2003, 2008; Li et al.,

2006), powder compaction (Ng, 1999; Kong and Lannutti, 2000; Thornton et al., 2004; Martin et al., 2006; Chung and Ooi, 2008; Mehrotra et al., 2009), direct shear test (Thornton and Zhang, 2003, 2006; Zhang and Thornton, 2007; Hartl and Ooi, 2008), biaxial and triaxial compression (Thornton and Barnes, 1986; Thornton, 2000; Williams and Rege, 1997; Rock et al., 2008; Ng, 2005; David et al., 2007), vibrating beds (Lee, 1997; Rosato et al., 2008; Zeilstra et al., 2006, 2008), hopper flow (Kohring et al., 1995; Langston et al., 1997, 2004; Baxter et al., 2000; Tüzün et al., 2004; Ketterhangen et al., 2007, 2008), rotational mixers and drums (Kuo et al., 2002; Lemieux et al., 2008; Dury et al., 1998; Portillo et al., 2007), gas fluidization (Tsuji et al., 1993, 2008; Xu an Yu, 1998; Xu et al., 2000; Kafui et al., 2002; Li and Kuipers, 2007; Gui et al., 2008), and pneumatic conveying (Xiang and McGlinchey, 2004; Lim et al., 2006; Kuang et al., 2008). Zhu et al. (2008) summarized the DEM studies in the past thirty years or so, which were categorized into three subject areas: particle packing, particle flow and fluid-particle flow.

In recent years, DEM and coupled CFD/DEM approaches have also been used to study the filling of a die or a confined cavity, and some new insights have been drawn into the powder flow (Wu et al., 2003a; Coube et al., 2005; Wu and Cocks, 2006; Wu, 2008; Guo et al., 2007, 2009b; Bierwisch et al., 2009), segregation (Guo et al., 2008, 2009a) and density distribution (Wu and Cocks, 2006; Bierwisch et al., 2007, 2009) during the filling process. Wu and Cocks (2006) and Wu (2008) adopted various 2D polyhedral particles in their simulations, and the influence of particle shape on powder flow and density distribution was hence explored. In addition, the effects of particle size, size distribution, powder level in the shoe and filling speed were also examined (Wu, 2008). To consider the irregularity of particle shape, Bierwisch et al. (2009)

introduced complex shaped grains consisting of agglomerates of spheres. In their 3D simulations, the constituent spheres of contacting grains interact with each other due to the force laws of sphere-sphere contact; forces and torques are then summed up for every grain and thereafter the equations of motion are solved under the constraint of the stiffness of each grain. The simulated density distributions are in good agreement with the experimental measurements for different die geometries. In order to model die filling in the presence of air, a simplified algorithm was incorporated in DEM by Wu and Cocks (2006) to take into account the effect of the build-up of air pressure. However, the air drag effect and the coupling effect of particle-air interaction were ignored. Although the study revealed that the simplified model can capture some essential features of the build-up of air pressure on the flow kinematics of powder, they envisaged that there was still a need to develop a more rigorous model, in which the dynamics of air and powder and their interactions are considered thoroughly in order to model the major effects of air during die filling as observed experimentally. Consequently, a coupled DEM/CFD method has been adopted, in which the air–particle interaction is determined by a combination of pressure gradient, viscous stress and drag force, to analyse the die filling process in the presence of air (Guo et al., 2009).

2.4. Methodology

In this work, a coupled DEM/CFD method, which was originally developed by Kafui et al. (2002) to model two-phase (gas-solid and liquid-solid) systems, is used to analyse the powder flow, mixing and segregation behaviours during die filling in the presence of air. The DEM/CFD code is an advanced version of TRUBAL, which is

the DEM code originally developed by Cundall (1988). The details of this method are provided below.

2.4.1. Equations for particle motion

The motion of discrete particles is governed by Newton's second law of motion. The net force acting on an individual particle i comprises a gravitational force $m_i\mathbf{g}$, a fluid-particle interaction force $\mathbf{F}_{\mathrm{fp}i}$, and solid particle-particle contact forces $\mathbf{F}_{\mathrm{c}i}$. The translational and rotational motions of particle i with mass m_i and moment of inertia I_i are governed by the following equations

$$m_i \frac{\mathrm{d}\mathbf{v}_i}{\mathrm{d}t} = \mathbf{F}_{\mathrm{c}i} + \mathbf{F}_{\mathrm{fp}i} + m_i\mathbf{g} \tag{2.1}$$

and

$$I_i \frac{\mathrm{d}\boldsymbol{\omega}_i}{\mathrm{d}t} = \mathbf{T}_i \tag{2.2}$$

in which, $\mathbf{v}_i$ and $\boldsymbol{\omega}_i$ are the translational velocity and angular velocity, respectively, of the particle, and $\mathbf{T}_i$ is the torque arising from the tangential components of the contact forces.

Explicit time integration of equations (2.1) and (2.2) using a central finite difference scheme with fixed time step Δt gives new velocities and positions of the individual particles:

$$\mathbf{v}_i^{t+\Delta t/2} = \mathbf{v}_i^{t-\Delta t/2} + \frac{d\mathbf{v}_i}{dt}\Delta t \qquad \text{and} \qquad \boldsymbol{\omega}_i^{t+\Delta t/2} = \boldsymbol{\omega}_i^{t-\Delta t/2} + \frac{d\boldsymbol{\omega}_i}{dt}\Delta t \tag{2.3}$$

$$\mathbf{x}_i^{t+\Delta t} = \mathbf{x}_i^{t} + \mathbf{v}_i^{t+\Delta t/2}\Delta t \qquad \text{and} \qquad \boldsymbol{\theta}_i^{t+\Delta t} = \boldsymbol{\theta}_i^{t} + \boldsymbol{\omega}_i^{t+\Delta t/2}\Delta t \tag{2.4}$$

where $\mathbf{x}_i$ and $\boldsymbol{\theta}_i$ are the coordinates and rotational displacements, respectively, of particle i. From the new positions and velocities of the particles new solid particle-particle contact forces and fluid-particle interaction forces can be then calculated.

2.4.2. Particle-particle interactions

A soft-sphere approach is adopted in the present DEM modelling and the particle-particle interaction is governed by models based on classic contact mechanics. For the frictional elastic contact of spherical particles, the theory of Hertz (1881; see also Johnson, 1985) is used to describe the normal force-displacement relationship while the theory of Mindlin and Deresiewicz (1953) is used for the tangential force-displacement calculations. For the frictional elastic contact with adhesion, the JKR theory (Johnson et al., 1971) that extends the Hertz theory to account for surface energy, and the theory of Thornton (1991) that combines the theories of Savkoor and Briggs (1977) and Mindlin and Deresiewicz (1953) are employed to evaluate the normal force-displacement and tangential force-displacement evolutions, respectively. The modelling of the frictional elastic-perfectly plastic contact of spherical particles with and without adhesion is also implemented in the current DEM/CFD code based on the theory of Thornton (1997) and Thornton and Ning (1998). However, in the work reported in this thesis, the effect of plastic deformation of particles is not considered so that only the models of frictional elastic contacts with and without adhesion are summarized below.

2.4.2.1. Frictional elastic contact without adhesion

For two spheres of radii R_i, Young's moduli E_i and Poisson's ratios ν_i (i =1, 2), the normal force-displacement (F_n-δ_n) relationship is given by Hertz (1881; also see Johnson, 1985):

$$F_n = \frac{4}{3} E^* R^{*1/2} \delta_n^{3/2} \tag{2.5}$$

where

$$\frac{1}{E^*} = \frac{1-\nu_1^2}{E_1} + \frac{1-\nu_2^2}{E_2} \tag{2.6}$$

and

$$\frac{1}{R^*} = \frac{1}{R_1} + \frac{1}{R_2} \tag{2.7}$$

Differentiating Eq. (2.5) with respect to δ_n gives the normal stiffness

$$K_n = \frac{dF_n}{d\delta_n} = 2E^* a \tag{2.8}$$

in which, a is the radius of the contact area given by

$$a = \sqrt{R^* \delta_n} \tag{2.9}$$

A theoretical study of the interaction between frictional elastic spheres in contact under varying oblique forces was presented by Mindlin and Deresiewicz (1953). Solutions were provided in the form of instantaneous compliances which, due to the dependence on both the current state and the previous loading history, could not be integrated *a priori*. However, several loading sequences involving variations of both normal and tangential forces were examined from which general procedural rules were identified. Adopting an incremental approach, the procedure is to update the normal force and contact area radius, using (2.5) and (2.9), followed by calculating the tangential incremental force ΔF_t using the relative tangential incremental surface displacement $\Delta\delta_t$ and the new values of F_n and a. By reanalysing the loading cases

considered by Mindlin and Deresiewicz (1953), it was shown by Thornton and Yin (1991) that, for all cases, the tangential stiffness may be expressed in a general form as

$$K_t = \frac{\Delta F_t}{\Delta \delta_t} = 8G^* a\theta \pm \mu(1-\theta)\frac{\Delta F_n}{\Delta \delta_t} \tag{2.10}$$

in which,

$$\frac{1}{G^*} = \frac{2-\nu_1}{G_1} + \frac{2-\nu_2}{G_2} \tag{2.11}$$

and G_i (i=1, 2) are the shear moduli of two contacting spheres.

If the conditions of $\Delta F_n > 0$ and $|\Delta \delta_t| < \frac{\mu \Delta F_n}{8G^* a}$ are satisfied, then θ should be set to one in Eq. (2.10); otherwise, θ follows

$$\theta^3 = 1 - \frac{(F_t + \mu \Delta F_n)}{\mu F_n} \qquad \Delta \delta_t > 0 \text{ (loading)} \tag{2.12a}$$

$$\theta^3 = 1 - \frac{(F_t^* - F_t + 2\mu \Delta F_n)}{2\mu F_n} \qquad \Delta \delta_t < 0 \text{ (unloading)} \tag{2.12b}$$

$$\theta^3 = 1 - \frac{(F_t - F_t^{**} + 2\mu \Delta F_n)}{2\mu F_n} \qquad \Delta \delta_t > 0 \text{ (reloading)} \tag{2.12c}$$

The negative sign in (2.10) is only invoked during unloading. F_t^* and F_t^{**} define the load reversal points for the transitions from loading-to-unloading and unloading-to-reloading, respectively. They need to be continuously updated to allow for the effect of varying normal force as

$$F_t^* = F_t^* + \mu \Delta F_n \qquad \text{and} \qquad F_t^{**} = F_t^{**} - \mu \Delta F_n \tag{2.13}$$

2.4.2.2. Frictional elastic contact with adhesion

For the frictional elastic contact of auto-adhesive particles, according to JKR theory (Johnson et al., 1971), the radius of the contact area is obtained from

$$a^3 = \frac{3R^* F_{\mathrm{n}}^{\mathrm{H}}}{4E^*} \tag{2.14}$$

where $F_{\mathrm{n}}^{\mathrm{H}}$ is the effective Hertzian force that would produce the same contact area and is given by

$$F_{\mathrm{n}}^{\mathrm{H}} = F_{\mathrm{n}} + 2F_{\mathrm{c}} \pm \sqrt{4F_{\mathrm{n}}F_{\mathrm{c}} + 4F_{\mathrm{c}}^2} \tag{2.15}$$

in which F_{n} is the applied normal force and F_{c} , known as the 'pull-off' force, is the minimum tensile force required to break the contact defined by

$$F_{\mathrm{c}} = 3\pi\gamma R^* \tag{2.16}$$

where γ is the surface energy.

The applied normal force and the relative normal displacement are related to the contact radius according to Johnson (1985), i.e.

$$F_{\mathrm{n}} = \frac{4E^* a^3}{3R^*} - 4\left(\pi\gamma E^* a^3\right)^{1/2} \tag{2.17}$$

$$\delta_{\mathrm{n}} = \frac{a^2}{R^*} - 2\left(\frac{\pi\gamma a}{E^*}\right)^{1/2} \tag{2.18}$$

Differentiating both (2.17) and (2.18) with respect to a and then combining to obtain $\mathrm{d}F_{\mathrm{n}} / \mathrm{d}\delta_{\mathrm{n}}$ leads to the following expression for the normal contact stiffness

$$K_{\mathrm{n}} = 2E^* a\left(\frac{3\sqrt{F_{\mathrm{n}}^{\mathrm{H}}} - 3\sqrt{F_{\mathrm{c}}}}{3\sqrt{F_{\mathrm{n}}^{\mathrm{H}}} - \sqrt{F_{\mathrm{c}}}}\right) \tag{2.19}$$

Following Savkoor and Briggs (1977), it was assumed by Thornton (1991) that, on initial application of a tangential force F_t, a peeling mechanism occurs resulting in a reduction of the contact area. During this peeling process, the contact radius is

$$a^3 = \frac{3R^*}{4E^*}\left(F_n + 2F_c \pm \sqrt{4F_nF_c + 4F_c^2 - \frac{F_t^2 E^*}{4G^*}} \right) \tag{2.20}$$

During the peeling process, Mindlin's (1949) no-slip solution applies and the tangential stiffness is

$$K_t = 8G^* a \tag{2.21}$$

The peeling process continues until the tangential force reaches a critical value of

$$F_t^{peel} = 4\sqrt{\frac{G^*}{E^*}\left(F_nF_c + F_c^2 \right)} \tag{2.22}$$

and then the contact radius reduces to

$$a^3 = \frac{3R^*}{4E^*}\left(F_n + 2F_c \right) \tag{2.23}$$

Thornton (1991) argued that peeling must occur before sliding, followed by a smooth transition to sliding. If at the end of the peeling process the critical tangential force F_t^{peel} given by (2.22) is less than the sliding force, a subsequent slip annulus is assumed to spread radially inwards and the micro-slip solution of Mindlin and Deresiewicz (1953) is applied until sliding occurs. The equations used in this case are (2.10) to (2.13) with substitution of $F_n + 2F_c$ for F_n. If the tangential force at the end of the peeling process is greater than the sliding force, the tangential force immediately falls to the sliding force.

Two sliding criteria are used to determine the tangential force F_t^{slide} when sliding occurs. For tensile normal loads when $F_n < -0.3F_c$,

$$F_t^{slide} = \mu F_n^H \left(1 - \frac{F_n^H - F_n}{3F_n^H}\right)^{3/2} \tag{2.24}$$

with F_n^H given by (2.15). If $F_n \geq -0.3F_c$, then

$$F_t^{slide} = \mu\left(F_n + 2F_c\right) \tag{2.25}$$

2.4.2.3. Damping

Contact damping is adopted to consider the energy dissipation due to the elastic wave propagation through a solid particle. This damping can be envisaged as the effect of dashpots that connect two particles in contact both in the normal and tangential directions. Thus, the damping forces are proportional to the relative velocities of two particles. The normal damping force F_{nd} and tangential damping force F_{td} are given by

$$F_{nd} = 2\beta\sqrt{m^* K_n}\,\Delta\delta_n / \Delta t \quad \text{and} \quad F_{td} = 2\beta\sqrt{m^* K_t}\,\Delta\delta_t / \Delta t \tag{2.26}$$

where

$$\frac{1}{m^*} = \frac{1}{m_1} + \frac{1}{m_2} \tag{2.27}$$

and m_1 and m_2 are the masses of two particles and β is the damping coefficient. The damping forces are added to the normal and tangential contact forces to provide the contribution to the out-of-balance forces acting on the particles from that contact. The damping coefficient β is specified in the range 0.05-0.1 to give a normal coefficient of restitution of about 0.98. The tangential damping force vanishes during sliding. It should be noted that, in agreement with the original Cundall and Strack (1979) concept, the damping forces are not part of the contact forces.

2.4.3. Fluid-particle interaction

Following the local average approach of Anderson and Jackson (1967), the force exerted by the fluid on each particle $\mathbf{F}_{\mathrm{fp}i}$ can be written as the sum of a component due to macroscopic variations in the fluid tensor, $\boldsymbol{\xi}_{\mathrm{f}}$, and a component, $\mathbf{F}'_{\mathrm{fp}i}$, due to detailed variations of the point stress tensor as the fluid flows around a particle:

$$\mathbf{F}_{\mathrm{fp}i} = V_{\mathrm{p}i}\nabla\cdot\boldsymbol{\xi}_{\mathrm{f}} + \mathbf{F}'_{\mathrm{fp}i} \tag{2.28}$$

in which $V_{\mathrm{p}i}$ is the volume of the particle i. The local average stress tensor in the fluid may be written as

$$\boldsymbol{\xi}_{\mathrm{f}} = -p\boldsymbol{\delta} + \boldsymbol{\tau}_{\mathrm{f}} \tag{2.29}$$

where p is the fluid pressure, $\boldsymbol{\delta}$ is the identity tensor and $\boldsymbol{\tau}_{\mathrm{f}}$ is the viscous stress or deviatoric stress tensor. The second term on the right of (2.28) includes skin friction and drag contributions comprising (i) an effective drag force in the direction of the relative velocity between the fluid and the particle and (ii) a virtual or added mass force accounting for the resistance of the fluid mass that is moving at the same acceleration as the particle. For gas-solid systems, the virtual mass can be neglected due to the very low density of gas compared to the solid and then $\mathbf{F}'_{\mathrm{fp}i}$ reduces to the effective drag force which, according to Anderson and Jackson (1967), is the drag force $\mathbf{F}_{\mathrm{d}i}$ obtained from the product of experimentally based correlations and the local void fraction ε. Consequently, substituting (2.29) into (2.28) and writing $\mathbf{F}'_{\mathrm{fp}i}$ in terms of $\mathbf{F}_{\mathrm{d}i}$ leads to the following expression for the fluid-particle interaction force

$$\mathbf{F}_{\mathrm{fp}i} = -V_{\mathrm{p}i}\nabla p + V_{\mathrm{p}i}\nabla\cdot\boldsymbol{\tau}_{\mathrm{f}} + \varepsilon\mathbf{F}_{\mathrm{d}i} \tag{2.30}$$

Assuming a Newtonian fluid with a viscous stress tensor, $\boldsymbol{\tau}_{\mathrm{f}}$, dependent only on the fluid motion, following Bird et al (1960), a general constitutive equation may be written as

$$\boldsymbol{\tau}_{\mathrm{f}} = \left[\left(\mu_{\mathrm{b}} - \tfrac{2}{3}\mu_{\mathrm{s}}\right)\nabla\cdot\mathbf{u}\right]\boldsymbol{\delta} + \mu_{\mathrm{s}}\left[\left(\nabla\mathbf{u}\right) + \left(\nabla\mathbf{u}\right)^{-1}\right] \tag{2.31}$$

where $\mathbf{u}$ is the fluid velocity; μ_{b} and μ_{s} are the bulk viscosity and shear viscosity, respectively, of the fluid.

The drag force $\mathbf{F}_{\mathrm{d}i}$ is calculated using the following empirical correlation of Di Felice (1994) which provides a continuous variation of drag force over the full practical range of flow regimes and particle porosities (i.e., void fractions):

$$\mathbf{F}_{\mathrm{d}i} = \tfrac{1}{2} C_{\mathrm{D}i}\rho_{\mathrm{f}}\frac{\pi d_{\mathrm{p}i}^2}{4}\varepsilon_j^2\left|\mathbf{u}_j - \mathbf{v}_i\right|\left(\mathbf{u}_j - \mathbf{v}_i\right)\varepsilon_j^{-(\chi+1)} \tag{2.32}$$

where ρ_{f}, $\mathbf{u}_j$ and ε_j are the fluid density, fluid velocity and the porosity of the computational fluid cell j in which particle i resides. $d_{\mathrm{p}i}$ is the diameter of particle i and $C_{\mathrm{D}i}$, the fluid drag coefficient for a single unhindered particle, is evaluated by

$$C_{\mathrm{D}i} = \left[0.63 + \frac{4.8}{\sqrt{Re_{\mathrm{p}i}}}\right]^2 \tag{2.33}$$

where the particle Reynolds number $Re_{\mathrm{p}i}$ is based on the superficial slip velocity between particle and fluid

$$Re_{\mathrm{p}i} = \frac{\rho_{\mathrm{f}} d_{\mathrm{p}i}\varepsilon_j\left|\mathbf{u}_j - \mathbf{v}_i\right|}{\mu_{\mathrm{s}}} \tag{2.34}$$

The porosity function $\varepsilon_j^{-(\chi+1)}$ in (2.32) corrects for the presence of other particles, and a dependence of this function on the flow was incorporated in the relation for χ

$$\chi = 3.7 - 0.65 \exp\left[-\frac{\left(1.5 - \log_{10} Re_{pi}\right)^2}{2} \right] \tag{2.35}$$

to take account of the variation of the exponent in the intermediate flow regimes as well as the near-constant values in the low and high Reynolds number flow regimes.

2.4.4. Equations for fluid flow

The continuity and momentum equations of the fluid are proposed by Anderson and Jackson (1967) in terms of local mean variables:

$$\frac{\partial \left(\varepsilon \rho_{\mathrm{f}}\right)}{\partial t} + \nabla \cdot \left(\varepsilon \rho_{\mathrm{f}} \mathbf{u}\right) = 0 \tag{2.36}$$

$$\frac{\partial \left(\varepsilon \rho_{\mathrm{f}} \mathbf{u}\right)}{\partial t} + \nabla \cdot \left(\varepsilon \rho_{\mathrm{f}} \mathbf{u}\mathbf{u}\right) = -\nabla p + \nabla \cdot \boldsymbol{\tau}_{\mathrm{f}} - \mathbf{F}_{\mathrm{fp}}^{*} + \varepsilon \rho_{\mathrm{f}} \mathbf{g} \tag{2.37}$$

in which the fluid-particle interaction force per unit volume, $\mathbf{F}_{\mathrm{fp}}^{*}$, is obtained by summing up the fluid-particle interaction forces $\mathbf{F}_{\mathrm{fp}i}$, Eq. (2.30), acting on all the particles in a fluid cell, n_{c}, and dividing by the volume of the fluid cell ΔV_{c}, thus

$$\mathbf{F}_{\mathrm{fp}}^{*} = \frac{\sum_{i=1}^{n_c} \mathbf{F}_{\mathrm{fp}i}}{\Delta V_{\mathrm{c}}} \tag{2.38}$$

In all the simulations reported in this thesis, only the air-solid particle systems are considered. Therefore, the ideal gas law is adopted to calculate the density of fluid (air):

$$\rho_{\mathrm{f}} = \frac{M_{\mathrm{f}}}{RT^{*}} p \tag{2.39}$$

where M_{f} is the average molar mass of air (0.0288 kg mol^{-1}), R is the ideal gas constant (8.314472 J K^{-1} mol^{-1}) and T^{*} is the temperature of air.

2.4.5. Determination of time step

As discussed above, during its movement, a particle may collide with neighbouring particles and interact with the surrounding fluid via momentum and energy exchanges. However, the particle movement is also affected by particles and fluid far beyond its local neighbourhood through the propagation of disturbance waves. This problem is solved by selecting a suitably small value for the time step such that, during a single time step, a disturbance can only propagate from a particle to other particles in contact with it and the local fluid cell. In the DEM model used in this study, it is assumed that all of the energy is transferred by Rayleigh waves. For an assembly of particles, the highest frequency of Rayleigh wave propagation is determined by the smallest particles, leading to a critical time step for the discrete particle model given by

$$\Delta t_{\mathrm{c}} = \frac{\pi d_{\mathrm{p}}^{\min}}{2\lambda}\sqrt{\frac{\rho_{\mathrm{s}}}{G}} \tag{2.40}$$

where

$$\lambda = 0.1631\nu + 0.8766 \tag{2.41}$$

$d_{\mathrm{p}}^{\min}$ is the minimum particle diameter in the assembly of particles of solid density ρ_{s}, G and ν are the shear modulus and Poisson's ratio, respectively, of the particle.

The maximum allowable time step in the numerical scheme for the fluid-phase equation is determined by the Courant condition and the viscosity stability criterion. As demonstrated by Kafui et al. (2002), the critical time step determined from the discrete particle scheme is generally much smaller than the maximum time step

determined from the fluid hydrodynamics scheme using the CFL criterion (MacCormarck, 1971). Therefore, a fraction of the critical time step determined from the discrete particle scheme, given by Eq. (2.40), is used as the time step in our coupled DEM/CFD simulations.

CHAPTER 3: POWDER FLOW DURING DIE FILLING

3.1. Introduction

In this chapter, the coupled DEM/CFD method, as discussed in Section 2.4, is used to simulate the die filling processes in a vacuum and in air, and the effect of air on powder flow behaviour during die filling is examined. The influences of powder characteristics (particle size, density and size distribution) are also investigated. Since most real powders, in particular, pharmaceutical powders, are more or less cohesive, simulations using cohesive powders are then performed to explore the influence of cohesion. Some of the results presented in this chapter have also been published in Guo et al. (2007; 2009b).

3.2. Computational set-up

All simulations presented in this chapter were performed in two dimensions. However, the void fraction is calculated by treating the powder bed as a monolayer of spheres with the average diameter as the thickness of the powder bed (Kafui et al., 2002). Schematics of die filling from a stationary shoe and a moving shoe are shown in Figures 3.1a and 3.1b, respectively. The simulated die filling system is composed of a top container, which is generally referred to as a shoe, and a bottom container which is the die. For die filling from a stationary shoe (Figure 3.1a), a shutter is set at the top of the die to hold the powder before die filling. Initially, a specified number of particles were randomly generated in the shoe, then deposited under gravity in the absence of air until they settled to a steady state with negligible kinetic energy, i.e.,

when the mean particle velocity is of the order of 10^{-6} m/s or smaller. The powder bed is then colour-banded so that the macroscopic flow patterns can be visualised. For die filling from a stationary shoe, the filling process is started by suddenly removing the shutter so that the powder starts to flow into the die under the influence of gravity. For die filling from a moving shoe (Figure 3.1b), the powder is delivered into the die when the shoe translates over the die opening from the right hand side to the left hand side at a constant velocity.

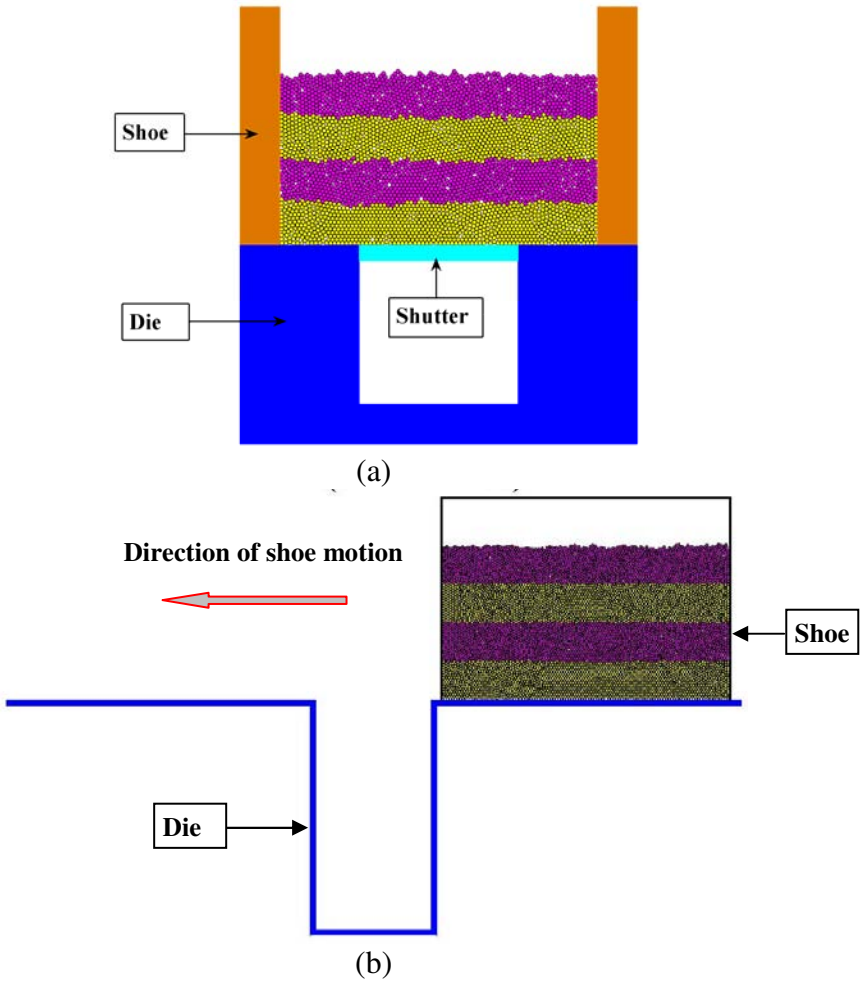

Figure 3.1 The numerical models for die filling from (a) a stationary shoe and (b) a moving shoe.

To consider the effect of air on the powder flow, air initially fills the void space in the shoe and die regions at uniform pressure (no pressure gradients). The computational

fluid cells and boundary conditions for the die filling from a stationary shoe and a moving shoe are schematically shown in Figures 3.2a and 3.2b, respectively. The computational domain for the gas phase (i.e., air) is uniformly discretised with interior fluid cells (1), the solid boundaries are treated as impermeable with no slip boundaries (3) for air flow, and the top of the shoe is modelled using continuous gas outflow wall cells with free slip boundaries (6). All quantities such as air pressure and air velocity are averaged in the fluid cells, and the void fraction of each cell is defined by the total volume of particles inside the cell. As argued by Tsuji et al. (1993), the size of the fluid cells should be smaller than the macroscopic motion of bubbles (to simulate the evolution of bubbles and the detailed fluid flow inside the bubbles) but larger than the particle size (to avoid zero void fractions). As typically adopted in simulations of fluidized beds (Tsuji et al., 1993), the size of the fluid cells is set in the range of 3-5 times the average particle diameter in this study. Initially, air with standard atmospheric pressure (1.01325×10^5 Pa) and a viscosity of 1.8E-5 kg $m^{-1}s^{-1}$ was uniformly distributed in the void space and was assumed to be static. Once the particles start to move, the air flows accordingly. The temperature of air is fixed at 293 K during the die filling process. It should be noted that for die filling from a moving shoe, only the interaction between the air and particles is considered. The interaction of the air with the walls of the moving shoe is neglected. This assumption is believed to be reasonable since the powder flow is mainly affected by the entrapped air in the die region (Wu and Cocks, 2004, 2006; Wu et al., 2003b, 2003c).

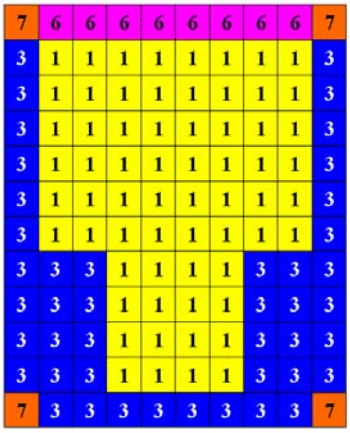

(a)

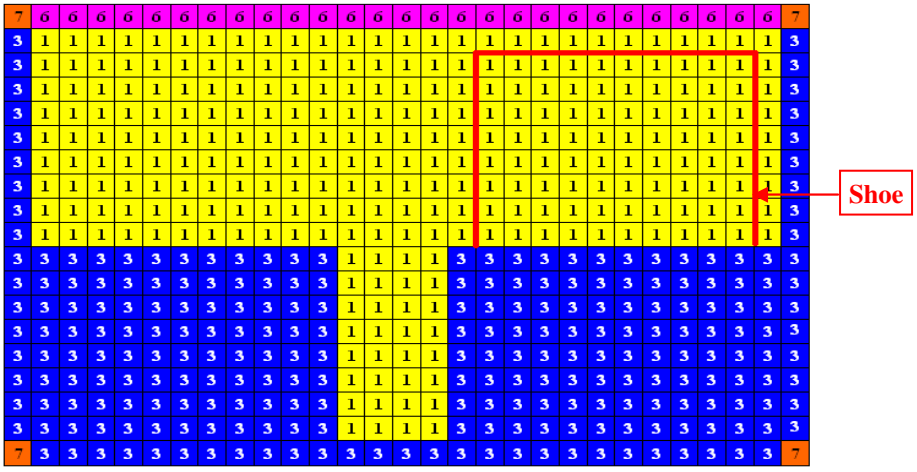

(b)

Figure 3.2 Schematic diagrams of the computational fluid cells and boundary conditions for die filling from (a) a stationary shoe and (b) a moving shoe. [1: interior fluid cell; 3: impermeable wall, no slip boundaries; 6: continuous gas outflow wall cell, free slip; 7: corner cell.]

In this study, except when stated otherwise, the particles are assumed to be elastic with a Young's modulus of 8.7GPa and Poisson's ratio of 0.3, which corresponds to the material properties of microcrystalline cellulose, a commonly-encountered pharmaceutical material. The solid walls are assumed to be steel with Young's modulus of 210 GPa, Poisson's ratio of 0.29 and density of 7800 kg/m^3. The interparticle and particle-wall friction coefficients are set to a value of 0.3.

Table 3.1 Simulation groups for die filling from a stationary shoe

	Die size (Width×Depth)	Particle diameter d_p (μm)	Solid density ρ_s (kg/m^3)	Void fraction ε
Group 1	2×2 mm	25	1500	0.448
		40		0.450
		50		0.447
		60		0.449
	7×7 mm	90	1500	0.447
		130		0.450
		180		0.449
		260		0.453
		340		0.447
		430		0.457
Group 2	7×7 mm	130	400	0.447
			700	0.451
			1500	0.450
			2500	0.449
			3500	0.448
			5500	0.449
			7800	0.450
Group 3	18×18 mm	500	1500	0.448
		600		0.447
		700		0.448
		800		0.448
		900		0.449
Group 4	7×7 mm	340	3000	0.447
			5000	0.448
			7000	0.447

For die filling from a stationary shoe, dies with a square shape are used and the width of the shoe is set as twice that of the die. Four groups of simulations with monodispersed powders have been performed to investigate the effects of particle size and density, as shown in Table 3.1. In Group 1, the solid particle density ρ_s is fixed at a value of 1500 kg/m^3, and different particle sizes d_p are used to investigate the effect of particle size. In Group 2, the particle size is fixed at 130 μm and different solid densities are used to investigate the effect of particle density. In Group 3, powders with particle sizes equal to or larger than 500 μm are used and a larger die is used to maintain the ratio of particle size to the width of die opening. In Group 4, powders with a relatively large particle size of 340 μm and higher solid densities are used.

Groups 3 and 4 are special cases with larger particle sizes and densities, for which the influence of air on the flow behaviour is expected to be negligible. After initial deposition, all the powder beds considered have similar void fractions in the range of 0.447- 0.457. In order to investigate the influences of particle size distribution and surface energy for cohesive powders, simulations with polydisperse and cohesive powders were also performed. The details are presented in Sections 3.3.3 and 3.3.4.

Table 3.2 Three cases for die filling from a moving shoe

	Die size (Width×Depth)	**Particle diameter d_p (μm)**	**Solid density ρ_s (kg/m^3)**	**Void fraction ε**
Case 1	4×8 mm	90	1500	0.450
Case 2	4×8 mm	340	3000	0.453
Case 3	4×16 mm	340	3000	0.452

For die filling from a moving shoe, a shallow die of width 4mm and depth 8 mm and a deep die of width 4mm and depth 16 mm are used and the width of the shoe is fixed as 10 mm. Three cases with monodisperse powders are considered, as shown in Table 3.2. In Case 1, a powder of particle diameter 90 μm and particle density 1500 kg/m^3 is used. In Case 2, a powder consisting of larger and heavier particles of diameter 340 μm and density 3000 kg/m^3 is used. The shallow die is used in both Cases 1 and 2. In Case 3, the large and heavy particles with the same particle properties as used in Case 2 are employed and the deep die is adopted to investigate the effect of die size.

3.3. Die filling from a stationary shoe

Die filling from a stationary shoe, which might be the simplest filling process, was studied first. Powders of various properties were used in the simulations.

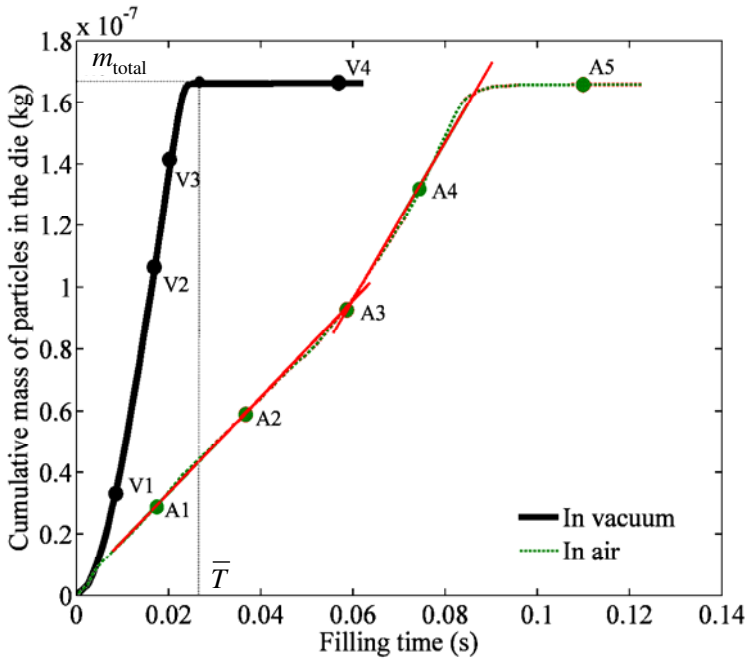

Figure 3.3 The variation of the mass of particles deposited into the die with filling time for die filling in a vacuum and in air. (Die size: 2 mm×2 mm)

3.3.1. Die filling in air and in a vacuum

In order to compare the flow behaviour of powder during die filling in air and in a vacuum, simulations with a monodispersed powder composed of particles of diameter 50μm and density 1500kg/m^3 were performed. Figure 3.3 shows the time history of the mass of particles fed into the die for die filling in a vacuum and in air. It is found that for die filling in a vacuum the flow of powder into a die is accelerated from the initial static state. A relatively low mass flow rate is observed at the very early stage of the process immediately after the shutter is removed (say $t < 0.005$ s). The flow rate increases very sharply thereafter and remains constant during most of the filling process until the die is almost completely filled when a deceleration stage is then observed. For die filling in air, it is also observed that there is an acceleration stage at the beginning of die filling and a deceleration stage when the die is almost completely

filled. However, the powder flow process in air can be divided into two distinct regimes: a slow flow regime at the early stage of die filling up to the instant A3 (as labelled in Figure 3.3) and a fast flow regime thereafter. It is evident that the die is filled much more slowly in air than in a vacuum. This is due to the counter-flow of the air against the direction of the powder flow. In order to explore the mass flow behaviour presented in Figure 3.3, a detailed examination of the flow patterns of powder and air was carried out and the results are presented in Figures 3.4 – 3.8, in which typical features at various instants labelled in Figure 3.3 are shown.

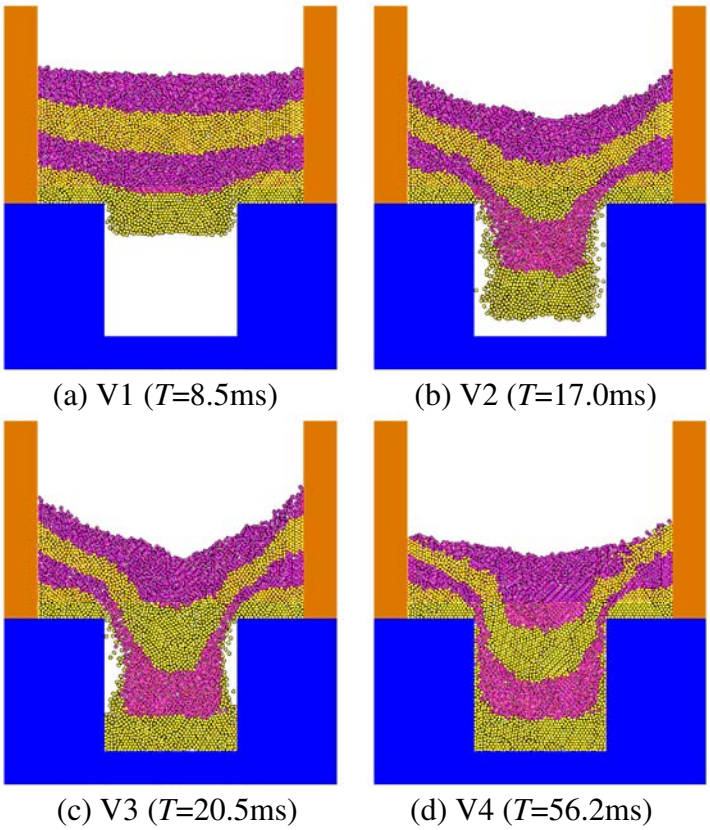

Figure 3.4 Powder flow behaviour during die filling in a vacuum.

Figure 3.4 shows the powder flow patterns for die filling in a vacuum. It can be seen that the powder flows into the die smoothly and quickly with two narrow regions of retarded flow adjacent to the edge of the die opening, forming two narrow empty

regions close to the die walls. This pattern is consistent with the experimental observation of powder discharge from a bin and is generally referred to as the 'empty annulus' (Seville et al., 1997).

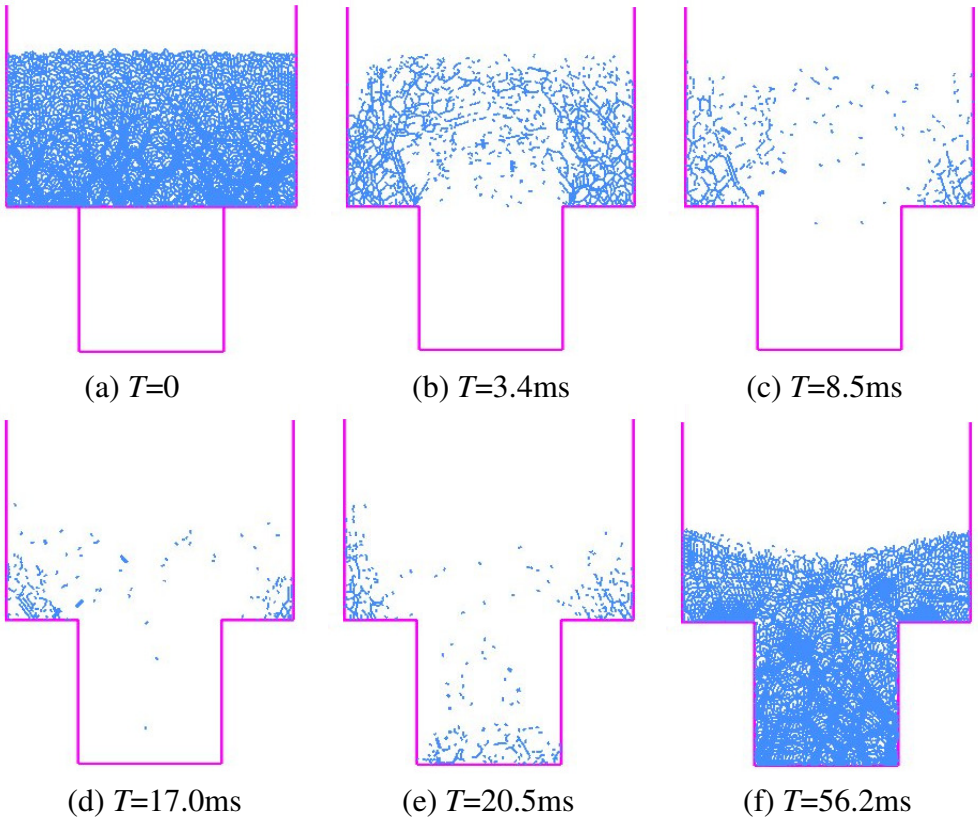

(a) T=0 (b) T=3.4ms (c) T=8.5ms

(d) T=17.0ms (e) T=20.5ms (f) T=56.2ms

Figure 3.5 Contact force distributions during die filling in a vacuum.

The contact force distributions for the powder at various instants are shown in Figure 3.5, in which the lines are drawn passing through the contact points in the direction of the forces, with the thickness of the lines indicating the magnitude of the local contact force relative to the current maximum contact force. It is observed that as the powder flow into the die commences, the contact forces disappear quickly from the bottom of the powder bed over the die opening (Figures 3.5b-e). This absence of any significant number of inter-particle contact forces persists until the die is almost completely filled whereupon a dense enduring contact force network is formed (Figure 3.5f).

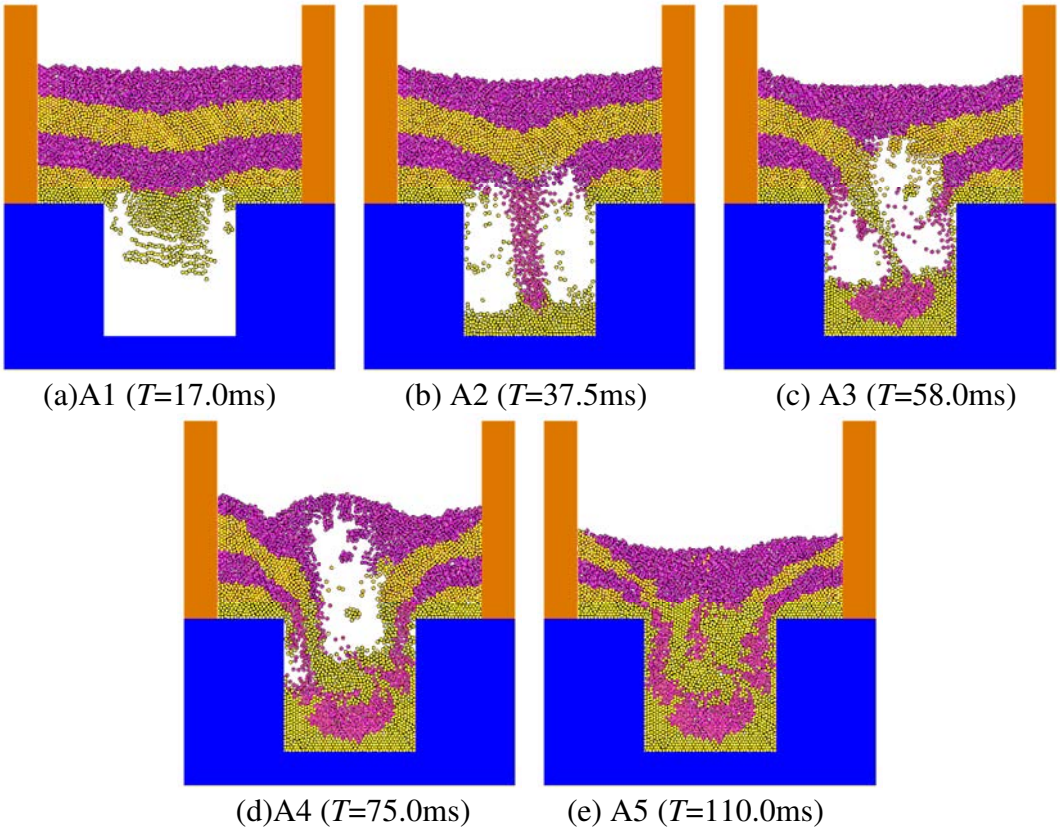

Figure 3.6 Powder flow behaviour during die filling in air.

The powder flow behaviour during die filling in air is shown in Figure 3.6, and the corresponding contact force distributions and air velocity and pressure distributions are given in Figures 3.7 and 3.8, respectively. In Figure 3.8, the length of the vectors represents the relative magnitude of the local air velocity scaled to the maximum air velocity during the whole die filling process. It can be seen that due to the presence of air in the die, the powder initially flows into the die very slowly and mainly from the centre of the die opening (Figures 3.6a, b). Thus, two air bubbles are formed next to the die walls and separated by the flowing powder at the centre (Figure 3.6b). The contact force network above the die opening persists over an extended period of time compared to that in a vacuum (Figures 3.7a-c). The air is initially dragged by the flowing powder to flow downwards at the centre of the die. Due to the restriction of

the die boundaries, the air flows sideways at the bottom and then turns upwards (Figure 3.8a). As shown in Figure 3.8b, the air flows upwards at a higher velocity in the centres of the bubbles, and it is also observed that the air, dragged by downward flowing clusters of particles along the die walls (Figure 3.6b), flows downwards near the die walls.

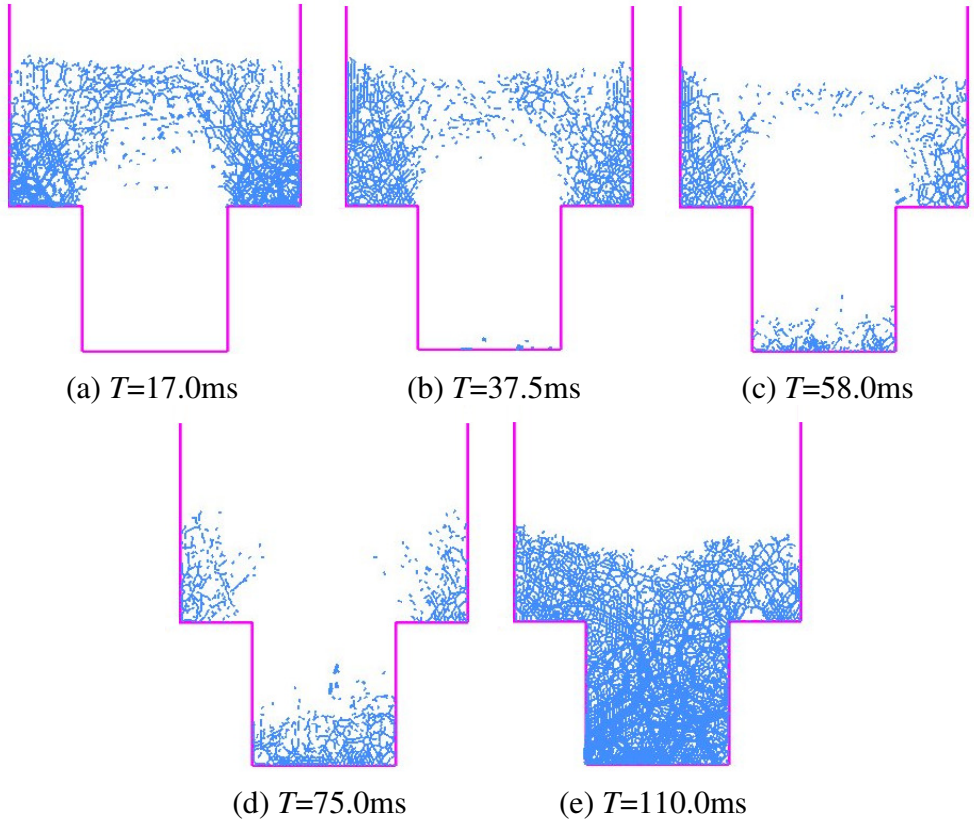

Figure 3.7 Contact force distributions during die filling in air.

As the powder flows into the die, the volume of the free space occupied by air decreases and, therefore, the overall pressure of the entrapped air increases (Figures 3.8a, b). The pressure distribution with a striped pattern is observed in Figure 3.8b. This striped pattern is formed as a result of the air being compressed by the main powder stream flowing in the centre and clusters of particles falling close to the die walls. Consequently, low pressure bands are created along the flow paths of the main

powder stream and the clusters of particles and high pressure bands are induced in between. The filling process hence becomes much less steady and the entrapped air bubbles hinder and disturb the powder flow, which induces a slow powder flow as observed in Figure 3.3.

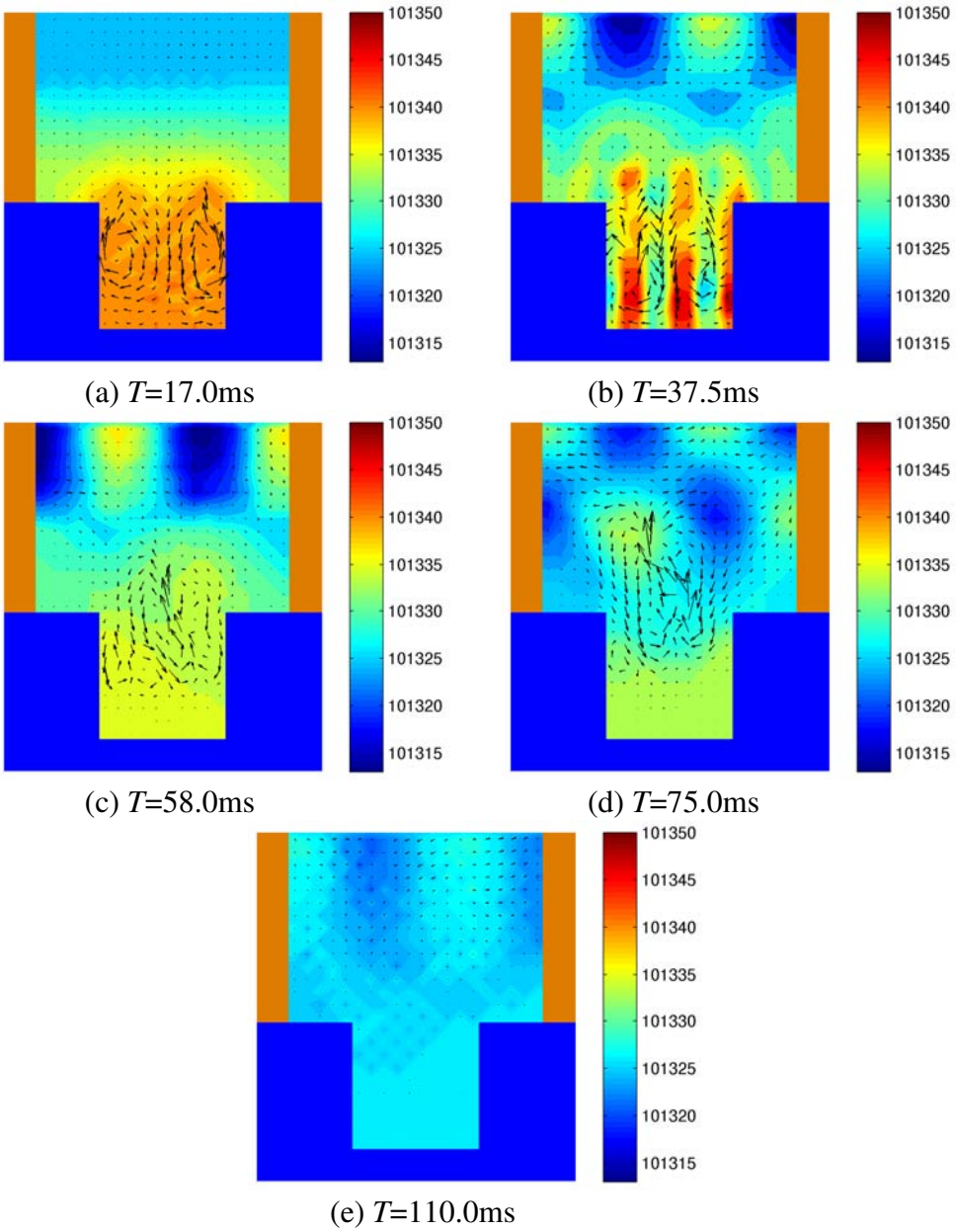

(a) T=17.0ms (b) T=37.5ms

(c) T=58.0ms (d) T=75.0ms

(e) T=110.0ms

Figure 3.8 Air velocity and pressure distributions during die filling in air.

As more powder flows into the die, the bubbles rise. One of them gradually shrinks and disappears, whilst the other one grows and continues to rise until it erupts at the

top surface of the powder bed (Figures 3.6c, d). It is interesting to note that once the centre of the larger entrapped bubble reaches the top of the die (Figure 3.6c), the powder flows easily into the die from the sides of the larger bubble. As a result, the mass flow rate is increased after the instant A3 shown in Figure 3.3. With the larger bubble moving out of the die, the contact force network above the die opening gradually disappears (Figures 3.7c, d). As the air permeates through the expanded loose powder layers above the die opening, the air pressure inside the bubbles decreases (Figures 3.8c, d). The strong interaction between the powder and the entrapped air leads to a significant mixing of particles when they are deposited into the die (Figure 3.6e). Once the die filling process is completed, an enduring contact force network is re-established (Figure 3.7e). Simultaneously, the air velocity decelerates to zero and the air pressure in the pores of the deposited powder reverts to atmosphere pressure (Figure 3.8e).

3.3.2. Mass flow rate

3.3.2.1. Theoretical aspects

In order to quantify the powder flow during die filling, an average mass flow rate $\overline{M}$ is defined as

$$\overline{M} = \frac{m_{\text{total}}}{\overline{T}} \tag{3.1}$$

in which m_{total} is the total mass of particles deposited into the die, $\overline{T}$ is the duration of die filling and is the time when the deposition of powder into the die is just completed (see Figure 3.3). For the die filling cases considered in Figure 3.3, the

average mass flow rate in air ($\overline{M} = 1.71\times10^{-6}$ kg/s) is much lower than that in a vacuum ($\overline{M} = 6.51\times10^{-6}$ kg/s).

The process of powder flow from a stationary shoe is somewhat analogous to hopper flow and the flow of a powder from a bin, for which Beverloo et al. (1961) proposed a well-known empirical equation for the solid discharge rate from a circular orifice in the form:

$$M = C\rho_b g^{1/2} D_0^{5/2}\left(1 - k\frac{d_p}{D_0}\right)^{5/2} \tag{3.2}$$

in which M is the mass flow rate, C is a dimensionless constant, ρ_b is the bulk density of the powder, g is the acceleration due to gravity, D_0 is the diameter of the circular orifice, d_p is the mean particle diameter, k is a constant that is found to depend only on the particle shape and has a value of about 1.5 for spherical particles (Seville et al., 1997). Note that $\left[1 - k\left(d_p/D_0\right)\right]$ is a correction for the orifice size due to the presence of an 'empty annulus', which is a region of retarded flow adjacent to the orifice edge (see also Figure 3.4).

Theoretical models have also been proposed to predict the discharge rates of granular materials from storage bins or hoppers. Many of these models are based on the concept of the 'free-fall arch', which is an arch located at the lower boundary surface of the powder bed. Above the free-fall arch, particles are in contact with each other. Below the arch, particles are no longer in contact and freely accelerate under gravity. Based upon experimental observations, Harmens (1963) assumed that the powder flow from a container is independent of the bed depth, H, and the shape of the free-

fall arch is independent of the scale so that the arch height above the circular orifice is of the order of the diameter D_0. When the particles are accelerating freely under gravity after detaching from the arch, their velocities on passing through the orifice are of the order of $(gD_0)^{1/2}$. By considering the cross sectional area of the orifice $\pi D_0^2/4$, the flow rate is thus proportional to $g^{1/2}D_0^{5/2}$, which is the same dependence as in Eq. (3.2). If the thickness of the container is far smaller than the width of the orifice, the powder flow can be treated as a quasi-two-dimensional planar flow. The shape of the orifice is then a narrow rectangle of dimensions $b_0 \times l$, where b_0 is the width of the orifice and l is the thickness of the container. Under this condition, by a similar analysis to that above, the height of the free-fall arch is shown to be of the order b_0. Thus, the particle velocity passing through the orifice is of the order $(gb_0)^{1/2}$. Considering the sectional area $b_0 l$, the flow rate is proportional to $g^{1/2}lb_0^{3/2}$.

Brown and Richards (1965) developed a 'minimum energy theorem' to describe powder flow with a spherical free fall arch. They obtained a volumetric flow rate equation for the powder discharge from a circular orifice in the form:

$$M_V = \frac{\sqrt{2\pi}}{6} g^{1/2} D_0^{5/2} \left(1 - \cos^{3/2}\kappa\right) \Big/ \sin^{5/2}\kappa \qquad (3.3)$$

in which M_V represents volumetric flow rate and κ is the half-angle of the flowing zone. It can be seen that the flow rate is proportional to $g^{1/2}D_0^{5/2}$, which is consistent with the Beverloo equation (3.2) irrespective of the effect of the 'empty annulus'.

Based on this theory, a volumetric flow rate for planar flow can also be derived. As indicated by Brown and Richards (1965), the radial velocity in plane strain is given by

$$v_{\mathrm{r}} = \frac{g^{1/2} r_0^{3/2} \cos^{1/2}\theta}{r} \tag{3.4}$$

where r_0 is the radius of curvature of the free-fall arch, r and θ are the radial and angular coordinates, respectively, for a position in the flowing zone. Thus, the volumetric flow rate for planar flow can be written as

$$M_{\mathrm{V}} = 2\int_0^{\kappa} v_{\mathrm{r}}\, l\, r\, \mathrm{d}\theta = 2\,\mathrm{g}^{1/2} l\, r_0^{3/2} \int_0^{\kappa} \cos^{1/2}\theta\, \mathrm{d}\theta \tag{3.5}$$

where l is the thickness of the powder bed. Since the width of the orifice, $b_0 = 2r_0 \sin\kappa$,

$$M_{\mathrm{V}} = \frac{\sqrt{2}}{2} \mathrm{g}^{1/2} l\, b_0^{3/2} \frac{\int_0^{\kappa} \cos^{1/2}\theta\, \mathrm{d}\theta}{\sin^{3/2}\kappa} \tag{3.6}$$

Davidson and Nedderman (1973) proposed a mass flow rate equation for quasi-two-dimensional hopper flow as

$$M = \frac{\rho_{\mathrm{b}} \mathrm{g}^{1/2} l b_0^{3/2}}{\sin^{1/2}\kappa_{\mathrm{h}}} \left[\frac{1+K}{2(K\text{-}2)}\right]^{1/2} \tag{3.7}$$

in which b_0 is the orifice width, l is the hopper thickness, κ_{h} is the hopper half-angle, K is a function of the internal friction angle and is in the range of 2.5-7.5 for commonly encountered materials (Seville et al., 1997).

3.3.2.2. Dimensional analysis

The analyses in Section 3.3.2.1 independently demonstrate that the flow rate is proportional to $g^{1/2} l b_0^{3/2}$ for the quasi-two-dimensional planar flow. Hence, a dimensionless flow rate M^* is proposed as

$$M^* = \frac{\overline{M}}{\rho_b g^{1/2} l b_0^{3/2} \left(1 - k\frac{d_p}{b_0}\right)^{3/2}} \tag{3.8}$$

where $\overline{M}$ is the average mass flow rate defined in Eq. (3.1). In Eq. (3.8), the presence of the retarded flow region adjacent to the orifice edge (empty annulus) is also considered, so $\left[1 - k\left(d_p/b_0\right)\right]$ is a correction for the die opening size. Schneider et al. (2005) indicated that under conditions where core flow occurs in a vacuum, M^* depends only on particle-particle and particle-wall frictions for a given shape of orifice, i.e.,

$$M^* = f(\mu_p, \mu_{pw}) \tag{3.9}$$

where μ_p is the friction coefficient between particles, and μ_{pw} is the friction coefficient between a particle and a wall. For given materials (with load-independent friction coefficients) therefore, M^* is expected to be constant.

As the powder flows into a die in the presence of air, a negative pressure gradient is created that opposes the powder flow. The built-up air pressure in the closed die enhances this negative pressure gradient to further slow down the powder flow, as demonstrated in Figures 3.6-3.8. By decreasing the void fraction ε, the permeability of the bulk material is decreased, so that it is more difficult for the entrapped air to escape and the powder flow is hindered further. The drag force exerted by the air on the particles is proportional to the square of the superficial relative velocity v_r (relative velocity between the air and the particle), which is related to the width of die opening b_0, because both the air and particle velocities are functions of position which is scaled by b_0. The air drag also depends on the particle size d_p and air

viscosity η. In addition, by increasing the solid density ρ_s, the ratio of the drag force to the inertia of particles is decreased so that the impact of air on particles is decreased. In summary, during die filling in the presence of air, the dimensional flow rate M^* can be influenced by a number of additional factors, including the particle size d_p (and shape), solid density ρ_s, air viscosity η, width of the die opening b_0, and void fraction ε.

Following Schneider et al. (2005), taking the bulk density $\rho_b = (1-\varepsilon)\rho_s$, g and b_0 as the independent variables, the following two dimensionless groups are introduced

$$\eta^* = \frac{\eta}{\rho_b g^{1/2} b_0^{3/2}} \tag{3.10}$$

and

$$d_p^* = \frac{d_p}{b_0} \tag{3.11}$$

The dimensionless flow rate during die filling in air can then be written as

$$M^* = f(\eta^*, d_p^*, \varepsilon, \mu_p, \mu_{pw}, \text{particle shape}) \tag{3.12}$$

To a first approximation, the relationship between M^* and η^*, d_p^* is assumed to be a power law in the form of

$$M^* = A\left(\eta^*\right)^{-m}\left(d_p^*\right)^n \tag{3.13}$$

where A, m and n are dimensionless parameters depending on void fraction ε, friction coefficients μ_p and μ_{pw}, and particle shape. These parameters can be determined by fitting the power law relationship to the data over a range of values of η^* and d_p^*.

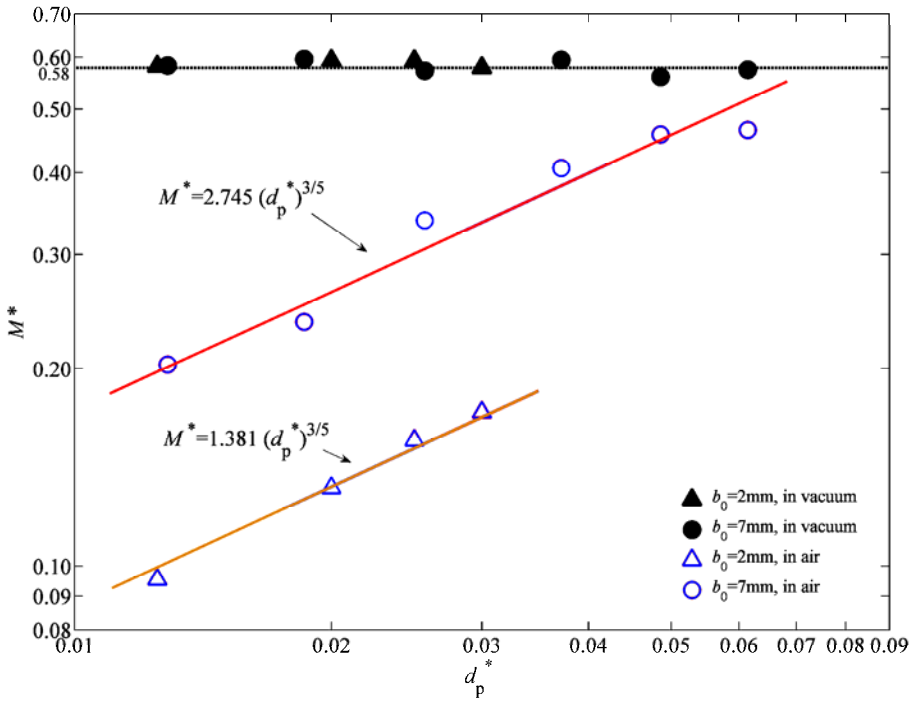

Figure 3.9 M^* versus d_p^* for die filling in a vacuum and in air

For die filling using monodisperse systems with a constant particle density and varying particle size (Group 1 in Table 3.1) the dimensionless flow rate M^* is plotted as a function of d_p^* in Figure 3.9. It can be seen that for die filling in a vacuum, the dimensionless flow rate M^* is essentially constant with an average value of 0.58. This is in excellent agreement with the Beverloo constant C determined experimentally (Seville et al., 1997), which is reported to be in the range 0.55-0.65. For die filling in air, M^* increases with increasing size ratio d_p^* for a given die opening size b_0. This can be explained as follows. The air drag force on each particle is proportional to $C_D d_p^2$, where C_D is the particle drag coefficient, and the gravity force on the particle is proportional to d_p^3, so the ratio of drag force to gravity is proportional to $C_D\left(1/d_p\right)$. Considering that C_D decreases with increasing particle size

d_p, the air drag effect becomes less significant as the particle size increases. As a result, the mass flow rate becomes higher with larger particles due to the reduced effect of air drag. It is interesting to note in Figure 3.9 that, on a log-log plot, the M^* versus d_p^* curves for different die opening sizes are essentially straight lines and parallel to each other. The best fit curves reveal that M^* is proportional to $(d_p^*)^{3/5}$, i.e.

$$M^* = \xi \left(d_p^* \right)^{3/5} \tag{3.14}$$

where ξ is a parameter depending upon the particle density and the die opening size.

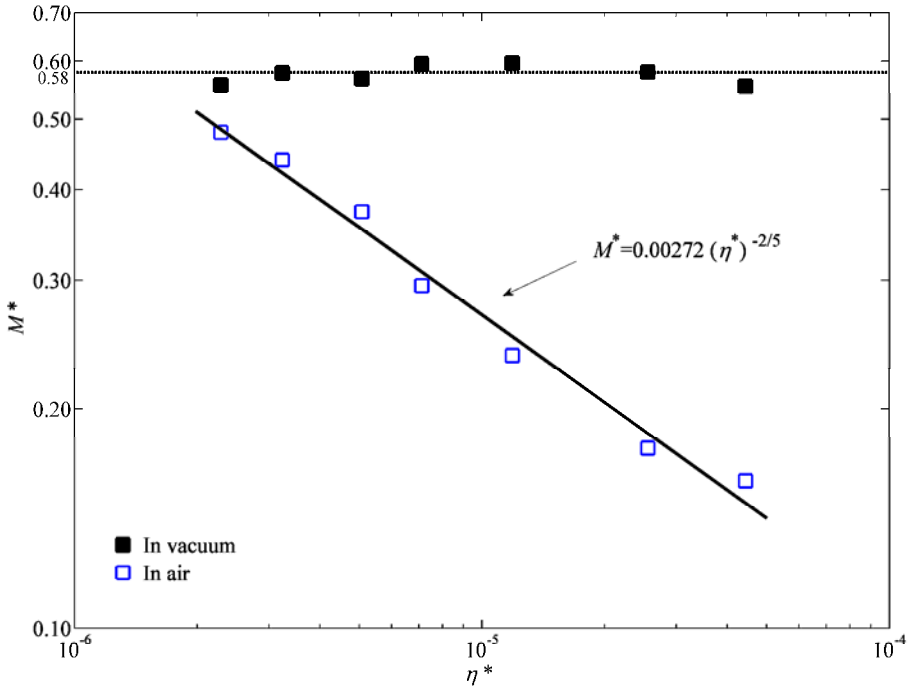

Figure 3.10 M^* versus η^* for die filling in a vacuum and in air.

From the results of the simulations using the parameters given for Group 2 in Table 3.1, M^* is plotted against η^* in Figure 3.10. It is clear that, for die filling in a vacuum, M^* is again constant at a value of 0.58. For die filling in air, M^* decreases as η^* increases. The relationship between M^* and η^* can be approximated as

$$M^* = 0.00272\left(\eta^*\right)^{-2/5} \tag{3.15}$$

From Eqs. (3.10) and (3.15) with $\rho_b = (1-\varepsilon)\rho_s$, we obtain

$$M^* \propto \rho_s^{2/5} \tag{3.16}$$

for die filling in air. This indicates that the dimensionless flow rate M^* in air increases with increasing solid density of the particles, due to the reduced effect of drag force relative to the inertia of particles.

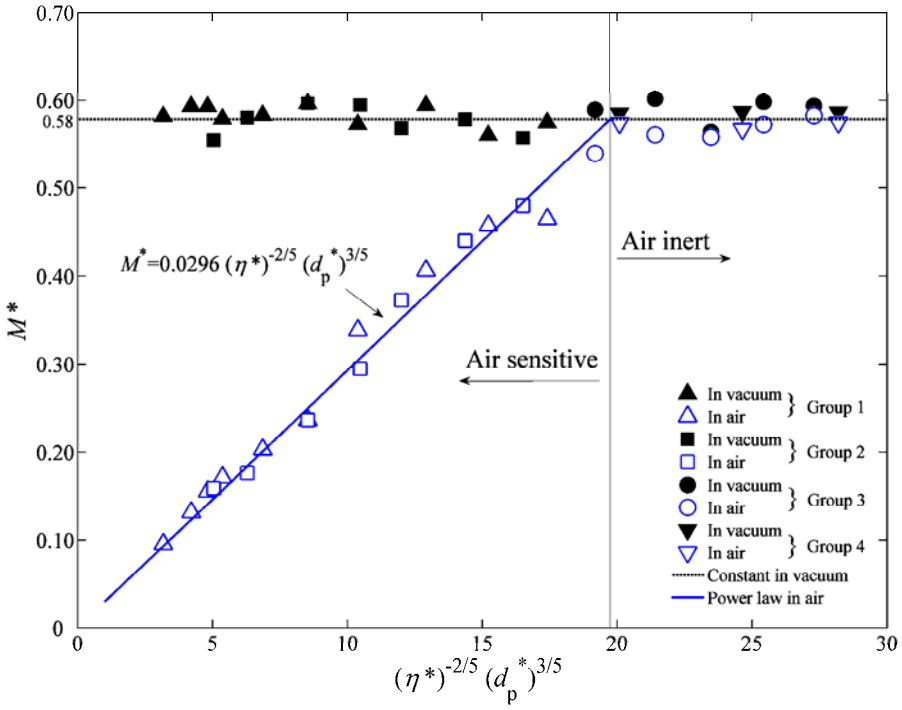

Figure 3.11 M^* versus $\left(\eta^*\right)^{-2/5}\left(d_p^*\right)^{3/5}$ for die filling in a vacuum and in air.

From Eqs. (3.13), (3.14) and (3.15), we can write

$$M^* = A\left(\eta^*\right)^{-2/5}\left(d_p^*\right)^{3/5} \tag{3.17}$$

The dimensionless mass flow rates M^* for all the cases listed in Table 3.1 are plotted against $\left(\eta^*\right)^{-2/5}\left(d_p^*\right)^{3/5}$ in Figure 3.11. It is clear that the data coalesce onto two master curves for die filling in air and in a vacuum, respectively. For die filling in a vacuum,

the dimensionless flow rate M^* is essentially constant at a value of 0.58 and is independent of particle size and particle density. This result is in excellent agreement with the previous studies of hopper flow and powder flow from bins (Seville et al., 1997; Beverloo et al., 1961; Rhodes, 1998), in which the effect of air could be neglected as coarse powders were used. For die filling in air, the results are distinguished by two regions. For high values of $\left(\eta^*\right)^{-2/5}\left(d_{\mathrm{p}}^*\right)^{3/5}$, M^* is essentially constant and close to the result obtained for die filling in a vacuum. For smaller values of $\left(\eta^*\right)^{-2/5}\left(d_{\mathrm{p}}^*\right)^{3/5}$, M^* increases linearly with $\left(\eta^*\right)^{-2/5}\left(d_{\mathrm{p}}^*\right)^{3/5}$, and the best fit to the data in this regime gives

$$M^* = 0.0296\left(\eta^*\right)^{-2/5}\left(d_p^*\right)^{3/5} \tag{3.18}$$

The demarcation between these two regimes can be determined by setting $M^* = 0.58$ in Eq. (3.18). This leads to

$$\left(\eta^*\right)^{-2/5}\left(d_p^*\right)^{3/5} = 19.6 \tag{3.19}$$

Therefore, the intersection point $\left(\eta^*\right)^{-2/5}\left(d_{\mathrm{p}}^*\right)^{3/5}$=19.6 can be treated as a critical value to classify the two distinct regimes of flow behaviour during die filling in air. If the value of $\left(\eta^*\right)^{-2/5}\left(d_{\mathrm{p}}^*\right)^{3/5}$ is less than this critical value, indicating that smaller and/or lighter particles are used, the powder flow rate is influenced and reduced significantly by the presence of air, and the flow rate is given by Eq. (3.18). This regime is referred to as the air-sensitive regime. If the value of $\left(\eta^*\right)^{-2/5}\left(d_{\mathrm{p}}^*\right)^{3/5}$ is greater than the critical value, indicating that larger or heavier particles are used, then the effect of air on the powder flow becomes negligible and the flow rate in air is close to that in a vacuum. We refer to this regime as the air-inert regime. This distinction should be a useful

guide for evaluating the influence of the presence of air on the powder flow behaviour during die filling.

By substituting for η^* and d_p^* using Eqs. (3.10) and (3.11), Eq. (3.17) can be written as

$$M^* = B\left(\frac{\rho_s^{\,2} g d_p^{\,3}}{\eta^2}\right)^{1/5} \tag{3.20}$$

where $B = A(1-\varepsilon)^{2/5}$.

Considering the particle solid density ρ_s is generally much greater than the air density ρ_a (1.2 kg/m^3), the Archimedes number (Seville et al., 1997) for the particles flowing in air can be written as

$$\mathrm{Ar} = \frac{\rho_a(\rho_s - \rho_a) g d_p^{\,3}}{\eta^2} \approx \frac{\rho_a \rho_s g d_p^{\,3}}{\eta^2} \tag{3.21}$$

From Eqs. (3.20) and (3.21), the dimensionless mass flow rate M^* can be rewritten in terms of the Archimedes number and particle-air density ratio as

$$M^* = B\left(\mathrm{Ar}\cdot\Phi_\rho\right)^{1/5} \tag{3.22}$$

where Φ_ρ represents particle-air density ratio (i.e. $\Phi_\rho = \rho_s/\rho_a$). A re-plot of Figure 3.11 is shown in Figure 3.12, in which M^* is plotted against $\mathrm{Ar}\cdot\Phi_\rho$. It is clear that two distinct regimes (i.e., air-sensitive and air-inert) can also be classified by a critical value of $\mathrm{Ar}\cdot\Phi_\rho = 9.56\times10^6$. The best fit to the data in the air-sensitive regime gives

$$M^* = 0.0233\left(\mathrm{Ar}\cdot\Phi_\rho\right)^{1/5} \tag{3.23}$$

as shown by the solid line in Figure 3.12.

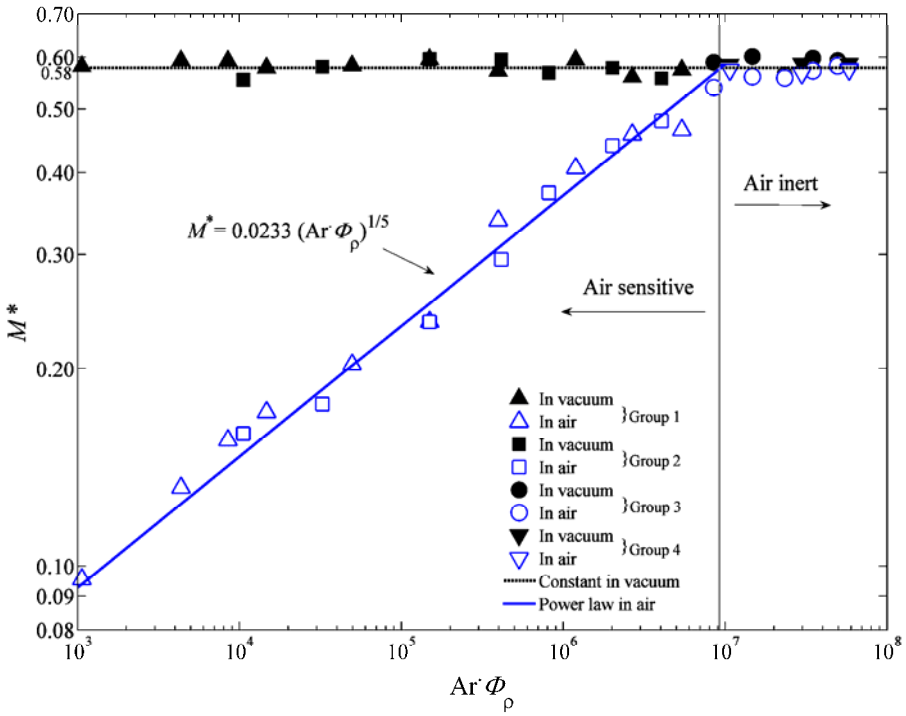

Figure 3.12 M^* versus $\mathrm{Ar}\cdot\Phi_\rho$ in a vacuum and in air

3.3.3. Die filling with polydisperse powders

In reality, monodisperse particle systems are rare. Most powders are polydisperse. Hence, die filling of polydisperse powders was also investigated. Two groups of polydisperse powders were examined. For these two groups, normal (Gaussian) particle size distributions were assumed with the average particle size set to 130 μm and 180 μm respectively. For each group, nine different size fractions were considered. The particle size distribution for the polydisperse system with an average particle diameter of 130μm and a particle size in the range 50 – 210 μm is shown in Figure 3.13. For the system with an average particle diameter of 180μm, the range of particle sizes was 100 – 260 μm. After initial deposition in the shoe, the void fractions of the polydisperse powders with the average particle diameters of 130μm and 180μm were 0.382 and 0.415 respectively.

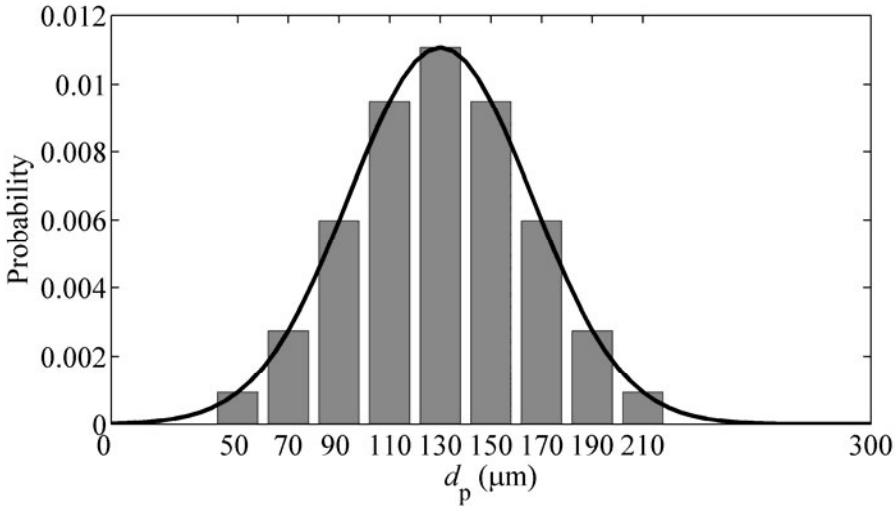

Figure 3.13 Typical particle size distribution.

Figure 3.14a shows a comparison of mass flow between the polydisperse powder system and a corresponding monodisperse system, having the same average particle diameter of 130μm. For die filling in a vacuum, the mass flow rate is higher for the polydisperse system. For die filling in air, the mass flow rate is slightly higher when a monodisperse system is used, rather than a polydisperse one. In addition, a larger mass of powder in a fully-filled die is obtained when the polydisperse system is used whether in a vacuum or in air, because of the effect of dispersion on final void fraction. To compensate for this, the volumetric flow is also presented in Figure 3.14b, in which the apparent volume is defined as the mass divided by the initial bulk density. It is clear that, for die filling in a vacuum, the volumetric flow rates are the same for both polydisperse and monodisperse powders. For die filling in air, the volumetric flow rate is lower for the polydisperse powder compared to the monodisperse one. This implies, not surprisingly, that the influence of air becomes more significant when a polydisperse powder is considered. Similar trends were found for die filling with monodisperse and polydisperse powders with an average particle diameter of 180 μm.

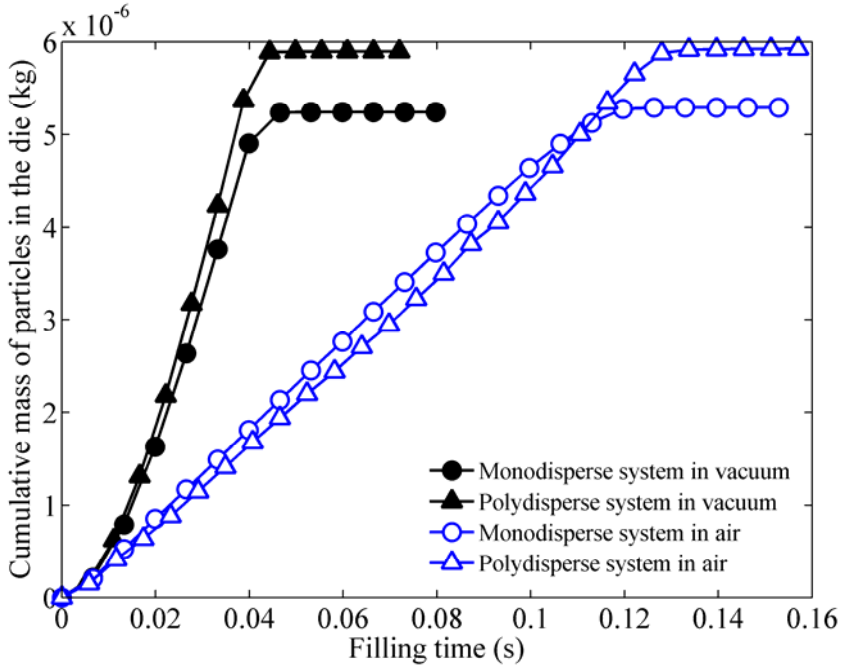

(a) Mass flow

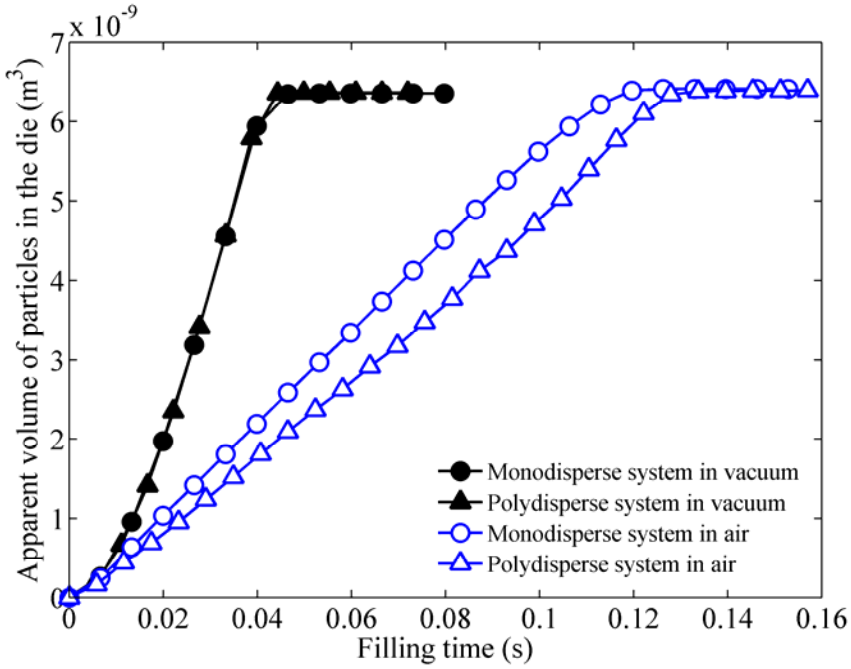

(b) Volumetric flow

Figure 3.14 (a) Mass flow and (b) volumetric flow for monodisperse and polydisperse powder systems with average particle diameter of 130 µm. (Die size: 7 mm×7 mm)

For powders with the same average particle diameter, the void fraction is lower for the polydisperse powder compared to the monodisperse powder. Therefore, during die filling with a polydisperse powder, the mass flow rate could be higher due to the

denser packing regardless of the effect of air. However, the volumetric flow rate could be lower with a polydisperse powder in the presence of air, since the entrapped air in the die encounters a greater resistance in permeating the powder bed due to the lower void fraction and a higher negative pressure gradient is generated to hinder the powder flow. Consequently, larger air bubbles are formed and a narrower flow stream is induced during die filling with polydisperse powders, as shown in Figure 3.15, which leads to a slower powder flow rate.

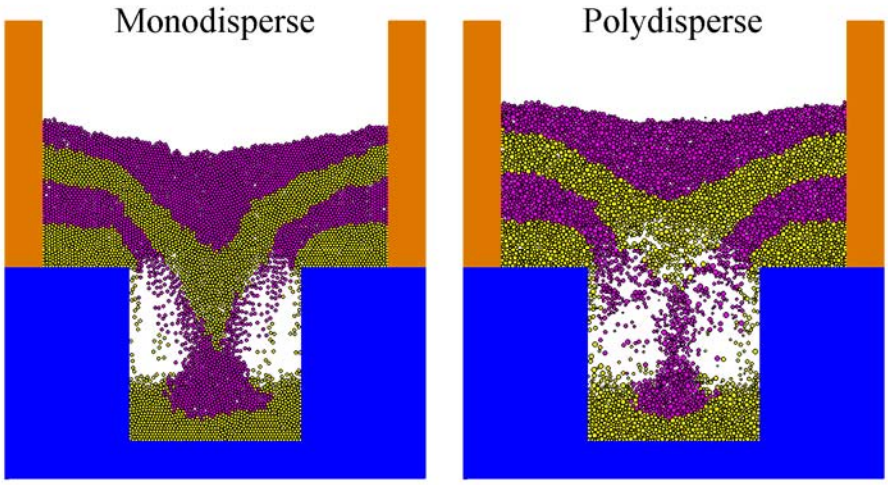

Figure 3.15 A comparison of powder flow patterns at the same moment in time during die filling for the monodisperse and polydisperse powder systems in the presence of air. The two powders have the same average particle diameter of 130μm.

Figure 3.16 shows a comparison of the dimensionless mass flow rate M^* obtained for the monodisperse and polydisperse powder systems. By different random generations of particles, three simulations with different initial configurations of the powder bed in the shoe have been performed for each set of conditions. The bar graph shows the mean value of M^* for each set with the error bar representing the standard deviation. It can be seen that, for die filling in a vacuum, M^* is almost identical for all systems. For die filling in air, M^* is reduced slightly for the polydisperse powders due to the lower void fraction.

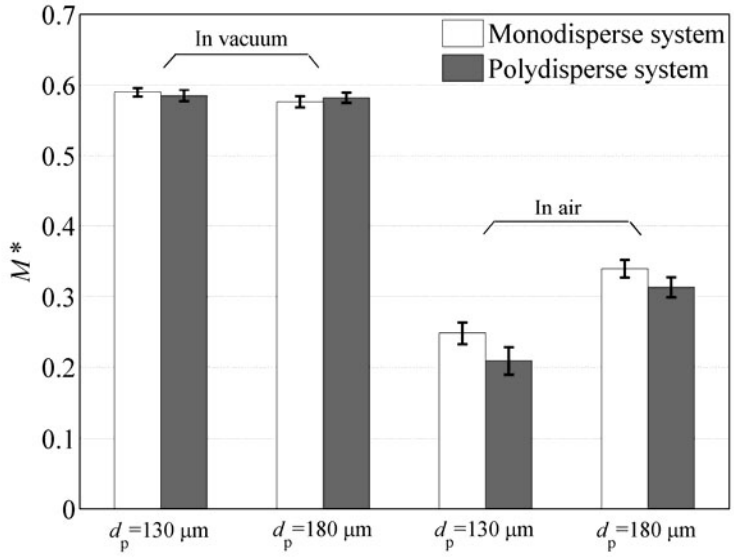

Figure 3.16 A comparison of dimensionless mass flow rates for monodisperse and polydisperse powder systems.

3.3.4. Die filling with cohesive powders

Most powders are to some extent cohesive, particularly in the case of powders with particle sizes less than 100 μm (Seville et al., 1997). In order to study the effect of adhesion on powder flow during die filling, surface energy was introduced for the monodisperse powder with particle diameter of 50 μm. In these simulations, the adhesive contacts for particle-particle and particle-wall are modelled according to the theories proposed by Johnson et al. (1971) and Thornton (1991). The surface energy γ is prescribed by assuming the 'pull-off' force F_c is equal to k times the weight of a particle, i.e.

$$F_c = 3\pi\gamma R^* = k \cdot m_p g \tag{3.24}$$

so,

$$\gamma = k \cdot \frac{m_p g}{3\pi R^*} \tag{3.25}$$

Thus, different surface energies γ can be specified to obtain different values of *k*. In addition, non-cohesive powder can be treated as a special case with *k* equal to zero.

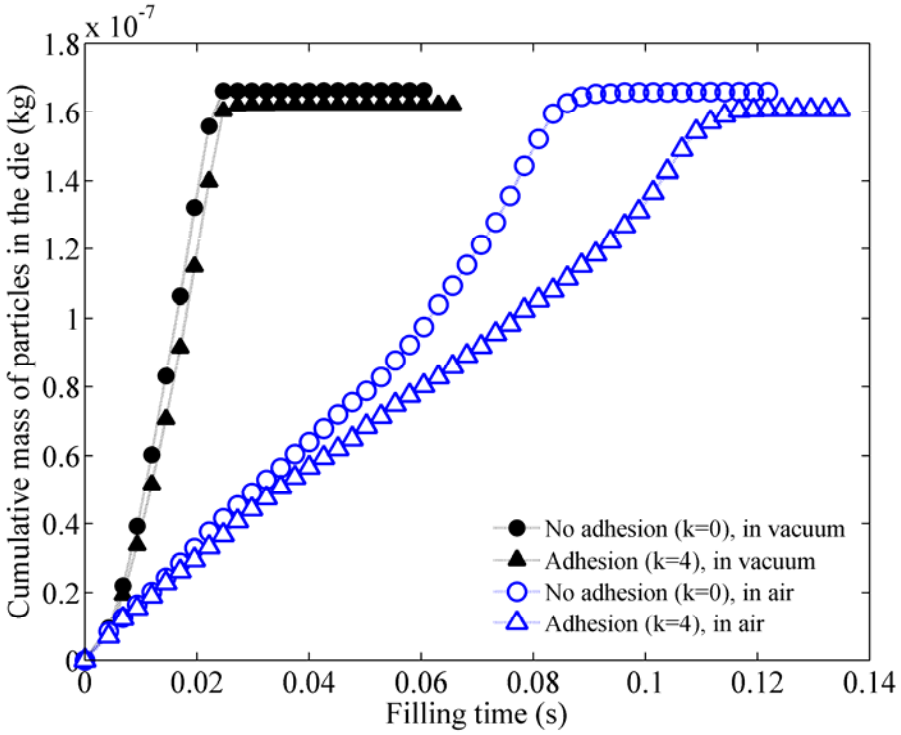

Figure 3.17 Mass flow with and without adhesion. (Die size: 2 mm×2 mm)

Figure 3.17 shows the comparison of mass flow with and without adhesion. For the powder with adhesion, *k* is set to 4 (i.e., $\gamma = 3.27\times10^{-5}\,\mathrm{J/m^2}$). It can be seen that for die filling in a vacuum, the flow of cohesive powder is slightly slower than that without adhesion, and slightly fewer particles flow into the die. For die filling in air, the flow of the cohesive powder is clearly slower than that of a non-cohesive powder, although the flow patterns are similar with a distinctive two-stage form, as discussed in Section 3.3.1. As expected, the powder flow in air is generally slower compared to the flow in a vacuum due to the effect of air.

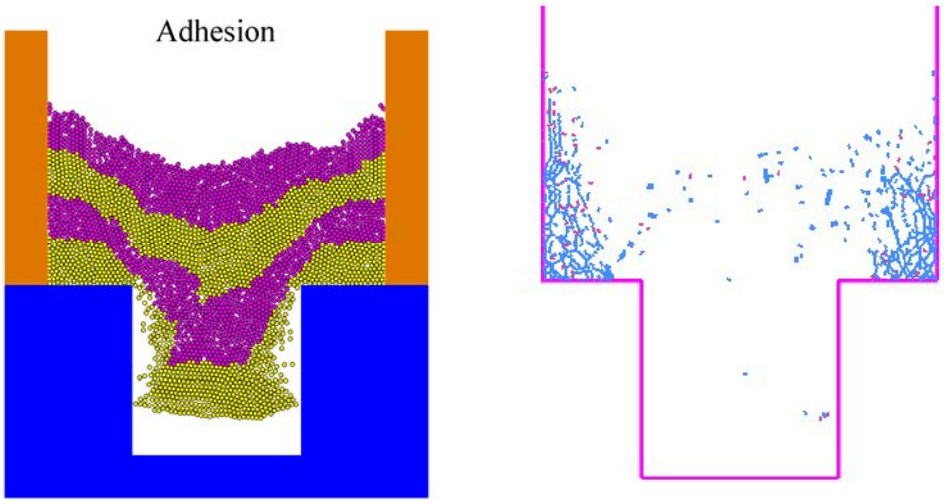

(a) Powder flow pattern (b) Contact force distribution

Figure 3.18 (a) Powder flow pattern and (b) contact force distribution for die filling with adhesion in a vacuum when T = 17 ms.

Figure 3.18 shows the powder flow pattern and contact force distribution in a vacuum at the same instant (T = 17.0 ms) as those shown in Figures 3.4b and 3.5d for die filling without adhesion. Compared to Figures 3.4b and 3.5d, it is clear that the die filling with a cohesive powder is slower than that for a non-cohesive powder (Figure 3.18a), and the stagnant zones on the ledges of the die are larger for the cohesive powder (Figure 3.18b).

The powder flow pattern and corresponding contact force distribution for die filling with a cohesive powder in the presence of air at the instant T = 75 ms are shown in Figure 3.19, which may be compared with Figures 3.6d and 3.7d. From the comparison, it is clear that for die filling with a cohesive powder in air, there are more particles still above the die opening at this instant (Figure 3.19a) and the contact force network can survive much longer when the particles are adhesive (Figure 3.19b). This is because of the adhesive particles sticking together and consequently, it becomes

harder for the air flow to break the particle bonds and permeate the more constricted air pockets. As a result, the die is filled more slowly in the case of cohesive powders.

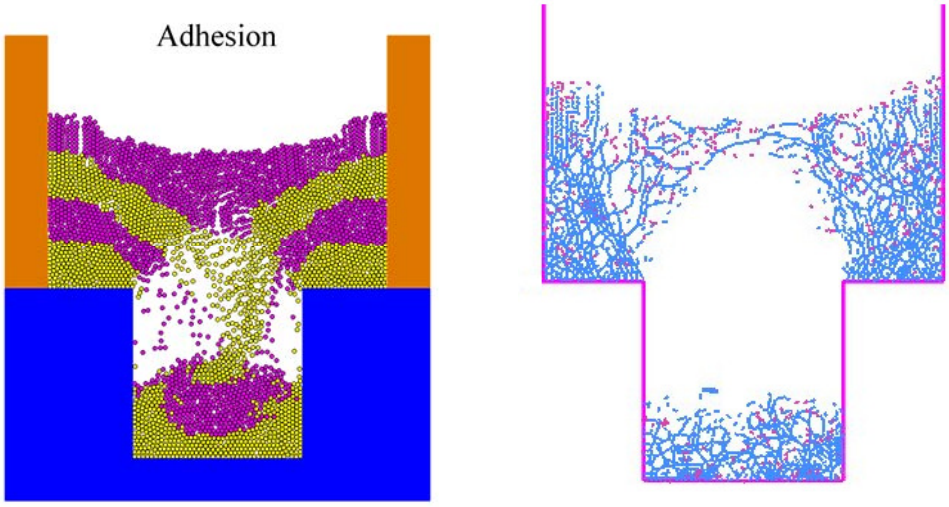

(a) Powder flow pattern (b) Contact force distribution

Figure 3.19 (a) Powder flow pattern and (b) contact force distribution for die filling with adhesion in the presence of air when T = 75 ms.

The dimensionless mass flow rates M^* for die fillings with and without adhesion in air and in a vacuum are compared in Figure 3.20. Again, each simulation was run in triplicate with different initial configurations of the powder bed in the shoe, and the mean value of M^* and the error bar representing the standard deviation are presented in Figure 3.20. It is clear that for die filling with the cohesive powder, M^* is slightly lower than with a non-cohesive powder. Furthermore, the dimensionless mass flow rates are much lower for die filling in air than those in a vacuum. This indicates that the presence of air has a more significant effect than adhesion on powder flow, at least for the cases considered here.

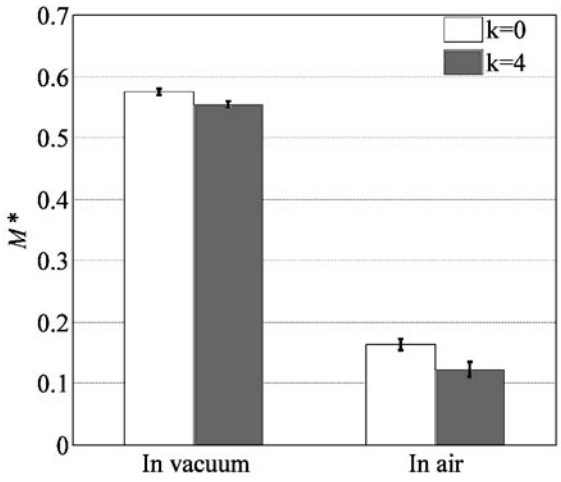

Figure 3.20 Dimensionless flow rates for different surface energies.

3.4. Die filling from a moving shoe

In the industrial powder compaction process, a moving shoe is generally used to deliver the powder. Simulations of die filling from a moving shoe are therefore performed. The three cases given in Table 3.2 are considered to investigate the effects of particle properties and the depth of die on the filling process.

3.4.1. Powder flow patterns in air and in a vacuum

Figures 3.21 and 3.22 show the snapshots of die filling in a vacuum and in air, respectively, for Case 1, in which the fine particles and a shallow die are used. In these simulations, the shoe moves at a velocity of 60 mm/s. During die filling at this shoe velocity, the powder flows into the die in a nose shaped profile (Figure 3.21a). The particles at the top of the powder mass cascade into the die over the top free surface, which is referred to as nose flow (Wu et al., 2003c), and the particles at the bottom region are delivered into the die by detaching from the bottom surface, which is referred to as bulk flow (Wu et al., 2003c). For die filling in a vacuum, the leading side of the die (referring to the direction of shoe motion, i.e., left hand side) is filled

by the particles from the top region of the powder mass in the shoe, and the tailing side of the die (i.e., right hand side) is occupied by the particles from the bottom region of the powder mass in the shoe (Figures 3.21b and c). For die filling in the presence of air, the air can be entrapped inside the die resulting in the formation of an air bubble (Figures 3.22a and b). The entrapped air prevents the flow of powder into the die, so that the particles at the top region have difficulty in flowing into the die and at the late stage of die filling the particles are fed into the die by detaching from the bottom surface (Figure 3.22b). As a result, the top region of the die cavity is mainly filled by the particles from the bottom layer of the powder mass (Figures 3.22b and c).

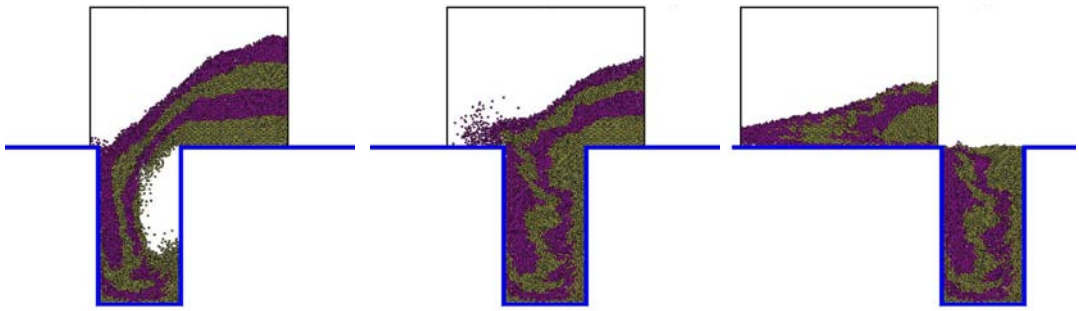

(a) 81.3 ms (b) 122.7ms (c) 245.4 ms

Figure 3.21 Snapshots of die filling in a vacuum at a shoe velocity of 60 mm/s. (with fine particles and a shallow die)

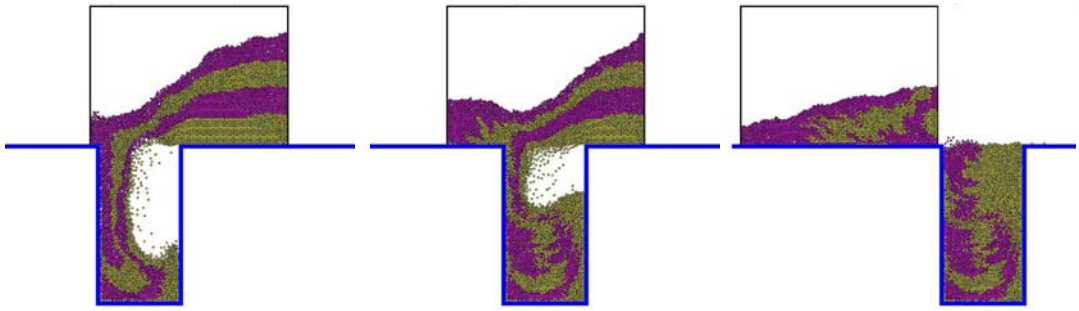

(a) 81.3 ms (b) 122.7ms (c) 245.4 ms

Figure 3.22 Snapshots of die filling in air at a shoe velocity of 60 mm/s. (with fine particles and a shallow die)

The snapshots of die filling in a vacuum and in air at a shoe velocity of 140 mm/s for Case 1 are shown in Figures 3.23 and 3.24, respectively. For die filling in a vacuum, the front of the flow stream rapidly moves across the die opening at this shoe velocity (Figure 3.23a), and therefore the particles at the top layer of powder mass can not flow into the die (Figures 3.23b and c). For die filling in air, the die is fed mainly by the particles in the bottom layer of the powder mass due to the resistance of the entrapped air (Figures 3.24a and b), and after filling the die cavity is only partially filled.

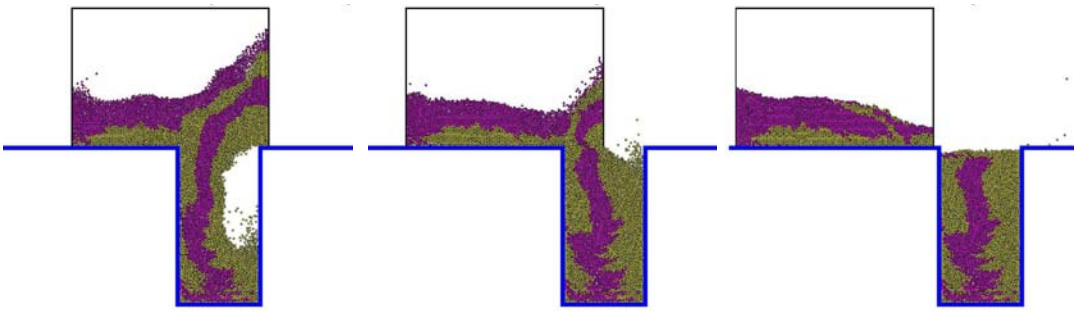

(a) 70.6 ms (b) 89.0 ms (c) 184.1 ms

Figure 3.23 Snapshots of die filling in a vacuum at a shoe velocity of 140 mm/s. (with fine particles and a shallow die)

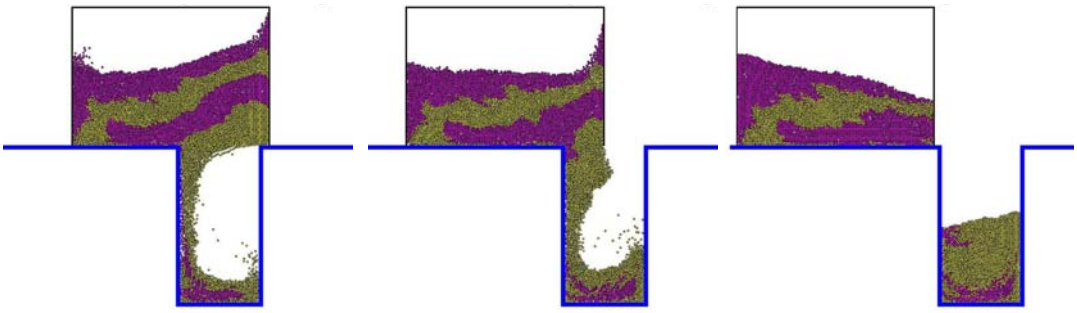

(a) 70.6 ms (b) 89.0 ms (c) 184.1 ms

Figure 3.24 Snapshots of die filling in air at a shoe velocity of 140 mm/s. (with fine particles and a shallow die)

When the shoe velocity is increased to 220 mm/s, as shown in Figures 3.25 and 3.26, the more rapid translation of powder mass over the die opening allows less time for

the particles to flow into the die, and only the particles at the bottom of powder mass are delivered into the die. As a result, the die cavity can no longer be completely filled in a vacuum (Figure 3.25c) and even fewer particles are obtained in the die in the presence of air (Figure 3.26c).

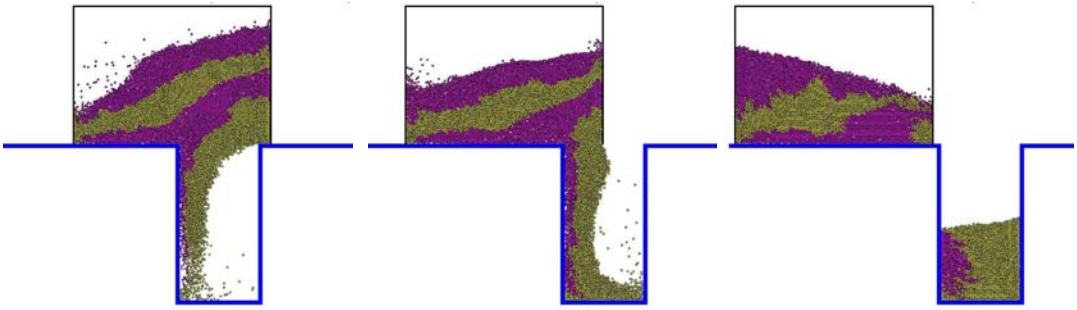

(a) 44.5 ms (b) 56.8 ms (c) 153.4 ms

Figure 3.25 Snapshots of die filling in a vacuum at a shoe velocity of 220 mm/s. (with fine particles and a shallow die)

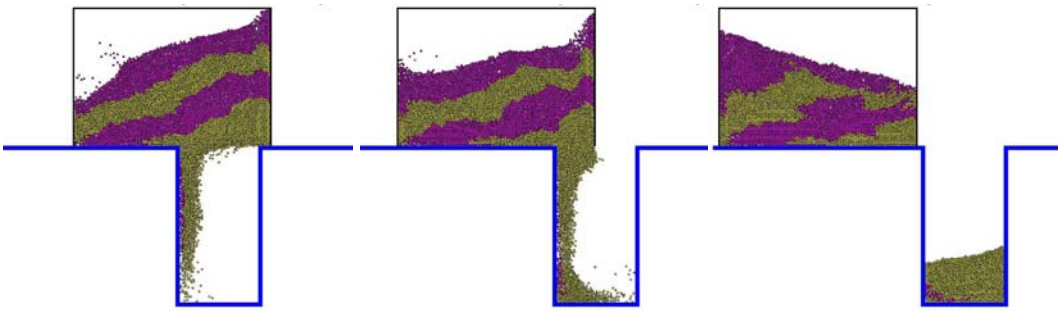

(a) 44.5 ms (b) 56.8 ms (c) 153.4 ms

Figure 3.26 Snapshots of die filling in air at a shoe velocity of 220 mm/s. (with fine particles and a shallow die)

In Case 2, the coarse particles, that are inert to the effect of air during die filling from a stationary shoe as discussed in Section 3.3.2, are also used in die filling from a moving shoe with a shallow die. It is found that the filling process with the coarse particles in the presence of air is very similar to that in a vacuum, indicating that the air also has a negligible impact on the die filling in this case. As a result, only the snapshots of die filling in air at various shoe velocities are shown in Figures 3.27-3.29.

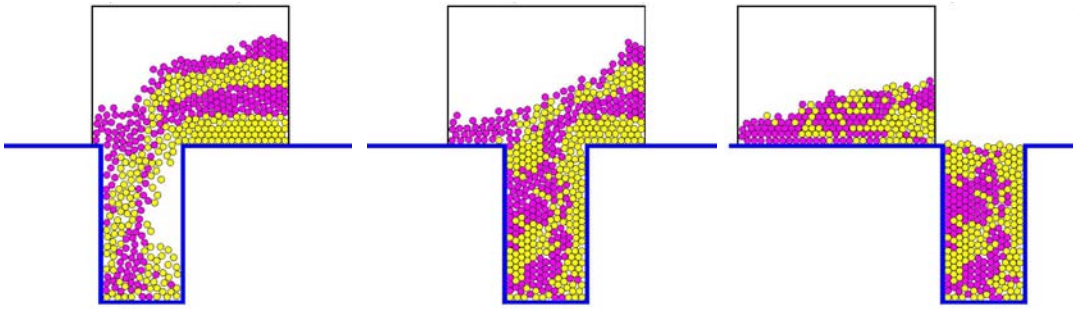

(a) 82.0 ms (b) 122.9ms (c) 248.6 ms

Figure 3.27 Snapshots of die filling in air at a shoe velocity of 60 mm/s. (with coarse particles and a shallow die)

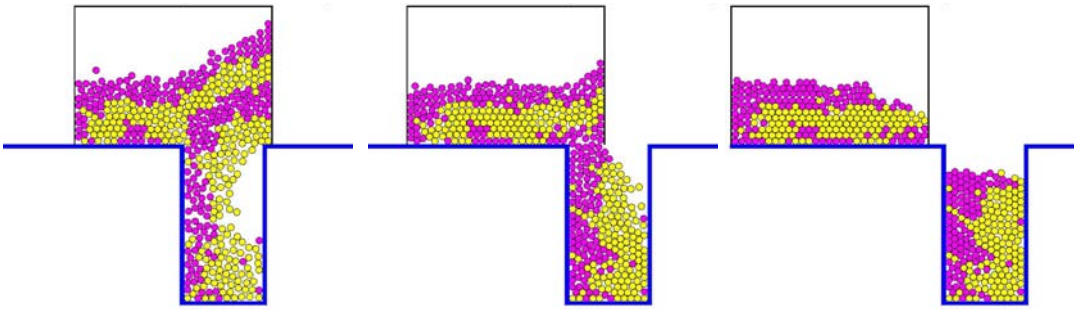

(a) 71.0 ms (b) 90.2 ms (c) 273.2 ms

Figure 3.28 Snapshots of die filling in air at a shoe velocity of 140 mm/s. (with coarse particles and a shallow die)

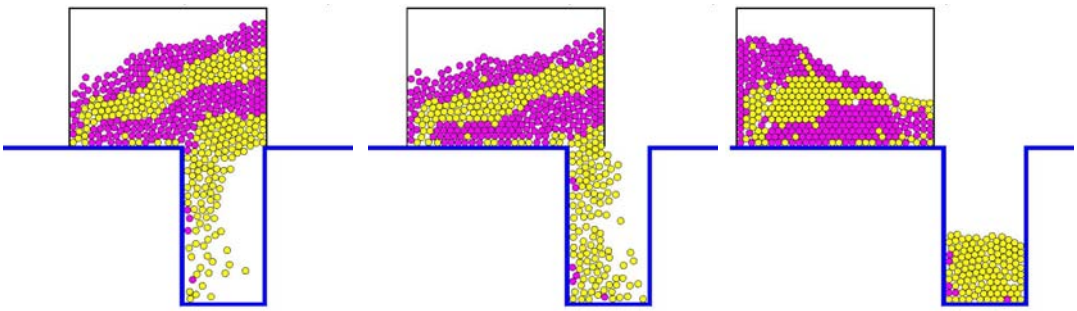

(a) 46.4 ms (b) 57.4 ms (c) 273.2 ms

Figure 3.29 Snapshots of die filling in air at a shoe velocity of 220 mm/s. (with coarse particles and a shallow die)

By comparing with the die filling processes with fine particles in Figures 3.22, 3.24 and 3.26, the powder flow streams in die filling with coarse particles seem to be thicker than those in die filling with fine particles. This is because the air can more

easily permeate through the larger channels formed between the coarse particles compared to the fine particles, and also the effect of air drag on coarse particles is much less pronounced due to the larger inertia. For die filling with coarse particles, when the shoe moves at a low velocity of 60 mm/s, the die is filled by the particles from both top and bottom of the powder mass in the shoe (Figure 3.27). When the shoe translates at higher velocities (i.e., 140 mm/s and 220 mm/s), the powder mass rapidly moves over the die opening and the particles are delivered into the die cavity by detaching from the bottom of the powder mass (Figures 3.28 and 3.29). As the shoe velocity increases, the amount of particles fed into the die is reduced due to the decreasing filling time and the increased interlocking of particles.

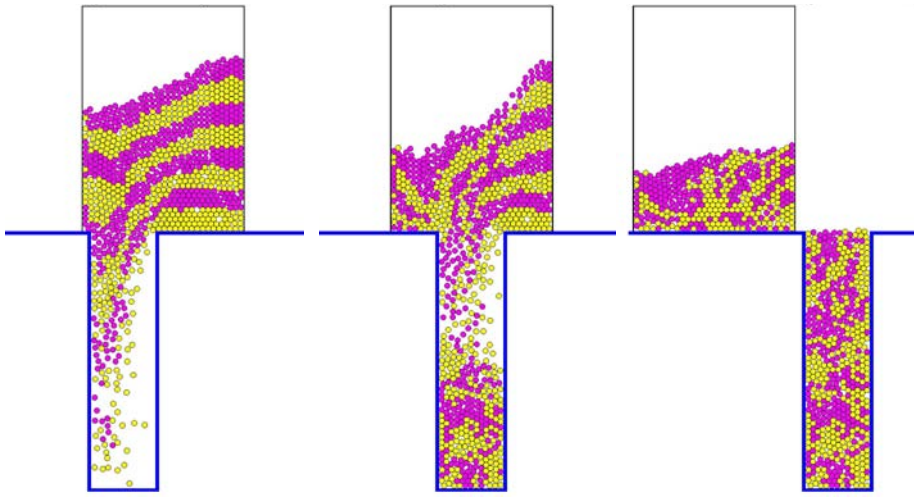

(a) 82.0 ms (b) 122.9ms (c) 251.3 ms

Figure 3.30 Snapshots of die filling in air at a shoe velocity of 60 mm/s. (with coarse particles and a deep die)

The same coarse particles as used in Case 2 are also employed in Case 3. However, a deep die having twice the depth of the shallow die (in Cases 1 and 2) is used in Case 3. Due to the negligible effect of air with coarse particles, the filling process in air is also similar to that in a vacuum for Case 3. Therefore only the snapshots of die filling in

air with various shoe velocities are shown in Figures 3.30-3.32. In general, the powder flow patterns with the deep die are similar to those with the shallow die.

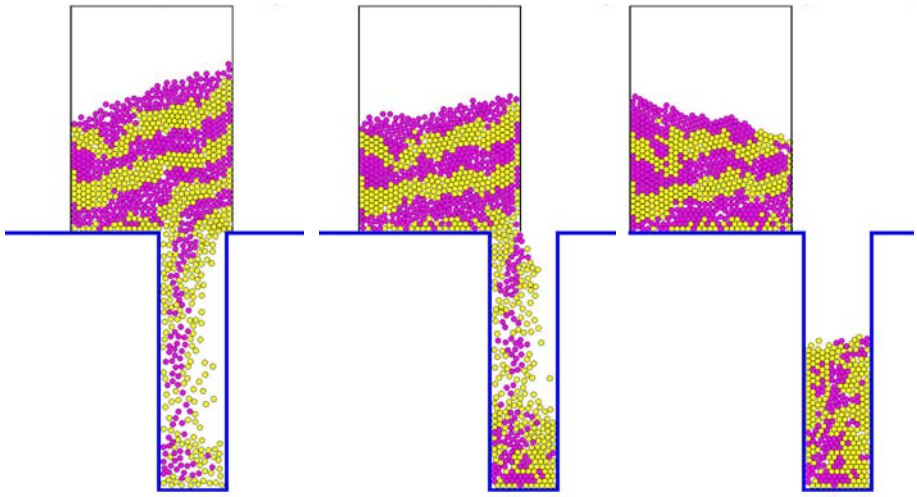

(a) 71.0 ms (b) 90.2 ms (c) 166.6 ms

Figure 3.31 Snapshots of die filling in air at a shoe velocity of 140 mm/s. (with coarse particles and a deep die)

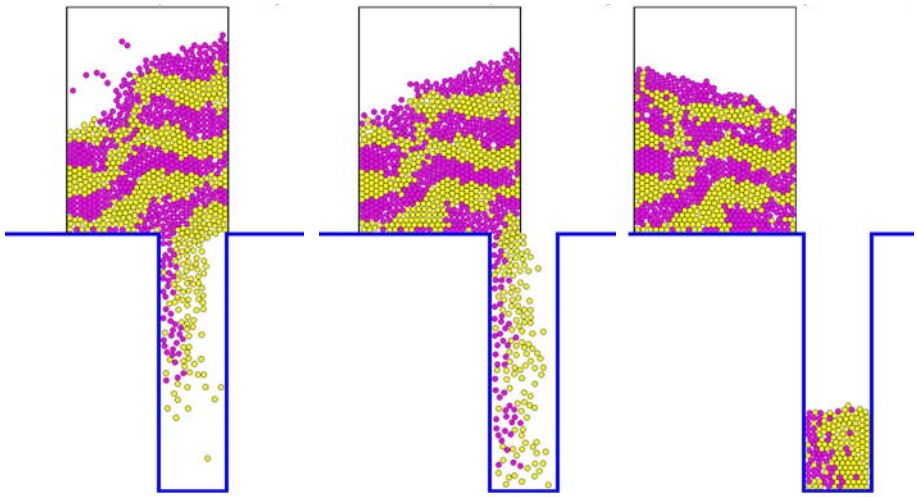

(a) 46.4 ms (b) 57.4 ms (c) 245.9ms

Figure 3.32 Snapshots of die filling in air at a shoe velocity of 220 mm/s. (with coarse particles and a deep die)

3.4.2. Mass flow rate and critical shoe velocity

In Figure 3.33, the average mass flow rate and fill ratio are plotted as a function of shoe velocity for Case 1. The average mass flow rate $\overline{M}$ is defined in Eq. (3.1). The fill ratio δ is the fraction of the die that is filled and it is defined as

$$\delta = \frac{m_{\text{total}}}{m_{\text{f}}} \tag{3.26}$$

where m_{total} is the total mass of particles deposited into the die at a given shoe velocity and m_{f} is the mass of particles in a fully filled die.

As shown in Figure 3.33a, the average mass flow rate in air is about half of that in a vacuum at a given shoe velocity due to the resistance of the entrapped air on the powder flow. It is also observed that at lower shoe velocities the average mass flow rate increases as the shoe velocity increases until it reaches a maximum, thereafter the average mass flow rate decreases with increasing shoe velocity. During die filling with a moving shoe, the effective discharging area (EDA) from which the powder flows into the die increases from zero to the whole die opening. When the shoe translates at a lower velocity, the filling process with a small EDA is prolonged thereby leading to a smaller overall mass flow rate. As the translational velocity of the shoe increases, the front of the powder mass moves rapidly across the cavity and the mass flow rate increases due to the fact that the powder can be delivered into the die through a larger area. However, the increase of shoe velocity can enhance the interlocking of particles, which is caused by the lateral compressive stresses generated by inertia effects (Wu et al., 2003c). Therefore, it can become more difficult for particles to be detached from the bulk due to the enhanced interlocking of particles as the shoe velocity increases, and the mass flow rate is hence reduced. In addition, as

the shoe moves at a higher velocity, there is less time for the newly mobilised particles to build up vertical speed above the die opening, thus, the particles flowing into the die cavity have a lower vertical velocity and consequently a lower mass flow rate is achieved.

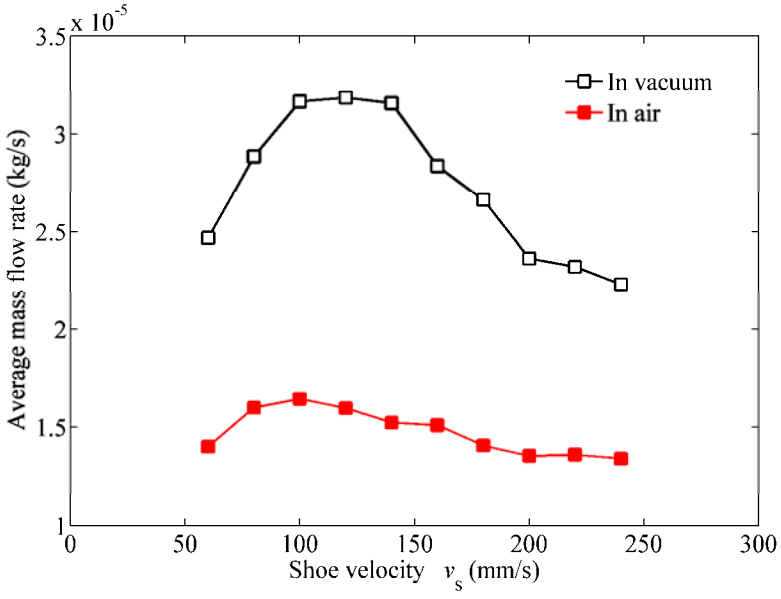

(a)

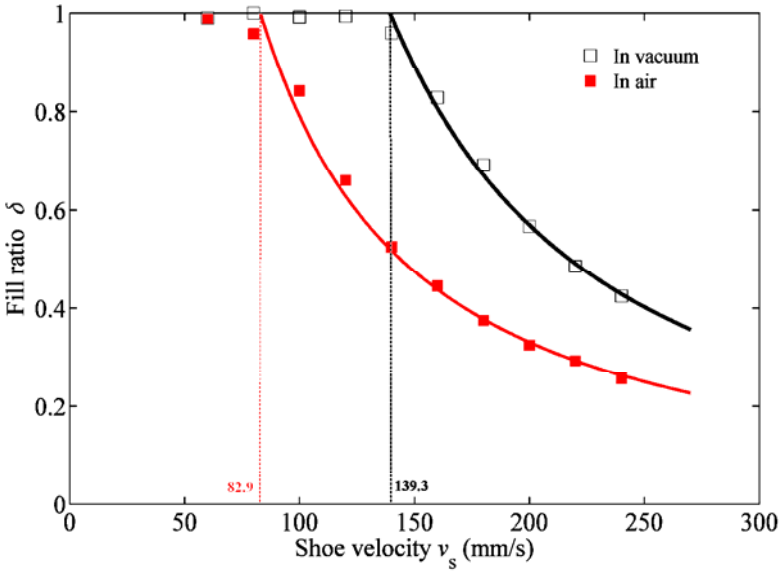

(b)

Figure 3.33 The variation of (a) average mass flow rate and (b) fill ratio with shoe velocity for Case 1.

It is observed from Figure 3.33b that the fill ratio δ is essentially equal to a value of unity at lower shoe velocities, implying the die is completely filled, and it is less than one at higher shoe velocities as the die is just partially filled. Obviously, there exists a maximum shoe velocity at which the die can be completely filled, which is referred to as critical shoe velocity (Wu et al., 2003c). It is also found from Figure 3.33b that the fill ratio decreases with the increasing shoe velocity when the die can not be completely filled (i.e., δ <1). For incomplete filling, experimental results (Wu and Cocks, 2004; Sinka et al., 2004; Shneider et al., 2005, 2007) showed that the fill ratio can be expressed in terms of the shoe velocity as

$$\delta = \left(\frac{v_c}{v_s} \right)^{\alpha} \tag{3.27}$$

where the shoe velocity v_s should be higher than the critical shoe velocity v_c, i.e., $v_s > v_c$. Parameter α depends on the powder properties and process conditions. Based on Eq.(3.27), the best fit to the data in Figure 3.33b gives

$$\delta = \left(\frac{139.3}{v_s} \right)^{1.56} \tag{3.28}$$

for die filling in a vacuum, and

$$\delta = \left(\frac{82.9}{v_s} \right)^{1.26} \tag{3.29}$$

for die filling in air. Therefore the critical shoe velocities are determined as 139.3 mm/s for die filling in a vacuum and 82.9 mm/s for die filling in air. It is evident that the critical shoe velocity in air is much lower than that in a vacuum due to the fact that the entrapped air resists the powder flowing into the die (Figures 3.22, 3.24 and 3.26). By comparing Figures 3.33a and 3.33b, it is found that the average mass flow rate appears to be highest when the shoe velocity is around the critical shoe velocity, which is consistent with the analysis of Wu (2008).

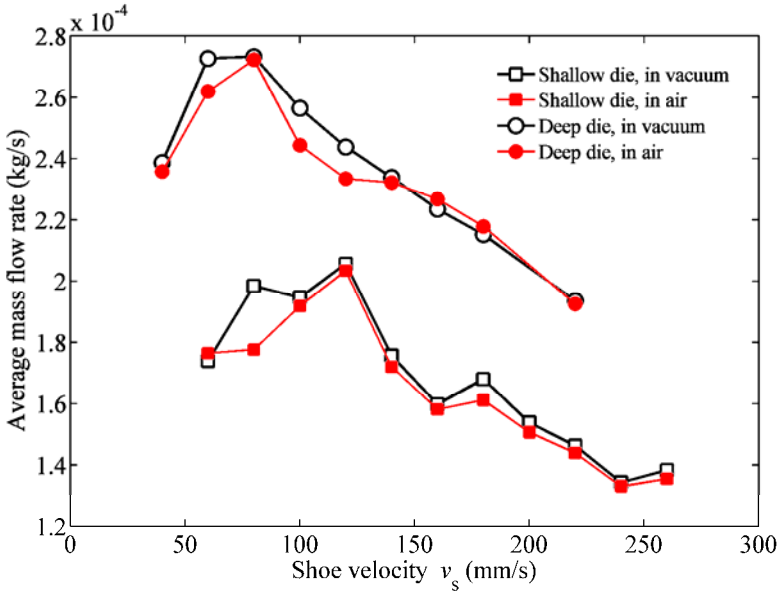

(a)

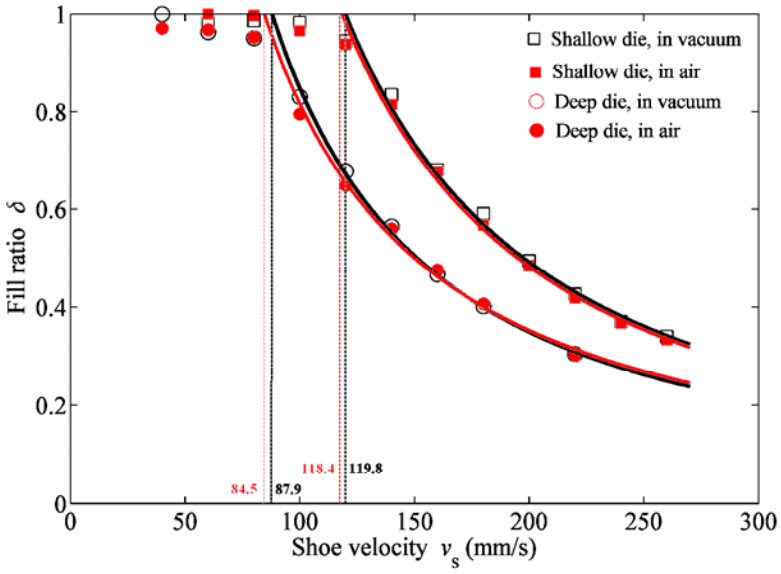

(b)

Figure 3.34 The variation of (a) average mass flow rate and (b) fill ratio with shoe velocity for Cases 2 and 3.

Figure 3.34 shows the average mass flow rates and fill ratios at various shoe velocities for Cases 2 and 3. As shown in Figure 3.34a, the trends are similar to those in Case 1 (Figure 3.33a): the average mass flow rate initially increases as the shoe velocity increases, until it reaches a maximum and thereafter the flow rate decreases with increasing shoe velocity. It is observed that the air does not have a pronounced impact

on the mass flow rate for die filling with these coarse particles, which are the air-inert particles as classified in Figure 3.12. It is noted that for die filling with a deep die, a higher powder bed consisting of more particles is introduced to the shoe in order to fully fill the enlarged die cavity. As indicated by Wu and Cocks (2004) and Wu (2008), a higher powder bed in the shoe can result in a higher powder flow rate due to the increased filling intensity. Therefore, as shown in Figure 3.34a, the average mass flow rate for die filling with a deep die is higher than that for die filling with a shallow die at a given shoe velocity due to the higher powder bed in the shoe.

Using Eq. (3.27), the critical shoe velocities and the fill ratio-shoe velocity relationships for incomplete filling can be determined by best fitting to the data in Figure 3.34b, which gives

$$\delta = \left(\frac{119.8}{v_s} \right)^{1.39} \tag{3.30}$$

and

$$\delta = \left(\frac{118.4}{v_s} \right)^{1.39} \tag{3.31}$$

for Case 2 in a vacuum and in air, respectively, and

$$\delta = \left(\frac{87.9}{v_s} \right)^{1.28} \tag{3.32}$$

and

$$\delta = \left(\frac{84.5}{v_s} \right)^{1.21} \tag{3.33}$$

for Case 3 in a vacuum and in air, respectively. The critical shoe velocities for die filling with a shallow die in a vacuum and in air are 119.4 mm/s and 118.4 mm/s, respectively. The critical shoe velocities for die filling with a deep die in a vacuum

and in air are 87.9 mm/s and 84.5 mm/s, respectively. Thus, for die filling with a given die cavity, the critical shoe velocity in air is very close to that in a vacuum due to the negligible effect of air on coarse particles. The critical shoe velocity is found to be reduced by increasing the depth of the die due to the enlarged capability of the cavity. By comparing Figures 3.34a and 3.34b, it is also observed that the average mass flow rate achieves the maximum value at the critical shoe velocity for die filling with coarse particles.

In Eq. (3.27), α generally has a value of 1.0-1.6 according to the extensive experimental data for a wide range of metal and pharmaceutical powders (Wu and Cocks, 2004, 2006;Sinka et al., 2004; Shneider et al., 2005, 2007). From the Eqs. (3.28)-(3.33), α is in the range of 1.21-1.56, which is in excellent agreement with the experimental results. This, to some extent, verifies our simulations.

3.5. Summary

In this chapter, simulations of powder flow during die filling are reported and the effect of air is examined. For die filling with a stationary shoe, the influences of particle size, density, size distribution and adhesion on the flow behaviour are investigated. It is found that the presence of air has a significant impact on the powder flow behaviour, especially for systems with smaller and lighter particles. The dimensionless mass flow rate M^* for the die filling in a vacuum is found to be constant with a value of 0.58, which is in excellent agreement with the Beverloo constant determined experimentally. The flow characteristics in air depend on the particle size and density. Two distinct regimes have been identified: (i) an air-

sensitive regime (for $\left(\eta^*\right)^{-2/5}\left(d_p^*\right)^{3/5} \le 19.6$ or $\mathrm{Ar}\cdot\Phi_\rho \le 9.56\times10^6$) with generally smaller and lighter particles, in which the presence of air has a significant impact on powder flow behaviour and the dimensionless mass flow rate increases as the particle size or density increases; (ii) an air-inert regime (for $\left(\eta^*\right)^{-2/5}\left(d_p^*\right)^{3/5} >19.6$ or $\mathrm{Ar}\cdot\Phi_\rho > 9.56\times10^6$), in which the particle size and density are sufficiently large that the effect of air flow becomes negligible and the dimensionless mass flow rate is essentially identical to that for the die filling in a vacuum. In addition, it is also found that for die filling in a vacuum, the dimensionless mass flow rate for polydisperse systems is essentially identical to that for monodisperse systems. The presence of air has a more significant impact on the flow of polydisperse powders than monodisperse powders, resulting in a lower dimensionless mass flow rate for polydisperse systems. Finally, it has been demonstrated that the presence of cohesion can reduce the powder flowability. Consequently, a lower dimensionless mass flow rate is obtained for die filling with a cohesive powder when compared to die filling with a non-cohesive powder.

For die filling with a moving shoe, the effects of shoe velocity, particle properties and die size on powder flow behaviour are explored. Nose flow dominates in the die filling process at a low shoe velocity, while bulk flow dominates when the shoe translates at a high velocity. It is observed that the average mass flow rate initially increases as the shoe velocity increases, until it reaches a maximum and thereafter the flow rate decreases with increasing shoe velocity. There exists a critical shoe velocity above which incomplete filling occurs. The higher the critical shoe velocity is, the better the powder flowability for a given die filling system. For die filling with small

and light particles, the average mass flow rate and critical shoe velocity are significantly reduced by the presence of air. For die filling with large and heavy particles, the effect of air is negligible. The critical shoe velocity is reduced by increasing the depth of the die due to the enlarged capability of the die cavity. It is also found that the maximum value of the average mass flow rate is achieved at the critical shoe velocity. In addition, for the incomplete filling, the fill ratio decreases as shoe velocity increases and it follows a power law relationship with the shoe velocity (i.e., Eq. (3.27)). The powers α in Eq. (3.37) determined from the simulations are consistent with those obtained experimentally.

CHAPTER 4: COMPETING FLOW OF DIFFERENT DENSITY PARTICLES

4.1. Introduction

The influence of air on powder flow depends on the particle diameter and density, as demonstrated in Chapter 3. The sensitivity of particles to the air is then characterized using a dimensionless parameter

$$\xi = A_r \Phi_\rho \tag{4.1}$$

where $\Phi_\rho (= \rho_s / \rho_a)$ is the ratio of solid density ρ_s to the air density ρ_a and A_r is the Archimedes number for particles flowing in air and is given as

$$A_r = \frac{\rho_a (\rho_s - \rho_a) g d_p^3}{\eta^2} \tag{4.2}$$

in which d_p is the particle diameter, η is the air viscosity and g is the gravitational acceleration. Granular materials can hence be classified into two regimes with a critical value of the dimensionless parameter ξ_c = 9.56x10^6: air-sensitive particles ($\xi < \xi_c$), for which the air has a significant effect on the granular flow, and air-inert particles ($\xi \geq \xi_c$), for which the effect of air is negligible. An air sensitivity index

$$\zeta = (\ln \xi_c - \ln \xi) / \ln \xi_c \tag{4.3}$$

can be introduced to quantify the sensitivity of particles to the presence of air. The particles are air-inert when $\zeta \leq 0$ and air-sensitive when $0 < \zeta < 1$. In the air-sensitive regime ($0 < \zeta < 1$), the larger the value of the index ζ, the more sensitive the particles are to the presence of air.

In this chapter, die filling with a binary mixture of particles of the same size but different densities is simulated. Two types of mixtures are employed in die filling: bi-column mixture and bi-layer mixture. The competing flow of particles of different densities during the die filling process is examined. For die filling with a binary mixture in the presence of air, the competing flow can be influenced by the difference in air sensitivities due to the difference in particle density.

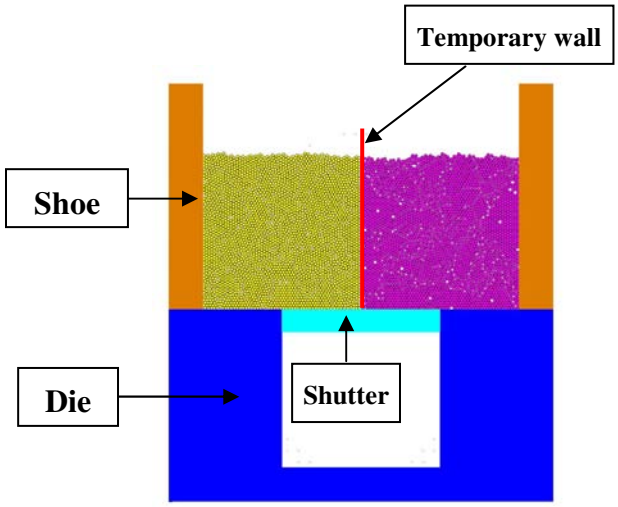

Figure 4.1 Numerical model for die filling with a bi-column mixture.

4.2. Die filling with bi-column mixtures

Die filling with bi-column mixtures and a stationary shoe is investigated. As shown in Figure 4.1, 3000 light particles (coloured in yellow) and 3000 heavy particles (in magenta) were randomly generated at the left and right hand sides, respectively, in the 14 mm wide shoe. The particles have the same diameter of 130 μm. A wall was temporarily positioned in the centre of the shoe to separate the light and heavy particles. In the presence of the shutter and the temporary wall, the particles then settled to a steady state under gravity. When removing the shutter and the temporary wall simultaneously, the particles are deposited into the die cavity of size 7×7 mm

under the influence of the gravitational force. For the simulations of die filling in the presence of air, the computational set-up of the air field is the same as that used previously in Session 3.2.

4.2.1. Powder flow patterns

Figure 4.2 shows the snapshots of the die filling process with a bi-column mixture in a vacuum. The corresponding particle velocity vectors are shown in Figure 4.3, where the length of the vector represents the relative magnitude of the velocity. In this simulation, the density of light particles ρ_l is set to 400 kg/m^3 and the density of heavy particles ρ_h is 7800 kg/m^3. When the die filling starts, the light and heavy particles are deposited into the die simultaneously (Figure 4.2a), and thereafter the flow of heavy particles pushes the light particles to the left hand side (Figure 4.2b). When the front of flow stream reaches the base of the die cavity, the heavy particles continue to move to the left hand side forcing some light particles at the top region of the die to flow out of the die (Figures 4.2c-e). During this process, as shown in Figures 4.3c-e, the light particles flow upwards under the effect of the flow of heavy particles. When the upward flowing stream of light particles meets the downward flowing stream on the top free surface, it is dragged down thereby forming a clockwise circling stream of light particles over the top of heavy particles, until a steady state is achieved with negligible particle velocities (Figures 4.2f and 4.3f). After die filling, most of die cavity is occupied by heavy particles and only a small part at the bottom-left hand side of the die is filled by light particles (Figure 4.2f).

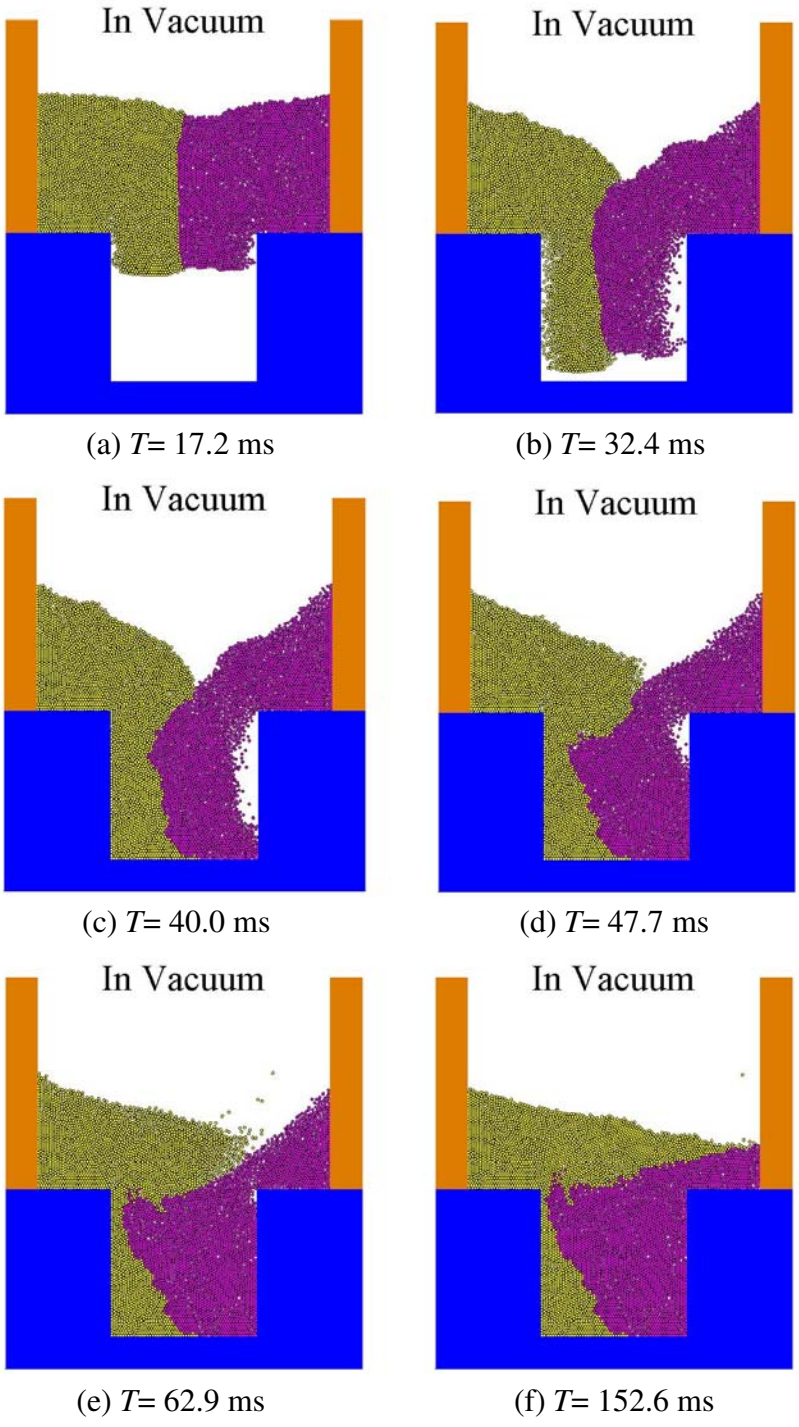

(a) T= 17.2 ms (b) T= 32.4 ms

(c) T= 40.0 ms (d) T= 47.7 ms

(e) T= 62.9 ms (f) T= 152.6 ms

Figure 4.2 Snapshots of die filling with a bi-column mixture in a vacuum. The light and heavy particles are coloured in yellow and magenta, respectively.

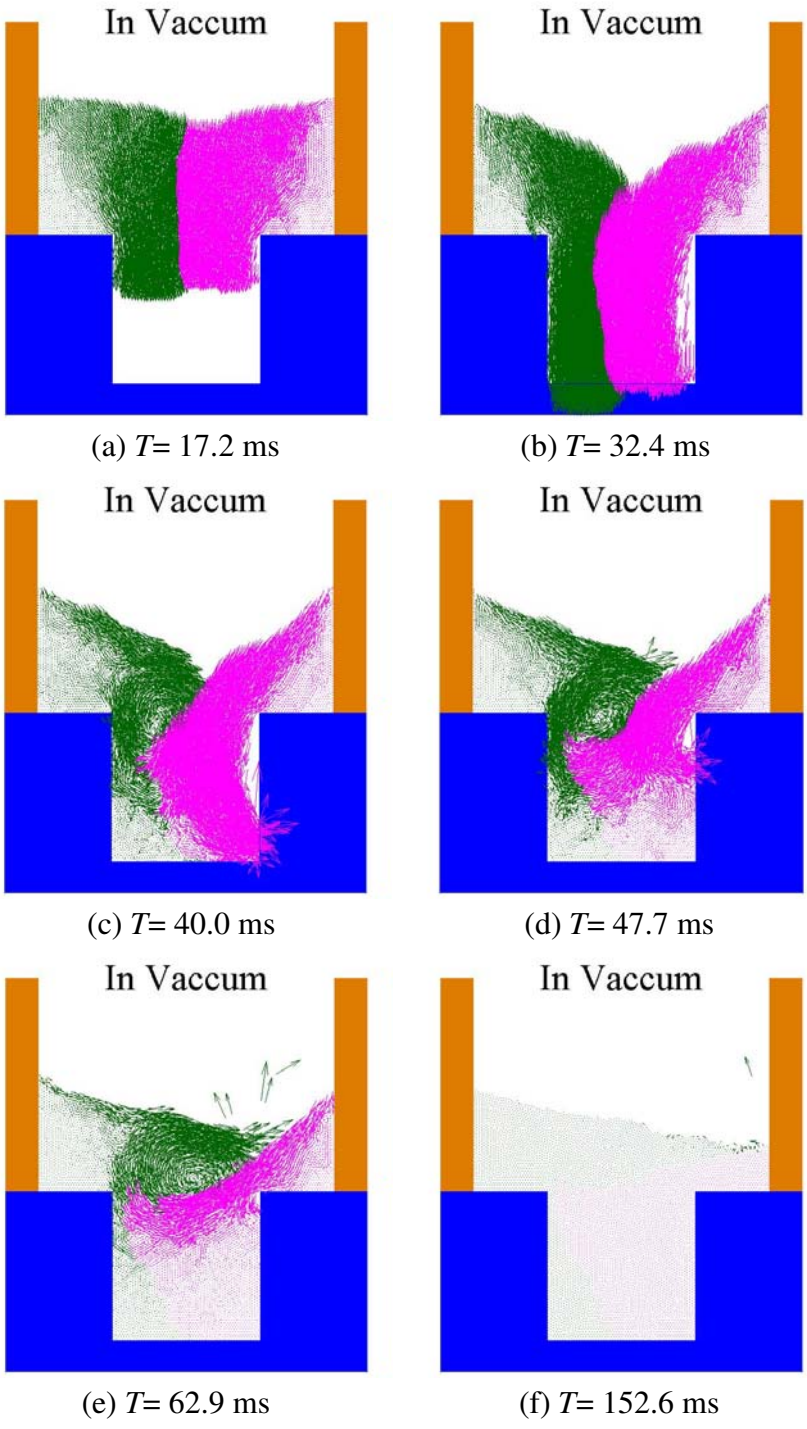

(a) T= 17.2 ms (b) T= 32.4 ms

(c) T= 40.0 ms (d) T= 47.7 ms

(e) T= 62.9 ms (f) T= 152.6 ms

Figure 4.3 Particle velocities during die filling with a bi-column mixture in a vacuum. The green and magenta vectors represent the velocity vectors of light and heavy particles, respectively.

The snapshots of die filling with a bi-column mixture in air are shown in Figure 4.4, in which the air velocity vectors are also superimposed and the length of the vector represents the relative magnitude of the air velocity. The corresponding particle velocity vectors are shown in Figure 4.5. According to Eqs.(4.1)-(4.3), the air sensitivity index of the light particles (ρ_l = 400 kg/m^3) is ζ_l =0.423 and is much greater than that of the heavy particles (ρ_h =7800 kg/m^3 and ζ_h = 0.054). This implies that the air flow should have a more significant impact on the motion of light particles than the heavy particles. As shown in Figure 4.4, the deposition of heavy particles drives the air to flow downwards initially, and then a 'U'-turn of air flow is observed when meeting the base and the side wall of the die cavity (Figures 4.4a and b). The light particles that have higher air sensitivity are blown upwards by the air, which flows upwards on the left hand side of die (Figures 4.4b and 4.5b). An air bubble is subsequently formed among the light particles (Figures 4.4c and d). As the entrapped air escapes through the void space between the particles, the light particles fall and flow down along the top surface of heavy particles (Figures 4.4d, 4.4e, 4.5d and 4.5e). Finally, the light particles settle down on the top of the heavy particles (Figure 4.4f). Due to the effect of air, it is difficult to deposit the air-sensitive particles (i.e., light particles) to the bottom region of the die, and the die is almost completely filled by the heavy particles except for a small part at the top of the die (Figure 4.4f).

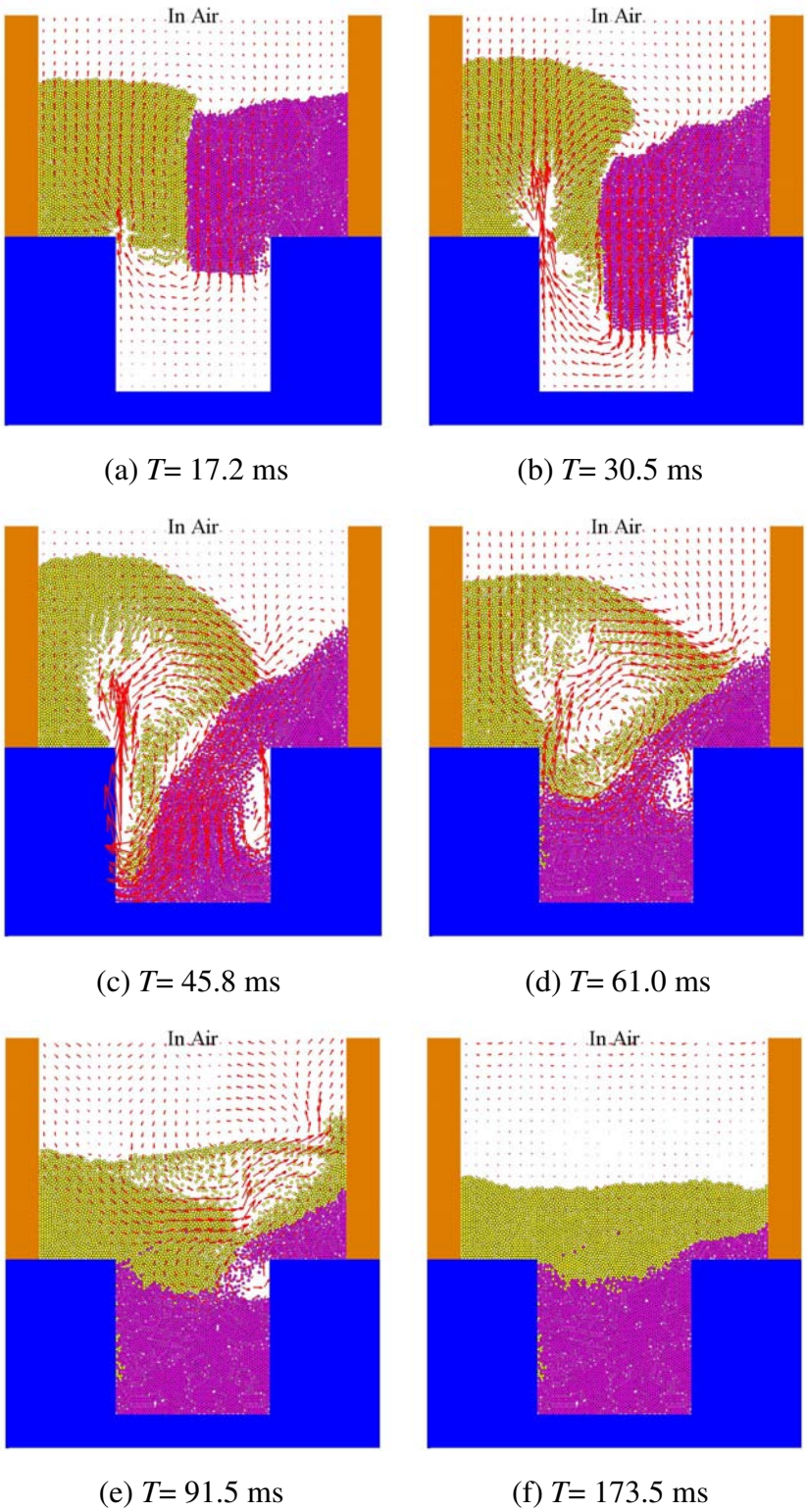

(a) T= 17.2 ms (b) T= 30.5 ms

(c) T= 45.8 ms (d) T= 61.0 ms

(e) T= 91.5 ms (f) T= 173.5 ms

Figure 4.4 Snapshots of die filling with a bi-column mixture in air with air velocity vectors superimposed. The light and heavy particles are coloured in yellow and magenta, respectively.

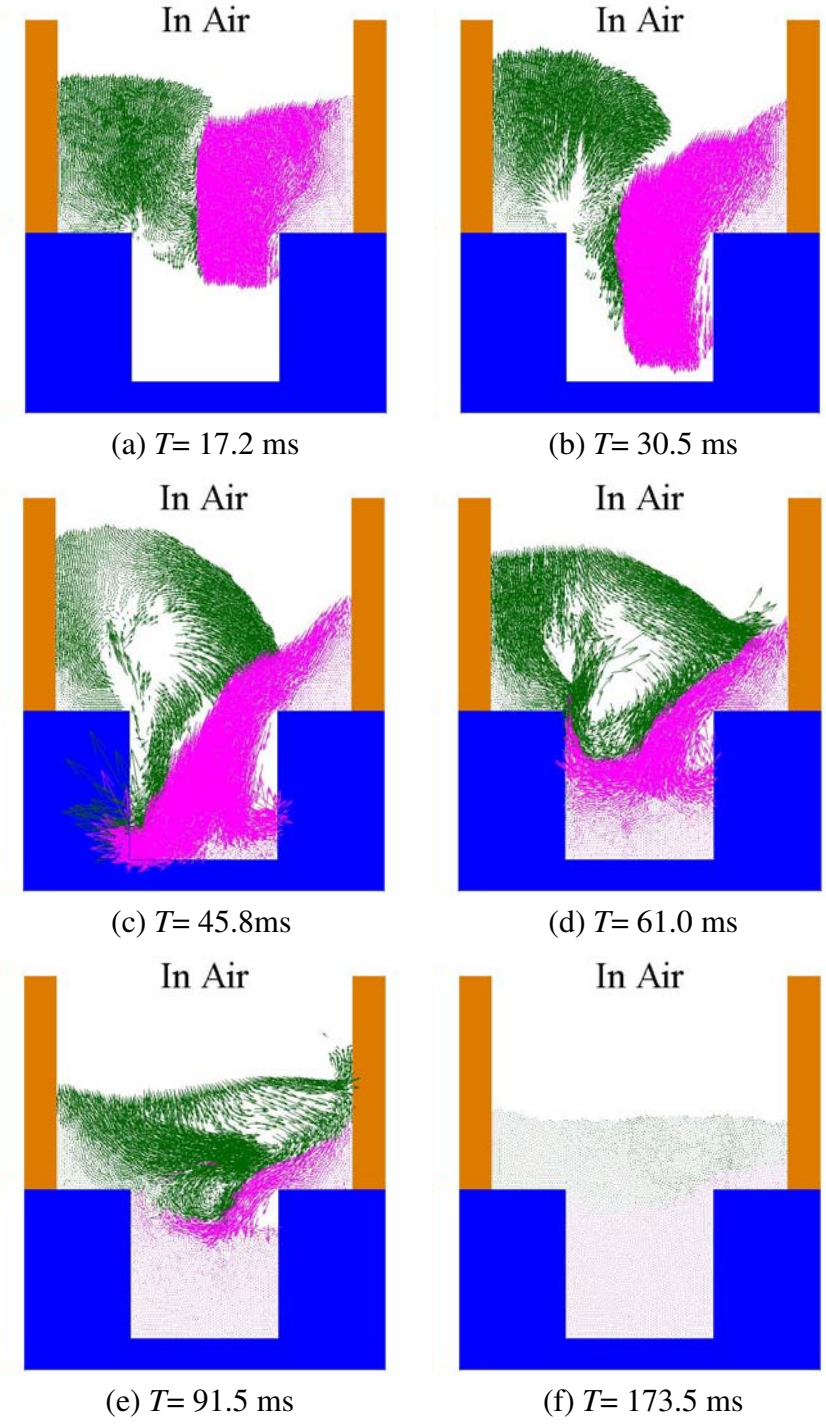

(a) T= 17.2 ms (b) T= 30.5 ms

(c) T= 45.8ms (d) T= 61.0 ms

(e) T= 91.5 ms (f) T= 173.5 ms

Figure 4.5 Particle velocity vectors during die filling with a bi-column mixture in air. The green and magenta vectors represent the velocity vectors of light and heavy particles, respectively.

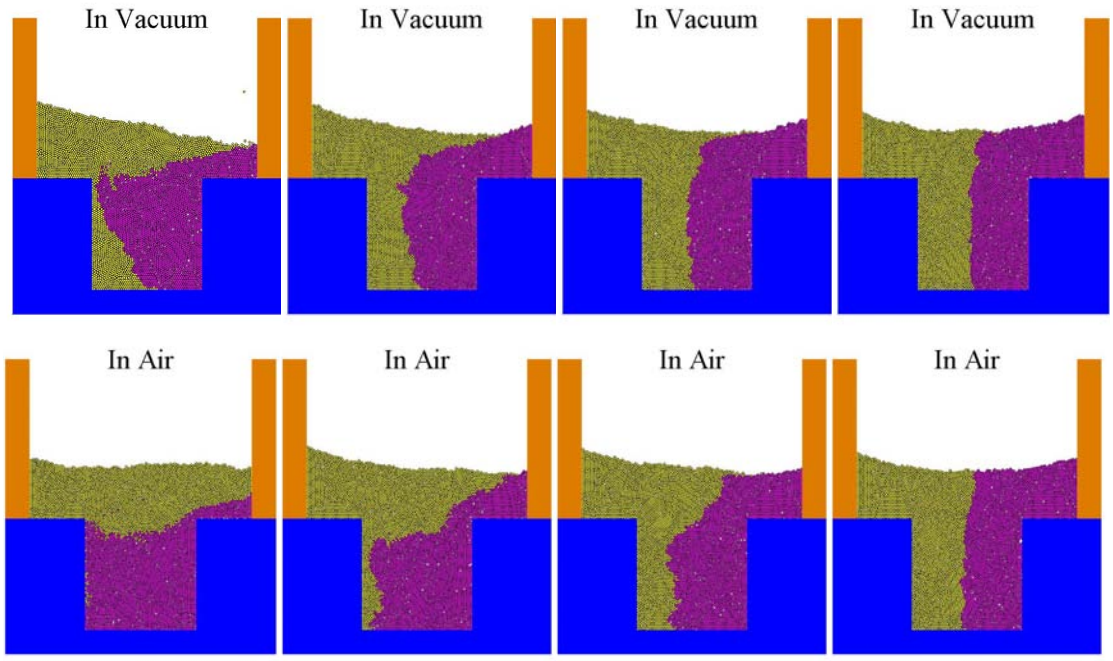

(a) $\rho_l / \rho_h = 0.05$ (b) $\rho_l / \rho_h = 0.2$ (c) $\rho_l / \rho_h = 0.4$ (d) $\rho_l / \rho_h = 0.8$

Figure 4.6 Final packing states for die filling with bi-column mixtures of various density ratios in a vacuum (top row) and in air (bottom row). The density of heavy particles ρ_h is fixed as 7800 kg/m^3.

4.2.2. The effect of density ratio

Bi-column mixtures of various density ratios were considered to investigate the effect of density ratio. Figure 4.6 shows the final packing states for die filling with bi-column mixtures of various density ratios. The density ratio is defined here as the ratio of the density of light particles to that of heavy particles (i.e., ρ_l / ρ_h). In Figure 4.6, the top row shows the states after die filling in a vacuum and the bottom row shows the states in air. For all the cases, the density of heavy particles ρ_h is fixed as 7800 kg/m^3. It is observed from Figure 4.6 that as the density ratio increases, the amount of light particles deposited into the die increases and the powder system becomes more symmetric to the centre line when the density ratio is close to one. During die filling with bi-column mixtures, competing flow occurs with the heavy

particles moving towards the side of the light particles due to the higher inertia, and this competition in flow becomes more balanced as the density difference is reduced. When air is present, the entrapped air prevents the air-sensitive particles (i.e., light particles) flowing into the die and consequently the air-inert particles (i.e., heavy particles) can be delivered into the die more easily. As a result, even fewer light particles are delivered into the die in air compared to in a vacuum for a given density ratio (see Figure 4.6).

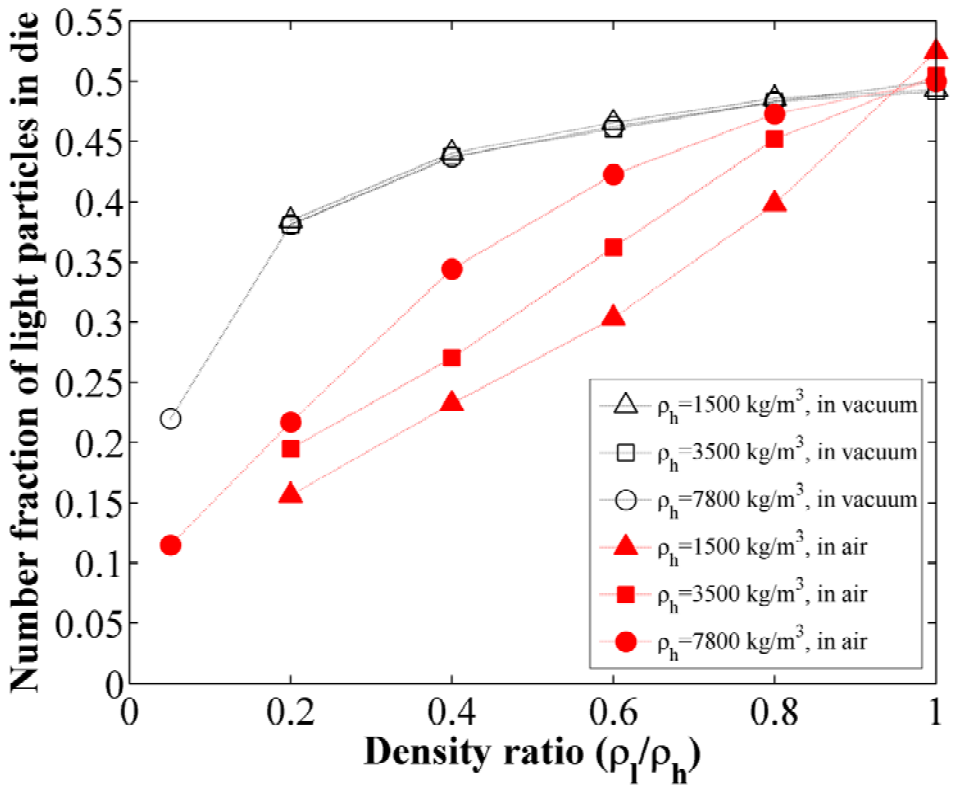

Figure 4.7 Number fraction of light particles in the die for die filling with bi-column mixtures of various density ratios.

In order to quantify the effect of density ratio on die filling with bi-column mixtures, the number fraction of light particles (NFLP) in the die is plotted as a function of density ratio ρ_l / ρ_h in Figure 4.7, in which the density of heavy particles ρ_h is fixed for each curve and three different densities of heavy particles (ρ_h = 1500 kg/m^3, 3500

kg/m^3 and 7800 /m^3) are considered. As observed in Figure 4.7, NFLP generally increases as the density ratio increases until it reaches a value around 0.5, when the density ratio is equal to unity, implying that two 'columns' of the particle system have the same particle density. For die filling in a vacuum, the NFLP-density ratio curves for three different values of ρ_h coalesce into one, which indicates that the NFLP depends only on the density ratio and it is insensitive to the absolute values of particle densities.

It is observed in Figure 4.7 that for die filling in air, the NFLP is lower than that in a vacuum for a specified density ratio which is not equal to unity, due to the fact that the flow of air hinders the delivery of light particles into the die. It is also observed that in the presence of air the NFLP increases as ρ_h increases for a specified density ratio which does not equal unity. This is because the particles become less sensitive to the effect of air as the particle densities increase so that the impact of airflow on the competing filling process is reduced. As a result, the dependence of NFLP on the density ratio for die filling in air is also governed by the absolute values of the particle densities.

4.3. Die filling with bi-layer mixtures

Bi-layer mixtures in which the particles in two layers have different densities were also used in die filling. As shown in Figure 4.8, two cases with bi-layer mixtures are

considered for die filling with a stationary shoe and a moving shoe: i) die filling with a HL mixture, in which the layer of heavy particles is located at the top and the layer of light particles at the bottom (Figure 4.8a) and ii) die filling with a LH mixture, in which the layer of light particles is at the top and the layer of heavy particles at the bottom (Figure 4.8b). The light and heavy particles are colour-coded in yellow and magenta, respectively. The light particles have a density of 400 kg/m^3 and an air sensitivity index of 0.423, and the heavy particles have a density of 7800 kg/m^3 and an air sensitivity index of 0.054. All the particles have the same diameter of 130μm. The die filling processes with HL mixture and LH mixture are discussed, respectively, in the following sections.

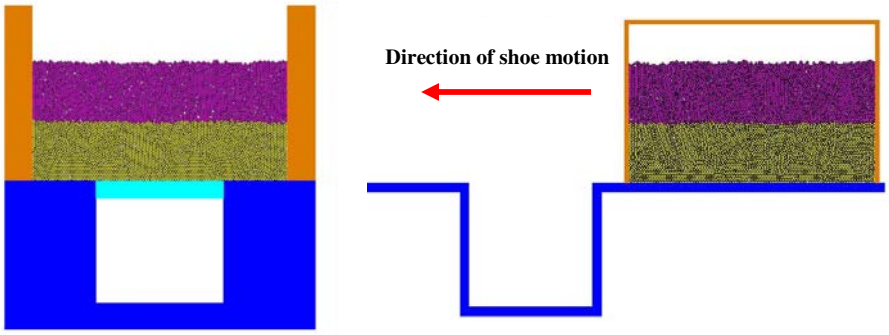

(a) Die filling with a HL mixture

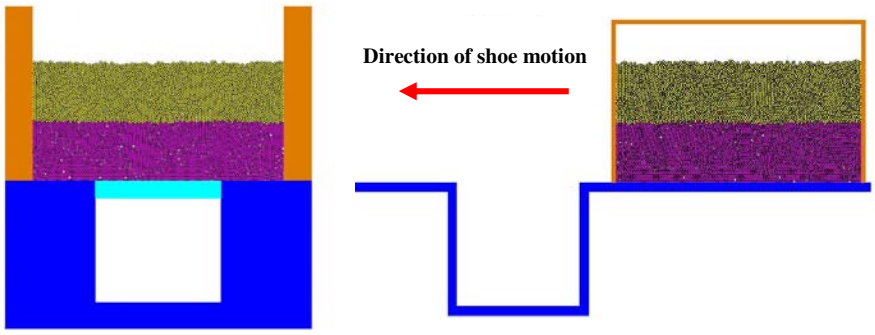

(b) Die filling with a LH mixture

Figure 4.8 Numerical models for die filling with bi-layer mixtures.

4.3.1. HL mixture

Figure 4.9 shows the powder flow patterns during die filling with a HL mixture from a stationary shoe. In a vacuum, the powder flows fast and smoothly, and the particles of different densities flow together (Figures 4.9a-d). In the presence of air, the downward flowing powder stream pushes the air aside and two air bubbles are formed adjacent to the die walls (Figures 4.9e–h). The light particles, which are sensitive to air, are inhibited by the entrapped air while flowing down along the edges of the die. As a result, more heavy particles are deposited into the die through the centre of the die opening (Figures 4.9f-h). Consequently, fewer light particles are delivered into the die (Figure 4.9h), compared to when filling in a vacuum (Figure 4.9d).

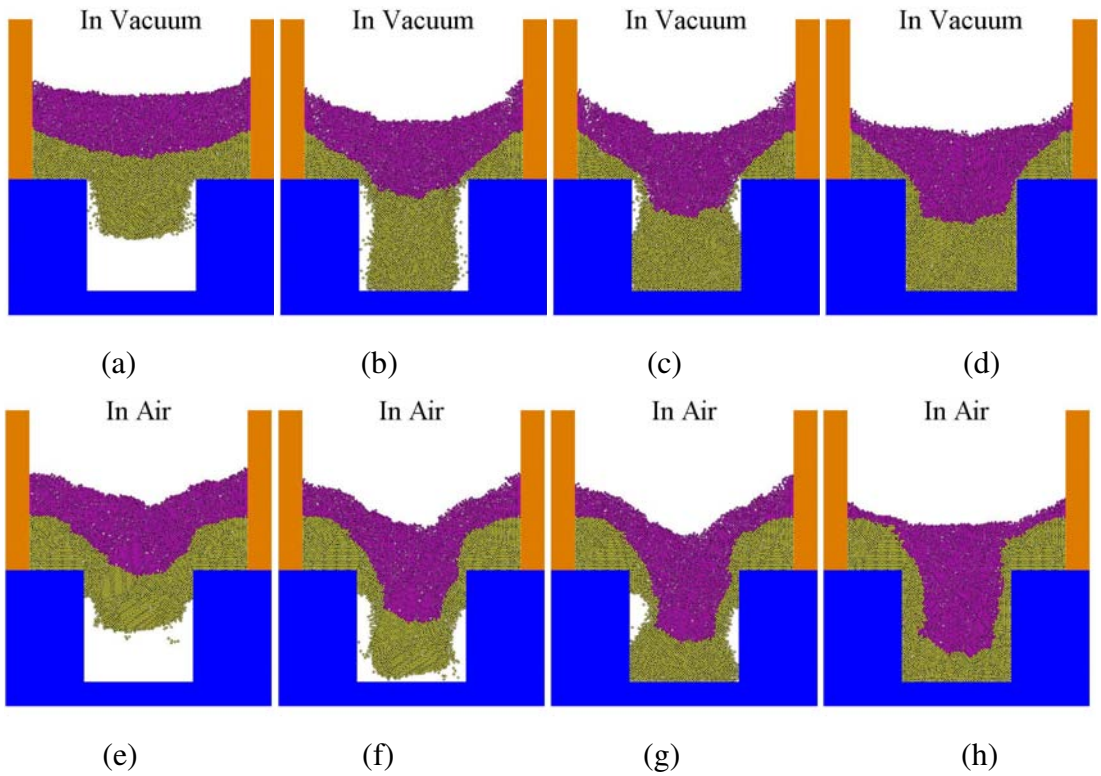

Figure 4.9 Powder flow patterns with HL mixture during die filling from a stationary shoe in a vacuum (top row) and in air (bottom row).

The die filling processes with the HL mixture from a moving shoe were also simulated. Figures 4.10 shows the powder flow patterns during die filling at a shoe speed of 70 mm/s in a vacuum and in air. At such a speed, nose flow (Wu et al., 2003c) dominates the die filling process, so that the air can easily escape from the die and it has a very limited impact on the powder flow behaviour. Hence the overall flow pattern in air (Figures 4.10e-h) is similar to that in a vacuum (Figures 4.10a-d). The light particles are firstly fed into the die from the bottom of the powder mass in the shoe, and then the heavy particles flow over the light layer and avalanche into the leading side (left hand side) of the die. The deposition of heavy particles forces the light particles to move upwards and backwards. Thus, after die filling the heavy particles occupy the bottom-left region of the die and the light particles are pushed to the top-right region with some light particles expelled out of the die (Figures 4.10d and h).

Figure 4.11 shows the powder flow patterns during die filling at a shoe velocity of 170 mm/s. It can be seen that by increasing the shoe velocity, the die opening is more rapidly covered by the powder mass. This reduces the chance for the heavy particles in the top layer to flow into the die, so that fewer heavy particles are delivered into the die after die filling. Comparing the powder flow patterns in a vacuum and in air, it is clear that the entrapped air can slow down the filling process (Figures 4.11c and 4.11g).

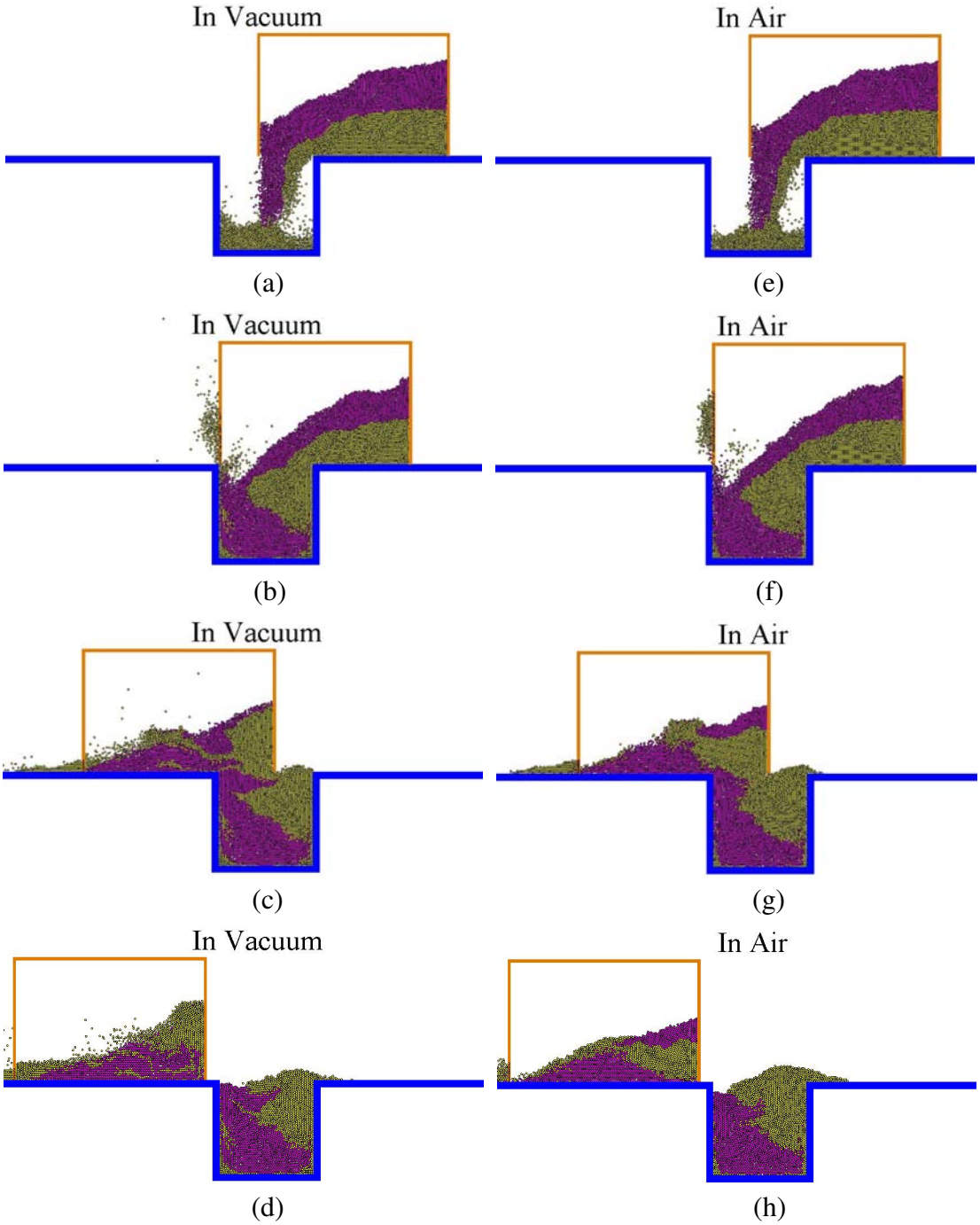

Figure 4.10 Powder flow patterns with HL mixture during die filling at a shoe velocity of 70mm/s in a vacuum (left column) and in air (right column).

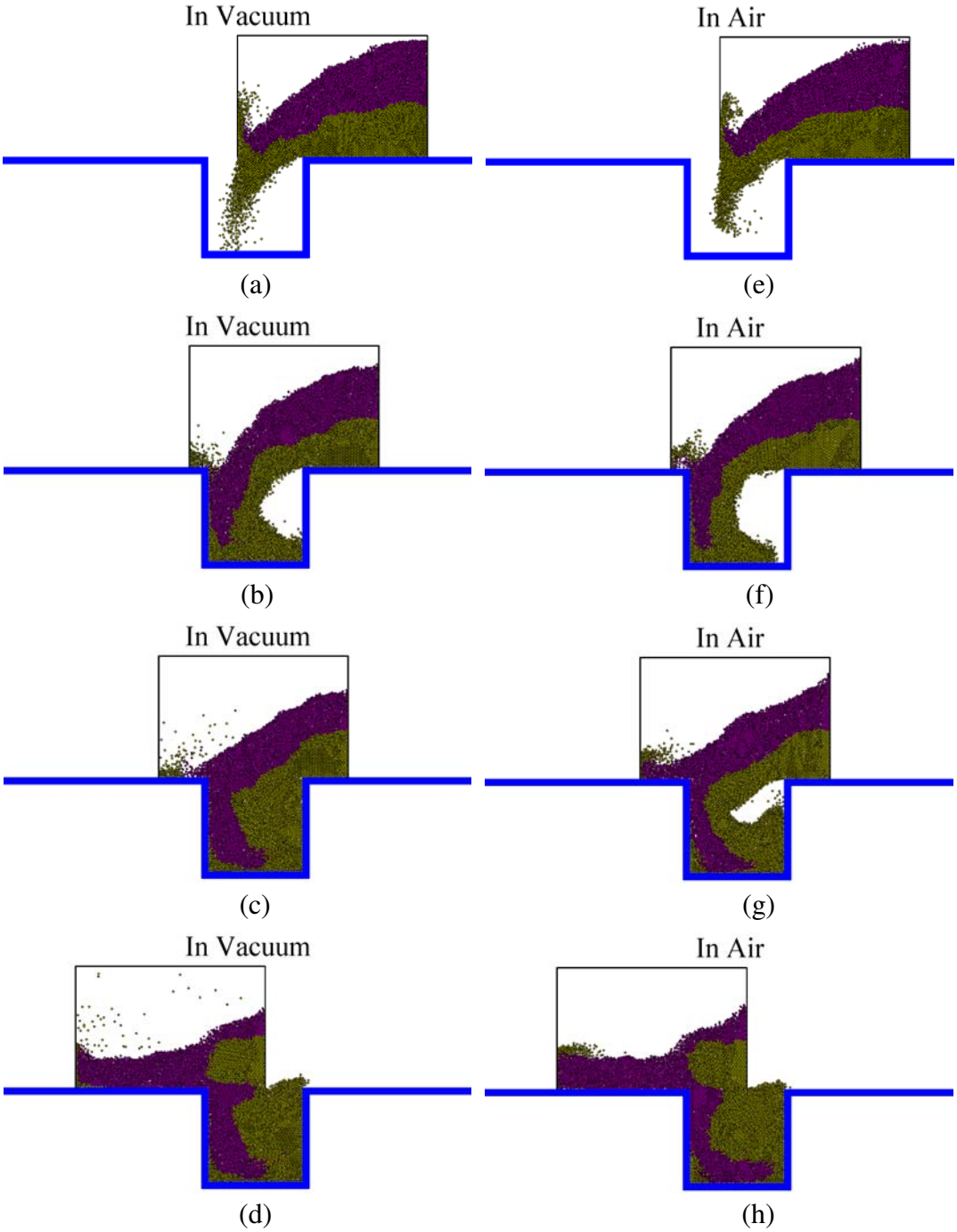

Figure 4.11 Powder flow patterns with HL mixture during die filling at a shoe velocity of 170mm/s in a vacuum (left column) and in air (right column).

Figure 4.12 shows the final powder packing states in the die for die filling with shoe velocities ranging from 35 – 170 mm/s. It can be seen that, for all cases considered, the heavy particles always occupy the bottom-left region of the die and the light particles are packed in the top-right region. Due to the density difference, the light particles are pushed upwards by the heavy particles forming a heap at the top of die. It is also observed that as the shoe speed increases, the amount of heavy particles deposited into the die decreases. The corresponding number fractions of light particles (NFLP) in the die are presented in Figure 4.13. For die filling at a zero shoe velocity (i.e. from a stationary shoe), the NFLP is much lower in the presence of air compared to in a vacuum. This is because the entrapped air prevents the light particles from flowing into the die (Figure 4.9). For die filling from a moving shoe, the NFLP generally increases with the shoe velocity. This is consistent with the observation in Figure 4.12. As the shoe velocity increases, the powder mass moves more rapidly over the die opening. This inhibits the heavy particles that are originally located at the top flowing into the die and provides more chances for light particles to flow into the die by detaching from the bottom of the powder mass in the shoe. Therefore, the NFLP in the die can be increased by increasing the shoe velocity. It is also observed from Figure 4.13 that the presence of air has a very limited effect on the NFLP as the nose flow dominates the flow process for all the shoe speeds considered.

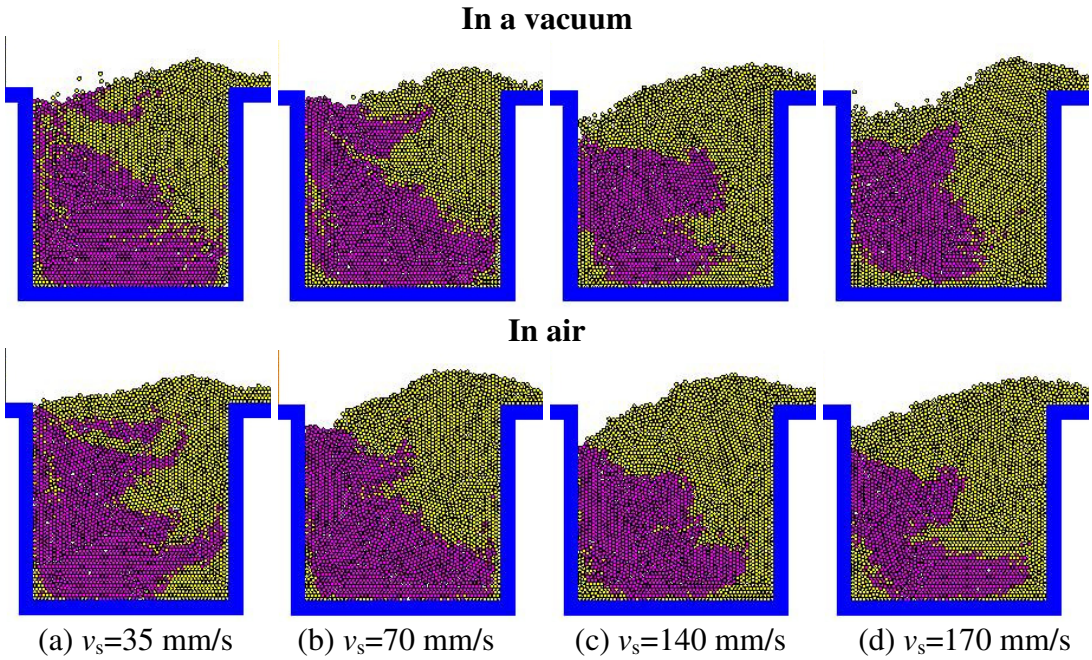

Figure 4.12 Final powder packing states in the die with HL mixture for die filling at different shoe velocities in a vacuum (top row) and in air (bottom row).

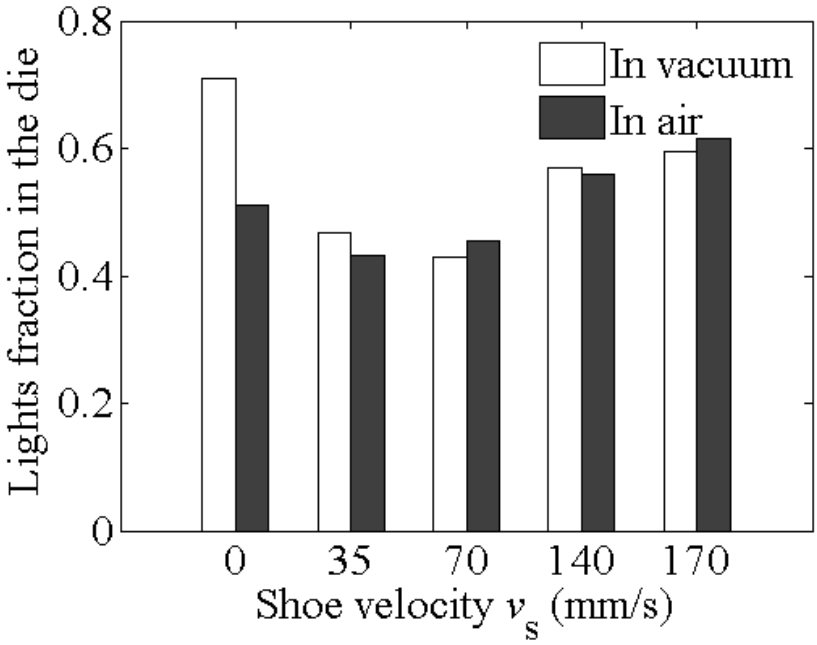

Figure 4.13 Number fractions of light particles in the die for die filling with a HL mixture at different shoe velocities.

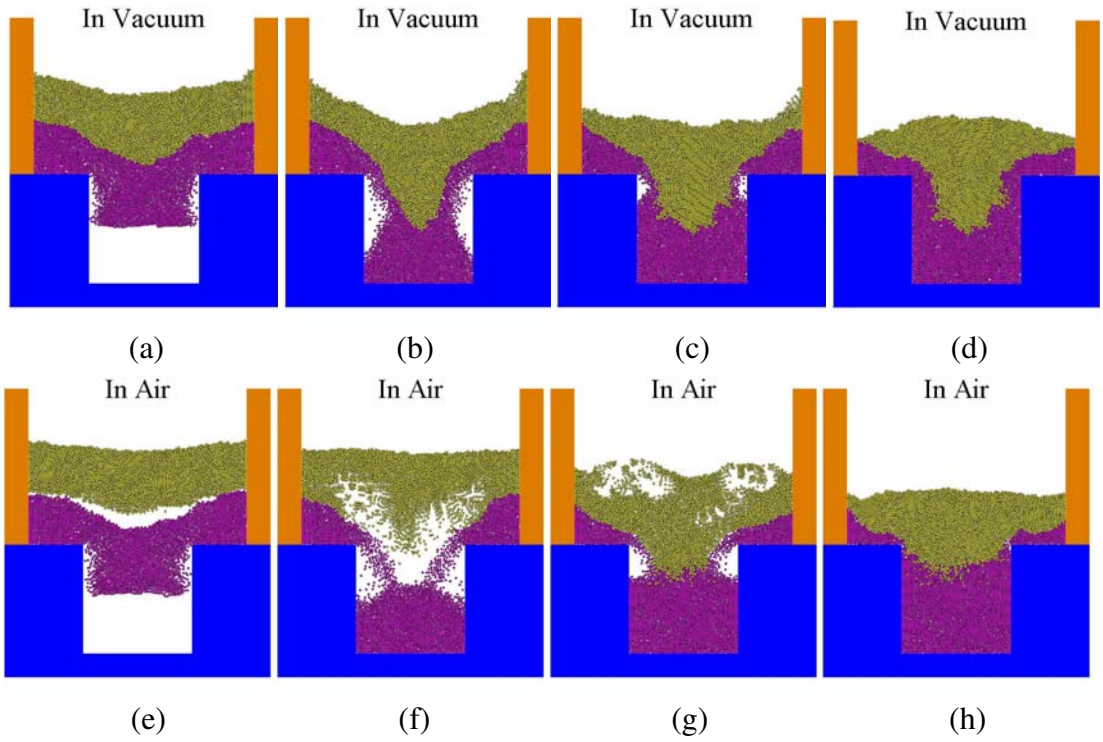

Figure 4.14 Powder flow patterns during die filling with a LH mixture from a stationary shoe in a vacuum (top row) and in air (bottom row).

4.3.2. LH mixture

The powder flow patterns during die filling from a stationary shoe with the LH mixture (i.e., the layer of light particles at the top and the layer of heavy ones at bottom), are shown in Figure 4.14. During die filling in a vacuum, powder flow is also smooth and rapid. Due to the large density difference, the region of light particles is squeezed upwards by the surrounding heavy particles. Therefore, a convex profile is formed on the top free surface after die filling (Figure 4.14d). In addition, a much sharper interface between light and heavy particles was created when compared to the flow with HL mixture (Figure 4.9d). In the presence of air, as the powder mixture starts to flow, due to the high air sensitivity of light particles the flow of light particles is significantly restricted by the air flow, therefore a gap is induced between the light

and heavy layers (Figures 4.14e and 4.14f). Several air bubbles are formed in the light particle layer and then erupt when they reach the top surface (Figures 4.14f and 4.14g). Because of the resistance of air to the flow of the light particles, fewer light particles are deposited into the die, compared to the filling in a vacuum (Figures 4.14d and 4.14h).

The powder flow patterns during die filling with the LH mixture from a move shoe at a velocity of 70 mm/s are shown in Figure 4.15. It can be seen that at this shoe speed, nose flow dominates the die filling process. Due to the density difference, the flow of heavy particles can push the light particles deposited in the die to the left hand side and even out of the die. In the presence of air, when the air is entrapped by the powder mass (Figures 4.15g and h), the entrapped air can also prevent the air-sensitive light particles from flowing into the die. Thus, even fewer light particles flow into the die during die filling in air. By increasing the shoe velocity to 170 mm/s and using the same LH mixture, as shown in Figure 4.16, the die opening is soon covered by the powder mass. The particles delivered into the die mainly come from the bottom layer (i.e. heavy particle layer) and the light particles initially located at the top have less chance to flow into the die. In the presence of air, the air can be entrapped inside the die cavity and several air bubbles are formed at the interface between two layers, which can prevent the light particles from flowing into the die.

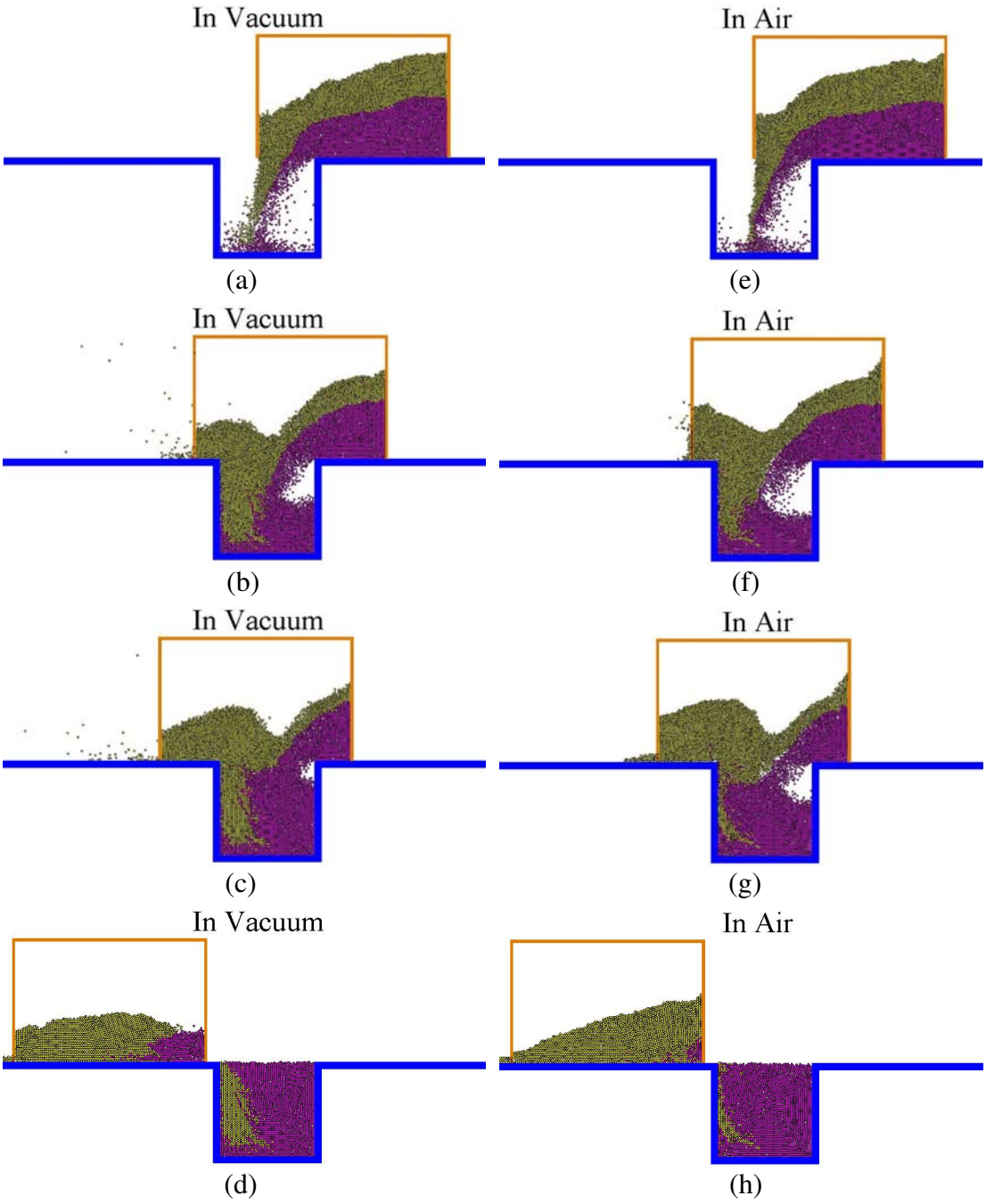

Figure 4.15 Powder flow patterns with the LH mixture during die filling at a shoe velocity of 70 mm/s in a vacuum (left column) and in air (right column).

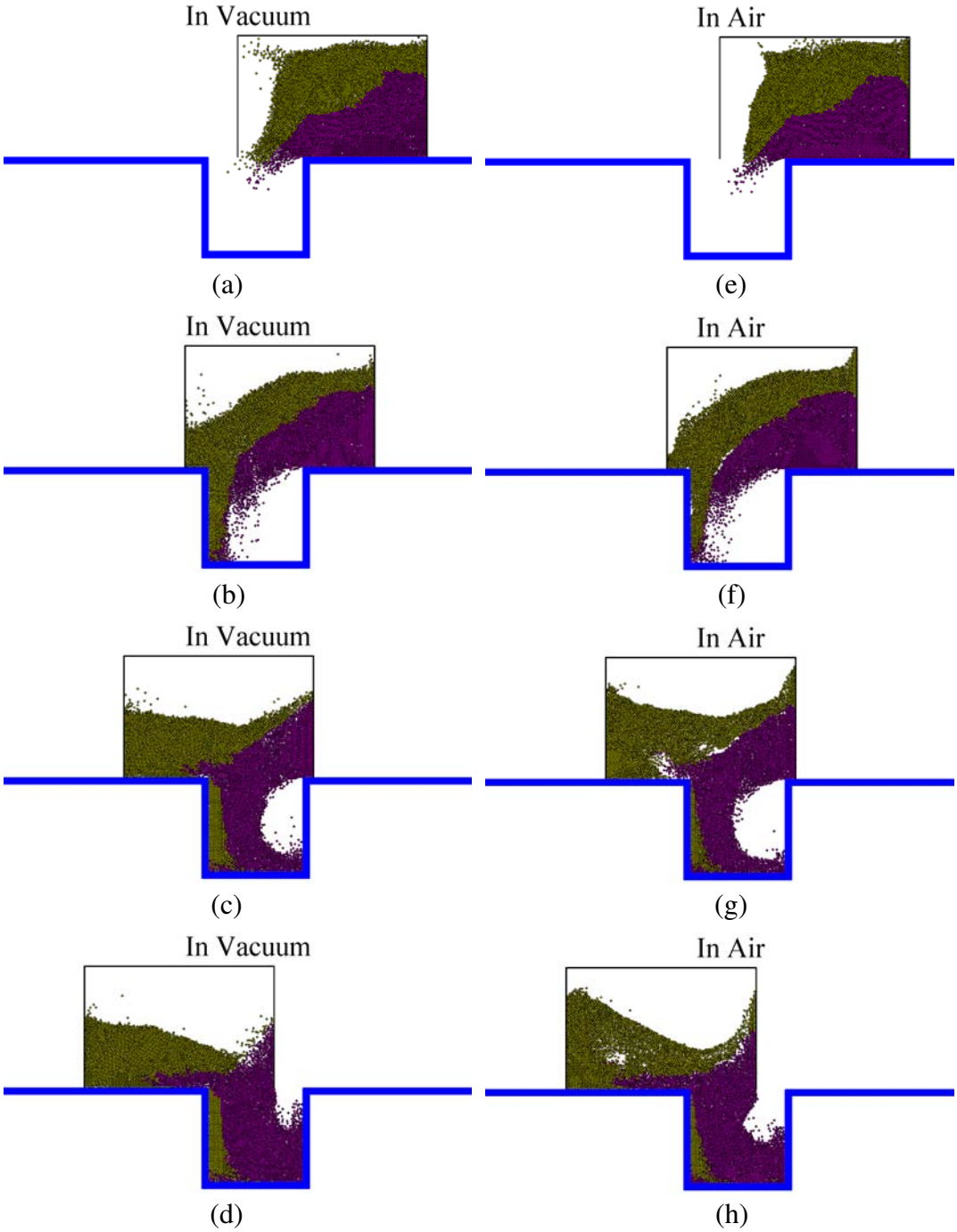

Figure 4.16 Powder flow patterns with the LH mixture during die filling at a shoe velocity of 170 mm/s in a vacuum (left column) and in air (right column).

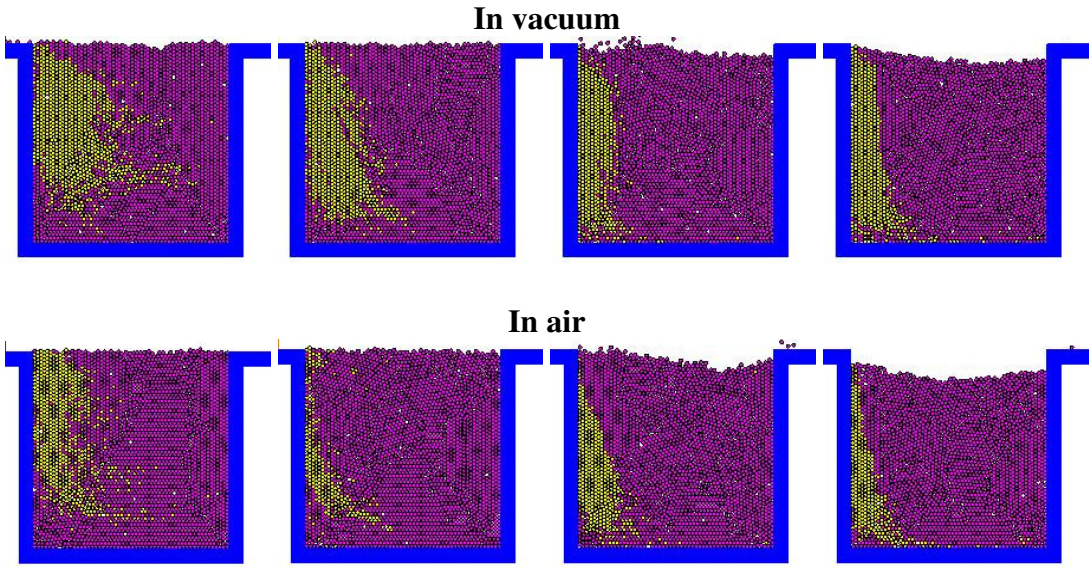

Figure 4.17 Final powder packing states in the die with the LH mixture for die filling at different shoe speeds in a vacuum (top row) and in air (bottom row).

Final packing states in the die for die filling at different shoe velocities with the LH mixture are shown in Figure 4.17. It is found that the light particles are predominantly filled into the left hand side region of the die with the majority of the die cavity occupied by heavy particles. During die filling with the LH mixture, the light particles are restrained by the surrounding heavy particles and the top free surface of the powder bed is even (Figure 4.17), unlike die filling with the HL mixture in which the light particles can rise out of the die opening and form a slope on the top surface (see Figure 4.12). By comparing die filling in a vacuum and in air, it is clear that fewer light particles are deposited into the die in the presence of air. The corresponding number fractions of light particles deposited into the die at various shoe velocities are shown in Figure 4.18. It is evident that the NFLP generally decreases with the shoe velocity as the deposition of light particle from the top layer is impeded during die filling at a higher shoe velocity, for which the bulk flow becomes dominant. The

presence of air can also reduce the NFLP, because the flow of the top light layer can be significantly inhibited by the entrapped air.

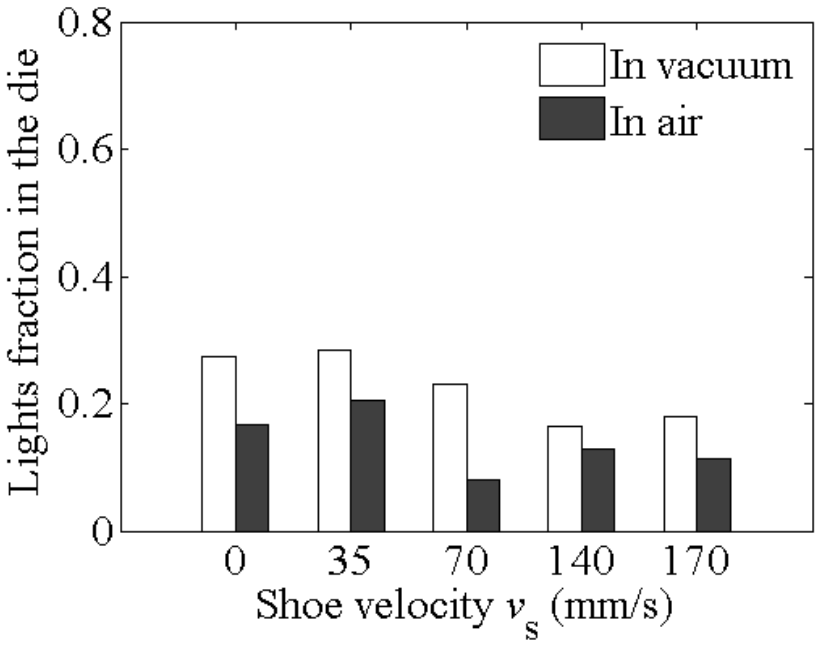

Figure 4.18 Number fraction of light particles in the die with the LH mixture for die filling at different shoe speeds.

4.4. Summary

In this chapter, die filling with bi-column and bi-layer mixtures has been reported. The mixtures comprise of identical sized particles but of different densities. The influence of the air on powder flow depends on the particle properties (e.g., density, size etc.). Therefore, an index is proposed to describe the air sensitivity of particles in terms of particle size and particle density.

During die filling with a bi-column mixture, the heavy particles prevent the light ones flowing into the die by pushing them due to the difference in inertia. In the presence of air, it is easier for the entrapped air to escape through the powder bed of light

particles which are more sensitive to the air. Therefore, even fewer light particles are deposited into the die in air compared to in a vacuum. The number fraction of light particles in the die (NFLP) increases as the density ratio ρ_l / ρ_h increases. The NFLP depends only on the particle density ratio for die filling in a vacuum but, for die filling in air, the NFLP depends not only on the particle density ratio but also on the absolute values of particle densities.

During die filling with a bi-layer mixture, the presence of air also prevents the light particles (i.e. air-sensitive particles) flowing into the die and therefore fewer light particles are deposited into the die in air compared to in a vacuum. As the shoe velocity increases, the powder mass covers the die opening more rapidly so that it becomes more difficult for the particles from the top layer of the powder bed to flow into the die. As a result, the number fraction of the component particles in the die, which were initially located at the top of the mixture, is reduced when the shoe moves faster.

CHAPTER 5: DENSITY-INDUCED SEGREGATION

5.1. Introduction

In this chapter, density-induced segregation during the die filling process was investigated using binary mixtures of particles with identical size but different densities. Die filling with random mixtures, which were generated by randomly mixing the light and heavy particles, was considered first. The powder flow patterns and the evolution of component concentrations in the die region were analyzed. Various shoe velocities and mixtures with a range of particle density ratios were employed to explore the effects of shoe velocity and particle density ratio on the segregation behaviour. The randomly generated mixtures are always slightly non-uniform. However, a perfectly uniform mixture (i.e., ordered mixture) can be generated by placing the particles in a regular way. Die filling with ordered mixtures was then simulated and compared with die filling with random mixtures, from which the effect of non-uniformity of the random mixtures on the segregation behaviour was examined. Some of the results presented in this chapter have also been reported in our recent publications (Guo et al., 2008; 2009a).

5.2. Die filling with random mixtures

A binary random mixture was generated as follows. First, 3000 particles of low density (ρ_l = 400 kg/m^3) were randomly generated in a specified region within the shoe and then 3000 particles of high density (ρ_h = 7800 kg/m^3) were randomly generated in the same region, filling the void space between the light particles. All the

particles have an identical diameter of 130 μm. The initial generation resulted in a loosely packed bed without interparticle contacts. The particles were then deposited under the gravitational force in the shoe until reaching a stable state with negligible kinetic energy. Thereby, a randomly packed binary mixture was produced in the shoe. A typical packing pattern of the generated binary mixture is shown in Figure 5.1, in which the light and heavy particles are colour-coded in yellow and magenta, respectively.

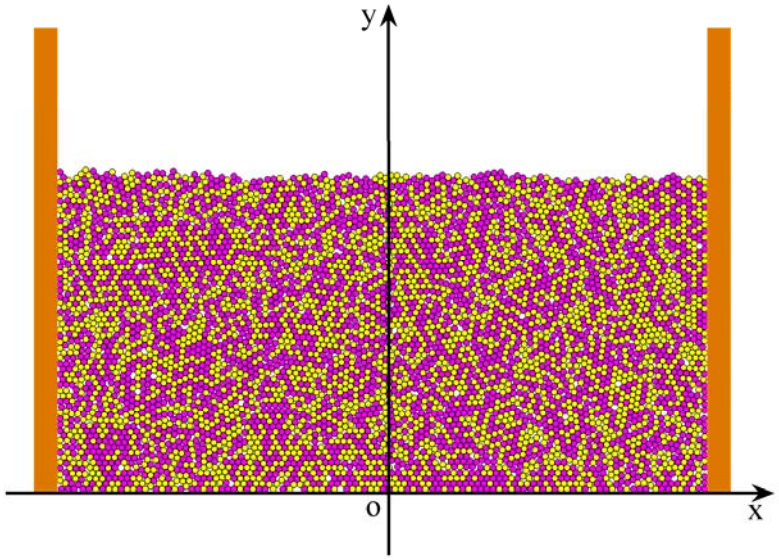

Figure 5.1 A random mixture of particles with the same size but different densities. (light and heavy particles are coloured in yellow and magenta, respectively)

5.2.1. Powder flow patterns

Powder flow patterns during die filling with the random mixture from a stationary shoe in a vacuum and in air are shown in Figure 5.2. During die filling in a vacuum (Figures 5.2a-d), the mixture flows smoothly and rapidly into the die as a single column. At an early stage (Figures 5.2a and b), it is observed that there is a gap between the flowing powder stream and the edges of the die opening. This corresponds to the so-called ‘empty annulus’ observed in hopper flow due to the

boundary effect (Seville et al., 1997). In the presence of air (Figures 5.2e-h), the air is entrapped inside the die cavity and two air pockets are formed near the die walls (Figures 5.2f and g). The light particles (ζ_l = 0.423) are more sensitive to the air compared to the heavy particles (ζ_h = 0.054), hence light particles are much easier to be entrained in the air and fall down more slowly compared to heavy particles during die filling in air. Consequently, a layer of air-sensitive particles (i.e. light particles) is observed to float over the top of the mixture and is separated from the main powder stream (Figures 5.2e-g). Once this powder layer settles onto the inclined top surface, the particles cascade down along the top free surface towards the centre. Therefore, a small pile of light particles is formed at the middle of the top surface after die filling in air (Figure 5.2h).

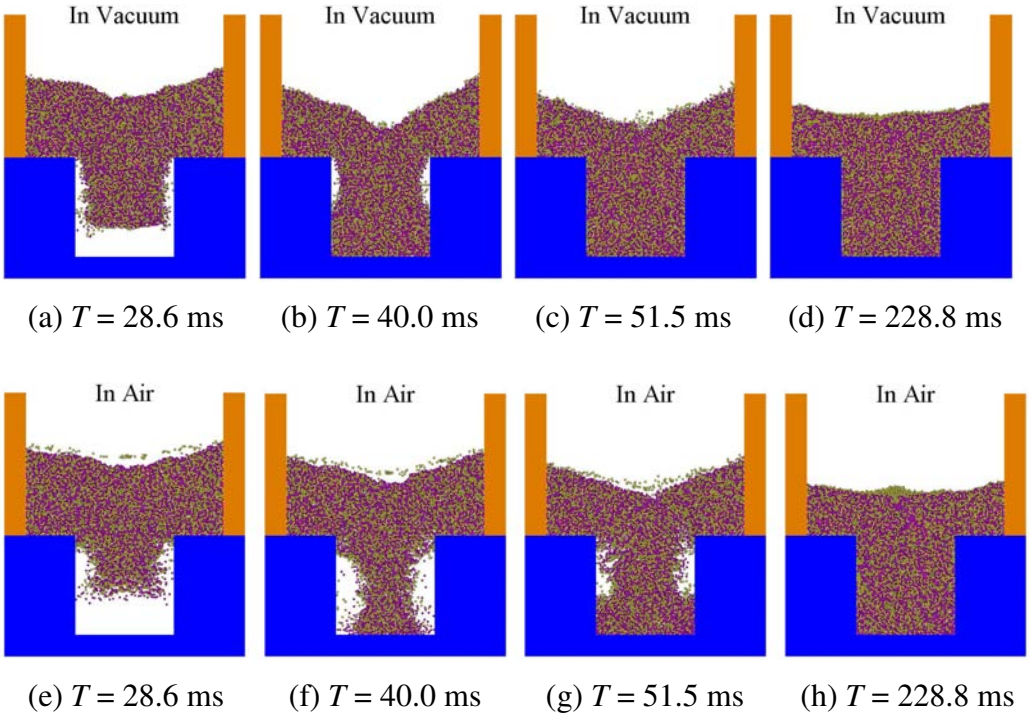

(a) T = 28.6 ms (b) T = 40.0 ms (c) T = 51.5 ms (d) T = 228.8 ms

(e) T = 28.6 ms (f) T = 40.0 ms (g) T = 51.5 ms (h) T = 228.8 ms

Figure 5.2 Die filling from a stationary shoe in a vacuum (top row) and in air (bottom row).

Figure 5.3 shows the powder flow patterns during die filling in a vacuum and in air with a moving shoe at a velocity of 70 mm/s. For this particular case, the die filling is dominated by nose-flow, which is referred to as the flow pattern in which the filling process involves the rapid cascading of powder particles from the top surface of the powder bed to the die cavity (Wu et al., 2003a). Once the main flowing powder stream hits the base of the die (Figure 5.3a) or the deposited powder bed in the die (Figure 5.3b), it divides into two 'rebounding' streams: one bounces forwards and the other one flows backwards. During this process, the light particles located at the front of these two flow streams usually gain higher velocities due to the smaller inertia. Thus, the fronts of rebounding flow streams are rich in light particles. The front of the forward rebounding flow stream can be expelled from the top of the die but the front of the backward rebounding stream is entrapped inside the die by the powder mass above the die opening (Figure 5.3b). Furthermore, a slope is gradually formed on the top free surface in the shoe. When the mixed particles flow down along the slope, the light particles rebound higher and further after collision due to the small inertia and therefore it is easier for the light particles to flow over the heavy ones. These light particles flow down along the surface and finally accumulate at the far front end (Figures 5.3c and d). This feature is consistent with the experimental observation of free surface segregation in heap formation (Drahun and Bridgwater, 1983). During die filling in air at this particular shoe velocity (Figures 5.3e-h), most of air in the die can escape before the powder mass completely covers the die opening, so that the air only slightly affects the powder flow and the flow patterns in air and in a vacuum are similar, as shown in Figure 5.3.

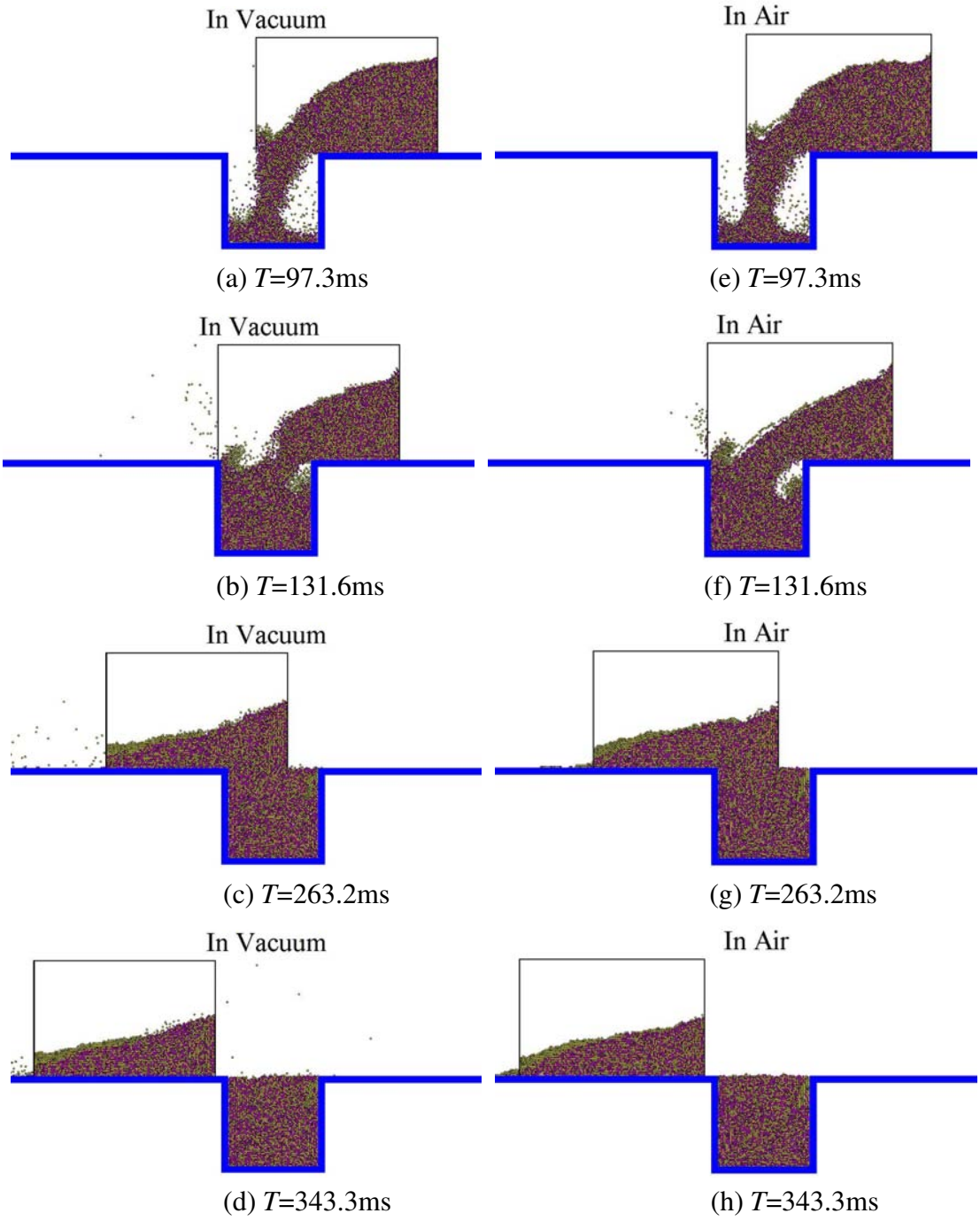

Figure 5.3 Die filling with a moving shoe at a velocity of 70mm/s in a vacuum (left column) and in air (right column).

However, when the shoe velocity is increased to 170 mm/s, as shown in Figure 5.4, the die opening is quickly covered with the powder mass in the shoe. The powder is delivered into the die mainly from the bottom of the powder mass in the shoe rather than from the top free surface, which is referred to as bulk-flow (Wu et al., 2003a). In other word, this die filling process is dominated by bulk-flow. The powder flowing stream first hits the front (left) boundary of the die and then the base; and then bounces backwards (Figure 5.4a). For die filling in a vacuum, the lights-rich front of the backward flowing stream is entrapped by the powder mass above the die opening (Figures 5.4b-d). For die filling in the presence of air (Figures 5.4e-h), an air pocket is formed in the top-right corner of the die (Figure 5.4f) and, when the back of the shoe moves across the right hand edge of the die, the lights-rich front of the flowing stream is expelled out of the die from the right hand side together with the release of the entrapped air (Figures 5.4g and h).

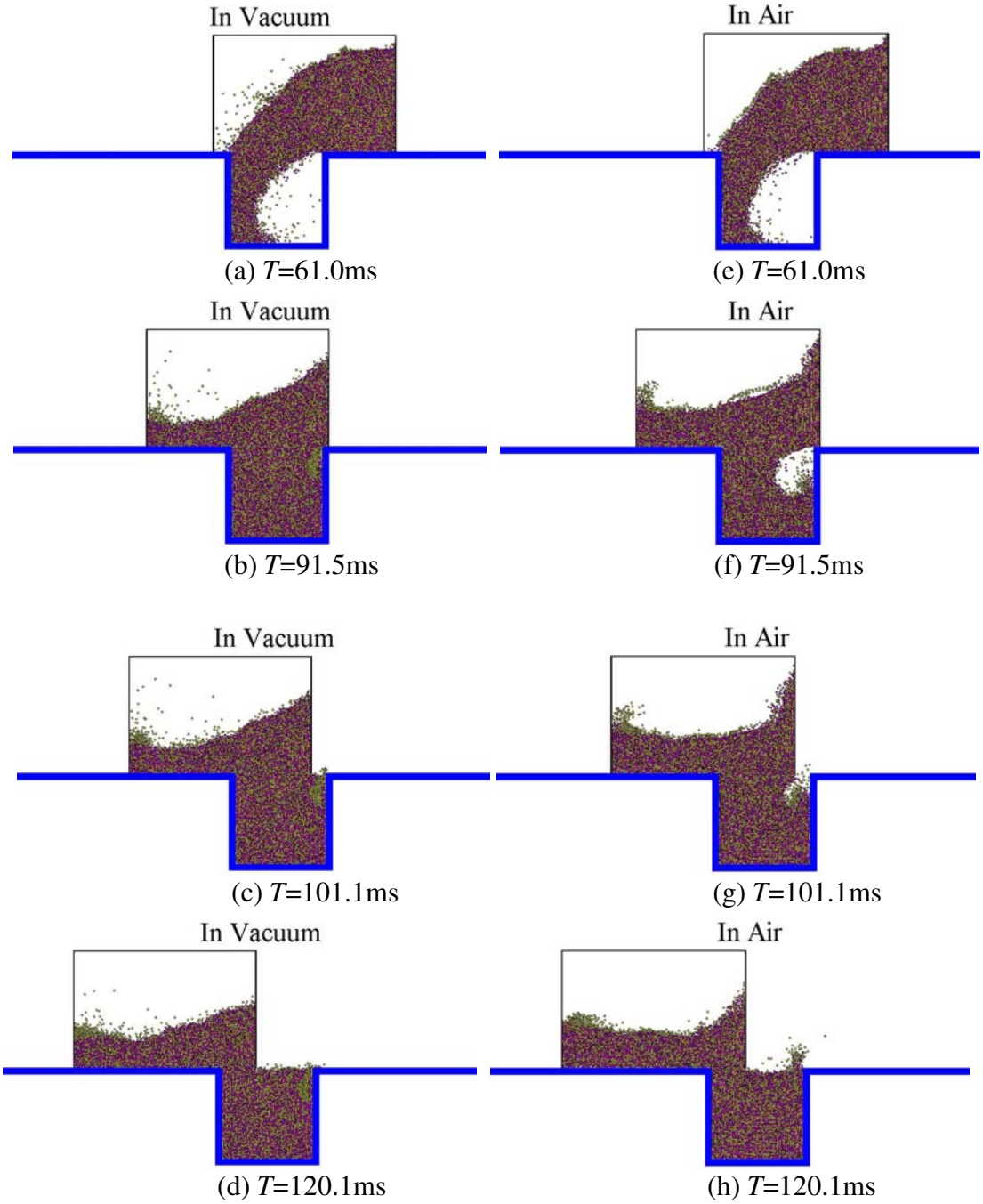

Figure 5.4 Die filling with a moving shoe at a velocity of 170mm/s in a vacuum (left column) and in air (right column).

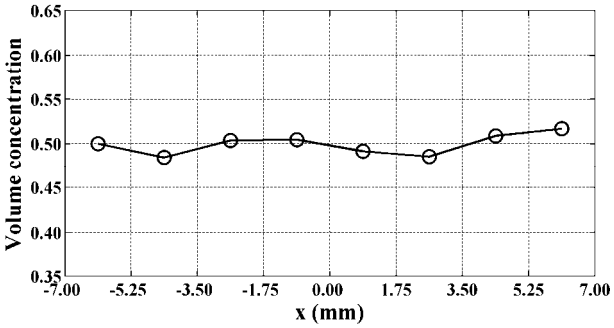

(a) Horizontal distribution

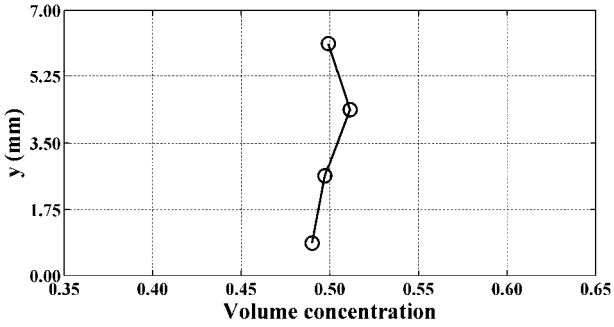

(b) Vertical distribution

Figure 5.5 (a) Horizontal and (b) vertical concentration distributions of the random mixture initially in the shoe before die filling.

5.2.2. Segregation during filling process

To examine the initial packing uniformity, the random mixture generated in the shoe before die filling (Figure 5.1) is partitioned into 8 identical columns in the horizontal direction and 4 identical layers in the vertical direction, respectively. The volume concentration of light particles c_i can be calculated for each cell i by

$$c_i = \tilde{V}_i / V_i \tag{5.1}$$

where $\tilde{V}_i$ and V_i are the solid volume of light particles and the total solid volume of the mixture in a specified cell i, respectively. The horizontal and vertical concentration distributions of the random mixture initially in the shoe before die filling (Figure 5.1) are then obtained and shown in Figure 5.5, in which the volume

concentrations of light particles in the columns are plotted against the horizontal positions x of the columns and the volume concentrations of light particles in the layers against the vertical positions y of the layers. In Figure 5.5, very small fluctuations from the average concentration (i.e., 0.5) are observed for the concentration profiles in both horizontal and vertical directions, indicating that the generated random mixture is slightly heterogeneous.

In order to evaluate the degree of segregation (i.e., non-uniformity), a concentration deviation D_{c} is adopted and can be calculated from

$$D_{\mathrm{c}} = \sqrt{\sum_i \frac{V_i}{V_{\mathrm{bed}}} \times \left[\frac{c_i - c_{\mathrm{m}}}{c_{\mathrm{m}}} \right]^2} \tag{5.2}$$

which is analogous to the definition of segregation index proposed by Zigan et al. (2008). In Eq. (5.2), c_i is the volume concentration of light particles in cell i as defined in Eq. (5.1), c_{m} is the mean volume concentration of light particles in the initial system and V_{bed}, the total solid volume of the powder bed considered, is equal to $\sum_i V_i$. According to Eq. (5.2), the concentration deviation D_{c} equals zero if the volume concentrations of light particles are identical in all cells and equal to the mean value c_{m} in the initial system, which implies that no segregation occurs and a homogeneous packing is obtained. On the other hand, the larger the concentration deviation D_{c} is, the more significant the segregation and the more heterogeneous the packing. In this study, Eq. (5.2) is used to determine the degree of segregation in the horizontal and vertical directions. Hence, two types of concentration deviations are defined: the horizontal concentration deviation, which is referred to as the concentration deviation with the powder bed partitioned horizontally with columns, is

used to quantify the degree of horizontal segregation and the vertical concentration deviation, which is referred to as the concentration deviation with the powder bed partitioned vertically with layers, is used to quantify the degree of vertical segregation. For the random mixture in the shoe before die filling (Figure 5.1), the horizontal concentration deviation is 0.025 with the powder bed partitioned into 8 equal-sized columns and the vertical concentration deviation is 0.018 with the powder bed partitioned into 4 equal-sized layers.

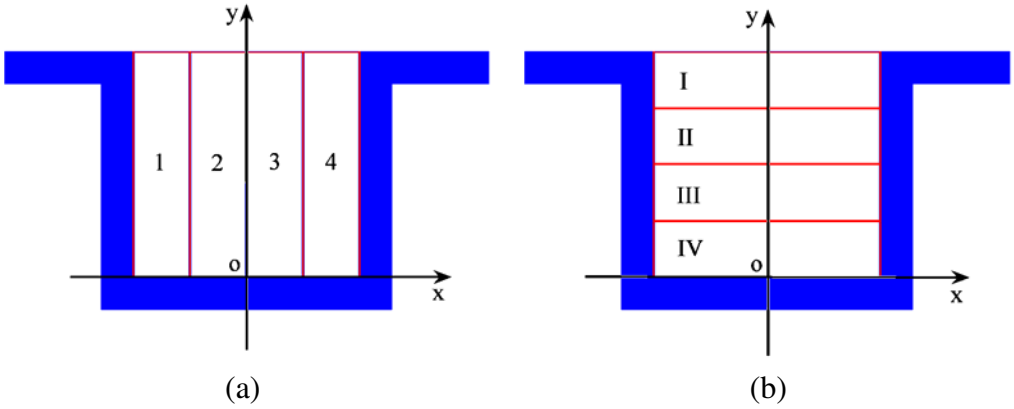

(a) (b)

Figure 5.6 An illustration of partitions for the die region (a) in the horizontal direction and (b) in the vertical direction.

The die region is partitioned by the identical cells in both horizontal and vertical directions as shown in Figure 5.6. The volume concentrations of light particles in the cells can be calculated according to Eq. (5.1) for each stage of die filling to examine the evolution of the concentrations in different parts of the die during the die filling process. Figure 5.7 shows the volume concentrations of light particles c_i in cells 1-4 and cells I-IV (see Figure 5.6) as a function of fractional solid volume discharged V/V_{total} during die filling with a stationary shoe, in which V is the cumulative solid volume of the particles deposited into the die and V_{total} is the total solid volume of the particles that are eventually discharged into the die.

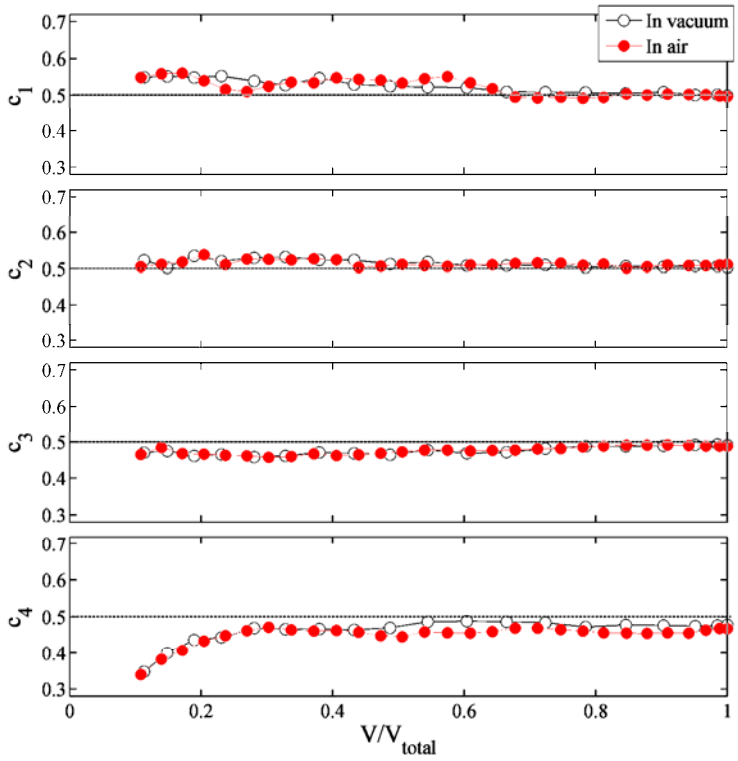

(a) Cells 1-4

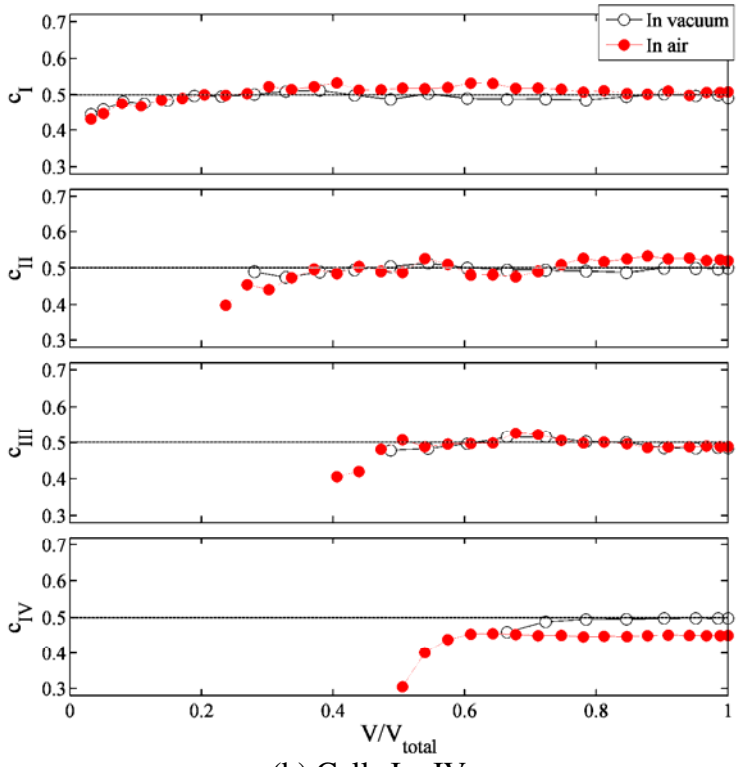

(b) Cells I – IV

Figure 5.7 Volume concentrations of light particles in (a) cells 1-4 and (b) cells I - IV as a function of fractional solid volume discharged during die filling with a stationary shoe (v_s = 0 mm/s).

As shown in Figure 5.7a, in cells 1 and 2, the concentration of light particles is slightly higher than the average value of the system (i.e. 0.5) at the early stage, and thereafter it decreases gradually until reaching a value close to 0.5 at the end of the filling process. In cells 3 and 4, the concentration of light particles is lower than 0.5 at early stage, and then it increases to the final concentration which is slightly lower than 0.5. During die filling with a stationary shoe, as shown in Figure 5.2, the die is filled by the powder right above the die opening, so that the initial concentration distribution in this region could influence the concentration in the die after die filling. As shown in Figure 5.5a, the concentration of light particles is lower than 0.5 in the region $0 < x < 3.5$, which is just above cells 3 and 4 in the die. As a result, a lower concentration of light particles is obtained in cells 3 and 4 during the die filling process.

Figure 5.7b shows the evolution of the volume concentration of light particles in different layers of the die. During die filling in a vacuum, the concentration of light particles oscillates slightly around the average value in each layer. In the presence of air, the concentration of light particles at the early stage is much lower than 0.5 in each layer and it decreases from the top layer to the bottom, which indicates a reduction in the concentration of light particles in the front of the powder flow stream during the filling process as the front reaches each layer. This is due to the different air sensitivities between light and heavy particles. The motion of light particles which have high air sensitivity can be significantly inhibited by the entrapped air so that the deposition of light particles is slower compared to the heavy ones, which leads to an increasing depletion of light particles in the front of the flow stream when the mixture flows down from top to bottom. Finally, a lower concentration of light particles is

obtained in the bottom layer of the die (i.e. cell IV) for die filling in air, compared to the filling in a vacuum.

Figure 5.8 shows volume concentrations of light particles in different cells as a function of fractional solid volume discharged during die filling with a shoe velocity of 70 mm/s. In Figure 5.8a, a higher concentration of light particles is observed in cells 1 and 4 when $0.2 < V/V_{total} < 0.4$. During this period ($0.2 < V/V_{total} < 0.4$), the main flowing stream divides into two 'rebounding' streams (Figures 5.3a and e) and the fronts of forward and backward flowing streams just approach cell 1 and cell 4, respectively. Therefore, the high concentration of light particles in cells 1 and 4 during $0.2 < V/V_{total} < 0.4$ indicates that the fronts of rebounding streams are rich in light particles. At a late stage of the filling process ($0.8 < V/V_{total} < 1$), a sharp reduction in concentration of light particles is observed in cell 1 due to the outflow of light particles from the edge of the die opening (see Figures 5.3b and f).

In Figure 5.8b, the concentration of light particles in the bottom layer c_{IV} decreases during $0.2 < V/V_{total} < 0.5$, and at the same time the concentrations of light particles at the upper layers c_{III} and c_{II} increase as the lights-rich fronts of the powder flowing streams rise up (Figures 5.3a and e). When $V/V_{total} > 0.5$, c_{III} and c_{II} begin to decrease and the concentration of light particles in the top layer c_{I} initially increases due to the inflow of the lights-rich flowing stream and then decreases during the final stage ($0.8 < V/V_{total} < 1$) due to the outflow of light particles from the top (Figures 5.3b and f).

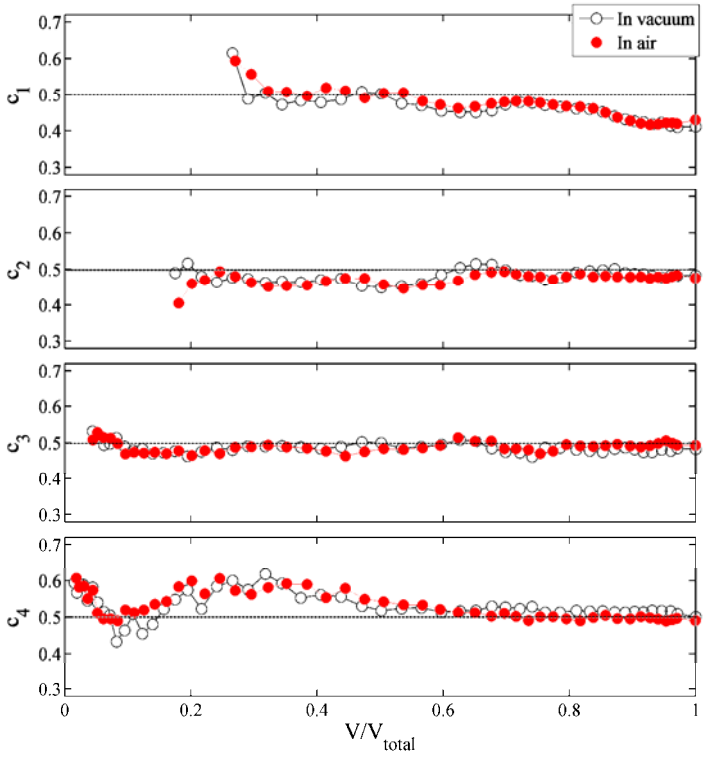

(a) Cells 1-4

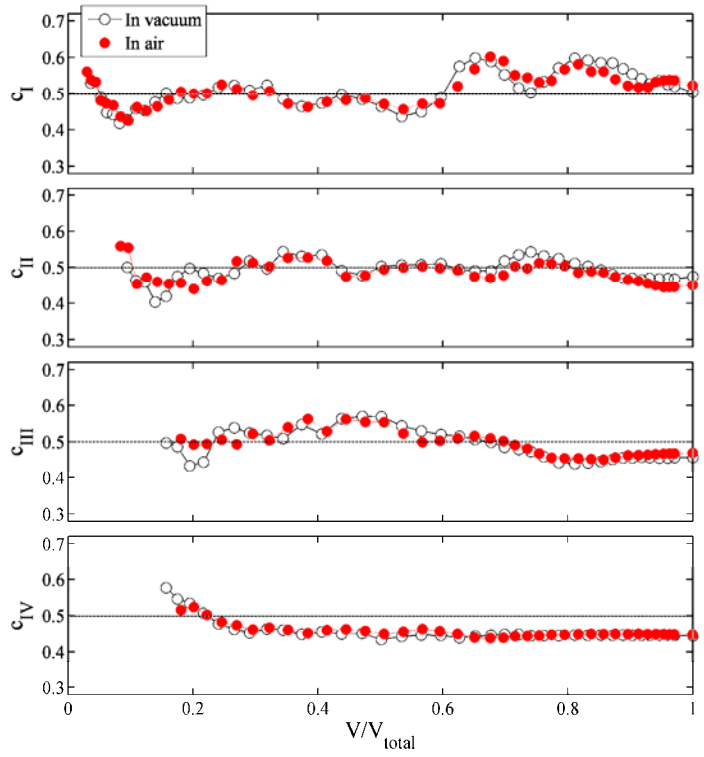

(b) Cells I - IV

Figure 5.8 Volume concentrations of light particles in (a) cells 1-4 and (b) cells I - IV as a function of fractional solid volume discharged during die filling with a moving shoe at a velocity of 70 mm/s.

The evolutions of volume concentrations of light particles in different cells during die filling with a moving shoe at a relatively high velocity of 170 mm/s are shown in Figure 5.9. During this process, the powder stream firstly flows into the leading (left hand) side of the die due to the high horizontal velocity and then bounces back by hitting the die boundaries (Figures 5.4a and e). Therefore, as shown in Figure 5.9a, the powder enters cells 1, 2 and 3 first and, when the bouncing stream reaches cell 4, the concentration of light particles c_4 is initially high due to the lights-rich front of the bouncing powder stream but then decreases as more particles flow in. Close to the end of the filling process in air, the concentration of light particles in cell 4 is further reduced due to the outflow of the lights-rich stream (see Figure 5.4h).

In Figure 5.9b, the concentration of light particles c_{I} in the top layer fluctuates around 0.5 at the early stage and then increases as a result of the arrival of the lights-rich stream front (Figures 5.4b and f) at the final stage of the filling process ($V/V_{\mathrm{total}} > 0.7$). For die filling in air, at the end of the filling process, c_{I} decreases eventually as a light particles-rich stream is expelled from the top of the die (Figure 5.4h). In the middle of the die, the concentrations of light particles c_{II} and c_{III} have a value around 0.5 during the filling process. In the bottom layer, the concentration of light particles c_{IV} decreases gradually and then remains constant with a value less than the specified average volume concentration of light particles initially in the system (i.e., 0.5) at the final stage of die filling ($V/V_{\mathrm{total}} > 0.8$).

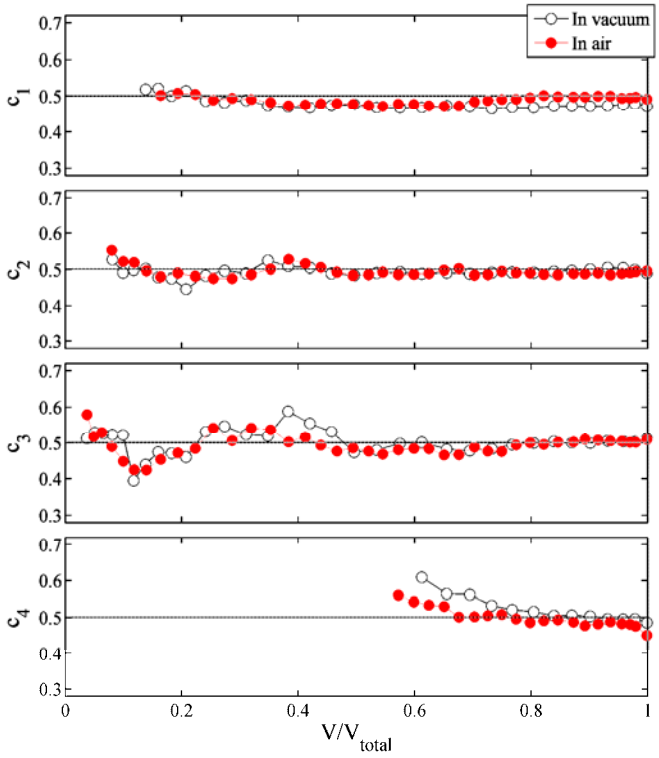

(a) Cells 1-4

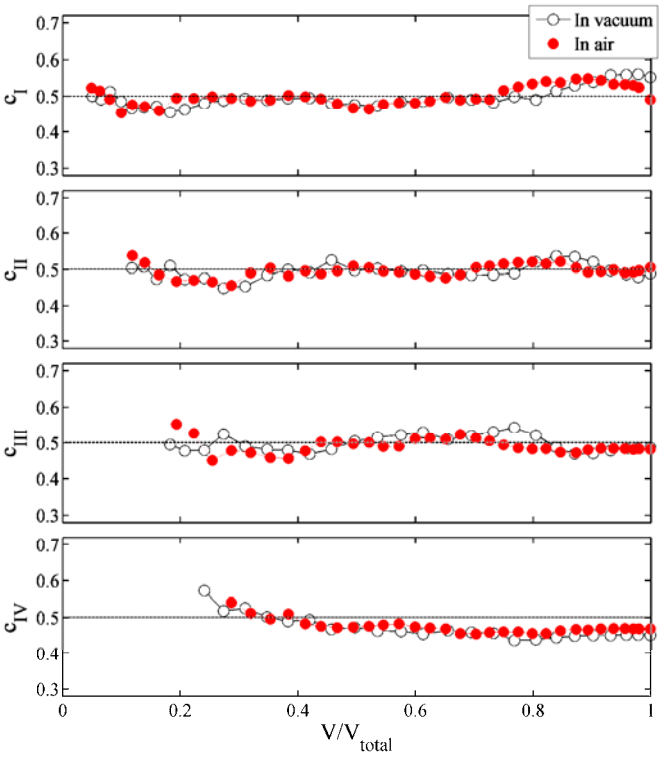

(b) Cells I - IV

Figure 5.9 Volume concentrations of light particles in (a) cells 1-4 and (b) cells I - IV as a function of fractional solid volume discharged during die filling with a moving shoe at a velocity of 170 mm/s.

5.2.3. The effect of shoe velocity

The concentration profiles in the die after die filling are obtained according to the partition of the die region as shown in Figure 5.6. Figure 5.10 shows the horizontal concentration distributions of light particles in the die after die filling at different shoe velocities. For die filling in a vacuum (see Figure 5.10a), segregation occurs at low shoe velocities (say 35 mm/s and 70 mm/s) with a lower concentration of light particles on the left hand side of the die. This is due to the fact that nose-flow dominates these flow processes and the outflow of the lights-rich front of the rebounding stream from the left hand side of the die takes place, as observed in Figures 5.3a and b. When a stationary shoe ($v_s = 0$) or relatively high shoe velocity (v_s = 140 mm/s or 170 mm/s) is employed, the concentration distributes uniformly in the horizontal direction. This is because bulk-flow becomes dominant (Figures. 5.2 and 5.4) and no lights-rich powder stream flows out of the die. In the presence of air, as shown in Figure 5.10b, segregation patterns are generally similar to those in a vacuum, i.e., a depletion of light particles is obtained on the left hand side of the die for die filling with shoe velocities of 35 mm/s and 70 mm/s (i.e., when nose-flow dominates) and more uniform concentration distributions are obtained when bulk-flow becomes dominant. In addition, it is interesting to observe from Figure 5.10b that for die filling in air with a shoe velocity of 170 mm/s, the concentration of light particles is lower on the right hand side of the die. This is caused by the outflow of the lights-rich front of the backward bouncing powder stream from the right hand side of the die as shown in Figure 5.4h.

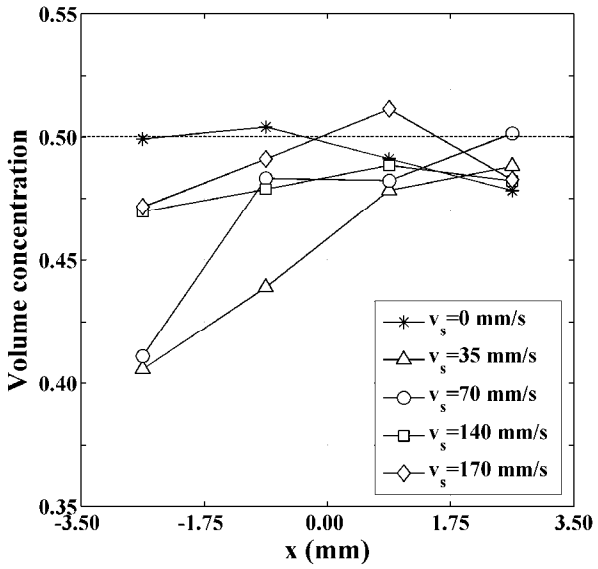

(a) In a vacuum

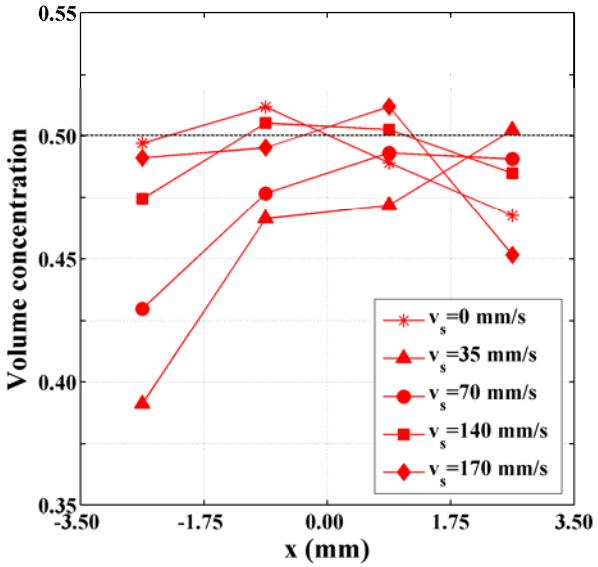

(b) In air

Figure 5.10 Horizontal concentration distributions of light particles in the die after die filling with a random mixture (ρ_h / ρ_l = 19.5) at different shoe velocities.

The vertical concentration distributions of light particles in the die for different shoe velocities are shown in Figure 5.11. For die filling in a vacuum (see Figure 5.11a), no significant segregation occurs when a stationary shoe is used (v_s = 0). However, when a moving shoe is used, the concentration of light particles is lower at the bottom and higher at the top and the overall concentration of light particles in the die decreases as

the shoe velocity decreases, for which nose-flow becomes dominant. When air is present, as shown in Figure 5.11b, segregation with a depletion of light particles at the bottom is also obtained for die filling with a stationary shoe due to the resistance of the entrapped air on the flow of light particles, which are more sensitive to the air. For die filling with a moving shoe, segregation patterns in air are similar to those in a vacuum.

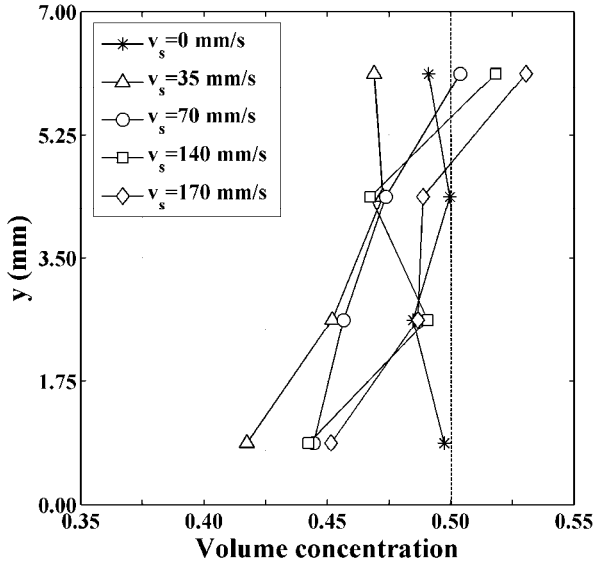

(a) In a vacuum

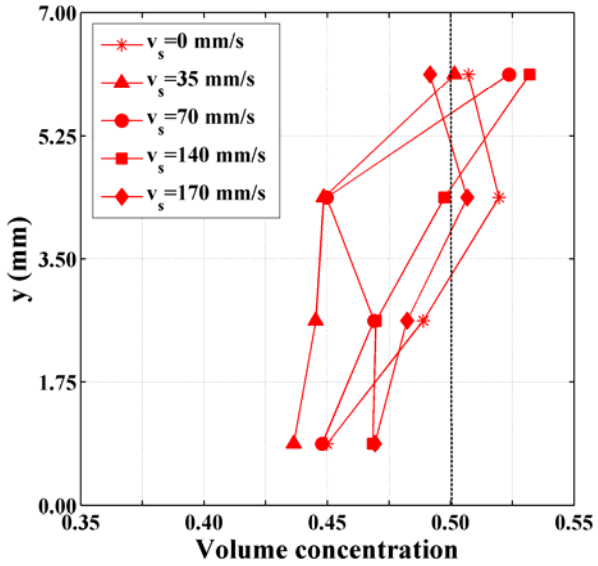

(b) In air

Figure 5.11 Vertical concentration distributions of light particles in the die after die filling with a random mixture (ρ_h / ρ_l = 19.5) at different shoe velocities.

The horizontal and vertical concentration deviations, as defined in Eq. (5.2), of the mixture deposited into the die are also calculated using the same partitions of the die (as shown in Figure 5.6). Figure 5.12 shows the horizontal and vertical concentration deviations in the die after die fillings at different shoe velocities. For the die filling with a stationary shoe (v_s = 0), both the horizontal and vertical concentration deviations are lower in a vacuum than in air, indicating that the presence of air can cause more significant segregation. When a moving shoe is used, the highest concentration deviations are obtained at a shoe velocity of 35 mm/s and the concentration deviation generally decreases with further increase in shoe velocity. It is interesting to find that the concentration deviations for the nose-flow dominated die filling (say v_s = 35 and 70 mm/s) are generally higher than those for the bulk-flow dominated die filling processes (say v_s = 0, 140 and 170 mm/s). This implies that the segregation tendency can be reduced if the die filling process is dominated by bulk-flow and is attributed to the fact that, when the bulk-flow becomes dominant, the chance for the lights-rich powder stream to flow out of the die in front of the powder mass in the shoe is reduced. It can also be seen that the horizontal concentration deviation in the presence of air increases when the shoe velocity increases from 140 mm/s to 170 mm/s. This is because when the shoe moves at a high velocity (e.g., 170 mm/s) the lights-rich powder stream can then flow out of the die at the trailing edge of the die (Figure 5.4h), which leads to a depletion of light particles in this region (Figure 5.10b).

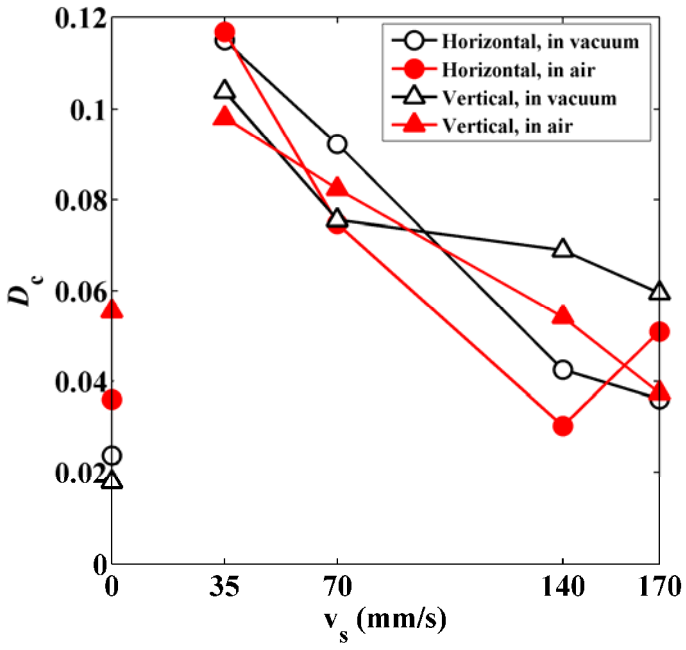

Figure 5.12 Horizontal and vertical concentration deviations in the die with a random mixture (ρ_h / ρ_l = 19.5) as a function of shoe velocity.

5.2.4. The effect of density ratio

The effect of density ratio on the segregation behaviour in die filling was also investigated by fixing the density of light particles ρ_l at 400 kg/m^3 (ζ = 0.423) and varying the density of heavy particles using ρ_h = 500 kg/m^3 (ζ = 0.396), 1000 kg/m^3 (ζ = 0.309), 1600 kg/m^3 (ζ = 0.251) and 7800 kg/m^3 (ζ = 0.053). All particles have the same diameter of 130μm. As the particle density increases, the air-sensitivity index ζ decreases, indicating that the influence of air flow on the flow of particles is reduced. The horizontal concentration distributions of light particles in the die after die filling with random mixtures of different density ratios and a stationary shoe (v_s =0 mm/s) are shown in Figure 5.13. For die filling in a vacuum the concentration of light particles is slightly lower on the right hand side of the die (Figure 5.13a), and this tendency is augmented if air is present (Figure 5.13b). This non-uniform packing is

primarily due to the heterogeneity of the initial mixture in the shoe before die filling, as discussed above.

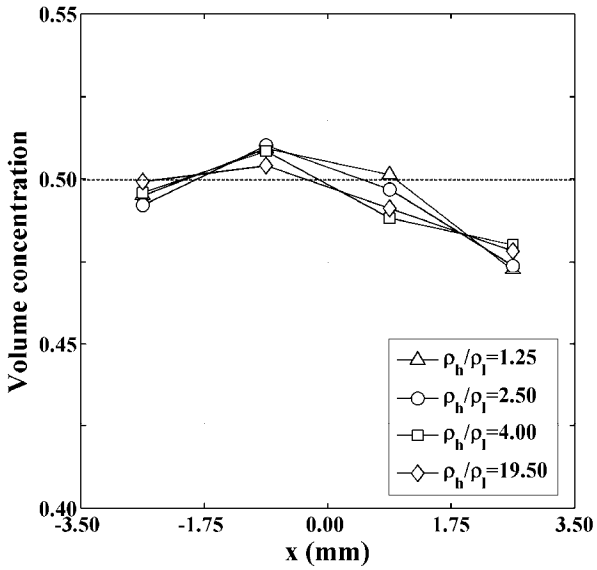

(a) In a vacuum

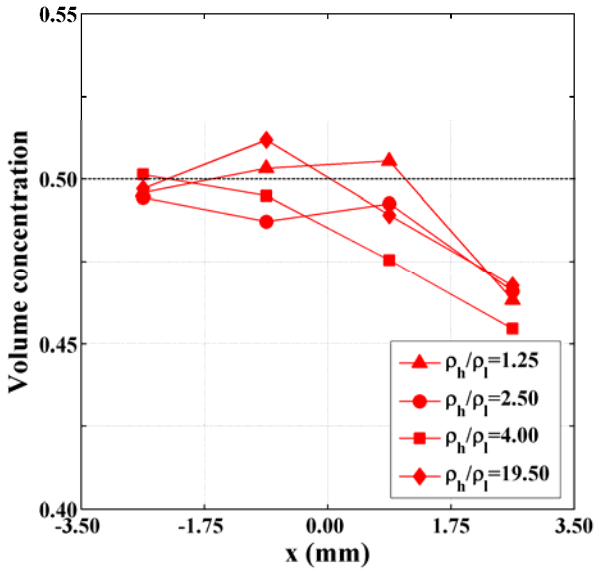

(b) In air

Figure 5.13 Horizontal concentration distributions of light particles in the die after die filling with random mixtures of different density ratios and a stationary shoe (v_s=0).

Figure 5.14 shows the corresponding vertical concentration distributions of light particles in the die. In a vacuum, the fluctuations in the concentration of light particles are very small and no obvious vertical segregation occurs for all density ratios

considered. In the presence of air, a low concentration of light particles is obtained at the bottom of the die for the various density ratios considered. As the density ratio increases, the concentration of light particles decreases at the bottom of the die. In the upper region of the die, the concentration of light particles is higher than the initial average value of the system for die filling with relatively high density ratios (say ρ_h/ρ_l = 4 and 19.5).

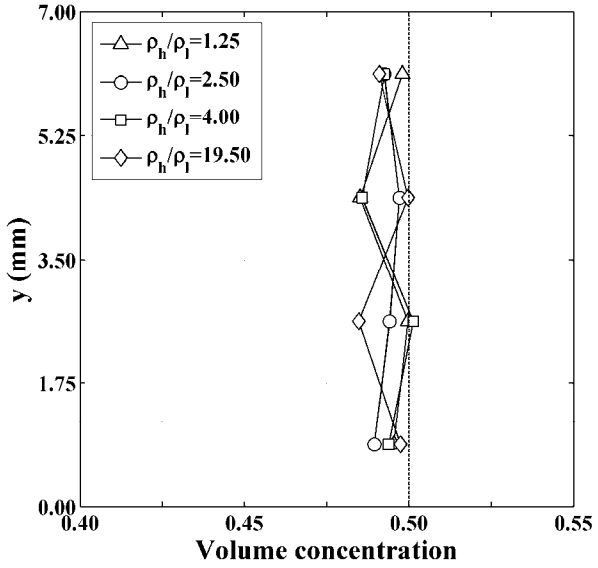

(a) In a vacuum

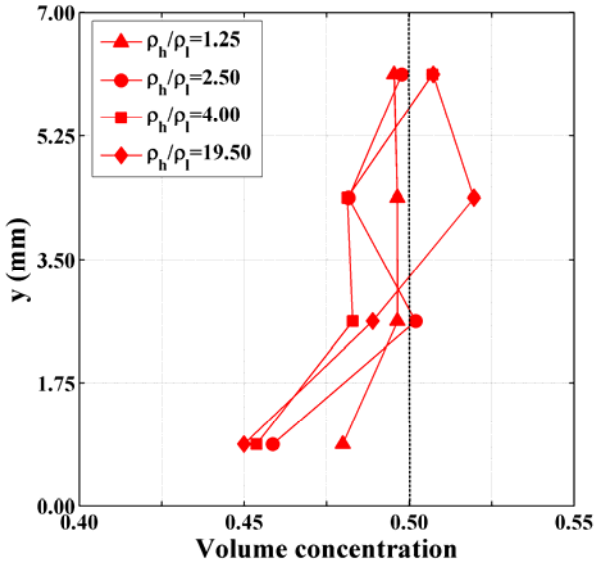

(b) In air

Figure 5.14 Vertical concentration distributions of light particles in the die after die filling with random mixtures of different density ratios and a stationary shoe (v_s=0).

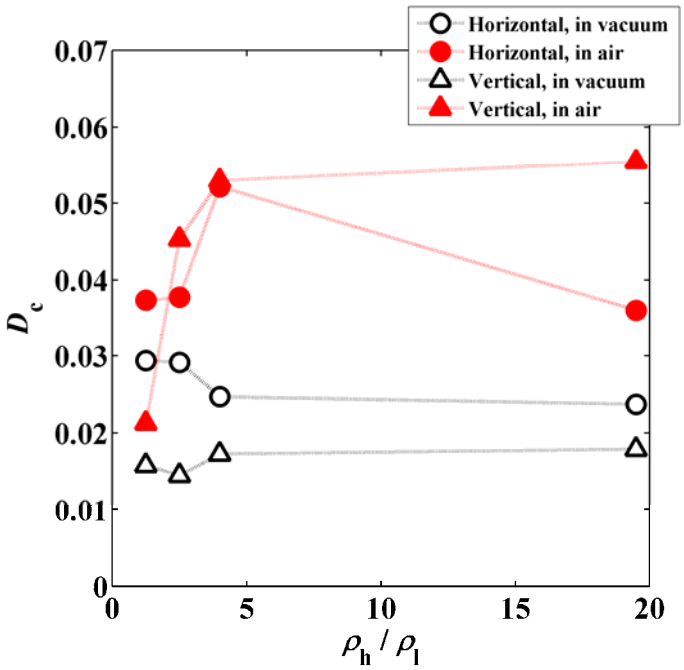

Figure 5.15 Horizontal and vertical concentration deviations as a function of density ratio after die filling with random mixtures and a stationary shoe (v_s =0 mm/s).

Figure 5.15 shows the horizontal and vertical concentration deviations for die filling with random mixtures of different density ratios using a stationary shoe. It is clear that, for die filling in a vacuum, the horizontal and vertical concentration deviations remain at a low level for each density ratio and that, for die filling in air, the concentration deviations are generally higher than those in a vacuum. Moreover, for die filling in the presence of air, as the density ratio increases, both the horizontal and vertical concentration deviations initially increase and then remain essentially constant (for vertical segregation) or even decrease (for horizontal segregation). This segregation behaviour is induced by the difference in falling acceleration due to the air drag, which causes the more air-sensitive particles (the light particles) to flow downwards at a lower speed compared to the less air-sensitive particles (the heavy particles). The segregation tendency is suppressed if the powder flows in a dense form because there is less void space for the particles to percolate through the packing of the powder

mass. With the increase in density ratio, the segregation is augmented by the increase of the difference in falling acceleration. However, the powder flow stream becomes more difficult to be diluted by air due to the increase of the particle density as they are less air sensitive, so that the chance for light particles to permeate through the voids formed between down-flowing heavy particles is reduced. Therefore, the degree of segregation no longer increases with the further increase in density ratio.

Die filling with random binary mixtures of different density ratios has also been investigated using a moving shoe. Figure 5.16 shows the horizontal concentration distributions of light particles in the die after die filling with random mixtures of different density ratios at a shoe velocity of 70 mm/s. During die filling at this shoe velocity, the powder can be delivered into the die over the surface of a nose-shaped flow stream (see Figures 5.3a, b, e and f) so that nose-flow dominates this filling process. It is clear that the concentration profiles for die filling in air and in a vacuum are similar and the concentration of light particles on the left hand side of the die is generally lower than that on the right hand side, which indicates that horizontal segregation takes place. The concentration of light particles on the left hand side of the die is found to decrease as the density ratio increases. Figure 5.17 shows the corresponding vertical concentration distributions of light particles in the die. It can be seen that the concentration of light particles in the lower region of the die is generally less than that in the upper region of the die, especially for mixtures of higher density ratios (i.e., ρ_h/ρ_l = 2.5, 4 and 19.5), indicating that segregation in the vertical direction also occurs. In general, the concentration of light particles at the bottom of the die decreases as the density ratio increases.

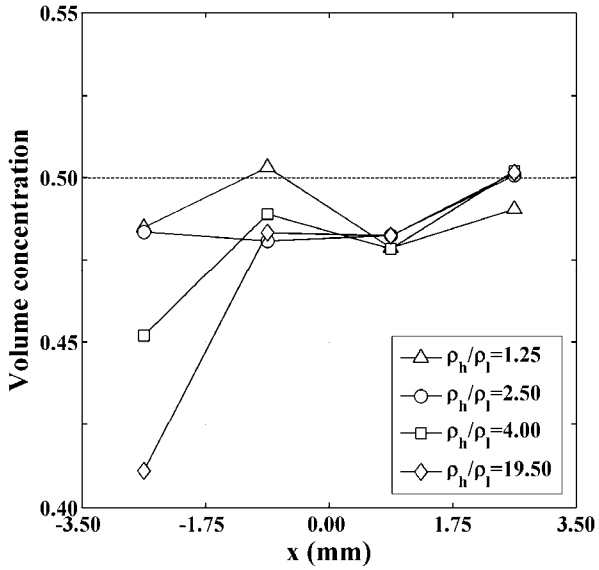

(a) In a vacuum

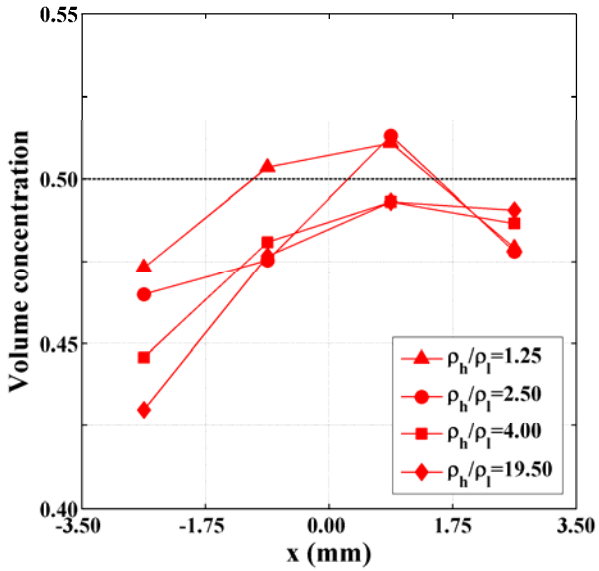

(b) In air

Figure 5.16 Horizontal concentration distributions of light particles in the die after die filling with random mixtures of different density ratios at a shoe velocity of 70 mm/s.

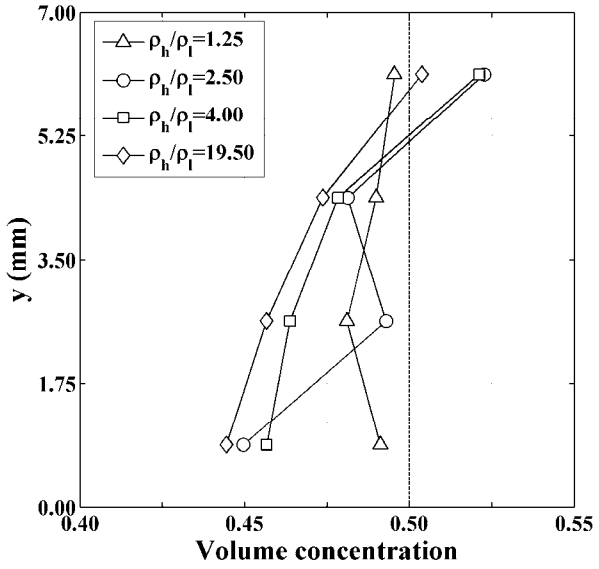

(a) In a vacuum

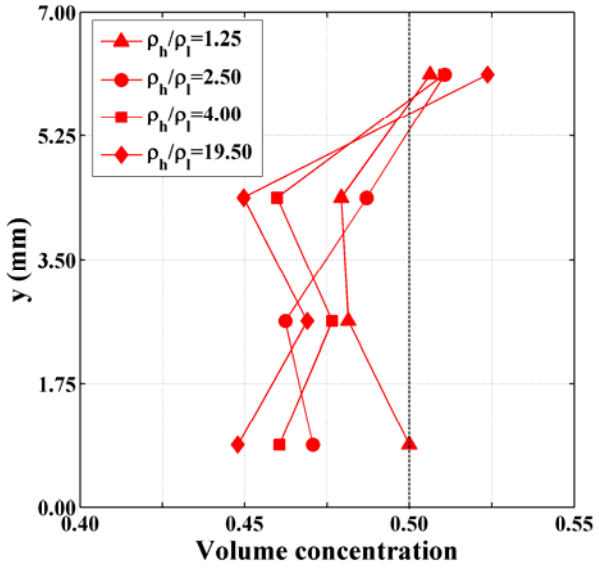

(b) In air

Figure 5.17 Vertical concentration distributions of light particles in the die after die filling with random mixtures of different density ratios at a shoe velocity of 70 mm/s.

The variations of the horizontal and vertical concentration deviations with density ratio for die filling with a moving shoe at a shoe velocity of 70mm/s are shown in Figure 5.18. It is observed that the horizontal and vertical concentration deviations increase as the density ratio increases. During this filling process, the nose-flow dominates. Due to the different particle inertia, the light particles rebound with higher

velocities during collisions and therefore they accumulate at the front of the powder flow stream, as shown in Figure 5.3. The increase of the difference in inertia by increasing the density ratio can facilitate the light particles to separate from the powder stream. As a result, the degree of segregation can be increased by increasing the density ratio. It is also observed that the air does not have a significant impact on the concentration deviations for die filling at this particular shoe speed. This is because, when the shoe travels at a velocity of 70 mm/s, the die filling is dominated by nose-flow and the air can escape from the die before the die opening is completely covered by the moving powder mass, as shown in Figures 5.3e and f.

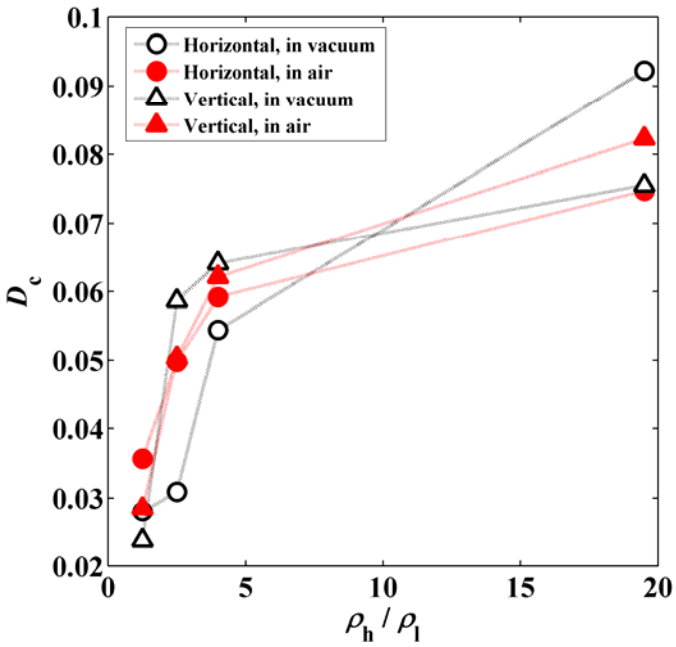

Figure 5.18 Horizontal and vertical concentration deviations as a function of density ratio for die filling with random mixtures at a shoe velocity of 70 mm/s.

The horizontal and vertical concentration distributions of light particles after die filling at a higher shoe velocity of 170 mm/s with random mixtures of different density ratios are shown in Figure 5.19 and Figure 5.20, respectively. During die filling at this shoe speed, the die opening is soon covered by the powder mass and the die cavity is filled by the powder detaching from the bottom of the powder mass

(Figure 5.4), so that the die filling is dominated by bulk-flow. As shown in Figure 5.19, no significant segregation in the horizontal direction is observed for die filling in a vacuum. For die filling in air, horizontal segregation occurs with a lower concentration of light particles on the right-hand side of the die with ρ_h/ρ_l = 19.5, i.e. the highest density ratio considered. This is due to the outflow of the lights-rich flow stream, as shown in Figure 5.4h.

The vertical concentration profiles are shown in Figure 5.20. For die filling in a vacuum, vertical segregation occurs with a lower concentration of light particles at the bottom and higher concentration at top. The concentration of light particles at the bottom generally decreases as the density ratio increases. It is noted that, for die filling in the presence of air, the die can not be completely filled with the mixtures of lower density ratios (ρ_h/ρ_l = 1.25, 2.5 and 4) due to the significant resistance from the entrapped air on the powder flow with low particle densities. As a result, the powder beds in the die are shallower than the depth of the die (7mm) after die filling in air with these mixtures. The shallow powder beds are then partitioned into three identical layers to obtain the vertical concentration profiles. In Figure 5.20b, mild segregation is observed for die filling with the mixture of ρ_h/ρ_l = 1.25. As the density ratio increases, vertical segregation occurs with a lower concentration of light particles at the bottom and a higher value at the top, except for die filling with the mixture of ρ_h/ρ_l = 19.5, in which a lower concentration of light particles is also obtained at the top of the die due to the outflow of the lights-rich powder flow stream (Figure 5.4h).

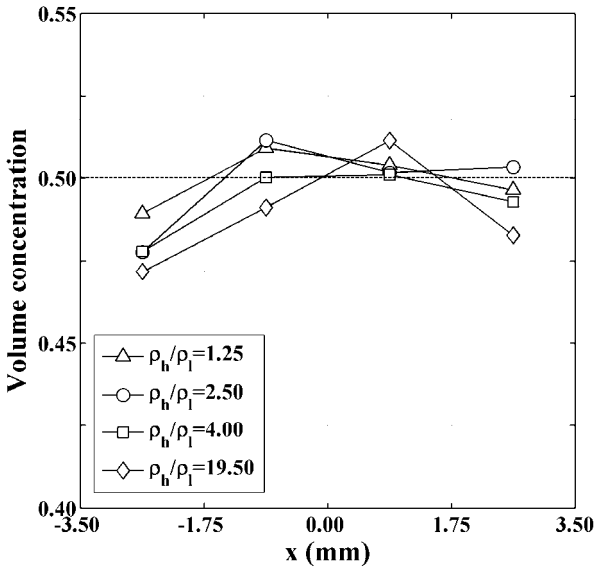

(a) In a vacuum

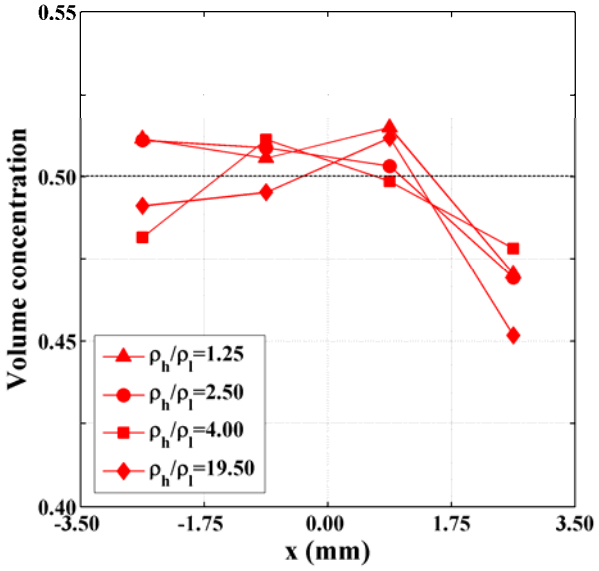

(b) In air

Figure 5.19 Horizontal concentration distributions of light particles in the die after die filling with random mixtures of different density ratios at a shoe velocity of 170 mm/s.

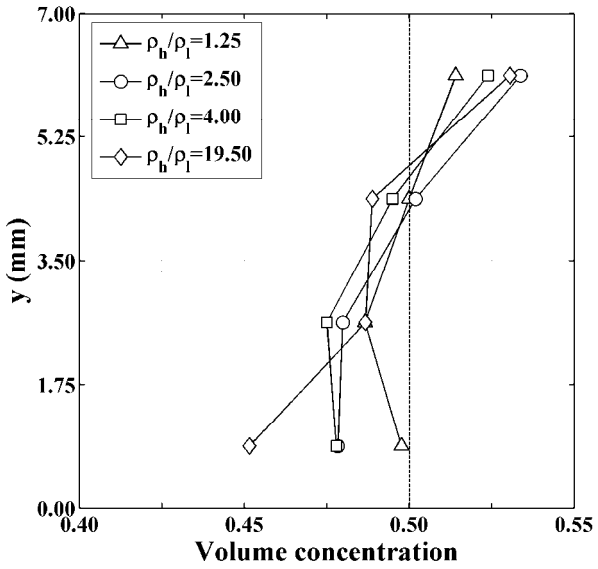

(a) In a vacuum

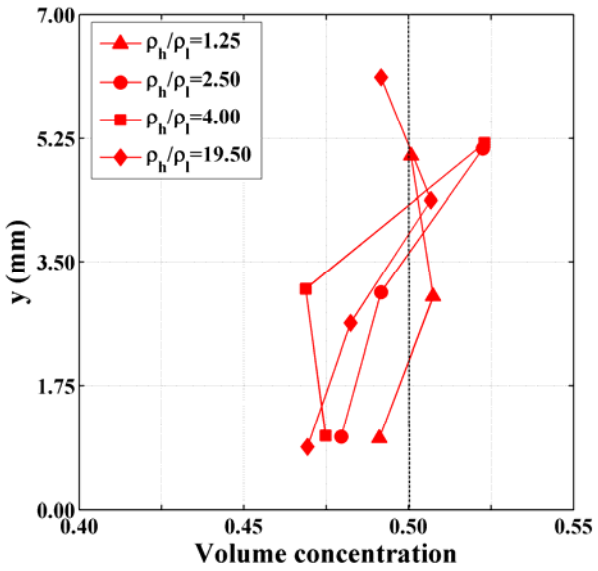

(b) In air

Figure 5.20 Vertical concentration distributions of light particles in the die after die filling with random mixtures of different density ratios at a shoe velocity of 170 mm/s.

Figure 5.21 shows the horizontal and vertical concentration deviations as a function of density ratio for die filling at a shoe velocity of 170mm/s. It is observed that the horizontal and vertical concentration deviations generally increase as the density ratio increases in a vacuum. When air is present, the segregation tendency is significantly influenced by the entrapped air which causes different powder flow behaviour from

that in a vacuum (Figure 5.4). The degree of horizontal segregation is increased by the presence of air. The vertical concentration deviation in air firstly increases and then decreases for a density ratio ρ_h/ρ_l = 19.5 due to the outflow of the lights-rich flow stream (Figure 5.4h) which avoids an excess of light particles in the upper region of the die (Figure 5.20b).

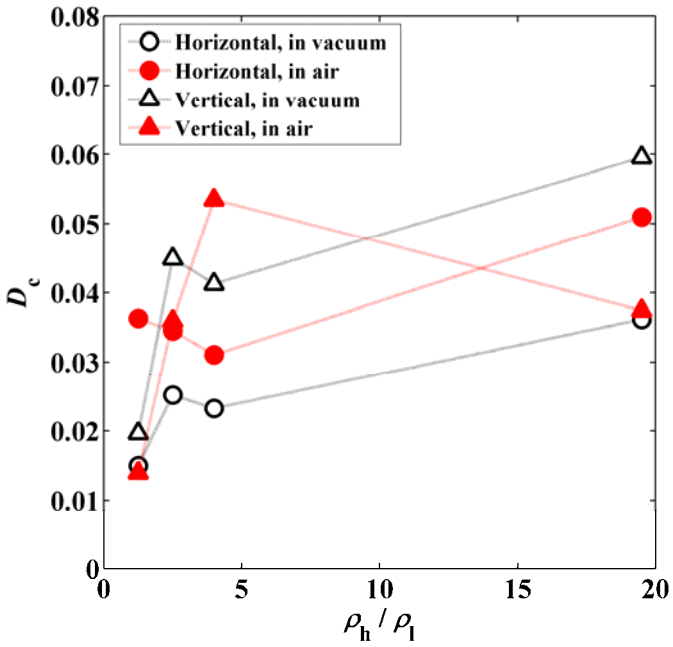

Figure 5.21 Horizontal and vertical concentration deviations as a function of density ratio for die filling with random mixtures at a shoe velocity of 170 mm/s.

5.3. Die filling with ordered mixtures

In order to examine how the initial non-uniformity in the random mixture (Figures 5.1 and 5.5) affects the segregation tendency, an ordered mixture which has a perfectly uniform concentration distribution was generated in the shoe before die filling. As shown in Figure 5.22, the ordered mixture is generated by alternately arranging the mono-sized light and heavy particles in the horizontal and vertical directions. To be consistent with the previous cases in which the random mixtures are used, die fillings with ordered mixtures of various density ratios and at various shoe velocities have

been simulated. The results show that the overall powder flow patterns with the ordered mixtures are similar to those with the random mixtures (Figures 5.2, 5.3 and 5.4). The segregation behaviour with the ordered mixtures will be discussed in the following sections.

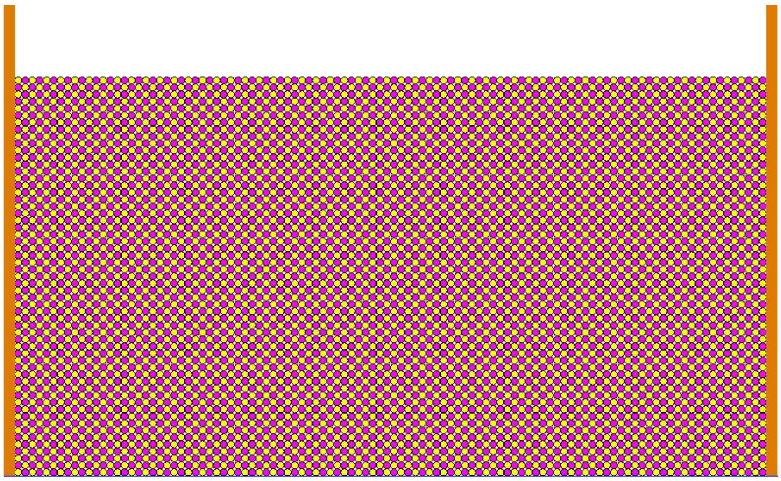

Figure 5.22 Configuration of the ordered mixture of the same size but different density particles. (light and heavy particles are coloured in yellow and magenta, respectively)

5.3.1. The effect of shoe velocity

The horizontal concentration distributions of light particles in the die after die filling with an ordered mixture (ρ_h / ρ_l = 19.5) at different shoe velocities are shown in Figure 5.23. Similar to those with a random mixture (Figure 5.10), significant segregation with a lower concentration of light particles on the left hand side is obtained for die filling with a moving shoe at low shoe velocities (i.e. 35 mm/s and 70 mm/s), and no obvious segregation in the horizontal direction is observed for die filling with a stationary shoe (i.e. 0 mm/s) and with a moving shoe at high shoe velocities (i.e. 140 mm/s and 170 mm/s). The corresponding vertical concentration distributions of light particles with the ordered mixture at different shoe velocities are shown in Figure 5.24. For die filling in a vacuum, a lower concentration of light

particles is obtained at the bottom of the die except for die filling with a stationary shoe, and the concentration of light particles in the die increases as shoe velocity increases for die filling with a moving shoe. In the presence of air, a lower concentration of light particles is also observed for die filling with a stationary shoe.

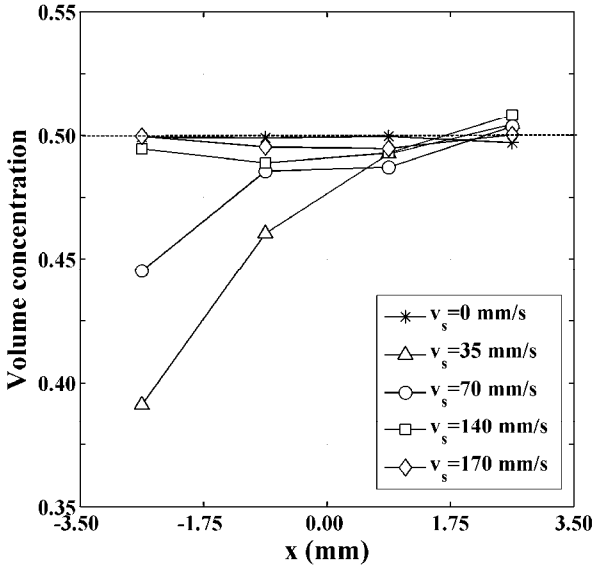

(a) In a vacuum

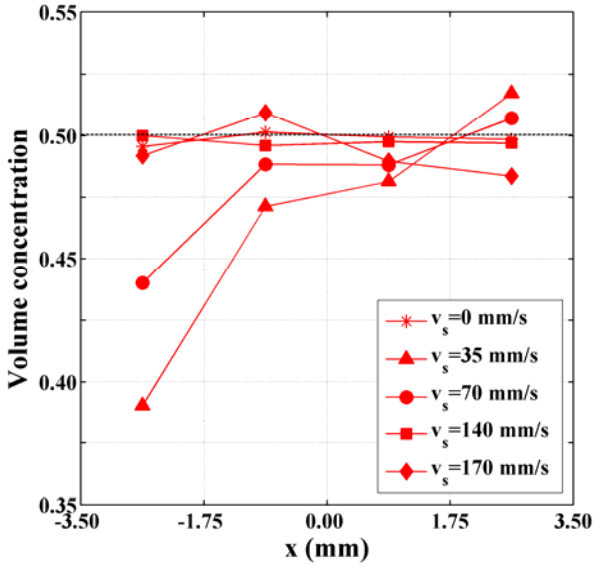

(b) In air

Figure 5.23 Horizontal concentration distributions of light particles in the die after die filling with an ordered mixture (ρ_h / ρ_l = 19.5) at different shoe velocities.

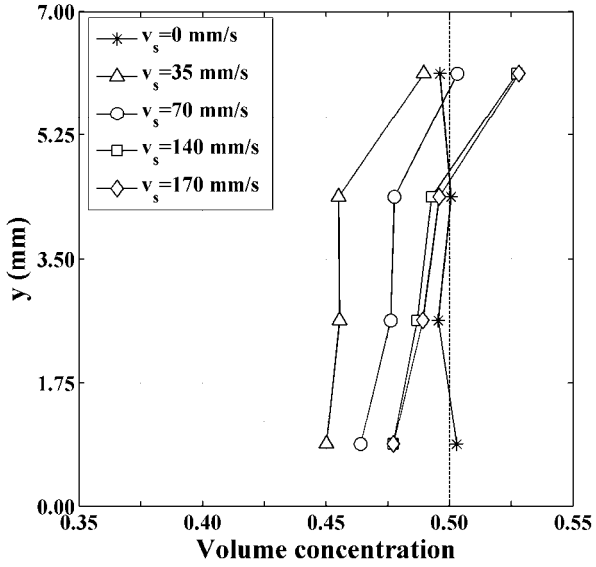

(a) In a vacuum

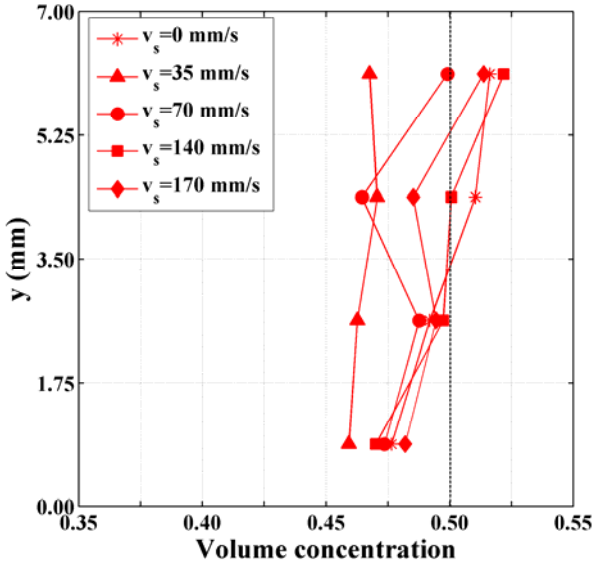

(b) In air

Figure 5.24 Vertical concentration distributions of light particles in the die after die filling with an ordered mixture (ρ_h / ρ_l = 19.5) at different shoe velocities.

Figure 5.25 shows the horizontal and vertical concentration deviations as a function of shoe velocity for die filling with the ordered mixture. Similarly as obtained from die filling with the random mixture (Figure 5.12), the larger concentration deviations are observed for die filling with a moving shoe at low shoe velocities (i.e. v_s = 35 mm/s and 70 mm/s) in which the nose-flow dominates, and the smaller concentration

deviations are observed for die filling with a stationary shoe (v_s =0) and with a moving shoe at higher shoe velocities (i.e. v_s = 140 mm/s and 170 mm/s) in which the bulk-flow dominates. For die filling with a moving shoe, the concentration deviations generally decrease as shoe velocity increases, but in the presence of air, the horizontal concentration deviation increases as shoe velocity increases from 140 mm/s to 170 mm/s due to outflow of light particles from the back of the shoe as observed during die filling with the random mixture (Figure 5.4h).

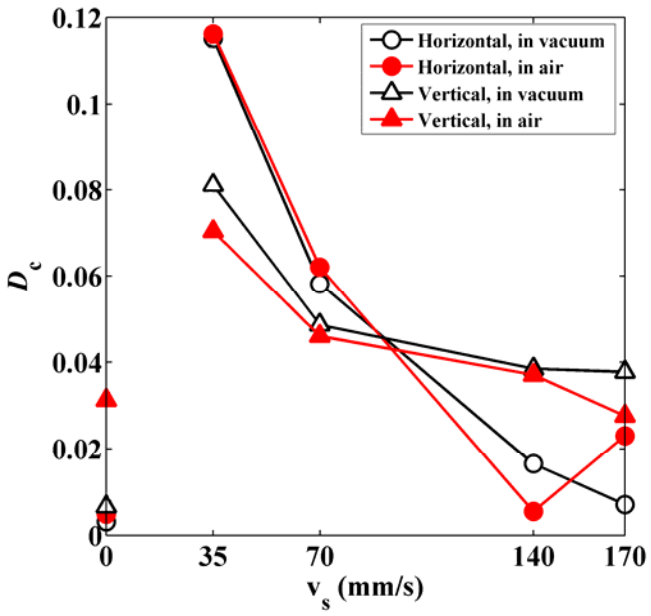

Figure 5.25 Horizontal and vertical concentration deviations as a function of shoe velocity for die filling with an ordered mixture (ρ_h / ρ_l = 19.5).

5.3.2. The effect of density ratio

Horizontal concentration distributions of light particles in the die after die filling from a stationary shoe (v_s=0) with ordered mixtures of different density ratios are shown in Figure 5.26. No segregation occurs in the horizontal direction for die filling in a vacuum. This proves that the horizontal concentration distribution in the die after die filling with a stationary shoe depends on the initial concentration profile in the shoe before die filling, as found in die filling with random mixtures. A low degree of

segregation is induced for die filling in the presence of air. The corresponding vertical concentration distributions of light particles in the die are shown in Figure 5.27. No vertical segregation occurs for die filling in a vacuum. For die filling in the presence of air, segregation occurs with a lower concentration of light particles at the bottom of the die and as the density ratio increases the concentration of light particles at the bottom of the die initially decreases and then increases.

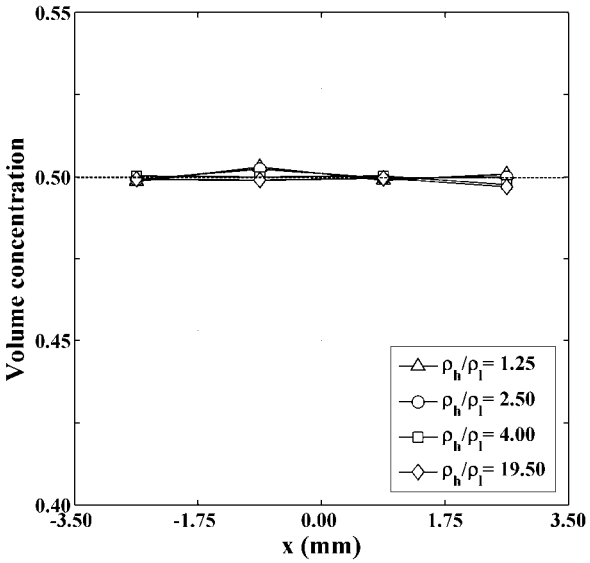

(a) In a vacuum

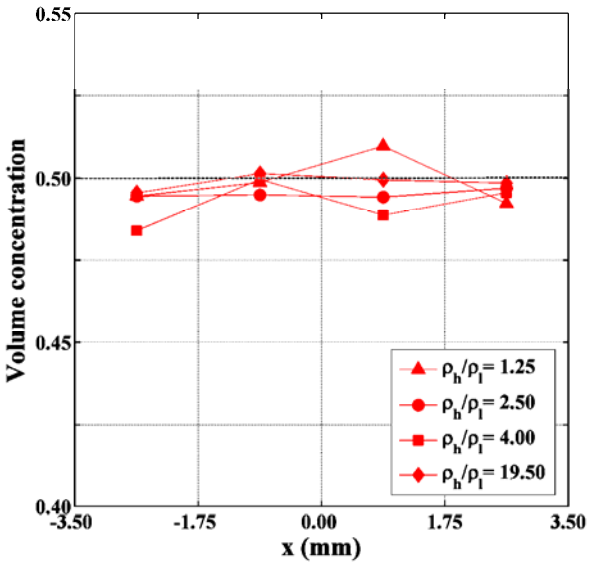

(b) In air

Figure 5.26 Horizontal concentration distributions of light particles in the die after die filling from a stationary shoe (v_s=0) with ordered mixtures of different density ratios.

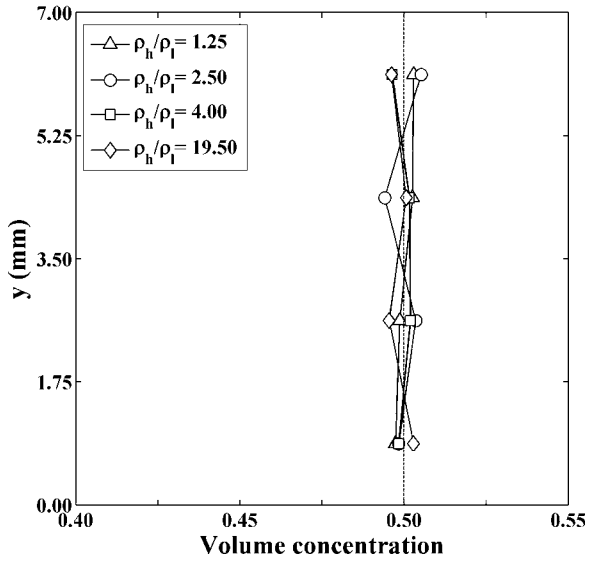

(a) In a vacuum

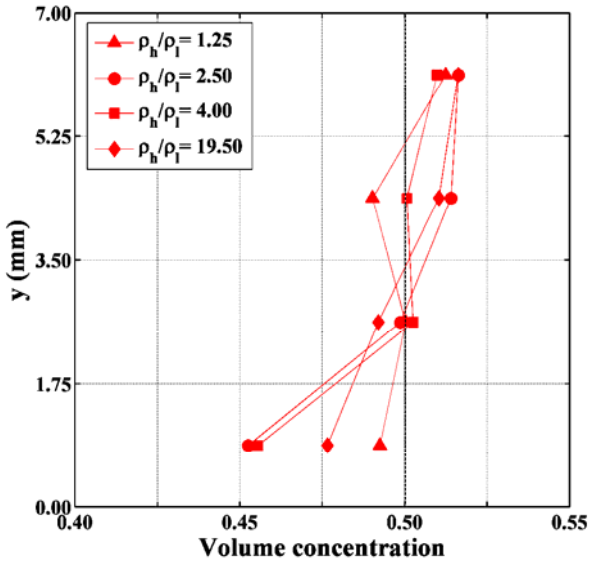

(b) In air

Figure 5.27 Vertical concentration distributions of light particles in the die after die filling from a stationary shoe (v_s=0) with ordered mixtures of different density ratios.

Figure 5.28 shows the horizontal and vertical concentration deviations as a function of density ratio for die filling with ordered mixtures and a stationary shoe. As observed in die filling with random mixtures (Figure 5.15), the concentration deviations in air are generally larger than those in a vacuum. This implies that the presence of air can

promote the segregation, especially in the vertical direction. For die filling in air, as the density ratio increases the vertical concentration deviation initially increases due to the increasing difference in falling velocities of light (air-sensitive) and heavy (air-inert) particles and then decreases due to the formation of denser powder flow streams with increasing particle densities.

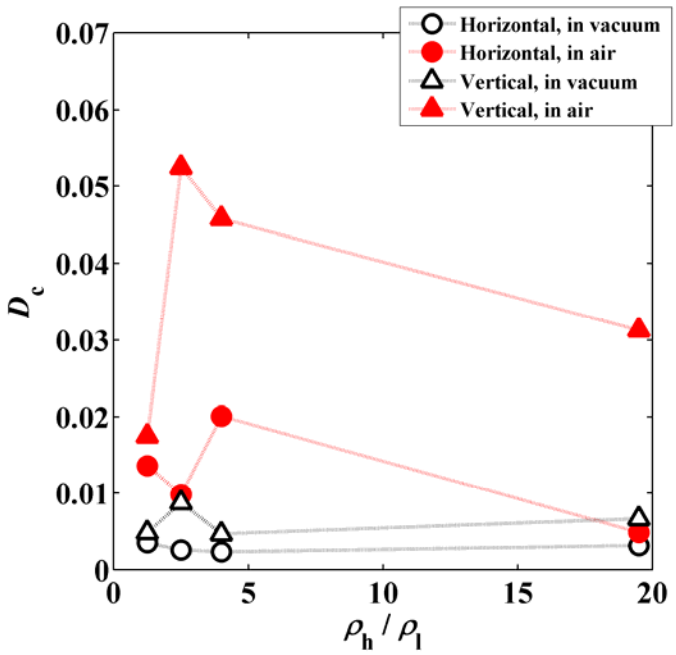

Figure 5.28 Horizontal and vertical concentration deviations as a function of density ratio for die filling with ordered mixtures and a stationary shoe.

Horizontal concentration distributions of light particles in the die after die filling with ordered mixtures of different density ratios at a shoe velocity of 70 mm/s are shown in Figure 5.29. In general, segregation occurs in the horizontal direction with a lower concentration of light particles on the left hand side of the die. As the density ratio increases, the concentration of light particles on the left hand side decreases. The corresponding vertical concentration distributions are shown in Figure 5.30. Segregation also occurs in the vertical direction with a lower concentration of light particles at the bottom of the die. As the density ratio increases, the concentration of light particles at the bottom decreases.

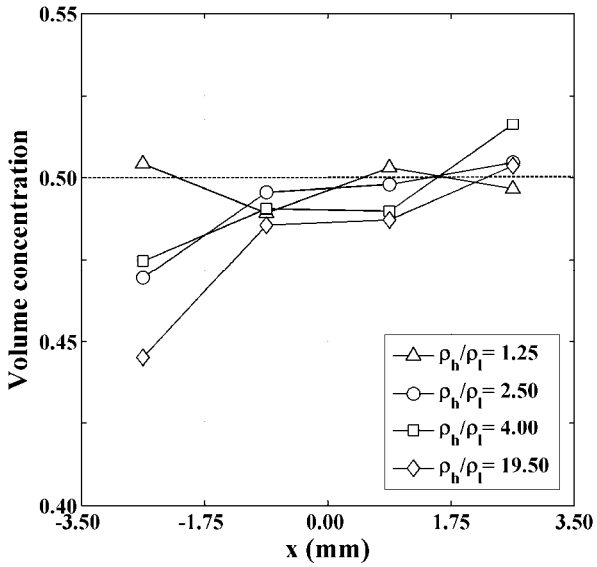

(a) In a vacuum

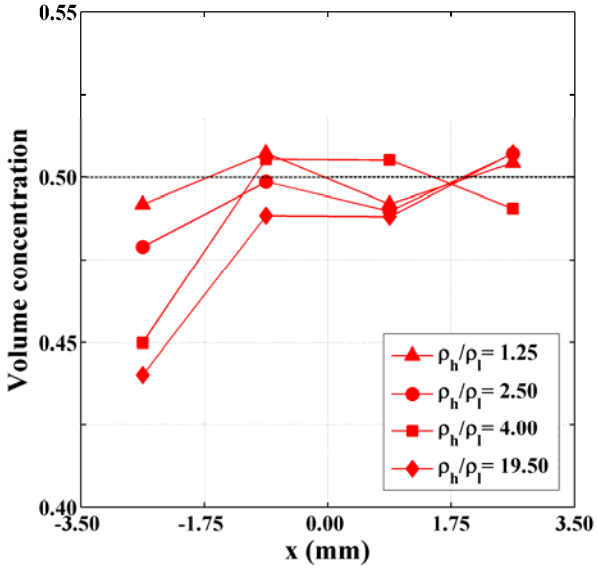

(b) In air

Figure 5.29 Horizontal concentration distributions of light particles in the die after die filling with ordered mixtures of different density ratios at a shoe velocity of 70 mm/s.

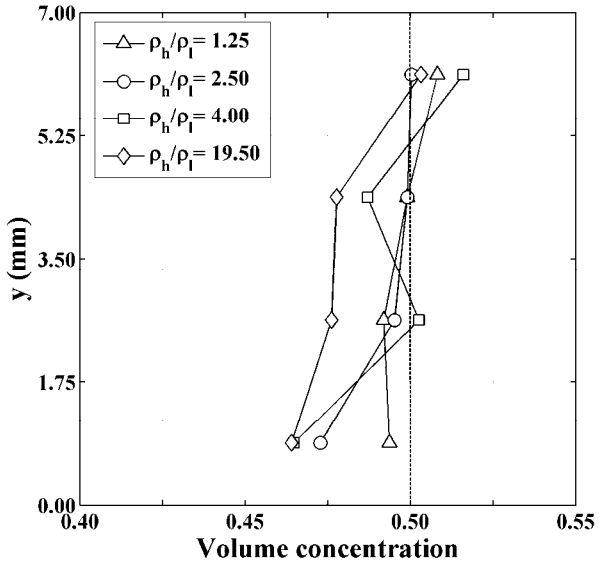

(a) In a vacuum

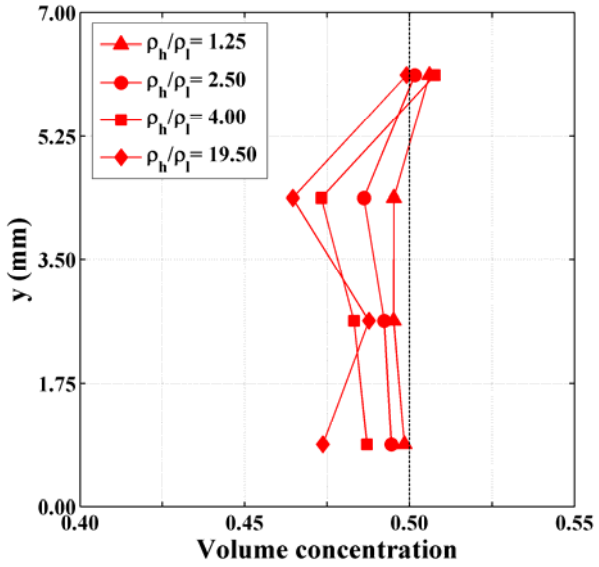

(b) In air

Figure 5.30 Vertical concentration distributions of light particles in the die after die filling with ordered mixtures of different density ratios at a shoe velocity of 70 mm/s.

Figure 5.31 shows the horizontal and vertical concentration deviations as a function of density ratio for die filling with ordered mixtures at a shoe velocity of 70 mm/s. In general, the concentration deviation increases as the density ratio increases due to the increasing difference in inertia that causes the light particles gaining higher rebound

velocities to segregate from the heavy ones. The effect of air is limited due to the easy release of the air from the die cavity in nose-flow dominant die filling process. These findings are also similar to those for the die filling with the random mixtures (Figure 5.18).

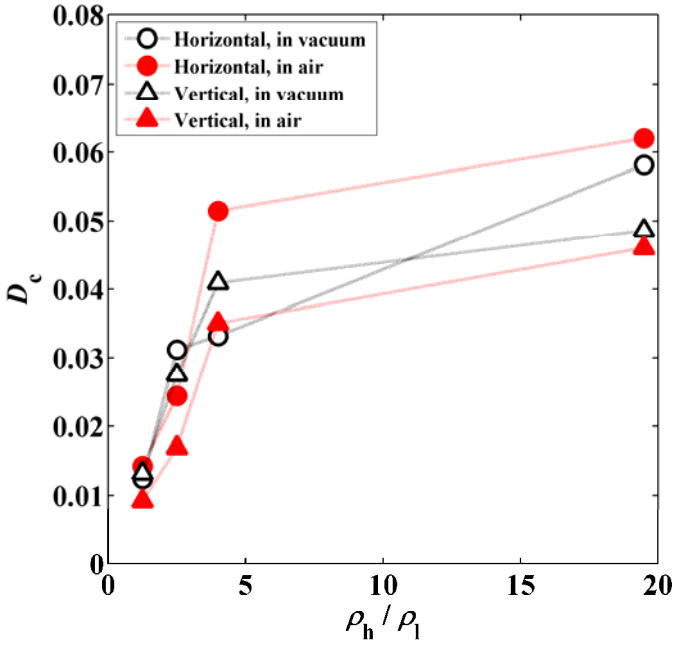

Figure 5.31 Horizontal and vertical concentration deviations as a function of density ratio for die filling with ordered mixtures at a shoe velocity of 70 mm/s.

5.4. Summary

Density-induced segregation during die filling with binary mixtures of mono-sized particles in air and in a vacuum was investigated using a coupled DEM/CFD method. Die filling with random mixtures, which were generated by randomly mixing the light particles (of low particle density) and the heavy particles (of high particle density), was considered first. The particles of different densities have different air sensitivities and the difference in air sensitivity was found to have a significant impact on the segregation behaviour during die filling in air. The effects of shoe velocity and density ratio on the segregation behaviour during die filling were also investigated.

For die filling with a stationary shoe, a low degree of segregation is observed in a vacuum, which is attributed to the non-uniformity of the initial random mixture in the shoe. When air is present, the entrapped air resists the downward flow of the air-sensitive particles (the light particles), so that vertical segregation is induced with a lower concentration of light particles at the bottom of the die. It is also observed that the air flow can disturb the flowing stream of particles, by which fluctuations of the horizontal concentration profile are promoted. As the density ratio (ρ_h / ρ_l) increases, the degree of segregation in air initially increases due to the increasing difference in falling acceleration from the effect of air drag; and then remains nearly constant or even decreases due to the formation of the denser powder flow stream that suppresses the segregation.

For die filling with a moving shoe, nose-flow and bulk-flow are observed to dominate die filling at low and high shoe velocities, respectively. The degree of segregation generally decreases as the shoe velocity increases with the transition of die filling from nose-flow dominated to bulk-flow dominated. For nose-flow dominated die filling, segregation occurs with a depletion of light particles not only at the bottom of the die but also at the leading side of the die that the shoe moves towards. When nose-flow occurs, the air can escape from the die before the die opening is completely covered by the moving powder mass, so that the influence of air on the powder flow and segregation behaviours is limited for the nose-flow dominated die filling. For bulk-flow dominated die filling in a vacuum, no obvious segregation occurs in the horizontal direction and only vertical segregation occurs with a low concentration of light particles at the bottom of the die. When air is present, the air can be entrapped in

the die by the fast moving powder mass in the shoe, and the entrapped air can cause an incomplete filling of the die (for low particle density) or the outflow of a lights-rich stream of particles from the trailing side of the die (referring to the direction of shoe motion). Consequently, the presence of air could have an impact on the segregation behaviour during the bulk-flow dominated die filling. It is also found that the degree of segregation during die filling with a moving shoe increases as the density ratio (ρ_h / ρ_l) increases, due to the increasing difference in inertia of the particles.

Finally, ordered mixtures, which are perfectly uniform, were employed to eliminate the initial heterogeneity which exists in the random mixtures. The results from die fillings with the ordered mixtures were in good agreement with those from die fillings with the random mixtures. This implies that the slight non-uniformity in the randomly generated mixtures has a negligible effect on the powder flow patterns and segregation tendency during die filling. Therefore, the density-induced segregation discussed in this study is a general consequence of die filling with well-mixed binary mixtures of the same size but different density particles.

CHAPTER 6: SUCTION FILLING

6.1. Introduction

In previous chapters, we have investigated the conventional gravity filling, in which powder is delivered into a fixed die cavity under gravity as the shoe translates over the die opening. There is also another die filling technique, namely suction filling, which is typically used on rotary presses during pharmaceutical tablet compaction (Jackson et al., 2007; Sinka and Cocks, 2009; Sinka et al., 2009). In this chapter, suction filling in the presence of air is simulated using the coupled DEM/CFD method. The effect of suction on the powder flow behaviour and density-induced segregation is examined by comparing suction filling with gravity filling.

6.2. Computational set-up

In suction filling, a movable punch is initially placed inside the die. As the powder mass in the shoe moves across the die opening, the punch moves downwards creating a low air pressure environment below the powder mass, which causes the powder to be 'sucked' into the die (Jackson et al., 2007; Sinka et al., 2009). The 2D numerical model of suction filling with a moving shoe is shown in Figure 6.1. The top of the punch, which is modelled using a physical wall of the same properties as the walls of the shoe and die, is located at the level of the die opening before the filling starts. When the powder mass in the shoe translates across the die opening, a constant downward velocity (v_p) is specified to the punch to perform the suction filling.

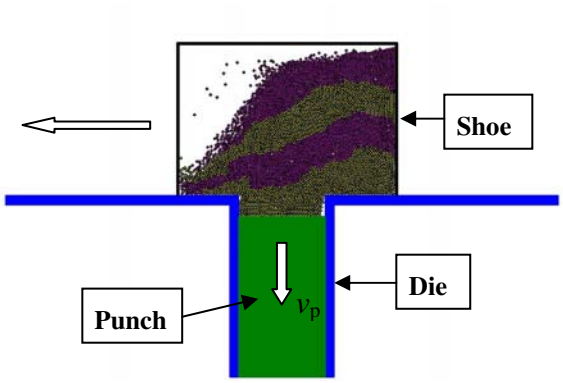

Figure 6.1 The numerical model for suction filling with a moving shoe.

A computational fluid dynamics (CFD) scheme is incorporated to consider the effect of suction, in which a low air pressure is created below the powder mass as the punch moves downwards. Figure 6.2 shows the schematic diagram of computational mesh of the fluid field and the boundary conditions. The field is partitioned uniformly using the identical cells. The die walls are treated as the impermeable static wall boundaries without slip (3), for which both normal and tangential components of air velocity should be equal to zero. The top of the system is open to the atmosphere, so that continuous air flow boundary (6) is assigned. During the suction filling process, the air flows into the die with the downward movement of the punch but it can not penetrate the top of punch. Hence, the cells, which are just located below the top of punch, are assigned as the impermeable moving wall boundary cells (2). On this boundary, the normal air velocity is equal to the punch velocity (v_p) and the tangential air velocity is zero (no-slip boundary). The cells below the moving wall boundary in the die are temporarily inactive, and they will be activated gradually as the punch moves downwards.

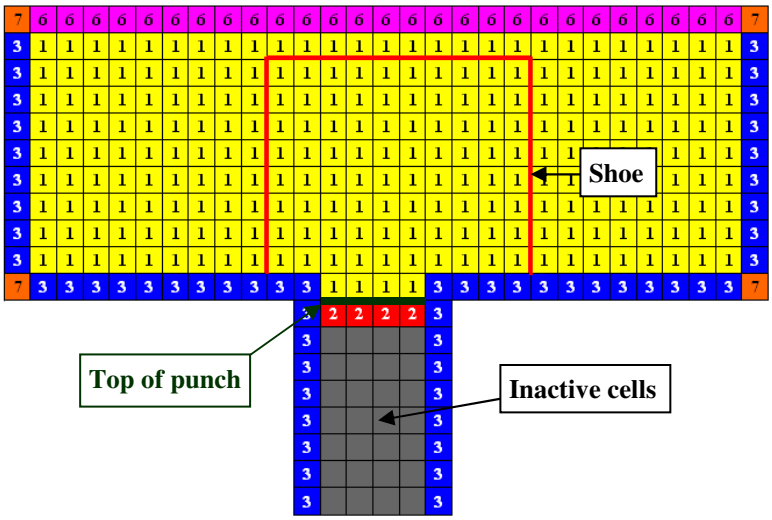

Figure 6.2 Schematic diagram of the computational mesh of fluid field and surrounding boundary conditions. [1: interior fluid cell; 2: impermeable moving wall cell, no-slip boundary; 3: impermeable static wall cell, no-slip boundary; 6: continuous air flow cell; 7: corner cell.]

Figure 6.3 shows the procedure to update the fluid cells in the die region during suction filling. As the top of punch moves down from the current layer to the layer below, the newly approached cells are activated as the interior fluid cells (1). Meanwhile, the cells immediately below the interior fluid cells are set to the impermeable moving wall cells (2). This procedure proceeds until the top of the punch reaches the bottom of the die region, and then the punch stops and the cells at the bottom layer are set to the impermeable static wall cells (3).

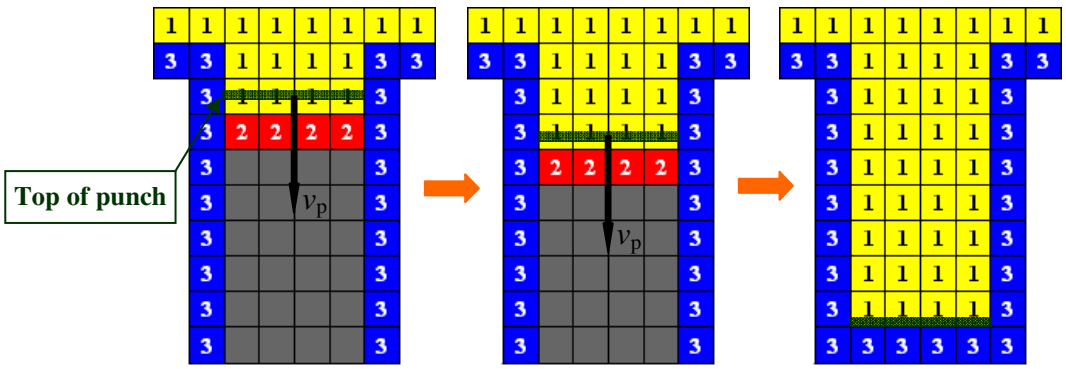

Figure 6.3 The update procedure of the fluid cells in the die region.

6.3. Powder flow behaviour during suction filling

Suction filling with a monodisperse powder is simulated first. In this simulation, a die of dimensions 2×4 mm is filled by the powder with a particle diameter of 50 μm and a particle density of 1500kg/m^3 from a shoe of 5 mm wide. As employed in the experiments, the punch velocity is typically in the range 100-500 mm/s (Motazedian et al., 2007; Sinka and Cocks, 2009; Sinka et al., 2009). Therefore, two punch velocities of 100mm/s and 276 mm/s are chosen to examine the effect of suction on the powder flow behaviour during die filling with a stationary shoe and a moving shoe.

6.3.1. Suction filling with a stationary shoe

Suction filling with a stationary shoe is first analyzed to explore the effect of suction. Figure 6.4 shows a comparison of the powder flow patterns during gravity filling in a vacuum, gravity filling in air and suction filling with a punch velocity of 100 mm/s. During gravity filling in a vacuum, the powder flows into the die smoothly as a column. However, during the filling process two narrow empty regions are formed close to die walls due to the effect of the boundary. This phenomenon is generally referred to as the 'empty annulus' (Seville et al., 1997). During gravity filling in air, as discussed in Chapter 3, the air can be entrapped inside the die and the build-up of air pressure hinders the flow of powder into the die. Two air bubbles are then formed close to the die walls, resulting in a much thinner powder flowing stream at the centre compared to the gravity filling in a vacuum. As more powder flows in, the air bubbles

rise up and finally burst out on the top surface of the powder mass. After gravity filling in air, the interfaces between different coloured layers appear obscurer than those in a vacuum, due to the chaotic powder flow in the presence of air. During suction filling with a punch velocity of 100 mm/s, a continuous draw of a powder plug into the die is obtained with the downward movement of the punch, and the empty regions as observed in gravity filling are no longer formed. Therefore, it can be concluded that the gravity filling in air is the slowest and most chaotic filling process, while suction filling can produce as quick and consistent filling process as gravity filling in a vacuum.

The corresponding air pressure distributions at the specified time instants during suction filling with a punch velocity of 100 mm/s are shown in Figure 6.5. It is observed that in the shoe region the air pressure decreases towards the die opening and a lower air pressure environment is developed in the die region. As the punch moves downwards, a decrease in air pressure is obtained close to the top of the punch. In the die region, the air pressure decreases from the top to the bottom, however, a uniform air pressure distribution in the horizontal direction is observed.

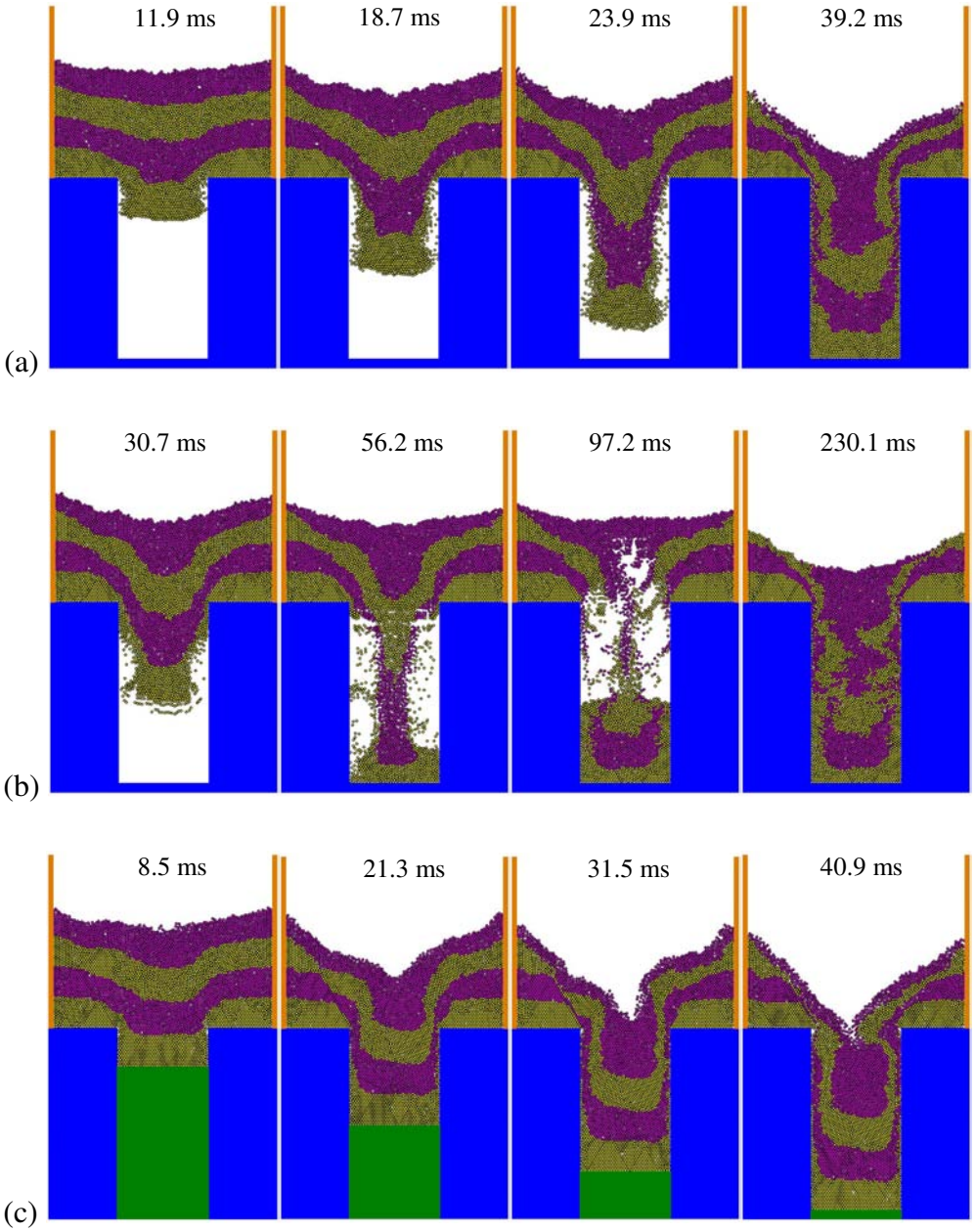

Figure 6.4 Power flow patterns during (a) gravity filling in a vacuum (top row), (b) gravity filling in air (middle row) and (c) suction filling (bottom row) with a punch velocity of 100 mm/s. A stationary shoe is used. The labels indicate the elapsed time from the start of die filling.

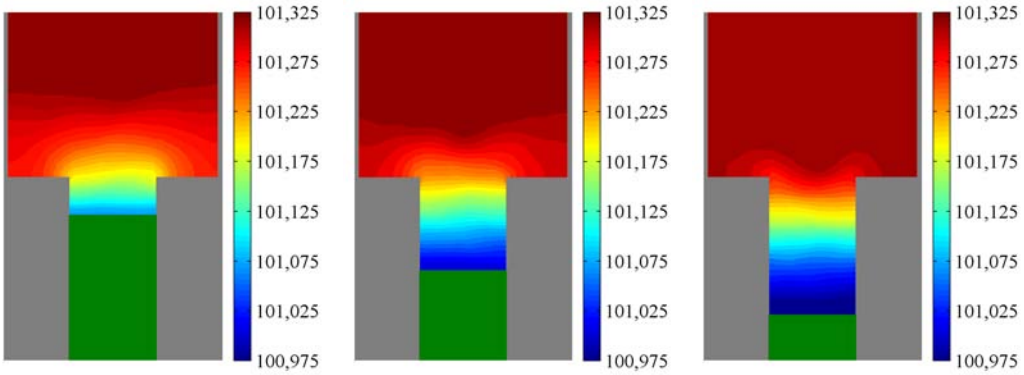

(a) T = 8.5 ms (b) T= 21.3 ms (c) T= 31.5 ms

Figure 6.5 Air pressure distributions at various time instants during suction filling with a punch velocity of 100 mm/s.

Figure 6.6 shows the vertical profiles of air pressure difference, P-P_0, vertical air velocity, u_y, and void fraction, ε, in the central column of the system at various time instants during suction filling with a punch velocity of 100 mm/s. P_0 represents the standard atmospheric pressure (i.e., P_0= 1.01325×10^5 Pa). From the profile plot of void fraction ε, it is easy to know the location of the powder bed, because ε is equal to one above the powder bed while less than one in the powder bed. As the punch moves downwards, a negative pressure gradient is generated with a linear decrease in air pressure through the powder bed from the top to the bottom. Above the powder bed, it is the pure air region, where the air remains the standard atmospheric pressure. Due to the pressure gradient, the air is driven to flow downwards dragging the particles into the die. In the profile plot of u_y, the negative sign indicates that the direction of vertical air velocity is downward. The magnitude of the vertical velocity of air in the interparticle pores of the powder bed is larger than the punch velocity. However, the air has to move in the same pace as the punch when it reaches the top of the punch. Therefore, the vertical air velocity falls to the punch velocity on the top of the punch. A sudden change in the vertical air velocity is observed at the interface between the pure air region and powder bed. This could be due to the sudden change in the void

fraction. When the air flows downwards from the pure air region into the pores of the powder bed, the decrease in void fraction causes a sharp decrease in the cross-sectional area for the flow of air. In order to keep the conservation of mass, the air velocity has to be increased as the cross-sectional area decreases. During the suction filling process, the pressure gradient increases with the downward movement of the punch until the punch stops at the lowest position. The air pressure in the die then increases as more air flows into the die and eventually reaches the surrounding atmospheric pressure, and meanwhile the air velocities vanish.

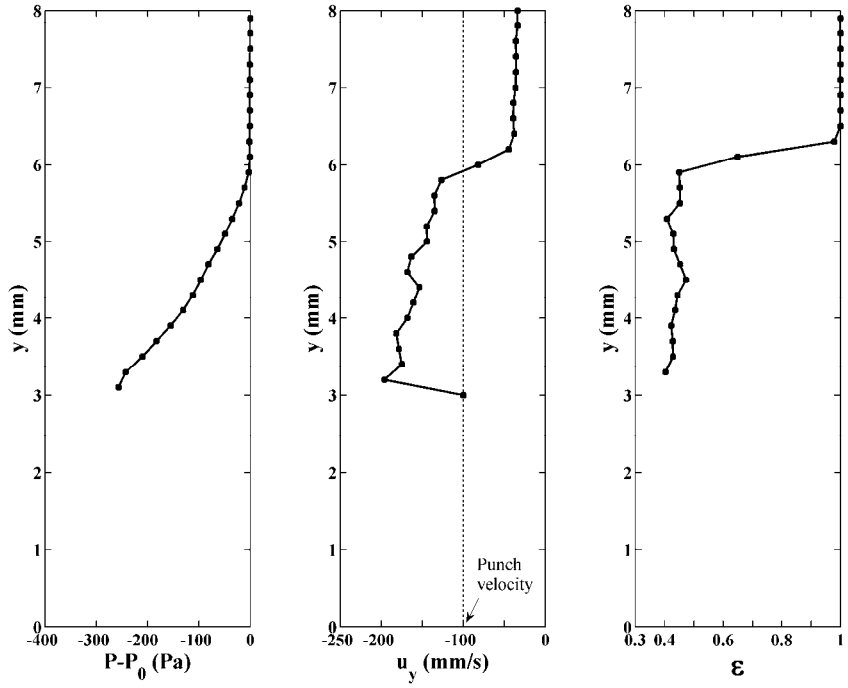

(a) T = 8.5 ms

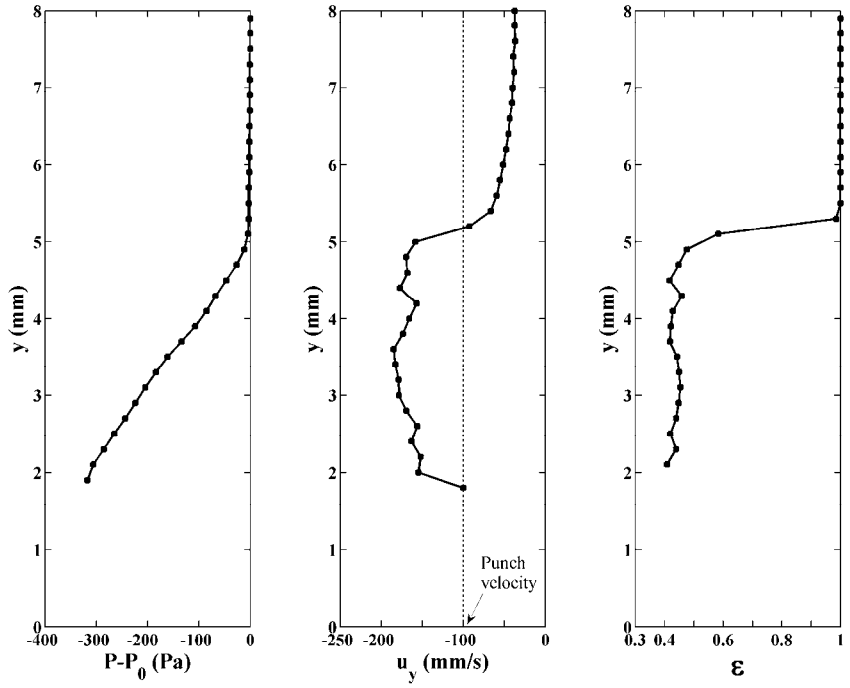

(b) T= 21.3 ms

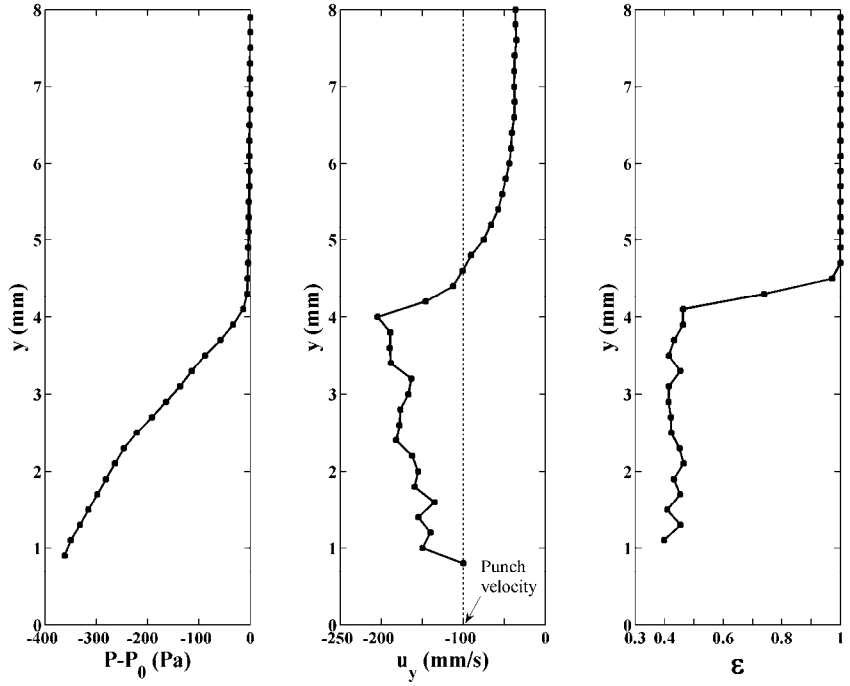

(c) T= 31.5 ms

Figure 6.6 Vertical profiles of air pressure difference, P-P_0, vertical air velocity, u_y, and void fraction, ε, in the central column of the system at various time instants during suction filling with a punch velocity of 100 mm/s.

A higher punch velocity of 276 mm/s was also employed in the suction filling with a stationary shoe. The powder flow patterns, air pressure distributions and vertical profiles of P-P_0, u_y and ε are plotted in Figures 6.7, 6.8 and 6.9, respectively. In this filling process, similar patterns as those with a lower punch velocity of 100 mm/s are observed: the powder flows into the die consistently as a plug, which fills the die tightly. However, a thin layer of particles lagging behind the main powder bed is observed at the top for suction filling with the punch velocity of 276 mm/s, as shown in Figure 6.7. This phenomenon does not occur with the punch velocity of 100 mm/s (Figure 6.4c). As shown in Figure 6.9a, the void fraction of the thin layer of particles is much higher than the main powder bed below, and consequently a lower vertical air velocity u_y is caused in the thin layer for the conservation of mass. Therefore, the particles in the top thin layer gain lower accelerations due to the air drag compared to the particles below. When the punch moves at a lower velocity (e.g., 100 mm/s), the movement of the main powder bed can be restrained by the punch, and this allows the particles in the top layer to catch up with the main powder bed below. However, when the punch moves at a sufficiently high velocity (e.g., 276 mm/s), the particles in the top layer are no longer quick enough to catch up with the fast-moving main powder bed, causing a gap at the top of system.

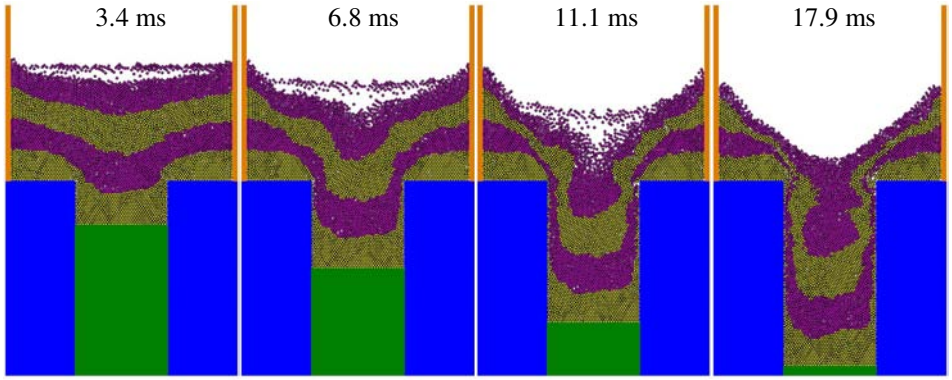

Figure 6.7 Powder flow patterns during suction filling with a stationary shoe and a punch velocity of 276 mm/s.

It is also observed in Figures 6.8 that the air pressure decreases towards the die opening in the shoe and a low air pressure environment is created in the die. The air pressure in the die decreases with the downward movement of punch. Figure 6.9 shows the similar profiles to those presented in Figure 6.6. For suction filling with a higher punch velocity of 276 mm/s, it is also observed that the air pressure decreases linearly through the powder bed from the top to the bottom and the pressure gradient increases as the punch moves downwards. By comparing Figure 6.9 to Figure 6.6, it is found that as the punch velocity increases from 100 mm/s to 276 mm/s, the magnitude of air pressure difference between the top and the bottom of the powder bed increases from 300-400 Pa to 500-1500 Pa, and the vertical velocity of the air flowing though the powder bed increases from 150-200 mm/s to 400-600 mm/s. The void fraction ε of the powder bed seems unaffected by the punch velocity and remains in a range 0.40-43.

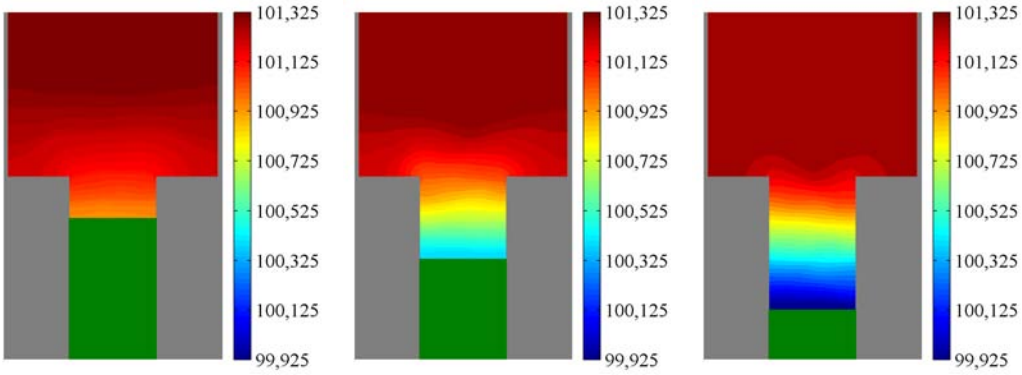

(a) T= 3.4 ms (b) T= 6.8 ms (c) T= 11.1 ms

Figure 6.8 Air pressure distributions at various time instants during suction filling with a punch velocity of 276 mm/s.

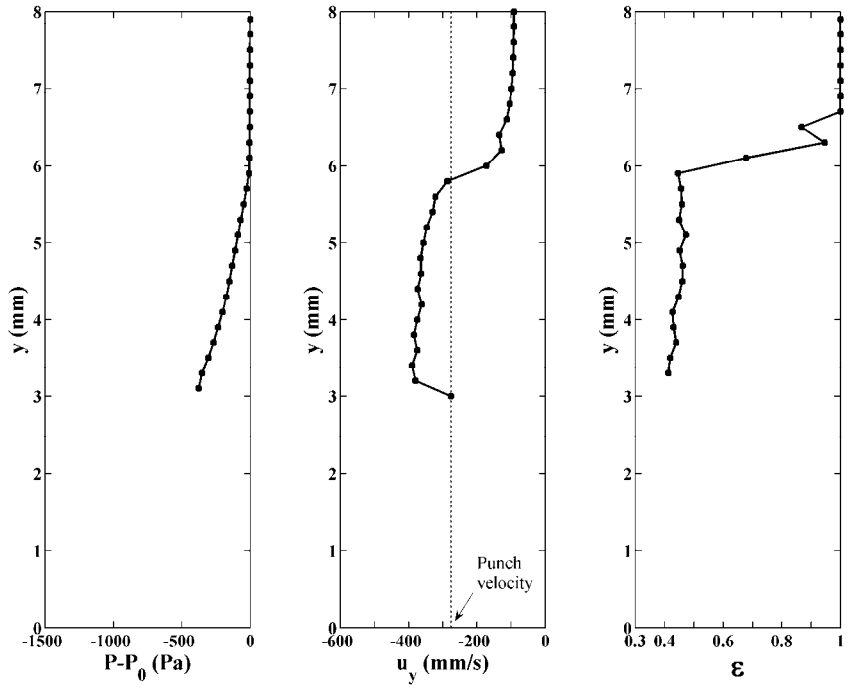

(a) T= 3.4 ms

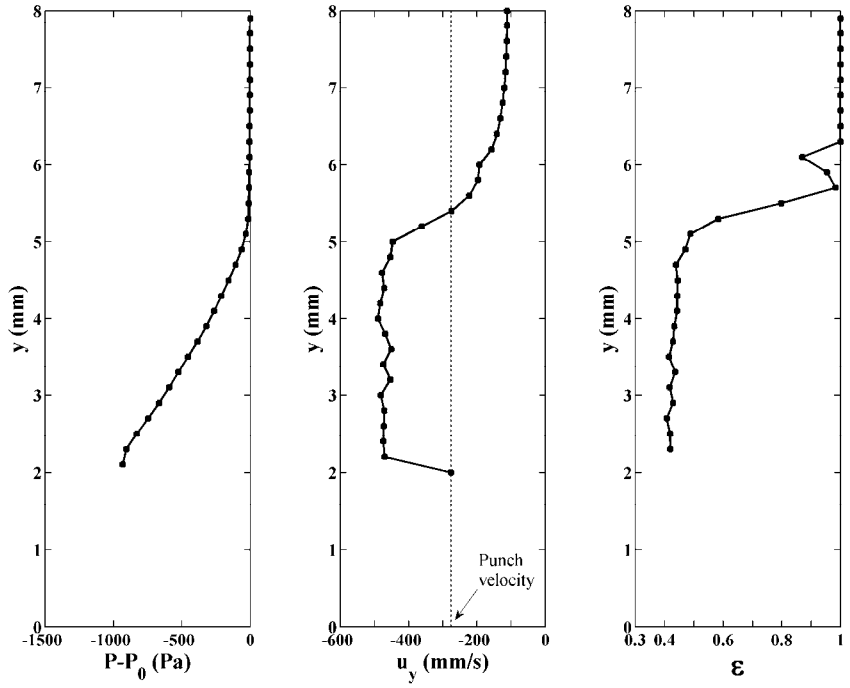

(b) T= 6.8 ms

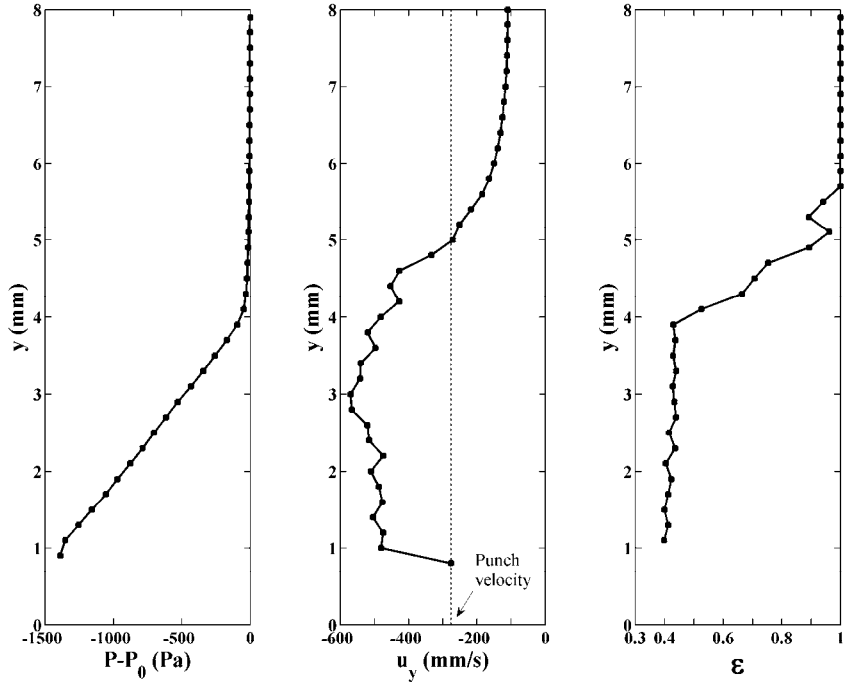

(c) T= 11.1 ms

Figure 6.9 Vertical profiles of air pressure difference, P-P_0, vertical air velocity, u_y, and void fraction, ε, in the central column of the system at various time instants during suction filling with a punch velocity of 276 mm/s.

A comparison of average mass flow rates (defined by Eq. (3.1)) under various filling conditions is shown in Figure 6.10. The lowest mass flow rate is obtained for gravity filling in air, in which the entrapped air inhibits the flow of particles into the die (Figure 6.4b). When the air is absent in gravity filling (i.e., gravity filling in a vacuum), the average mass flow rate is improved by 5 times. Suction filling with a punch velocity of 100 mm/s can produce the same average mass flow rate as gravity filling in a vacuum. Using a higher punch velocity of 276 mm/s, a very high flow rate with a value more than 10 times that in gravity filling in air is obtained in suction filling. In gravity filling, the powder flows into the die under gravity; while in suction filling, the powder is deposited into the die under the combined influences of gravity and air pressure gradient. Therefore, a higher powder flow rate is obtained in suction filling as expected. In conclusion, creating a vacuum condition and using suction are two ways to increase the powder flow rate during die filling. In the engineering practice, it is usually difficult and expensive to create the vacuum condition, so that suction filling could be a more promising technique in order to improve the filling efficiency effectively and economically.

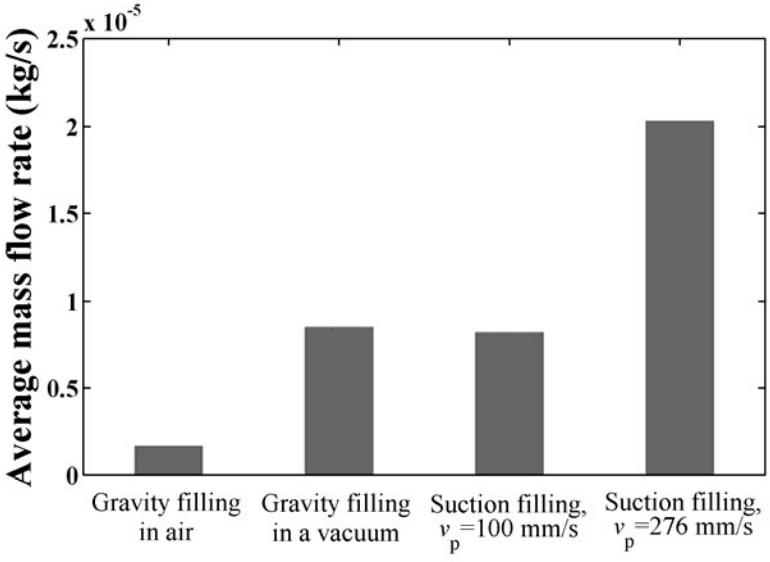

Figure 6.10 Average mass flow rates under various filling conditions.

6.3.2. Suction filling with a moving shoe

Suction filling with a moving shoe is also investigated. Figure 6.11 shows a comparison of powder flow patterns between gravity filling and suction filling. Thinner powder flow streams are observed in gravity filling. For gravity filling in a vacuum, the bottom two layers of the powder in the shoe are delivered into the die (Figure 6.11a). When air is present, the air can be entrapped in the die and the build-up of air pressure opposes the flow of powder. As a result, only the particles from the bottom layer can flow into the die (Figure 6.11b). During suction filling, the powder is 'sucked' into the die as a plug. This phenomenon is consistent with the experimental observations by Jackson et al. (2007) and Sinka et al. (2009). For suction filling with a lower punch velocity of 100 mm/s, the punch has not reached the lowest position yet when the powder mass in the shoe has moved across the die opening (Figure 6.11c). This causes a reduction of effective filling area at the late stage of filling process and a partially filled die. When the punch velocity is increased to 276 mm/s, the punch can reach the lowest position before the shoe moves across the die opening, and the die is completely filled under this condition (Figure 6.11d).

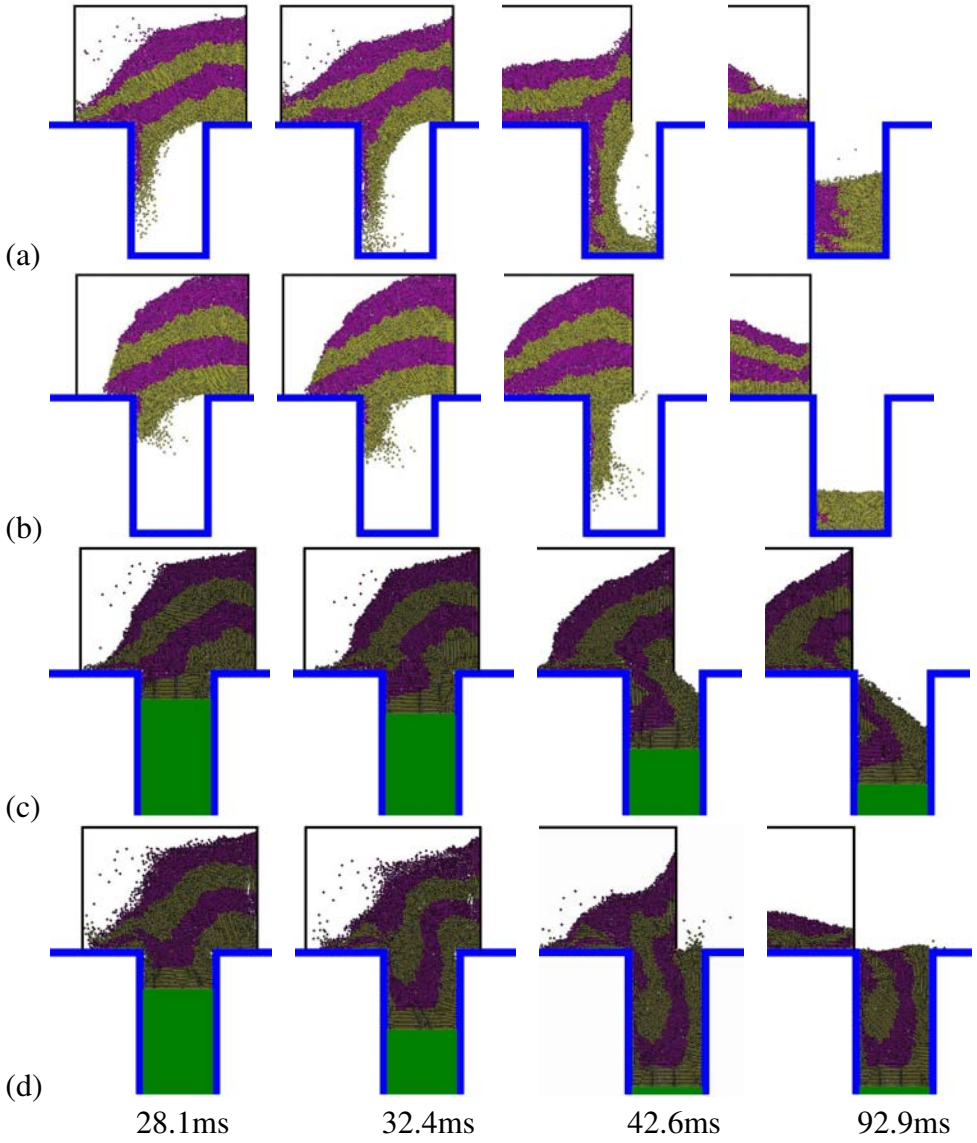

Figure 6.11 Power flow patterns during (a) gravity filling in a vacuum, (b) gravity filling in air, (c) suction filling with a punch velocity of 100 mm/s and (d) suction filling with a punch velocity of 276 mm/s. The shoe velocity is set to 140 mm/s. The labels indicate the elapsed time from the start of die filling.

Figure 6.12 shows the average mass flow rates for gravity filling and suction filling at various shoe velocities. The lowest average mass flow rates are obtained with gravity filling in air due to the effect of the entrapped air in the die. The flow rates are improved by a factor of 2 with gravity filling in a vacuum. It is evident that the mass

flow rates can be significantly increased in suction filling due to the effect of air pressure gradient. The mass flow rates in suction filling with a punch velocity of 100 mm/s are more than 3 times those with gravity filling in air. A higher punch velocity of 276 mm/s can lead to dramatically high mass flow rates, which are about 10 times those with gravity filling in air.

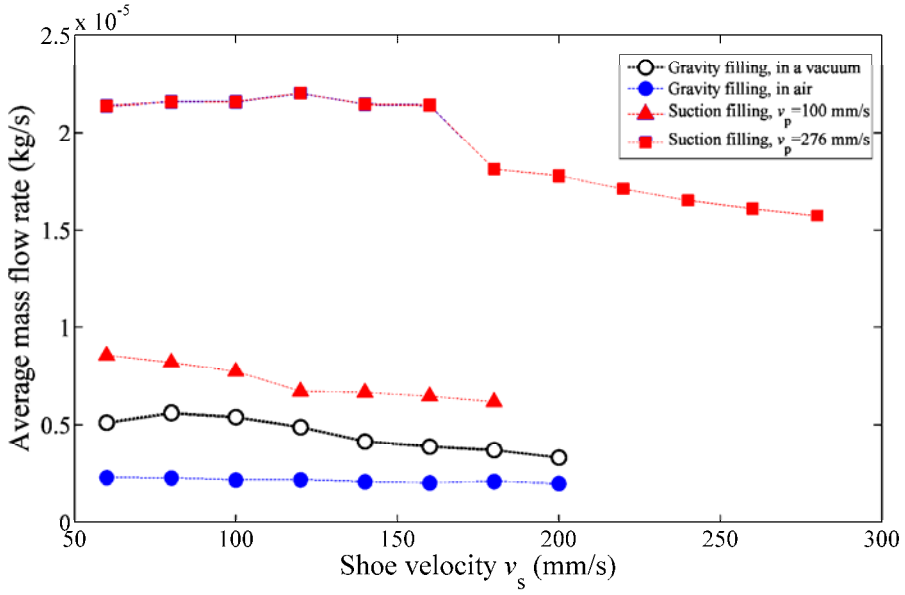

Figure 6.12 The variation of average mass flow rate with shoe velocity for gravity filling and suction filling.

As shown in Figure 6.12, the average mass flow rate decreases slightly with the shoe velocity for gravity filling in air, and it increases at the beginning and then decreases with the shoe velocity in a vacuum. The dependence of the average mass flow rate on the shoe velocity in gravity filling has been discussed in Chapter 3. In suction filling with a punch velocity of 100 mm/s, the average mass flow rate decreases as shoe velocity increases. In suction filling with a punch velocity of 276 mm/s, the average mass flow rate is essentially constant when the shoe velocity is not higher than 160 mm/s and a sudden decrease occurs when the shoe velocity exceeds 160 mm/s. For

suction filling with a low shoe velocity, the die is always filled by a consistent and thick powder plug, which moves in the same pace as the punch. Therefore, the mass flow rate of powder depends on the punch velocity rather than the shoe velocity in suction filling with a low shoe velocity. However, when a high shoe velocity (e.g. v_s >160 mm/s) is employed in suction filling, the punch has not reached the lowest position while the back wall of the shoe has arrived above the die opening. Under this condition, the filling still proceeds when the back wall of the shoe is moving across the die opening. During this period, the effective filling area (EFA) is smaller than the die opening and the powder flow stream becomes thinner. As a result, the average mass flow rate is reduced in suction filling when the shoe velocity is sufficiently high.

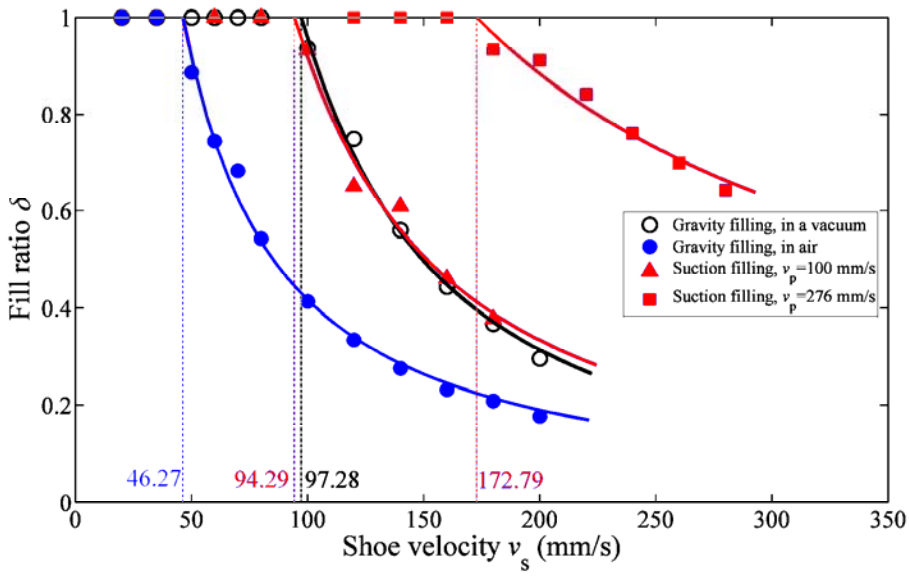

Figure 6.13 Fill ratio as a function of shoe velocity for gravity filling and suction filling.

Figure 6.13 shows fill ratio as a function of shoe velocity for gravity filling and suction filling. The fill ratio is defined as the ratio of the mass of the powder eventually delivered into the die to the mass of powder in a fully filled die. In suction filling, the delivery of powder into the die starts only after the die opening is

completely covered by the powder mass in the shoe. Although the delivery time is less than that in gravity filling, the mass of powder delivered into the die is significantly increased, especially with a high punch velocity, due to the high mass flow rate (see Figure 6.12). Therefore, the highest fill ratios are obtained in suction filling with a punch velocity of 276 mm/s. The delivery of powder can be restrained by the punch when the punch moves downwards at a low velocity. As a result, the fill ratios in suction filling with a punch velocity of 100 mm/s are close to those in gravity filling in a vacuum, although they are still higher than that in gravity filling in air.

According to Eq. (3.27), the fill ratio-shoe velocity relationships (for the incomplete filling) can be determined by best fitting to the data in Figure 6.13, which gives

$$\delta = \left(\frac{97.28}{v_s} \right)^{1.61} \tag{6.1}$$

and

$$\delta = \left(\frac{46.27}{v_s} \right)^{1.14} \tag{6.2}$$

for gravity filling in a vacuum and in air, respectively, and

$$\delta = \left(\frac{94.29}{v_s} \right)^{1.46} \tag{6.3}$$

and

$$\delta = \left(\frac{172.79}{v_s} \right)^{0.85} \tag{6.4}$$

for suction filling with punch velocities of 100 mm/s and 276 mm/s, respectively. The critical filling velocities, i.e., the maximum shoe velocities at which the die cavities can be completely filled, are then determined as 97.28 mm/s for gravity filling in a vacuum, 46.27 mm/s for gravity filling in air, 94.29 mm/s for suction filling with a

punch velocity of 100 mm/s and 172.79 mm/s for suction filling with a punch velocity of 276 mm/s. The critical filling velocity is improved by a factor of 2 in gravity filling in a vacuum compared to in the presence of air. Suction filling with a punch velocity of 100 mm/s leads to nearly the same critical filling velocity as gravity filling in a vacuum. By increasing the punch velocity to 276 mm/s, the critical filling velocity is increased dramatically due to the strong effect of suction. At shoe velocities above the critical filling velocity, the fill ratio in suction filling with a punch velocity of 276 mm/s decreases less abruptly than in other cases, indicating that relatively high fill ratios at speeds above the critical filling velocity can still be obtained using the suction filling. Similar results were ever obtained experimentally by Sinka et al. (2009).

Suction filling, especially with a high punch velocity, can dramatically improve the powder flow rate during die filling. However, it should be noted that an extremely high punch velocity can cause the occurrence of turbulence, thereby affecting powder flow behaviour and composition uniformity, as reported by Sinka and Cocks (2009). Therefore, great care must be taken when applying a very high suction velocity.

6.4. Density-induced segregation during suction filling

Suction filling with a random binary mixture of particles with the same size but different densities is also simulated. In this simulation, the random binary mixture and the dimensions of shoe and die are the same to those previously used in the gravity filling (see Section 5.2). The punch velocity is set to 150 mm/s.

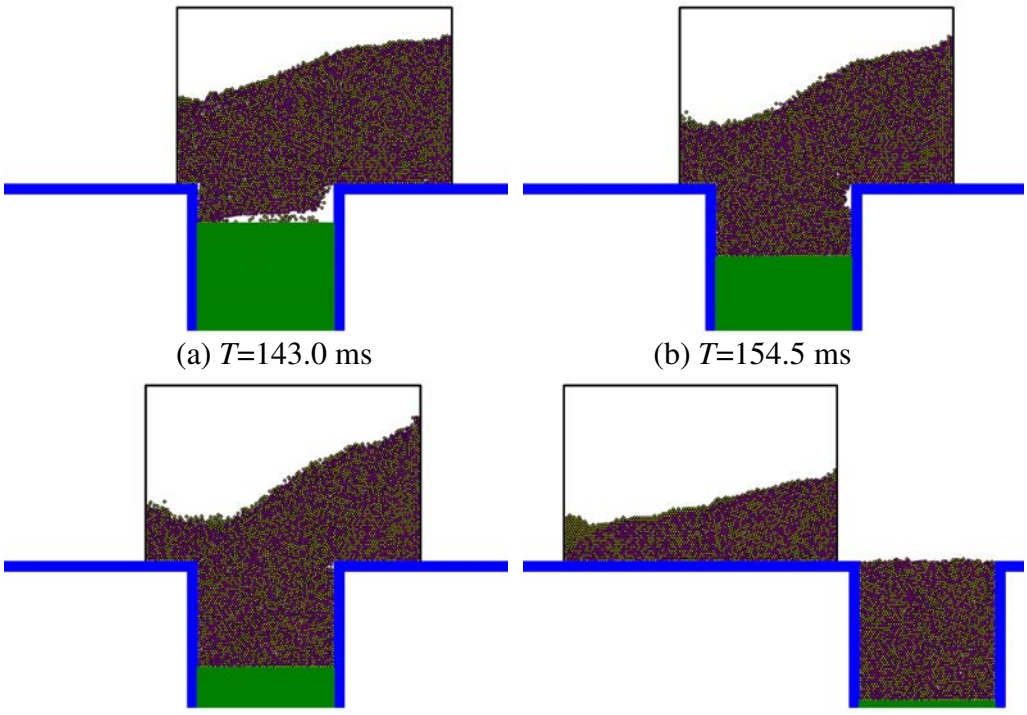

Figure 6.14 Suction filling with a binary mixture at a shoe velocity of 70mm/s. The labels indicate the elapsed time from the start of die filling.

Figure 6.14 shows the powder flow patterns during suction filling with the binary mixture at a shoe velocity of 70 mm/s. During suction filling, the powder is smoothly deposited into the die as a plug, unlike the process in gravity filling (see Figure 5.3), in which the powder flows in a nose-shaped profile and a light particles-rich stream can flow out of the die from the far end of the die. In suction filling, no nose flow occurs as the punch does not move downwards until the powder mass completely covers the die opening.

The horizontal and vertical volume concentration profiles of light particles in the die region for gravity filling and suction filling are plotted in Figure 6.15, in which the volume concentration of light particles is determined according to Eq. (5.1). The shoe velocity of 70 mm/s was employed in both gravity filling and suction filling. For gravity filling, a lower concentration of light particles is obtained on the left hand side

due to the outflow of powder stream which is rich in light particles (Figures 5.3b and f). A lower concentration of light particles is also observed at the bottom of the die in gravity filling. This is due to the fact that the light particles that have smaller inertia rebound higher and further than the heavy ones when the powder flow stream collides on the base of die or on the deposited powder bed, therefore the light particles migrate to the top region while heavy particles sink to the bottom (see Section 5.2).

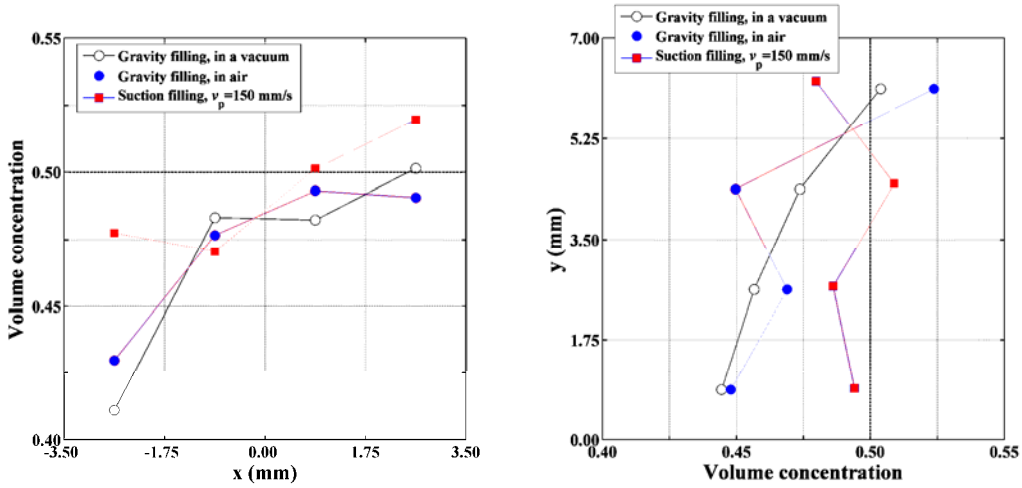

(a) Horizontal (b) Vertical

Figure 6.15 (a) Horizontal and (b) vertical volume concentration profiles of light particles in the die region for gravity filling and suction filling. The shoe velocity is 70 mm/s.

For suction filling, a more uniform concentration profile is observed in both horizontal and vertical directions (Figure 6.15). This is because during suction filling the die is filled by a powder plug that fills the die cavity tightly (Figure 6.14), so that there is very little space for particles to segregate. On the other hand, the particles 'sucked' into the die move nearly in the same pace as the downward moving punch therefore reducing the opportunity for the occurrence of severe collision and rebound, which can cause segregation during gravity filling as discussed in Section 5.2.

Using Eq.(5.2), the horizontal and vertical concentration deviations D_c for gravity filling and suction filling are also calculated and shown in Figure 6.16. The concentration deviation quantifies the degree of segregation: the larger the concentration deviation is, the more significant the segregation and the more heterogeneous the packing. It is evident that both horizontal and vertical concentration deviations are significantly reduced with suction filling and therefore the reduction in density-induced segregation can be achieved using suction filling.

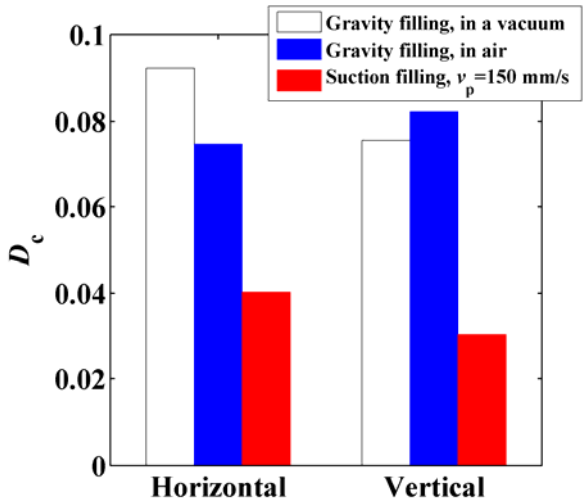

Figure 6.16 Horizontal and vertical concentration deviations for gravity filling and suction filling. The shoe velocity is 70 mm/s.

Suction filling with this binary mixture at a higher shoe velocity of 140 mm/s is also simulated. The powder flow patterns at this shoe velocity are generally similar to those at the shoe velocity of 70 mm/s (see Figure 6.14), except that a thinner powder flow stream is observed at the early stage of suction filling at the shoe velocity of 140 mm/s due to the higher momentum that particles can gain when the shoe moves faster.

Figure 6.17 shows the horizontal and vertical volume concentration profiles of light particles in the die for gravity filling and suction filling at a shoe velocity of 140 mm/s. During gravity filling at a shoe velocity of 140 mm/s, as discussed in Section 5.2, bulk

flow dominates and horizontal segregation is suppressed. Therefore, no significant segregation in the horizontal direction is observed for both gravity filling and suction filling at such a shoe velocity. In the vertical direction, segregation occurs with a lower concentration of light particles at the bottom and a higher value at the top for gravity filling. As discussed above, this is because the light particles rebound higher than heavy particles when the powder flow stream hits an obstacle during gravity filling. While no severe collision occurs and little space is provided for particles to segregate during suction filling, therefore a relatively uniform concentration profile in the vertical direction can be obtained in suction filling (Figure 6.17b).

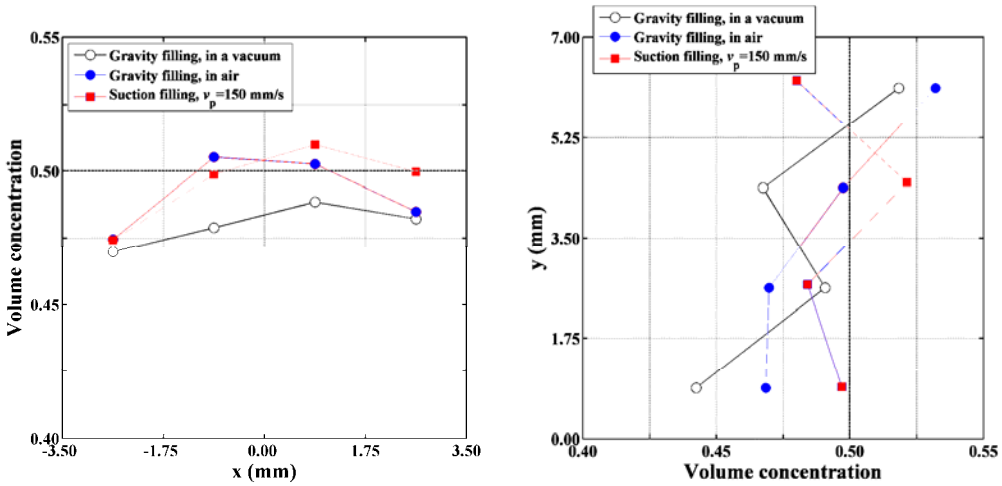

(a) Horizontal (b) Vertical

Figure 6.17 (a) Horizontal and (b) vertical volume concentration profiles of light particles in the die region for gravity filling and suction filling. The shoe velocity is 140 mm/s.

The corresponding horizontal and vertical concentration deviations D_c for gravity filling and suction filling are shown in Figure 6.18. It is found that with such a high shoe velocity (i.e. 140mm/s) suction has a limited impact on the low-degree segregation in the horizontal direction, while it can still significantly reduce the segregation in the vertical direction.

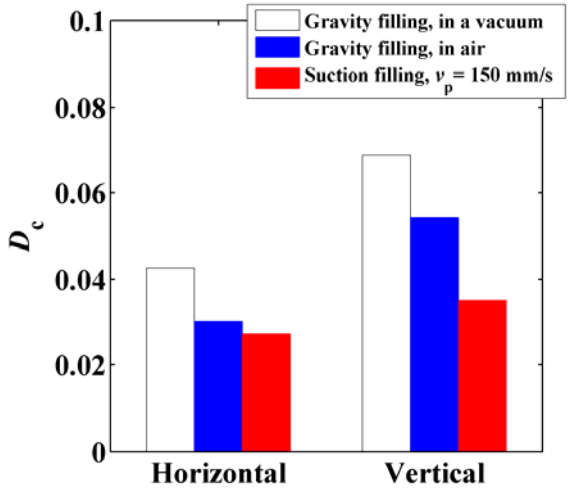

Figure 6.18 Horizontal and vertical concentration deviations for gravity filling and suction filling. The shoe velocity is 140 mm/s.

6.5. Summary

In this chapter, simulations of suction filling are reported and the results are compared with those obtained by gravity filling. In suction filling, a lower air pressure environment is created below the powder mass due to the downward motion of the punch and a thick powder plug is drawn into the die under the combined effects of gravity and air pressure gradient. As a result, the mass flow rate and critical shoe velocity are significantly improved with suction filling, compared to gravity filling in which the powder is deposited into the die only by gravitational force and the build-up of air pressure in the die opposes the flow of powder. A high punch velocity can enhance the effect of suction. However, the punch must not move too fast since turbulence can occur and this will influence powder flow and composition uniformity. Moreover, in suction filling no nose flow occurs and the powder flows into the die very smoothly without severe collisions and rebound. Therefore segregation induced by particle density differences can be suppressed.

CHAPTER 7: THREE-DIMENSIONAL SIMULATIONS OF DIE FILLING

7.1. Introduction

In Chapters 3-6, powder flow and segregation behaviours during die filling were reported based on results obtained from two dimensional (2D) simulations, in which the movements of particles were all restrained within a plane. However, since real die filling systems are three dimensional (3D), it is questionable as to how realistic are the results of 2D simulations. Therefore, 3D simulations have been performed and the results are presented in this chapter. A comparison is made between 2D and 3D simulation results.

7.2. Computational set-up

As shown in Figure 7.1, two types of 3D die filling models were employed: a thin-sliced model and a fully-3D model. In the thin-sliced model, two parallel periodic boundaries were introduced in the z-direction (i.e. thickness direction) and separated by a distance of 1.5 mm (t). In the fully-3D model, the thickness of the system t was 3 mm, and two physical wall boundaries were used at the back and front of the system. The die cavity was 7 mm wide (w) and 7 mm deep (h), and the shoe was 14 mm wide (L) for both models. A specified number of identical particles of diameter d_p=130 μm and density ρ=1500kg/m^3 were randomly generated and then deposited under gravity to form a dense packing in the shoe prior to die filling. After the initial deposition, the heights of powder beds in the shoe (H) were between 6.5mm and 7 mm. The powder

beds were initially colour-banded in order to visualize the macroscopic flow behaviour of particles.

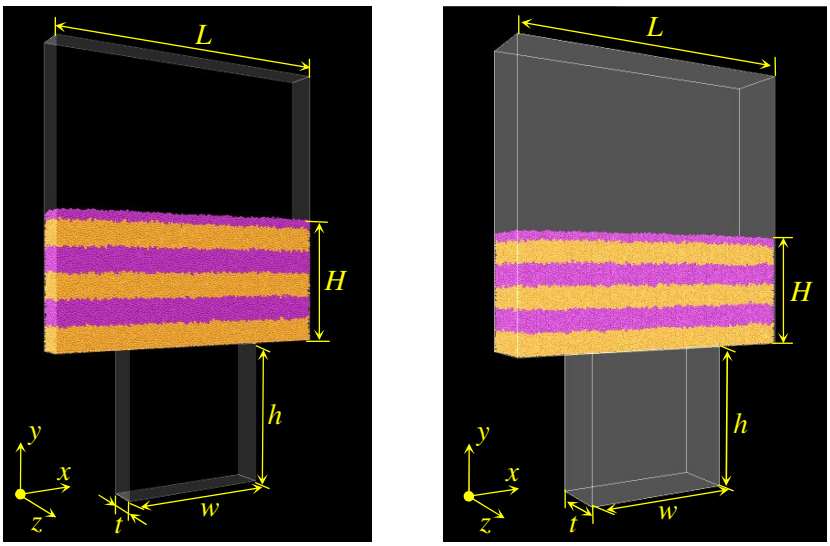

(a) Thin-sliced model (b) Fully-3D model

Figure 7.1 (a) Thin-sliced model and (b) fully-3D model for die filling with a stationary shoe.

The presence of air was modelled using computational fluid dynamic (CFD). Figure 7.2 shows the schematic diagrams of the computational fluid cells and boundary conditions for the thin-sliced model and the fully-3D model. The air domain was uniformly meshed with identical cells of dimensions 0.5×0.5×0.5 mm (yellow cells). In the *x*-*y* plane, the impermeable wall boundaries without slip (blue cells) were specified around the air domain except at the top where the continuous gas outflow boundary (pink cells) was assigned. In the thickness direction (i.e., *z*-direction), two periodic boundaries (green cells) were introduced for the thin-sliced model (Figure 7.2a), while two impermeable wall boundaries were adopted for the fully-3D model (Figure 7.2b). The air has a viscosity of 1.8E-5 kg $m^{-1}s^{-1}$ and an initial pressure equal to standard atmospheric pressure (101.325 KPa). The temperature of air is fixed at 293 K during the entire die filling process.

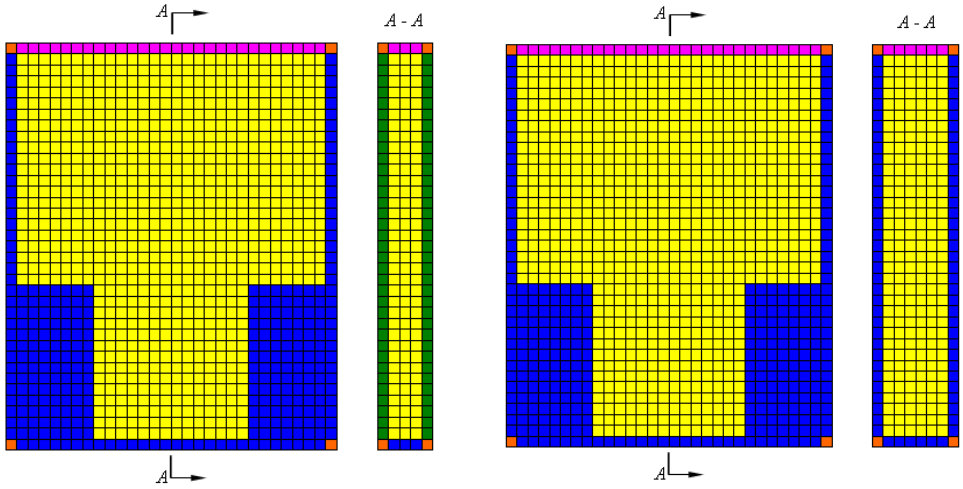

(a) Thin-sliced model (b) Fully-3D model

Figure 7.2 Schematic diagrams of the computational fluid cells and boundary conditions for the (a) thin-sliced model and (b) fully-3D model of die filling with a stationary shoe. [: interior fluid cell; : impermeable wall cell, no slip; : continuous gas outflow wall cell, free slip; : corner cell; : periodic boundary cell]

7.3. Powder flow during die filling

Three-dimensional simulations were performed to re-examine the powder flow behaviour (flow patterns and flowability) during die filling, which was previously investigated using 2D simulations (see Chapter 3).

Figure 7.3 shows a comparison of the die filling processes in a vacuum between the 2D model, thin-sliced model and fully-3D model. The powder flow patterns are very similar for all the models. The powder is filled into the die as a single column rapidly and smoothly. Due to the effect of the edge of the die opening, two empty regions are formed close to the die walls at an early stage. A concave surface is created at the top of the particle system due to discharge of particles from the centre of the shoe. The particles on the top surface (magenta particles) flow down along the slopes and eventually accumulate at the bottom of the concave surface.

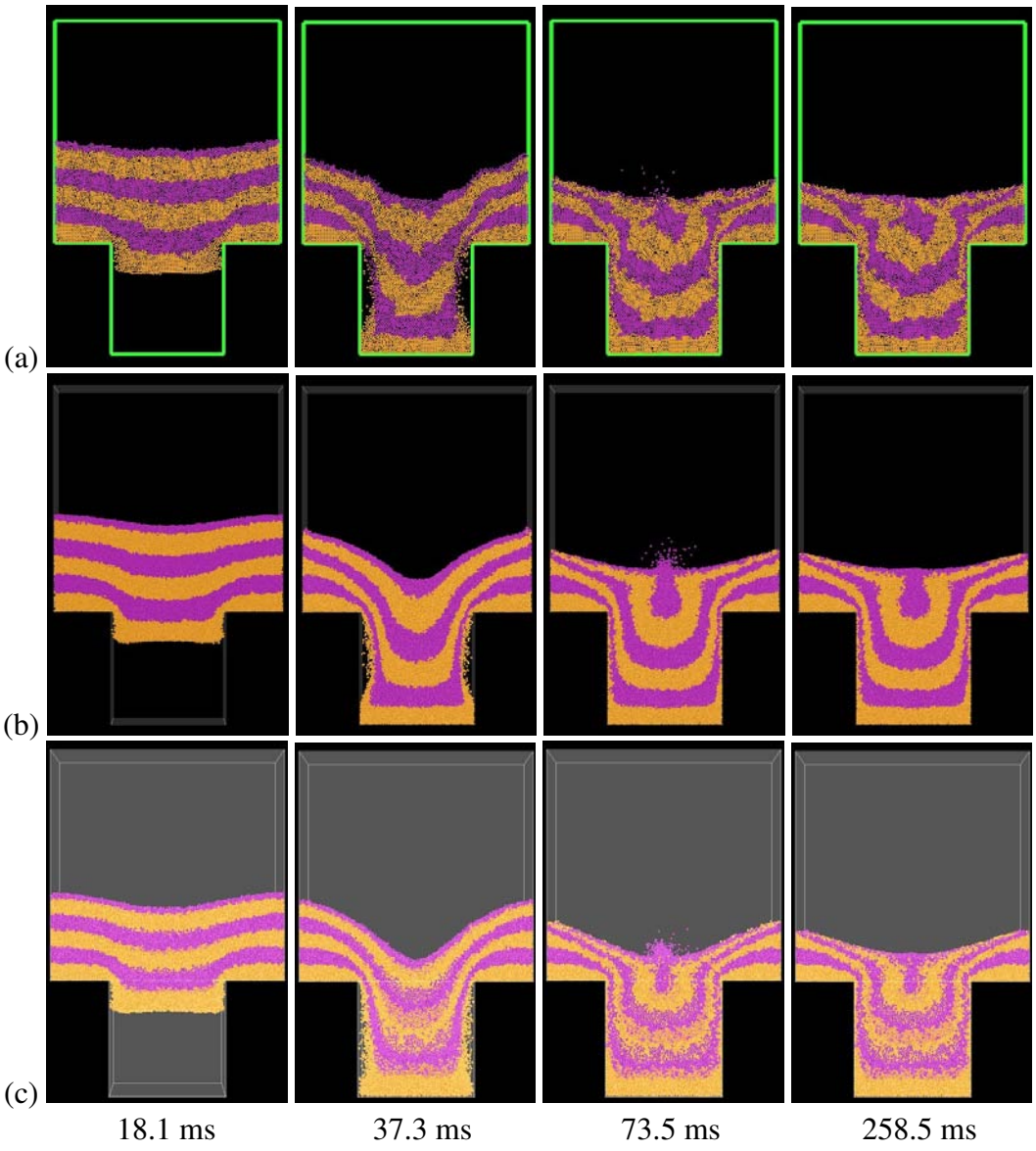

Figure 7.3 Comparison of die filling processes in a vacuum using the (a) 2D model (top row), (b) thin-sliced model (middle row) and (c) fully-3D model (bottom row). The labels indicate the elapsed time from the start of die filling.

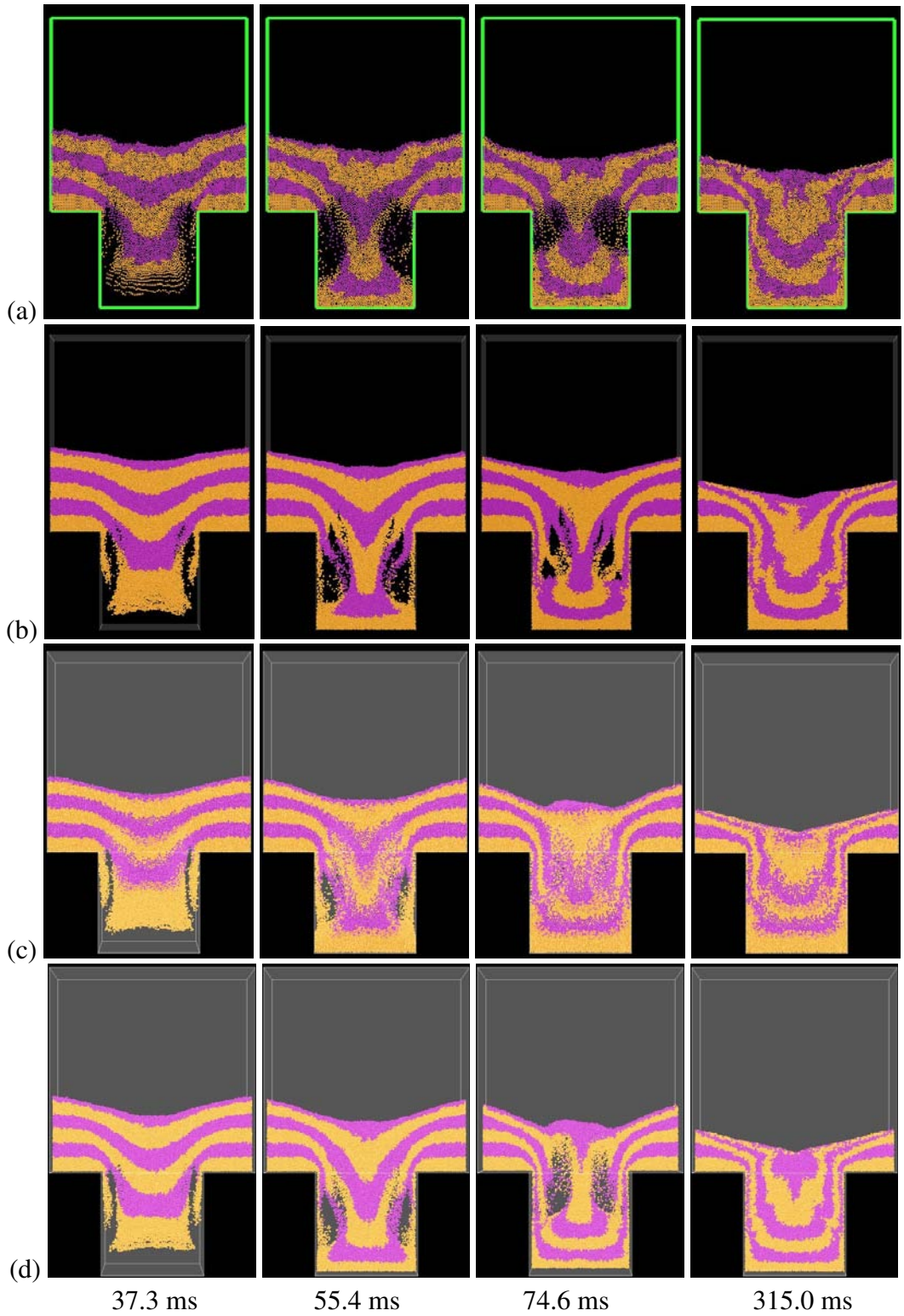

Figure 7.4 Comparison of die filling processes in air using the (a) 2D model (top row), (b) thin-sliced model (second row) and (c) fully-3D model (third row). The corresponding patterns of the slice in the centre of the fully-3D systems are shown in (d). The labels indicate the elapsed time from the start of die filling.

Figure 7.4 shows a comparison of the die filling processes in the presence of air for the three models. The air is entrapped in the die and slows down the filling process. The powder flows into the die mainly from the centre, and as a result, the air is dragged to flow downwards in the centre and then flow aside when meeting the base of the die. Two air bubbles are consequently formed close to the die walls. The bubbles gradually rise up and shrink until they disappear. Figure 7.4c shows the front view of the die filling process using the fully-3D model. From Figure 7.4c, it seems that the bubbles in the fully-3D model are smaller than those observed in the 2D model (Figure 7.4a) and in the thin-sliced model (Figure 7.4b). However, this is not true as demonstrated in Figure 7.4d that shows the corresponding patterns of the slice in the centre of the fully-3D system. It is observed that the patterns in the slice at the centre of the fully-3D system are similar to those in the 2D and thin-sliced models. Therefore, in the fully-3D model, the three dimensional air bubbles can be entrapped inside the particle system and they are difficult to be observed clearly from outside. The 2D model and the thin-sliced model can reproduce the patterns of the slice at the centre of the fully-3D system.

The normalized cumulative mass m/ϕ as a function of filling time is plotted in Figure 7.5, in which the cumulative mass of particles deposited into the die m is normalized by

$$\phi = \rho_b g^{1/2} l b_0^{3/2} \left(1 - k\frac{d_p}{b_0}\right)^{3/2} \tag{7.1}$$

According to Eqs. (3.1) and (3.8), the average slope of the inclined curve before reaching the horizontal line in Figure 7.5 gives the dimensionless mass flow rate M^*. It is clear from Figure 7.5 that the results predicted by three different models are in

very good agreement. During the filling process, the mass initially increases as the particles are deposited into the die until the die cavity is completely filled and then it remains constant. It takes around 0.05 s for the die to be completely filled in a vacuum but over 0.1 s in the presence of air, giving the dimensionless mass flow rates M^*=0.59 for die filling in a vacuum and M^*=0.24 for die filling in air. As shown in Figure 7.4, the powder flow is hindered by the entrapped air, so that a lower powder flow rate is induced for die filling in air.

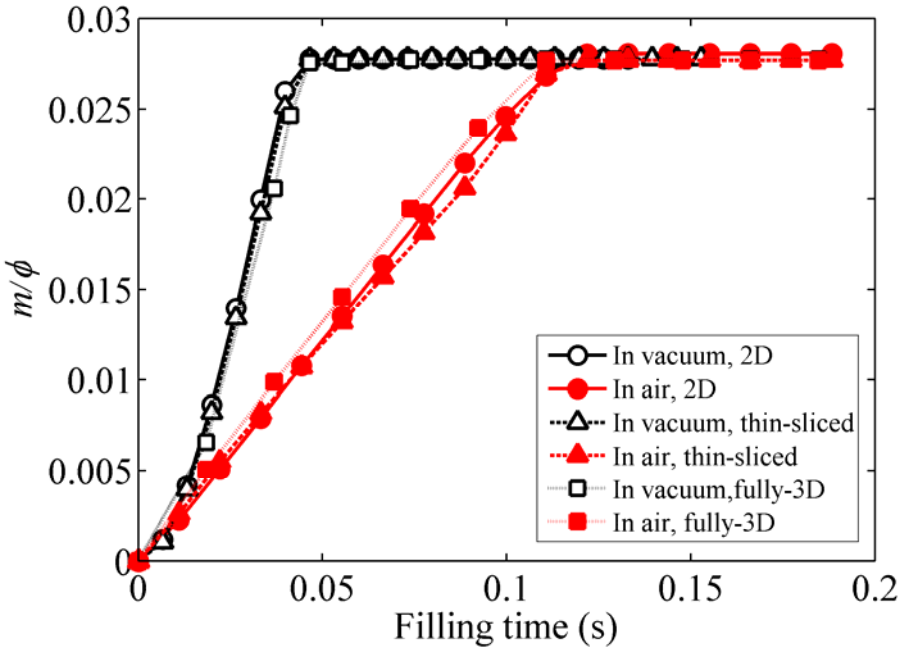

Figure 7.5 Variation of normalized cumulative mass in the die with filling time.

7.4. Density-induced segregation during die filling

As discussed in Chapter 5, the difference in particle density can cause segregation during die filling. In this section, as shown in Figure 7.6, three different models were used to investigate the density-induced segregation: 2D model, thin-sliced model and fully-3D model. Binary mixtures of the particles of the same size but different densities were employed in all three models. In Figure 7.6, the heavy particles of

density ρ_h = 7800 kg/m^3 are coloured in red and the light particles of density ρ_l = 2100 kg/m^3 are coloured in yellow. All the particles have the same diameter of 130 μm. In each binary granular system, the same number of light and heavy particles are employed so that the average volume concentration of each component is equal to 50%.

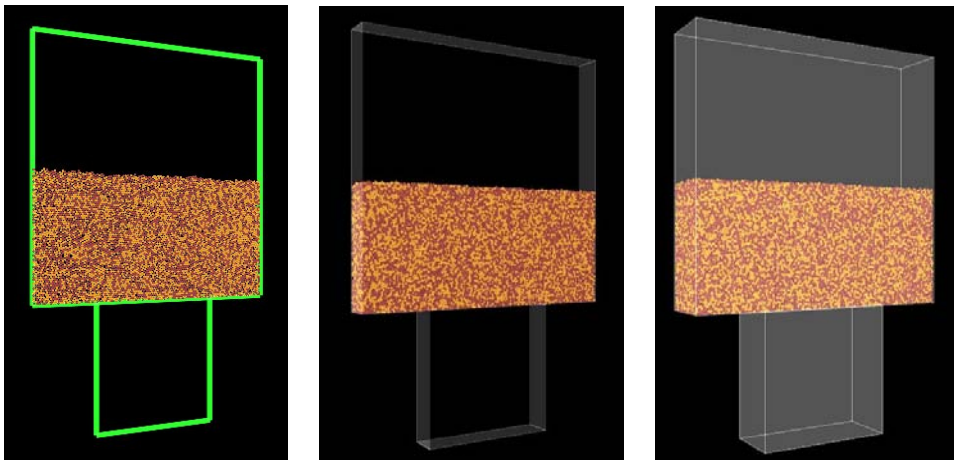

(a) 2D model (b) Thin-sliced model (c) Fully-3D model

Figure 7.6 (a) 2D model, (b) thin-sliced model and (c) fully-3D model for die filling with a stationary shoe and a binary mixture of different density particles.

Figure 7.7 shows the initial volume concentration distributions of the light particles in the powder bed in the shoe before die filling. In both horizontal and vertical directions, the concentration profiles are very uniform for the thin-sliced model and fully-3D model. However, a slight fluctuation of concentration around the average value (i.e. 0.5) is observed for the 2D model. The numbers of particles employed in the 2D model, thin-sliced model and fully-3D model are 6,000, 70,000 and 140,000 respectively. Therefore, much fewer particles are used in the 2D model, which could cause a statistical fluctuation in the concentrations between different parts of the powder bed.

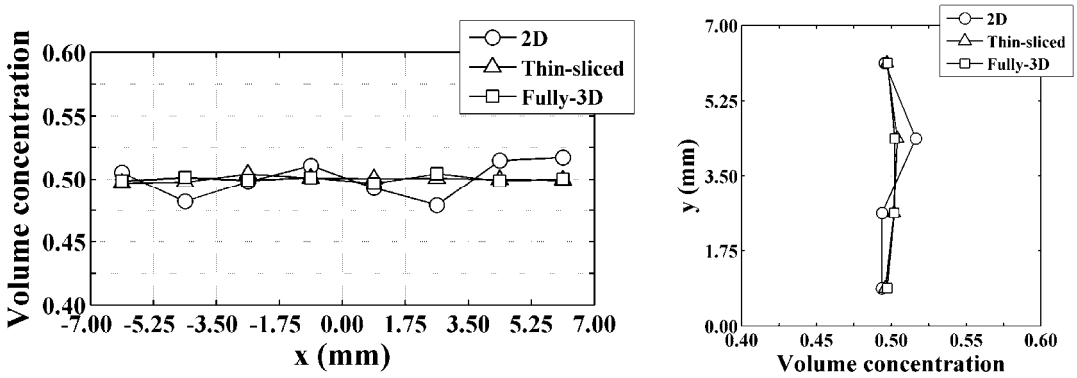

(a) Horizontal direction (b) Vertical direction

Figure 7.7 Initial volume concentration distributions of the light particles in the shoe in the (a) horizontal and (b) vertical directions.

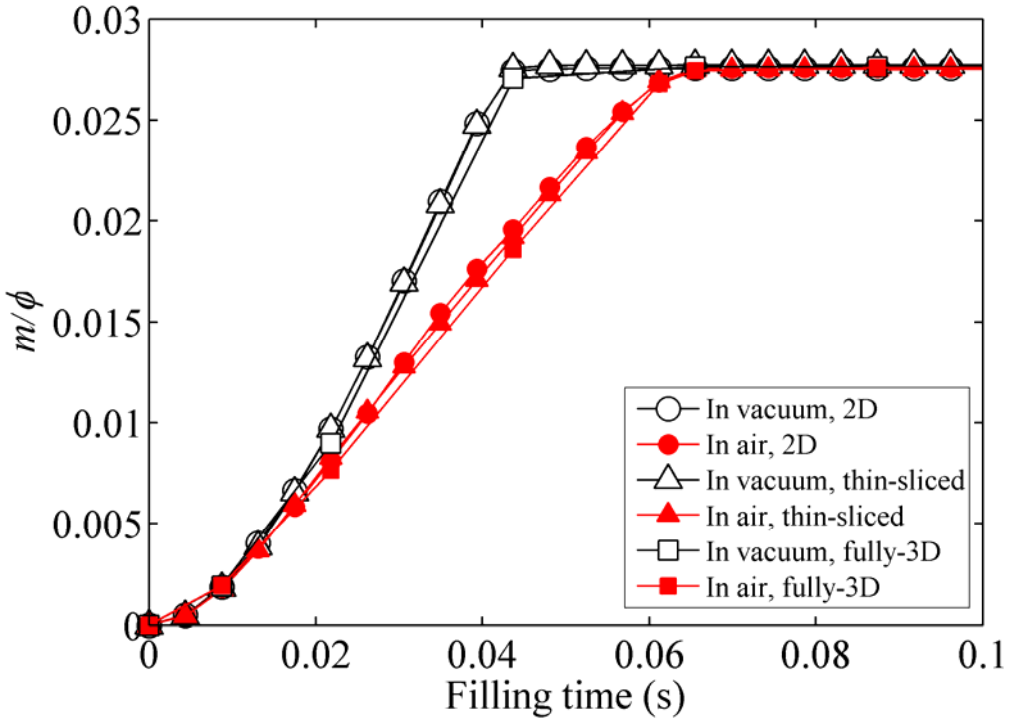

Figure 7.8 Normalized cumulative mass in the die as a function of filling time during die filling with a binary mixture and a stationary shoe.

The macroscopic powder flow patterns during die filling with the binary mixtures are similar to those previously observed during die filling with the monodisperse systems (see Figures 7.3 and 7.4). The normalized cumulative mass in the die m/ϕ as a function of filling time is plotted in Figure 7.8. It is observed that three different

models produce identical results. At an early stage, the normalized mass m/ϕ increases slowly due to the acceleration of particles from the static state, and then it increases more rapidly at a constant rate until the die is completely filled when the mass remains constant. It can be seen that the die is filled more quickly and a higher dimensionless mass flow rate is obtained in a vacuum (M^*=0.60) compared to in air (M^*=0.43).

After die filling, similar particle packing patterns are obtained with different models, as shown in Figure 7.9. The uniformity of the mixture in the die after die filling is subsequently examined. The horizontal concentration distributions of light particles in the die are plotted in Figure 7.10. In the 2D model, a lower concentration of light particles is observed on the right hand side of the die. This segregation is caused by the non-uniformity of the initial powder bed in the shoe before die filling, as discussed in Chapter 5. Due to the very good initial uniformity in the shoe for the thin-sliced model and fully-3D model (Figure 7.7), no horizontal segregation occurs in the die after die filling using these two models.

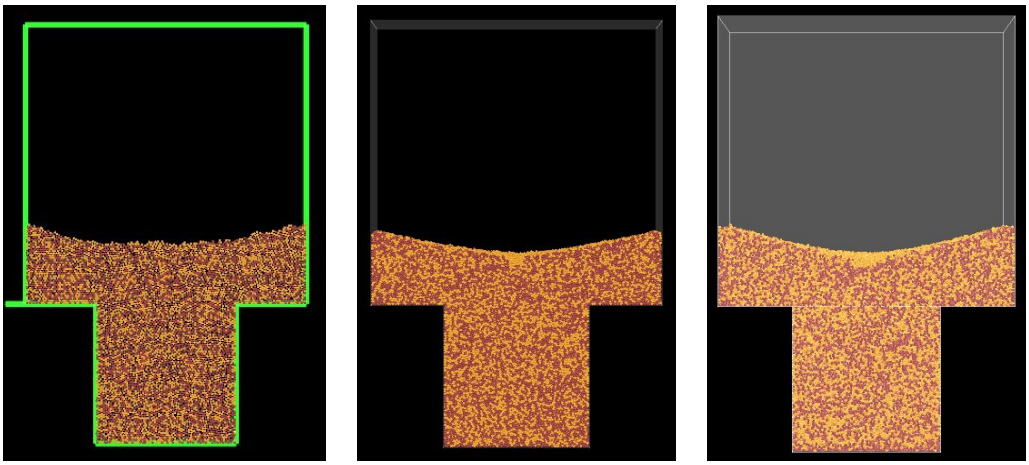

(a) 2D model (b) Thin-sliced model (c) Fully-3D model

Figure 7.9 Final packing patterns after die filling in air with a stationary shoe using three different models.

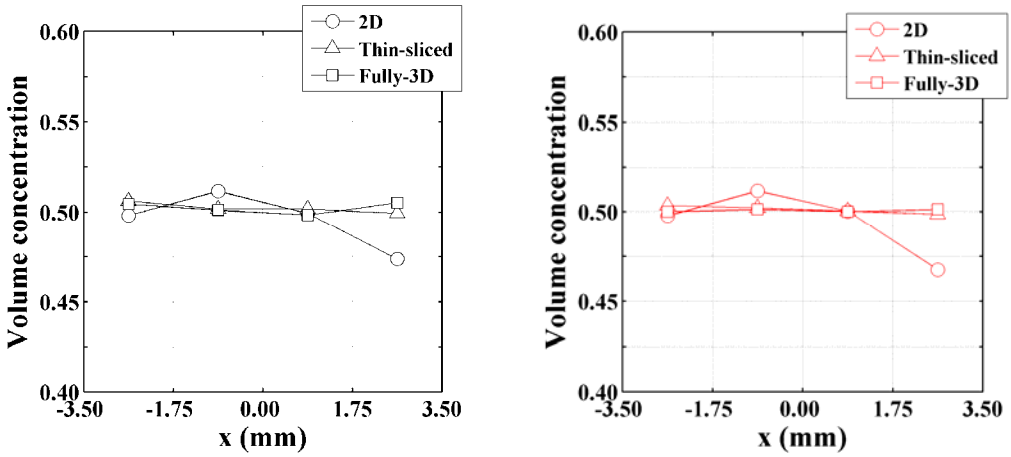

(a) In a vacuum (b) In air

Figure 7.10 Horizontal concentration distributions of light particles in the die after die filling with a stationary shoe (a) in a vacuum and (b) in air.

The corresponding vertical concentration distributions of light particles are plotted in Figure 7.11. For die filling in a vacuum, the concentration of light particles is slightly lower at the bottom of the die using the 2D model and no segregation is observed when the thin-sliced and fully-3D models are used. In the presence of air, segregation occurs and the concentration of light particles at the bottom of the die is generally lower than that at the top for all the three models.

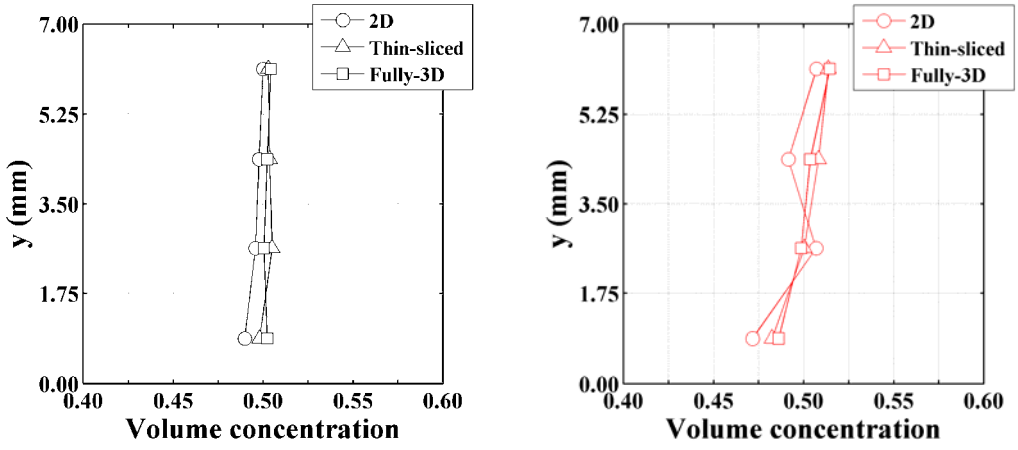

(a) In a vacuum (b) In air

Figure 7.11 Vertical concentration distributions of light particles in the die after die filling with a stationary shoe (a) in a vacuum and (b) in air.

Die filling with the binary mixture and a moving shoe at a velocity of 70 mm/s was also simulated using the thin-sliced model and fully-3D model. The powder flow patterns are similar to those observed using the 2D model, as shown in Figure 5.3. During this die filling process, nose-flow occurs with the cascading of particles from the top free surface into the die. When the flowing powder stream hits the base of die or the deposited powder bed, the light particles usually gain higher rebounding velocities due to the small inertia. Thus, segregation occurs with the fronts of the rebounding flow streams rich in light particles.

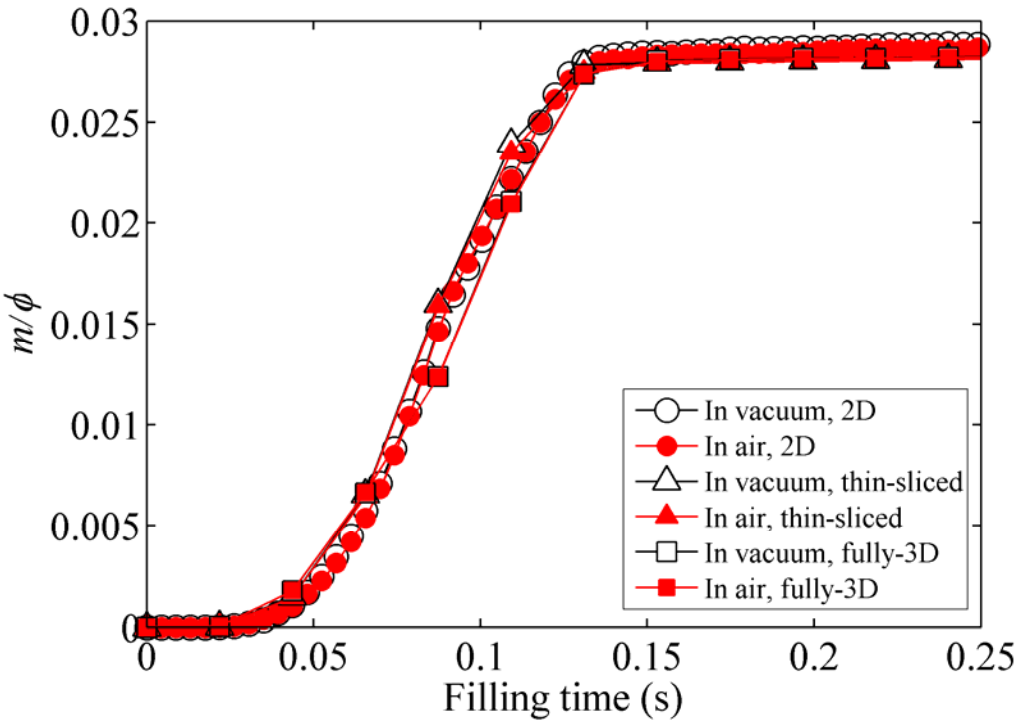

Figure 7.12 Normalized cumulative mass in the die as a function of filling time during die filling with a binary mixture and a moving shoe.

The normalized cumulative mass in the die as a function of filling time during die filling with a moving shoe is plotted in Figure 7.12. It is evident that identical results are obtained using the three different models; and also the curves for die filling in air are consistent with those for die filling in a vacuum. The latter is due to the fact that the nose-flow dominates this filling process and the air can easily escape from the die

before the die opening is completely covered by the powder mass (Figure 5.3). Therefore, the presence of air has a very limited effect on the powder flow during this type of die filling process. In addition, a smaller dimensionless mass flow rate is obtained for die filling with a moving shoe (M^*=0.28) compared to die filling with a stationary shoe in a vacuum (M^*=0.60) and in air (M^*=0.43). This is because for die filling with a stationary shoe, the powder can always be delivered into the die through nearly the entire die opening while, for die filling with a moving shoe, the effective area for the power to flow through into the die increases gradually from zero as the shoe moves over the die opening from one side to the other.

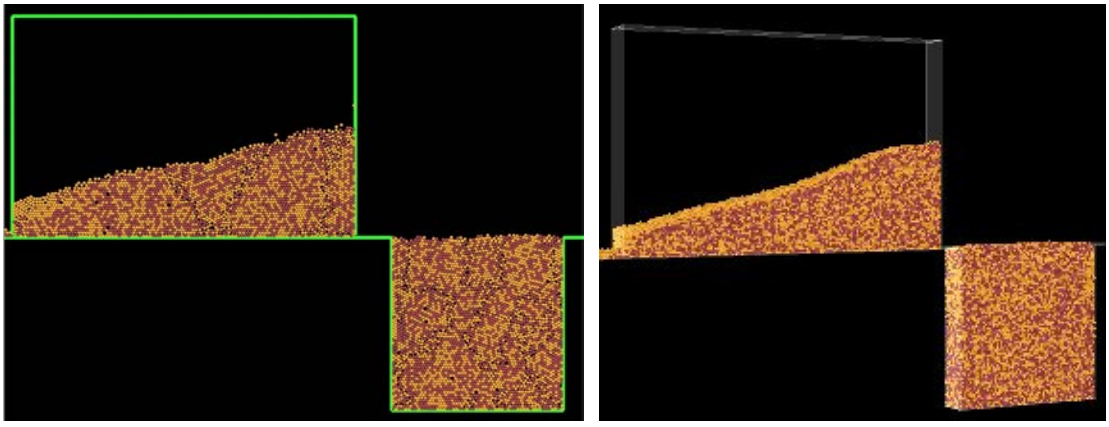

(a) 2D model (b) Thin-sliced model

(c) Fully-3D model (d) A slice in the centre of fully-3D model

Figure 7.13 Final packing patterns after die filling with a moving shoe at a velocity of 70 mm/s using the (a) 2D model, (b) thin-sliced model and (c) fully-3D model. A slice in the centre of fully-3D model is shown in (d).

The final packing patterns after die filling with a moving shoe using different models are shown in Figure 7.13. During the die filling process, a slope is formed in the shoe and the light particles migrate to the surface and then accumulate at the foot of the slope. Figure 7.13c shows the front view of the particle state in the fully-3D model. It is observed that the bottom region of the slope is covered by light particles. A slice in the centre of the fully-3D model is shown in Figure 7.13d to illustrate the situation inside the fully-3D model, and the state of this slice is very close to that of the thin-sliced model (Figure 7.13b).

The horizontal and vertical concentration distributions of light particles in the die after die filling with the moving shoe are shown in Figure 7.14 and Figure 7.15, respectively. Segregation occurs with a lower concentration of light particles on the leading side of the die (referring to the direction of shoe motion) and also a lower concentration of light particles at the bottom of the die. This segregation is caused by the difference in the inertia of particles: the light particles which have small inertia rebound higher and further than the heavy ones during collisions. This segregation mechanism has been discussed in detail in Chapter 5. By comparing the results with different models, it is found that although the same segregation pattern is obtained in all the models, the 2D model slightly exaggerates the degree of segregation. In the 2D model, the movements of particles are restrained within a plane. Therefore, the third dimension in the thin-sliced model and fully-3D model seems to facilitate the mixing of particles by offering more freedom for the particles to move. In addition, the small number of particles used in the 2D model can cause statistical fluctuations.

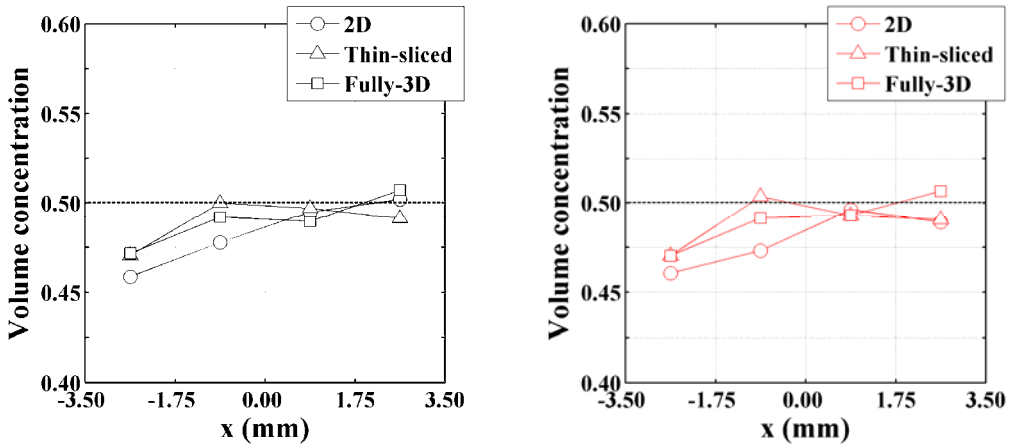

(a) In a vacuum (b) In air

Figure 7.14 Horizontal concentration distributions of light particles in the die after die filling with a moving shoe (a) in a vacuum and (b) in air.

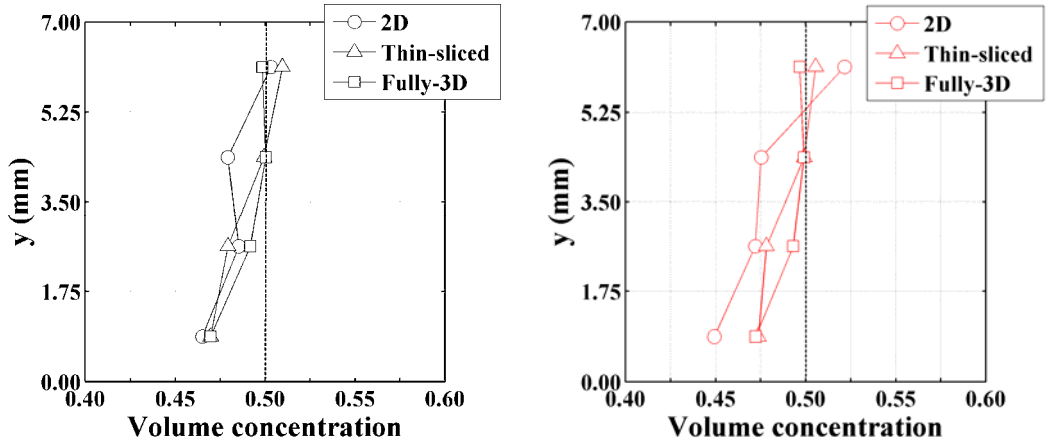

(a) In a vacuum (b) In air

Figure 7.15 Vertical concentration distributions of light particles in the die after die filling with a moving shoe (a) in a vacuum and (b) in air.

7.5. Summary

Three dimensional simulations were performed to investigate the powder flow behaviour and density-induced segregation in die filling. A comparison was made between the 3D simulations and 2D simulations. It was found that the powder flow patterns and die filling rate are in very good agreement using 2D and 3D models. The

tendencies of density-induced segregation predicted by 2D models are similar to those by 3D models. However, the 2D model slightly exaggerates the degree of segregation compared to the 3D models, implying that the third dimension can facilitate the mixing of particles by offering more freedom for particle movement.

CHAPTER 8: SIZE-INDUCED SEGREGATION

8.1. Introduction

This chapter reports the results of 3D simulations on the segregation of a binary mixture of different-sized particles during die filling. A parametric study is conducted to examine the effects of shoe velocity, particle size ratio, initial fines mass fraction, cohesion and the height of powder bed in the shoe on segregation tendency.

8.2. Computational set-up

Thin-sliced models were adopted to simulate die filling process with a stationary shoe and a moving shoe as illustrated in Figure 8.1 In each model, two parallel periodic boundaries are introduced in the *z*-direction (i.e. thickness direction) and separated by a distance of 1.4 mm (*t*). 2967 coarse particles of diameter d_c = 360 μm and 21096 fine particles of diameter d_f = 90 μm are randomly generated and mixed in a shoe of width *L*=14 mm. All the particles have the same density of 1500 kg/m^3. Thus, the initial fines mass fraction x_f, which is defined as the ratio of the mass of fine particles to the total mass of all particles, is equal to 10%. After initial deposition in the shoe under gravity, a densely packed powder bed of height 6.8 mm (*H*) is obtained. During die filling, the particles are delivered into a die of dimensions 7 mm × 7 mm (*w*× *h*). The coarse and fine particles are coloured in red and yellow, respectively, in all the plots of particle states in this chapter, as exemplified in Figure 8.1.

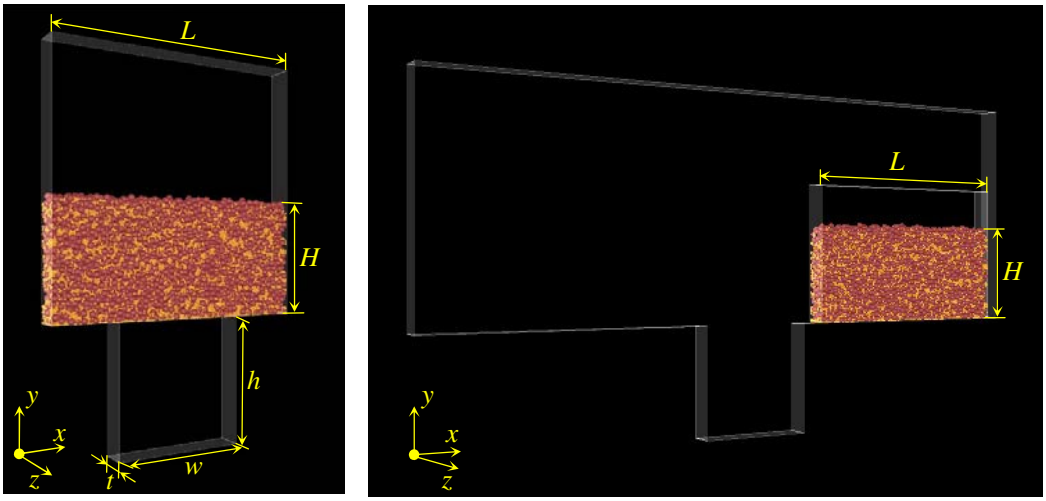

(a) Stationary shoe (b) Moving shoe

Figure 8.1 Thin-sliced models for die filling with a (a) stationary shoe and a (b) moving shoe.

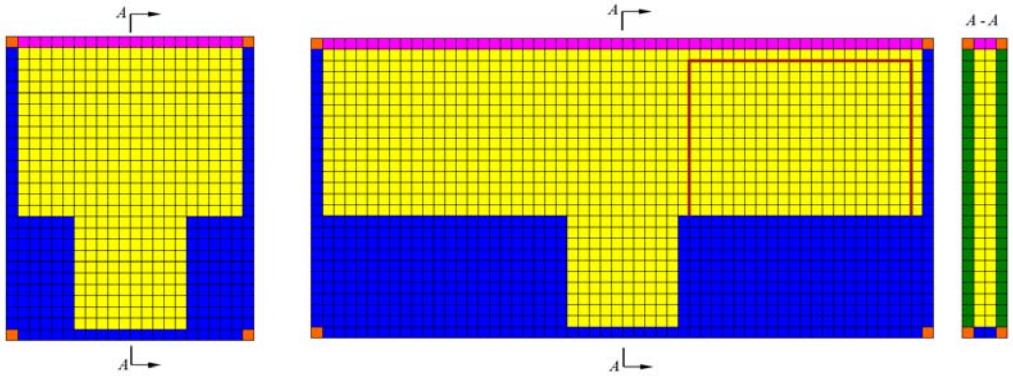

(a) Stationary shoe (b) Moving shoe

Figure 8.2 Schematic diagrams of the computational fluid cells and boundary conditions for the thin-sliced models of die filling with a (a) stationary shoe and a (b) moving shoe. [□: interior fluid cell; ■: impermeable wall cell, no slip; ■: continuous gas outflow wall cell, free slip; ■: corner cell; ■: periodic boundary cell]

Figure 8.2 shows the corresponding schematic diagrams of the computational fluid cells and boundary conditions. The air domain is uniformly meshed with the identical cells of dimensions 0.7×0.7×0.7 mm. In the *x*-*y* plane, the impermeable wall boundaries without slip are specified around the air field except at the top where the continuous gas outflow boundary is used. In the thickness direction (i.e., *z*-direction),

two periodic boundaries are introduced for the air flow. The air of the same properties as previously specified in Section 7.2 is also used here.

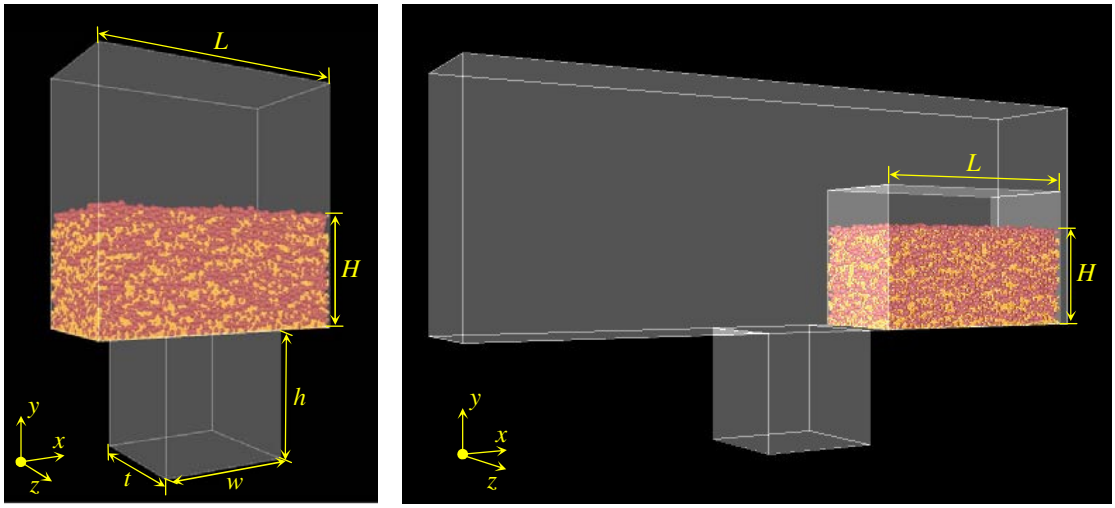

(a) Stationary shoe (b) Moving shoe

Figure 8.3 Fully-3D models for die filling with a (a) stationary shoe and a (b) moving shoe.

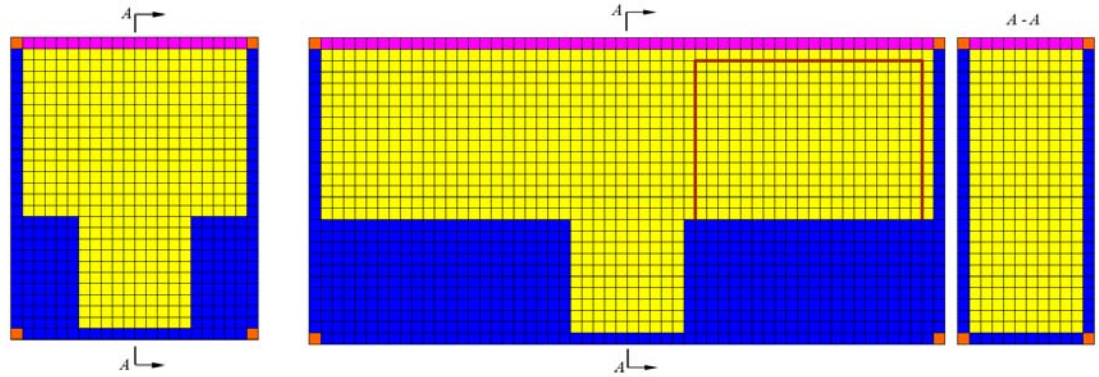

(a) Stationary shoe (b) Moving shoe

Figure 8.4 Schematic diagrams of the computational fluid cells and boundary conditions for the fully-3D models of die filling with a (a) stationary shoe and a (b) moving shoe. [□ : interior fluid cell; ■: impermeable wall cell, no slip; ■: continuous gas outflow wall cell, free slip; ■: corner cell]

Fully-3D models were also employed as shown in Figure 8.3. In the fully-3D models, the physical wall boundaries are introduced in the z-direction instead of the periodic boundaries that are used in the thin-sliced models. The thickness of the fully-3D model t is set to 7 mm, five times that of the thin-sliced model (t =1.4 mm). Therefore,

five times amount of the fine and coarse particles as used in the thin-sliced model are generated in the fully-3D model in order to keep the average fines mass fraction x_f and the height of powder bed H identical to those used in the thin-sliced model (i.e., x_f =10% and H=6.8 mm). The schematic diagrams of the computational mesh of the air domain for the fully-3D models are plotted in Figure 8.4. The air domain is also meshed using the identical cells of dimensions 0.7×0.7×0.7 mm. In the fully-3D model, the boundary conditions for the air in the *x-y* plane are the same to those used in the thin-sliced model; however, two parallel impermeable wall boundaries without slip are employed in the *z*-direction.

8.3. Powder flow patterns

Die filling processes with a stationary shoe in a vacuum using the thin-sliced and fully-3D models are shown in Figure 8.5. The powder flow patterns in a vacuum obtained using two different models are similar: the powder flows smoothly into the die, and the empty space is observed inside the die close to the vertical die walls at the early stage (say at T = 38.4ms) of die filling due to the effect of the 'empty annulus' as previously discussed in Section 3.3.1. During die filling, the particles located in the bottom corners of the shoe stay static, forming two stagnant zones. Due to the frictional interaction, the particles close to the stagnant zones flow down at a lower speed compared to the particles in the centre. As a result, a V-shaped concave profile is gradually formed at the top surface with the rapid discharge of particles from the centre of the powder bed. In this process, the coarse particles flow down the slopes more easily by rolling over the top of the fine particles and accumulate at the bottom of the concave. As a result, an excess of coarse particles is eventually generated in the centre of the shoe (Figure 8.5). This phenomenon is consistent with the previous

observations of the segregation in the discharge from the flat-bottomed bins obtained experimentally by Samadani et al. (1999) and numerically by Ketterhagen et al. (2008). After die filling, a layer of coarse particles is observed on the top surface. This is due to the fact that the fine particles have a higher probability to fill the voids in the lower layer below the surface, so that the fines sift down with the coarses remaining on the surface.

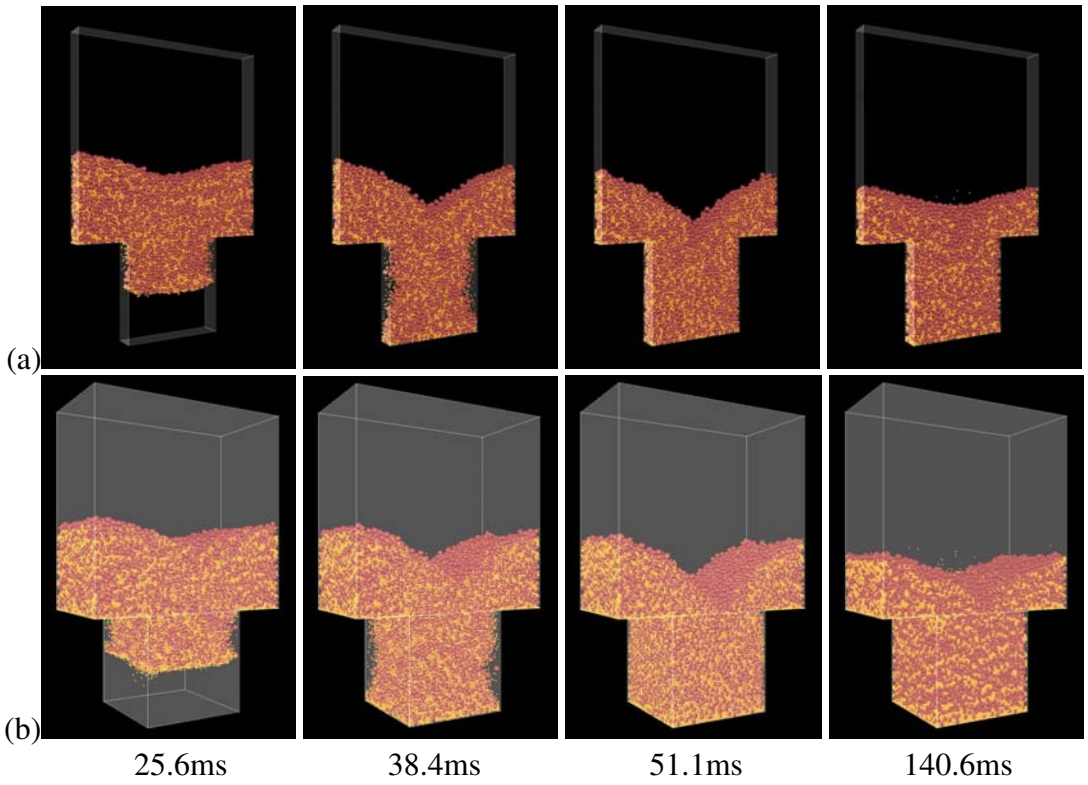

Figure 8.5 Die filling with a stationary shoe in a vacuum using the (a) thin-sliced model (top row) and (b) fully-3D model (bottom row). The labels indicate the elapsed time of filling process.

Figures 8.6 shows the powder flow patterns during die filling with a stationary shoe in the presence of air. Similar powder flow patterns are also obtained using the thin-sliced model and fully-3D model. As discussed in Chapter 3, the fine particles are more sensitive to the air and the presence of air has a more significant impact on the flow of the fine particles. As a result, the flow of fine particles is hindered in the

regions close to the vertical die walls where the air is entrapped (see Figure 8.6). During die filling in air, a concave profile is also generated on the top free surface. However, due to the entrapped air, the discharge rate of powder is reduced so that the concave profile formed in air is not as steep as that in a vacuum, which makes the coarse particles more difficult to flow down along the gentle slopes. Hence, a coarses-rich region in the centre of the shoe, which can be found for die filling in a vacuum (Figure 8.5), is not observed when air is present (Figure 8.6). After die filling, a layer of coarse particles is also obtained on the top surface due to the percolation of fine particles, although this effect is suppressed by the resistance from air.

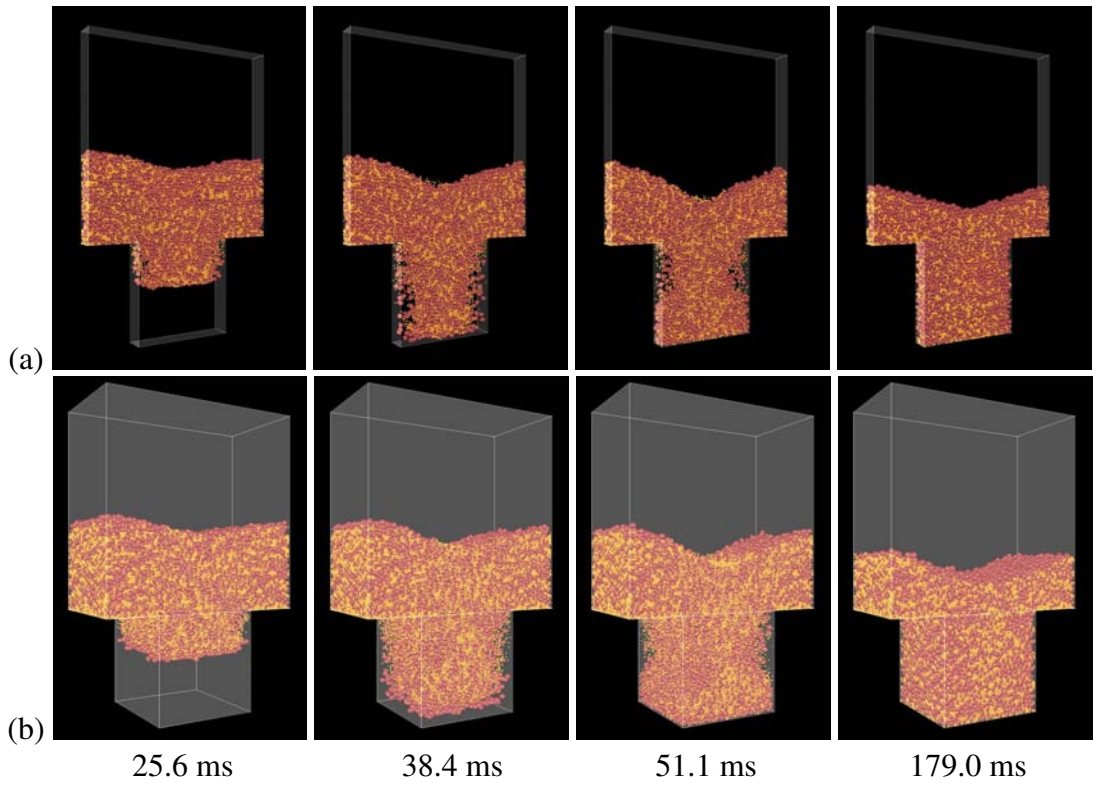

Figure 8.6 Die filling with a stationary shoe in air using (a) thin-sliced model and (b) fully-3D model. The labels indicate the elapsed time of filling process.

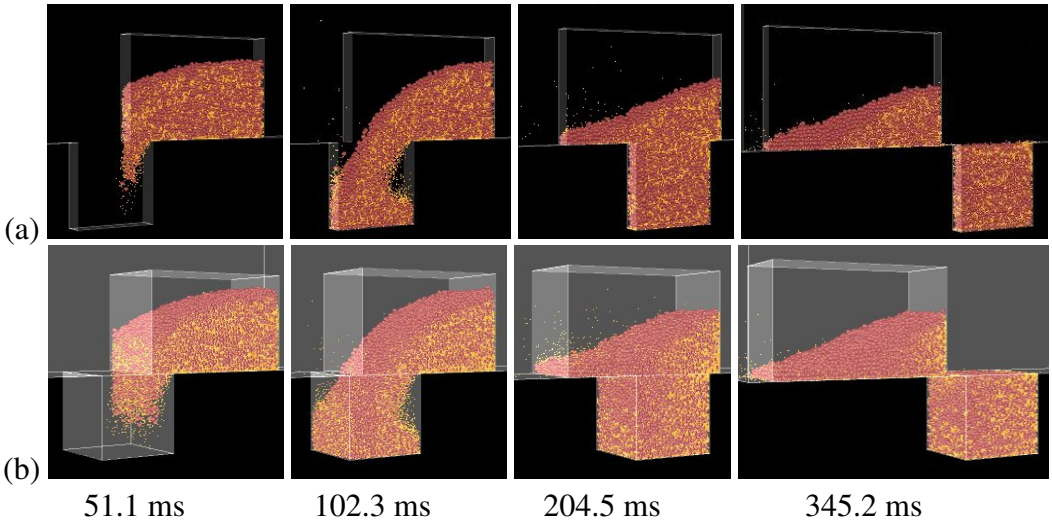

Figure 8.7 Die filling in a vacuum with a moving shoe at a velocity of 70 mm/s using (a) thin-sliced model and (b) fully-3D model. The labels indicate the elapsed time of die filling.

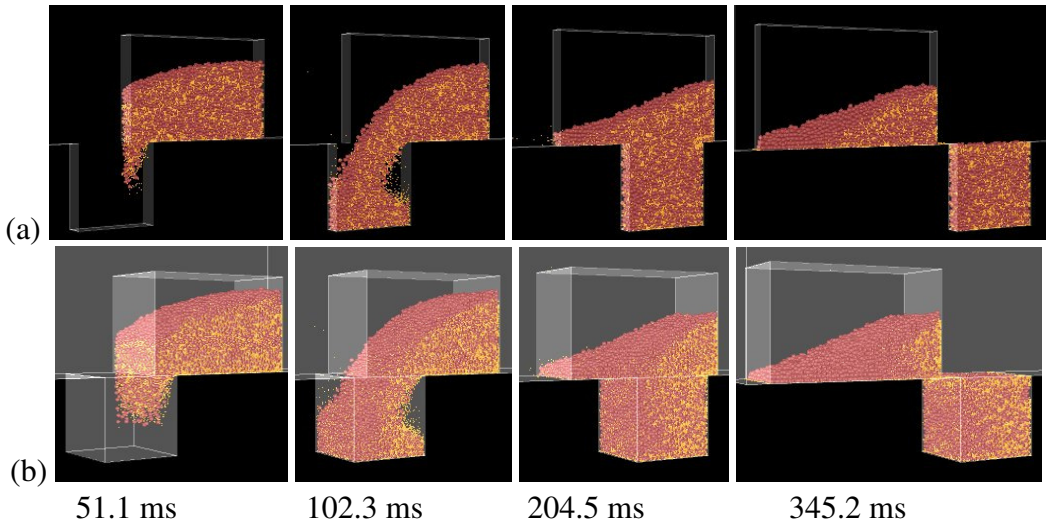

Figure 8.8 Die filling in air with a moving shoe at a velocity of 70 mm/s using (a) thin-sliced model and (b) fully-3D model. The labels indicate the elapsed time of die filling.

Figure 8.7 shows the die filling process with a moving shoe in a vacuum. The shoe velocity v_s is set to 70 mm/s. At the beginning, the powder only from the bottom of the shoe is delivered into the die. A nose-shaped flow stream is then formed, and the powder can flow into the die from the top free surface. In the free surface flow, the coarse particles can more easily roll over the top of the fines while the fines sift into

the powder bed. This results in a coarses-rich powder stream flowing into the die cavity from the top surface and occupying the leading side of the die, which the shoe moves towards. As the shoe moves across the die, a slope is gradually formed in the shoe. During this process, the coarse particles migrate to the surface and then accumulate at the bottom, whereas the fine particles sift to the bulk of the powder. Powder flow patterns during die filling at the same shoe velocity (i.e. v_s=70 mm/s) but in the presence of air are shown in Figure 8.8. For this particular die filling process, air can escape from the die before the die is completely covered by the powder bed. As a result, the effect of air is negligible and the powder flow patterns in air are similar to those in a vacuum (Figure 8.7). Similar powder flow patterns are also obtained using the thin-sliced model and fully-3D model for die filling with a moving shoe.

8.4. Segregation in powder flow

In order to examine the initial uniformity of the densely-packed bed in the shoe before die filling, the concentration distributions of fines along *x*, *y* and *z* directions for this powder bed are plotted in Figure 8.9. For the concentration distribution of fines in the *x*-direction, the powder bed is partitioned into several identical cells along the *x*-direction, and the fines mass fraction in each cell, x_i, normalized by the average fines mass fraction of the whole powder bed, x_f, is plotted as a function of the *x*-coordinate of the cells, *x*, normalized by the width of the powder bed, *L*, as shown in Figure 8.9a. Similarly, by partitioning the powder bed uniformly along the *y* and *z*-directions, the concentration distributions of fines along the *y* and *z*-directions are plotted in Figures 8.9b and c, in which, the *y* and *z*-coordinates of the cells, *y* and *z*, are normalized by the height (*H*) and thickness (*t*) of powder bed, respectively.

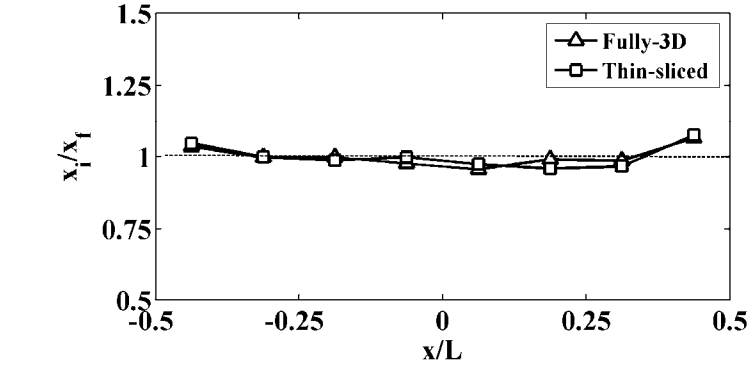

(a) *x*-direction

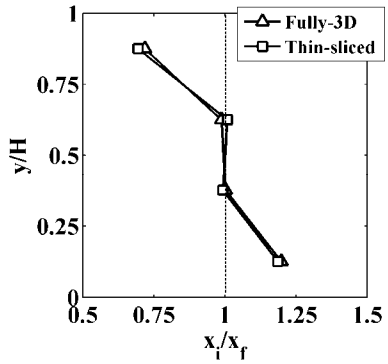

(b) *y*-direction

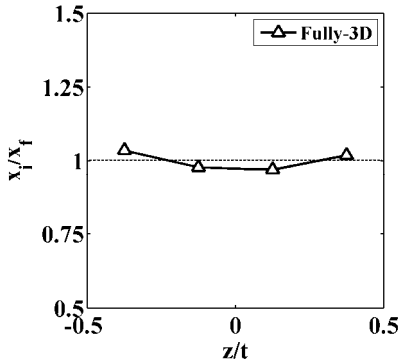

(c) *z*-direction

Figure 8.9 Initial concentration distributions of fines along (a) *x*-direction, (b) *y*-direction and (c) *z*-direction in the shoe.

In Figure 8.9, slight fluctuation of x_i/ x_f around unity is observed in the horizontal directions (i.e., *x*-direction for both thin-sliced and fully-3D models, and *z*-direction only for fully-3D model), indicating no segregation occurs with each cell having the average fines mass fraction (i.e. x_f). While significant segregation occurs in the vertical direction (i.e., *y*-direction) with a higher fines mass fraction at bottom and a lower value at top. This is due to the fact that during the initial deposition process the fines can pass through the void space in the matrix of coarse particles and sift to the bottom region, leading to an excess of fines at the bottom and a depletion of fines at the top. This is normally referred to as the segregation induced by the percolation or sifting mechanism (Ketterhagen et al., 2008).

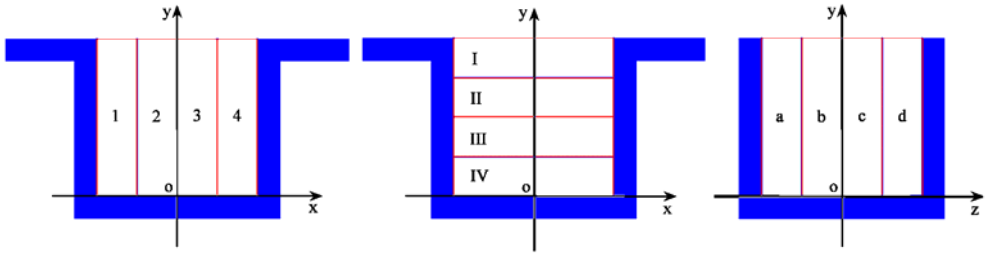

(a) (b) (c)

Figure 8.10 Partitions of die cavity in the (a) *x*-direction, (b) *y*-direction and (c) *z*-direction. The partition in the *z*-direction is only for the fully-3D model.

Size-induced segregation may also occur when powders start to flow from the shoe into the die. To examine the segregation in the die, the die cavity is partitioned using the identical cells along the *x*, *y* and *z*-directions, respectively, as shown in Figure 8.10. Since there is only a small thickness in the *z*-direction for the thin-sliced model (Figure 8.1), the partition in the *z*-direction is therefore only applicable to the fully-3D model. The fines mass fraction in each cell can be calculated at a given instant during die filling so that the time evolution of the concentration can be obtained in different parts of the die during die filling process. Size-induced segregation during die filling will be discussed as follows.

8.4.1. Die filling with a stationary shoe

Figure 8.11 shows the segregation results of powder discharge from a stationary shoe (v_s =0) in terms of the fines mass fraction in a given sample of mass Δm_i discharged from the shoe, x_i^s (see Appendix A), normalized by the initial average fines mass fraction, x_f, as a function of the fractional mass discharged, m/m_{total}, in which, m is the cumulative mass discharged from the shoe and equals to $\sum_i \Delta m_i$, and m_{total} is the total mass discharged during the entire die filling process. A high concentration of

fines is observed in the first sample as the powder from the lower region of the shoe, where the fines mass fraction is high (see Figure 8.9b), flows into the die first. Thereafter, the fines mass fraction fluctuates slightly around the initial average value x_f (i.e. $x_i^s/x_f \approx 1$) for die filling in a vacuum. While the fines mass fraction decreases to a level lower than x_f (i.e. $x_i^s/x_f < 1$) in the presence of air. This is because the entrapped air hinders the deposition of fines, resulting in a depletion of fines in the powder discharged from the shoe. When the die cavity is close to be completely filled, the fine particles have a better chance than the coarse ones to fill the limited space left in the die. Therefore, the fines mass fraction increases abruptly at the late stage during die filling in a vacuum and in air.

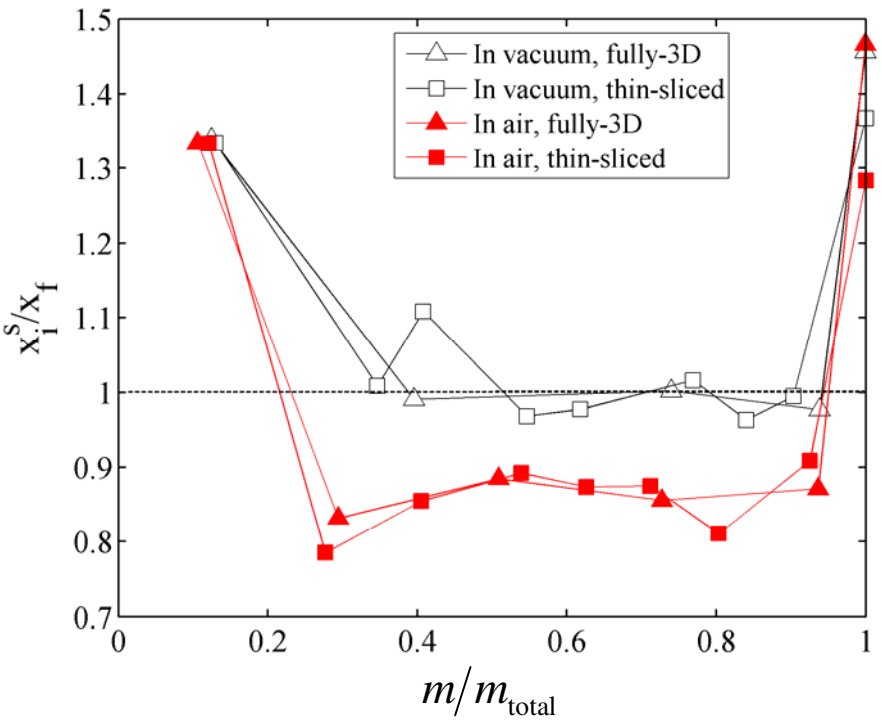

Figure 8.11 Variation of normalized fines mass fraction in a given sample discharged from the shoe, x_i^s/x_f, with the fractional mass discharged, m/m_{total}, during die filling with a stationary shoe (v_s =0).

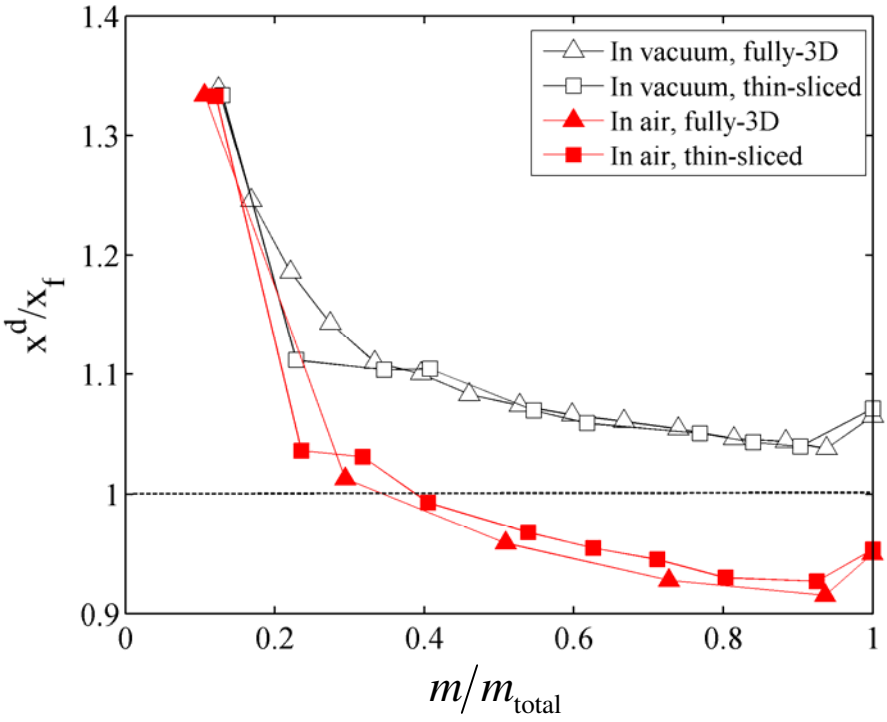

Figure 8.12 Variation of normalized transient fines mass fraction in the die, x^d/x_f, with the fractional mass discharged, m/m_{total}, during die filling with a stationary shoe (v_s =0).

Figure 8.12 plots the transient fines mass fraction in the die, x^d (see Appendix A), normalized by x_f, as a function of the fractional mass discharged from the shoe, m/m_{total}, during die filling with a stationary shoe. The transient fines mass fraction in the die x^d is referred to as the ratio of the mass of fine particles to the total mass of all particles in the die at a given instant during die filling. At the early stage, the fines mass fraction in the die decreases sharply until m/m_{total} is equal to 0.3. When 0.3< m/m_{total} <0.9, the fines mass fraction decreases at a much lower rate. When the die is close to being fully filled (i.e. m/m_{total} >0.9), an increase in the fines mass fraction is observed. The fines-rich powder from the bottom of the shoe flows into the die first causing a high concentration of fines in the die at the early stage, and this is followed by a well-mixed powder so that the overall concentration of fines decreases gradually

as more well-mixed powder flows in. When the die is almost fully filled, fines are easier to be filled into the limited space resulting in an increase in fines mass fraction in the die. It is also observed that due to the effect of air the fines mass fraction in the die x^d during die filling in air is always lower than that in a vacuum when m/m_{total} >0.2. In addition, when m/m_{total} >0.4, x^d becomes lower than the initial average value of the system x_f (i.e., x^d / x_f <1) for die filling in air while it still remains higher than x_f (i.e., x^d / x_f >1) for die filling in a vacuum. After die filling, an excess of fines is obtained in the die in a vacuum and a depletion of fines is obtained in air due to the resistance of the entrapped air on the flow of fines.

The die cavity has been partitioned into identical cells along the *x*, *y* and *z*-directions, respectively, as shown in Figure 8.10. Figure 8.13 shows the variation of normalized fines mass fraction in each cell with the fractional mass discharged, m/m_{total}, during die filling in a vacuum and in air. The results in Cells 1-4 (Figure 8.10a) are shown in Figure 8.13a. The fines mass fraction in each cell is initially higher and then decreases gradually at the early stage (m/m_{total} <0.4). In the central region (Cells 2 and 3), the fines mass fraction remains constant at the initial average value x_f after the early stage (m/m_{total} >0.4) for die filling in a vacuum and in air. In the regions close to the die walls (cells 1 and 4), the fines mass fraction for die filling in air is significantly lower than that in a vacuum when m/m_{total} >0.2. This is because the air is entrapped in the regions between the central flow stream and die walls and two air pockets are formed close to die walls (see Figure 8.6), and the entrapped air hinders the deposition of fines to the regions close to the die walls.

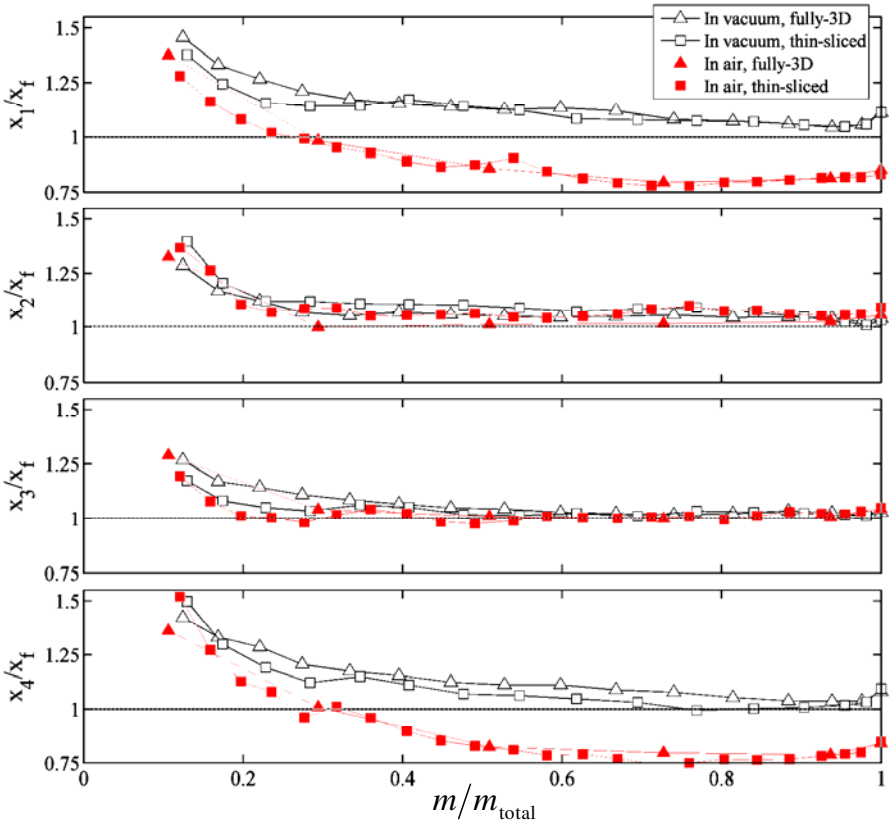

(a) Cells 1-4

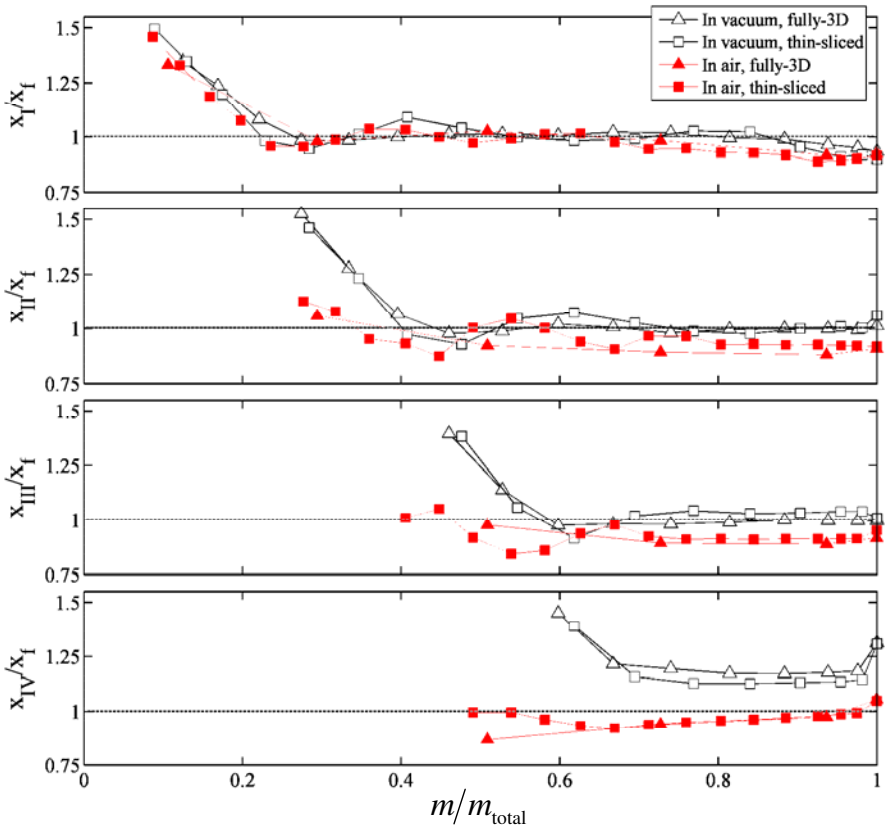

(b) Cells I-IV

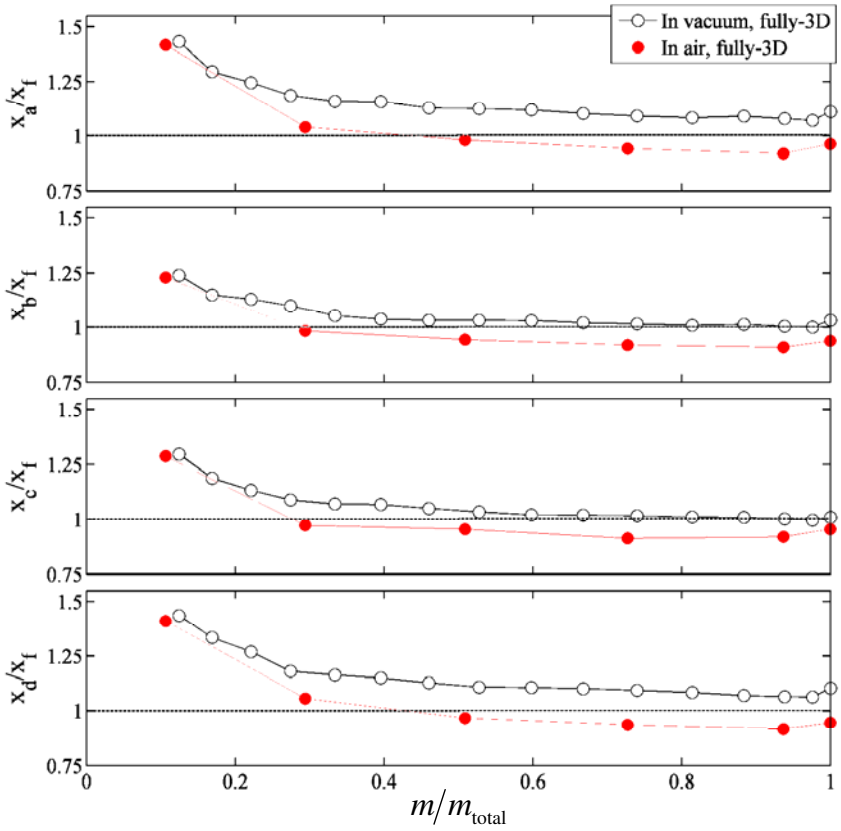

(c) Cells a-d

Figure 8.13 Fines mass fractions in (a) Cells 1, 2, 3 and 4 (obtained by partitioning the die in the *x*-direction), (b) Cells I, II, III and IV (in the *y*-direction) and (c) Cells a, b, c and d (in the *z*-direction) normalized by the initial average fines mass fraction, x_f, as a function of the fractional mass discharged, m/m_{total}, during die filling with a stationary shoe.

Figure 8.13b shows the evolution of the concentration of fines in each layer of the die (Figure 8.10b). For die filling in a vacuum, the fines mass fraction in the top three layers (Cells I, II and III) decreases as the front of the flow stream passes through the layer, and then the fines mass fraction fluctuates slightly around the initial average fines mass fraction x_f. The fines-rich front of the flow stream is eventually packed in the bottom layer, resulting in a very high fines mass fraction in Cell IV. At the late stage, an increase in fines mass fraction is observed in the bottom layer (Cell IV) due to the percolation of fines. For die filling in air, the fines mass fraction at the front of

powder flow stream decreases as the powder flows down from the top to the bottom, due to the effect of air drag on the flow of fine particles. At the late stage of die filling in air, the fines mass fraction is slightly lower than the initial average fraction x_f in the top three layers (Cells I, II and III), and only a mild excess of fines is observed in the bottom layer (Cell IV).

Figure 8.13c shows the evolution of the concentration of fines in the Cells a-d (Figure 8.10c) for the fully-3D model. The evolution of fines mass fraction in each cell follows the similar trend: the fines mass fraction decreases abruptly at the early stage and then decreases gradually and finally increases slightly when the die is close to be completely filled. The fines mass fraction in air is generally lower than that in a vacuum.

8.4.2. Die filling with a moving shoe

Figure 8.14 plots x_i^s / x_f as a function of m/m_{total} for die filling with a moving shoe at a shoe velocity of 70mm/s. A higher fines mass fraction is observed at the early stage due to the fact that the fines-rich powder at the bottom of the shoe flows into the die first (Figures 8.7 and 8.8). After that, the fines mass fraction decreases and falls below the initial average value x_f when $0.4 < m/m_{total} < 0.8$. During this period, the powder flows into the die in a nose-shaped profile and coarse particles are easier to be delivered into the die by cascading over the top free surface (Figures 8.7 and 8.8), leading to a depletion of fines in the flow stream. At the late stage ($m/m_{total} > 0.8$), a dramatic increase in fines mass fraction is observed. This is attributed to the following two factors. When the die cavity is close to being completely filled, the fine particles

can be more easily filled into the limited space left in the die compared to the coarse ones. On the other hand, when the shoe moves over the die opening a high shear strain is induced between the moving powder in the shoe and the static powder in the die (Figures 8.7 and 8.8), and this shearing process promotes the percolation of fines. As a result, an even higher fines mass fraction in the powder discharged from the shoe at the late stage is obtained for die filling with a moving shoe (x_i^s / x_f = 2.4 ~ 3.2) compared to die filling with a stationary shoe (x_i^s / x_f = 1.3 ~ 1.5).

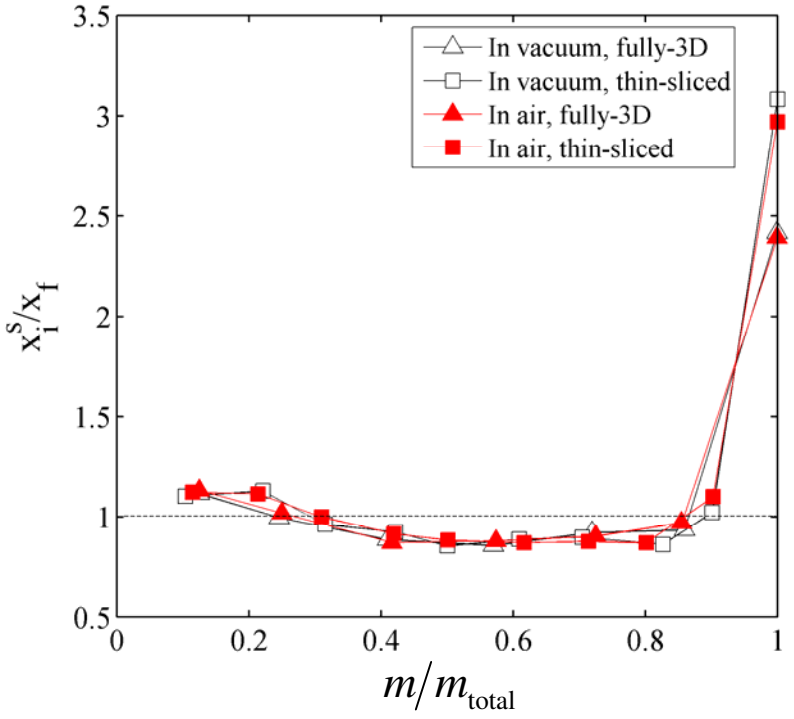

Figure 8.14 Variation of normalized fines mass fraction in a given sample discharged from the shoe, x_i^s / x_f, with the fractional mass discharged, m/m_{total}, during die filling with a moving shoe at a shoe velocity of 70 mm/s.

Figure 8.15 shows x^d/x_f as a function of m/m_{total} for die filling with a moving shoe at a velocity of 70mm/s. The transient fines mass fraction in the die is higher than the initial average value x_f at the early stage due to the flow of fines-rich powder from the bottom of the shoe, and it decreases gradually as the coarse particles avalanche

into the die over the top free surface (Figures 8.7 and 8.8). A sudden increase of fines mass fraction in the die occurs at the late stage due to the fact that the percolation of fines dominates when the die is almost completely filled. Consequently, the fines mass fraction in the die is eventually higher than x_f (i.e. $x^d/x_f > 1$).

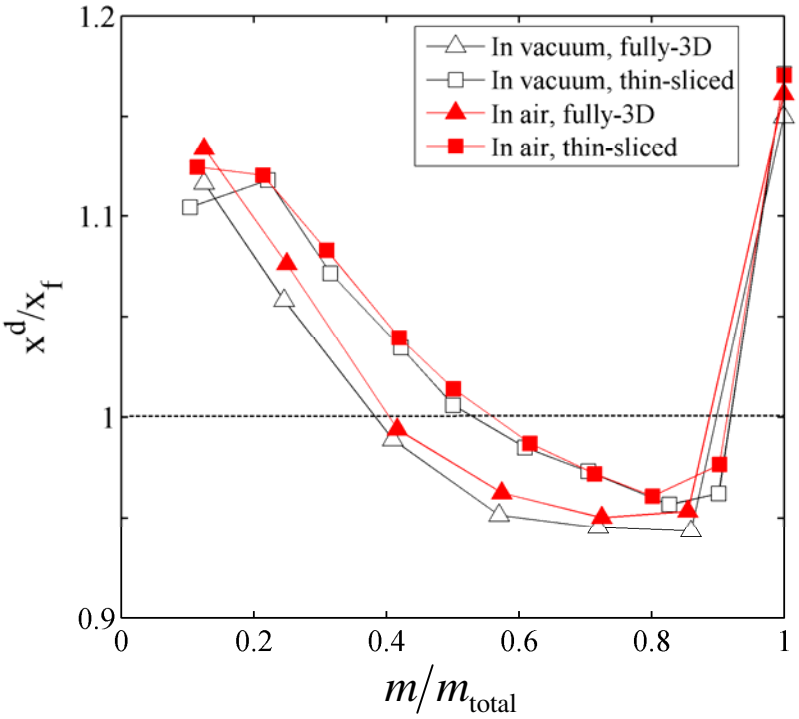

Figure 8.15 Variation of normalized transient fines mass fraction in the die, x^d/x_f, with the fractional mass discharged, m/m_{total}, during die filling with a moving shoe at a velocity of 70mm/s.

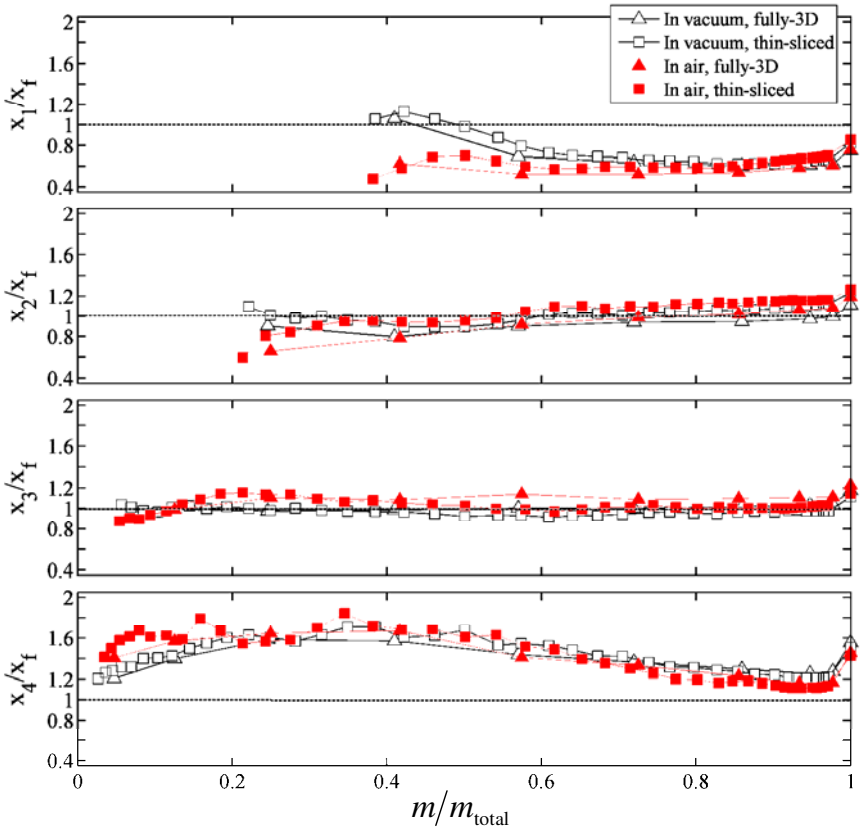

(a) Cells 1-4

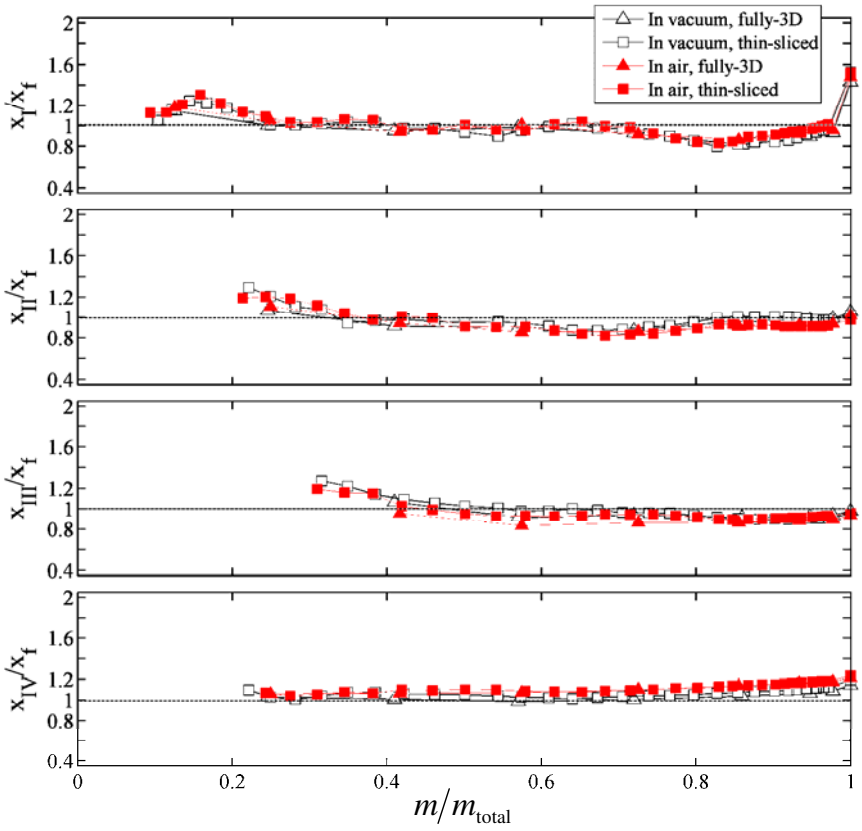

(b) Cells I-IV

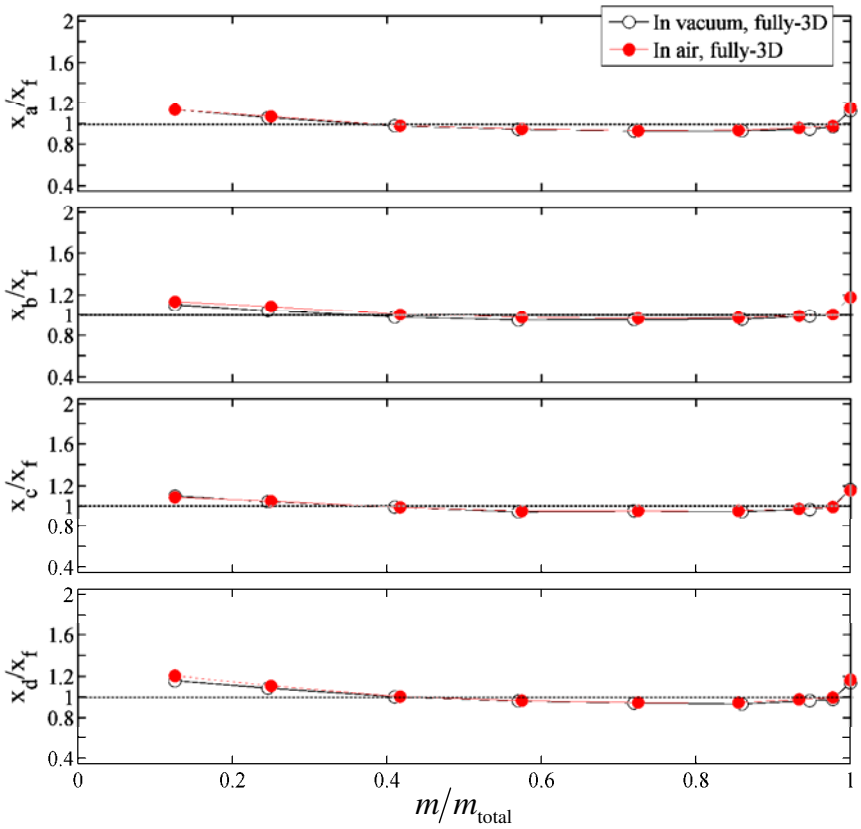

(c) Cells a-d

Figure 8.16 Fines mass fractions in (a) Cells 1, 2, 3 and 4 (partitioned in the *x*-direction), (b) Cells I, II, III and IV (in the *y*-direction) and (c) Cells a, b, c and d (in the *z*-direction) normalized by the initial average fines mass fraction, x_f, as a function of the fractional mass discharged, m/m_{total}, during die filling with a moving shoe at a velocity of 70mm/s.

Figure 8.16 plots the normalized fines mass fraction in each cell of the die (see Figure 8.10) as a function of m/m_{total} for this die filling process. The evolutions of the concentration of fines in Cells 1-4 are shown in Figure 8.16a. As the shoe moves from the right hand side to the left, the powder first approaches Cell 4, which is located on the trailing side of the die (referring to the motion of shoe). As indicated in Figures 8.7 and 8.8, the trailing side is mainly filled by the fines-rich powder from the bottom of the shoe. Therefore, a higher fines mass fraction is resulted in Cell 4. The fines mass fraction in the central region of the die (Cells 2 and 3) fluctuates slightly around initial average value x_f during the filling process. Cell 1 is located on the leading side

of the die, which is mainly filled by the coarse particles cascading from the top free surface (Figures 8.7 and 8.8). Thus, a depletion of fines is obtained in Cell 1.

Figure 8.16b shows the evolution of the concentration of fines in each layer of the die. The fines mass fraction in the top layer (Cell I) varies slightly during most of the die filling process but it increases sharply at the final stage, implying the occurrence of strong percolation of fines at the top of the die when die cavity is almost completely filled. A gentle fluctuation of the fines mass fraction around x_f in the middle two layers (Cells II and III) and a gradual increase in the fines mass fraction in the bottom layer (Cell IV) are observed during the filling process. Figure 8.16c shows the evolution of the concentration of fines in Cells a-d for the fully-3D model. It is clear that for all the cells in the *z*-direction the fines mass fraction decreases slowly during most of the filling process but increases suddenly at the final stage.

From Figures 8.14-8.16, it is evident that the segregation results for die filling in air are consistent with those for die filling in a vacuum, indicating that the air has a negligible effect on the segregation during this particular die filling process. This is because nose-flow dominates this filling process and the air can escape from the die before the die opening is completely covered by the powder mass (see Figure 8.8). Therefore, the air flow has less chance to go through the bulk of powder and to influence the segregation by entraining fine particles.

8.5. Concentration distributions in the die

To explore the uniformity of the deposited powder bed in the die after die filling, the concentration distributions of fines in *x*, *y* and *z*-directions are plotted, using the

partitions as shown in Figure 8.10. Figure 8.17 shows the concentration distributions of fines for die filling with a stationary shoe. The concentration distributions of fines in the *x*-direction are shown in Figure 8.17a, in which the normalized fines mass fraction, x_i / x_f, is plotted as a function of the *x*-coordinate of the centre of the cell, *x*, normalized by the width of the die, *w*. It is observed that for die filling in a vacuum, the fines mass fraction is slightly higher close to the die walls and lower in the centre. This is because a fines-depleted region is generated below the bottom of the V-shaped concave during die filling in a vacuum, as shown in Figure 8.5. In contrast, the fines mass fraction is remarkably lower close to the die walls for die filling in the presence of air. As discussed above, the air, which is entrapped in the regions close to the vertical walls of the die, opposes the deposition of fines to those regions during die filling in air (Figure 8.6). Therefore, a depletion of fines is induced in the regions close to the vertical walls of the die.

The concentration distributions of fines in the *y*-direction are shown in Figure 8.17b, in which the *y*-coordinate of the centre of the cell, *y*, is normalized by the height of the die, *h*. For die filling in a vacuum, an obvious segregation occurs with a higher concentration of fine particles at the bottom and a lower value at the top due to the percolation mechanism as discussed above. When air is present, the extent of this segregation is reduced. The presence of air hinders the fine particles from flowing down, so that the percolation of fine particles through the matrix of coarse particles is resisted. As a result, the segregation due to the percolation mechanism is suppressed when air is present.

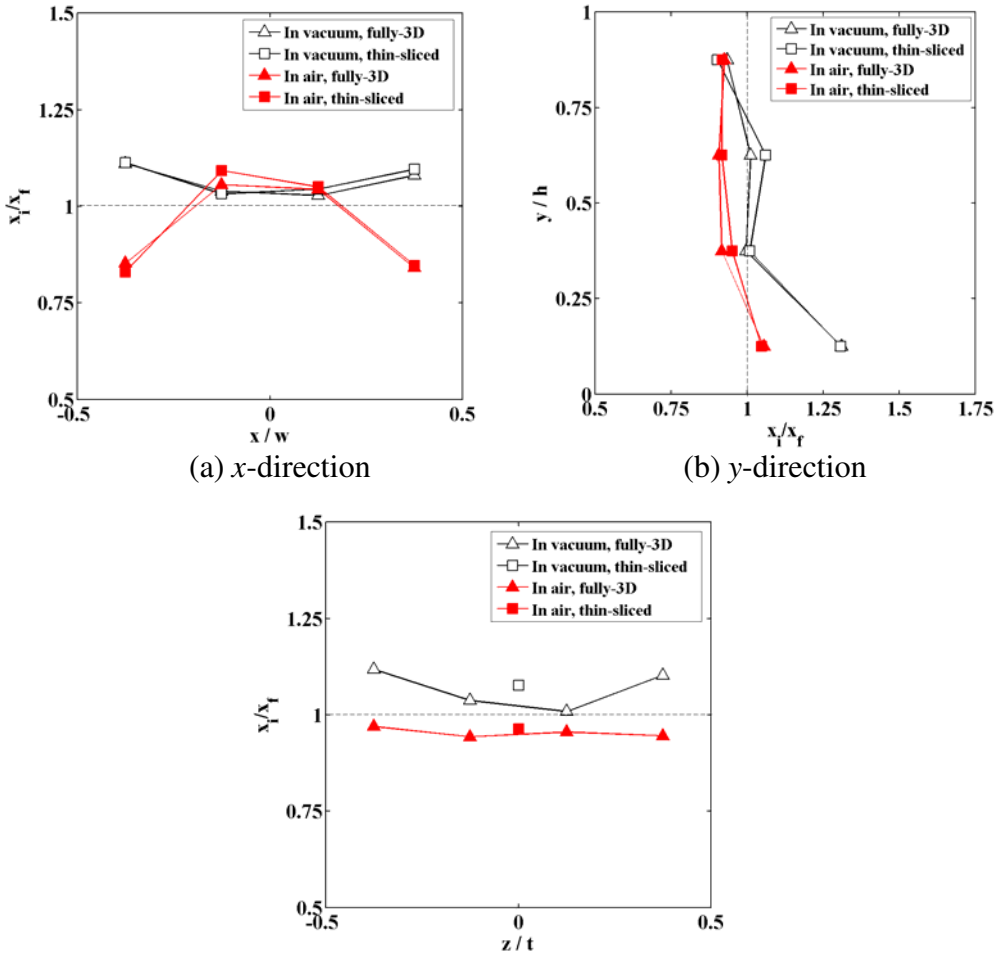

(a) x-direction (b) y-direction

(c) z-direction

Figure 8.17 Concentration distributions of fines in (a) x-direction, (b) y-direction and (c) z-direction for die filling with a stationary shoe.

The concentration distributions of fines in the z-direction are plotted in Figure 8.17c, in which the z-coordinate of the centre of the cell, z, is normalized by the thickness of the die, t. For the thin-sliced model, only a thin slice of the domain exists in the z-direction. By using the periodic boundaries, the concentration profile is assumed to be repeatable and uniform along the z-direction. The average fines mass fraction of this thin-sliced powder bed within the die region is calculated and added to Figure 8.17c. As shown in Figure 8.17c, for die filling in a vacuum, the fines mass fraction is slightly higher in the regions close to die walls in the fully-3D model, and the fines mass fraction in the thin-sliced model shows a small departure from the concentration

profile of the fully-3D model. For die filling in air, the concentration of fines distributes uniformly in the fully-3D model, and the concentration of fines obtained by using the thin-sliced model remains at the same level as the concentration profile of the fully-3D model. In general, the fully-3D model produces uniform concentration distributions in the *z*-direction and the fines mass fractions predicted using the thin-sliced model are consistent with those using the fully-3D model.

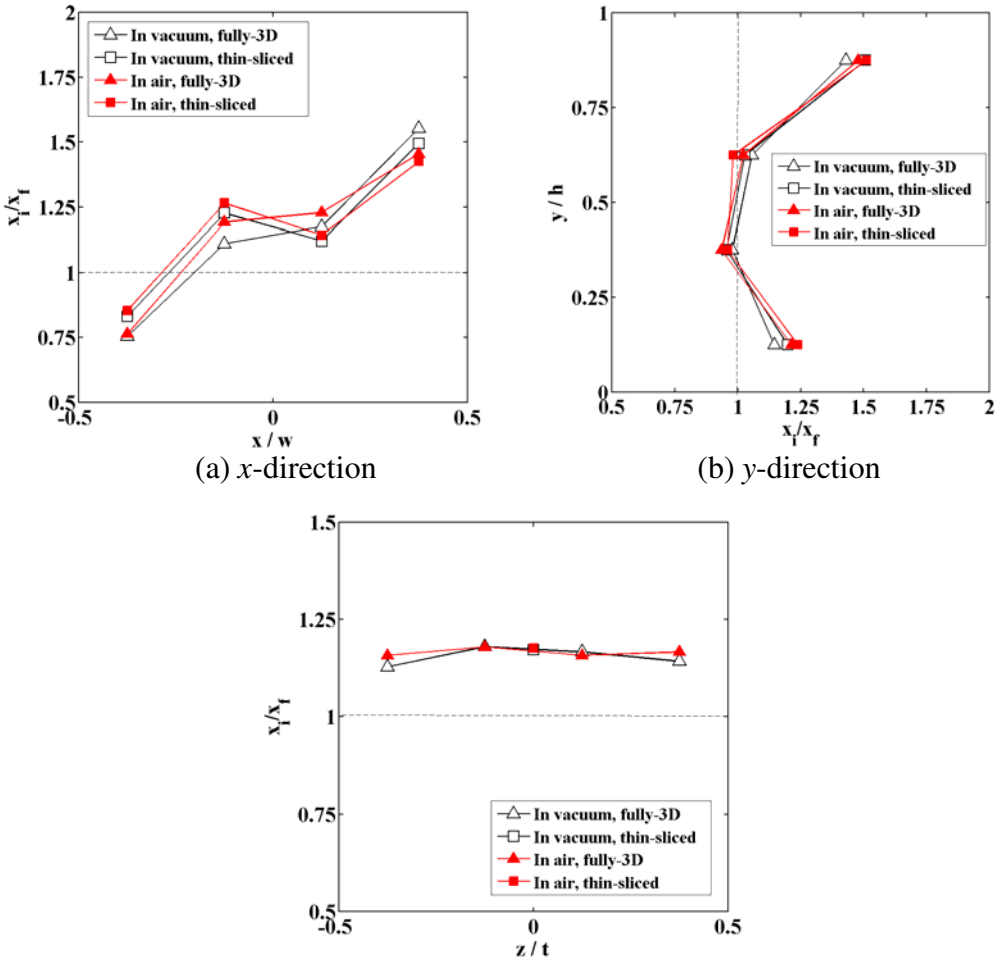

(a) *x*-direction (b) *y*-direction

(c) *z*-direction

Figure 8.18 Concentration distributions of fines in (a) *x*-direction, (b) *y*-direction and (c) *z*-direction for die filling with a moving shoe at a velocity of 70 mm/s.

The concentration distributions of fines in the *x*-, *y*- and *z*-directions for die filling with a moving shoe at a velocity of 70 mm/s are shown in Figure 8.18. As shown in Figure 8.18a, a lower fines mass fraction is observed on the leading side (i.e., left

hand side) of the die and a higher concentration of fines is observed on the trailing side (i.e., right hand side). This is because the leading side of the die is primarily filled by the coarses-rich powder which comes from the free surface flow, while the trailing side of the die is filled by the fines-rich powder from the bottom of the shoe (see Figures 8.7 and 8.8). As shown in Figure 8.18b, the fines mass fraction remains the initial average fraction x_f in the middle region, whereas it is higher at the bottom due to the percolation of fines and even higher at the top of the die due to the fact that the shearing between the moving powder in the shoe and the static powder bed in the die significantly promotes the percolation of fines into the top region of die from the bottom of the shoe. In Figure 8.18c, it can be seen that very uniform concentration profiles in the *z*-direction are obtained using the fully-3D model and the fines mass fractions are in good agreement using the thin-sliced model and fully-3D model. For this die filling, it is also clear that the presence of air does not have a significant impact on the concentration distributions, due to the fact that the air can escape from the die before the powder mass covers the whole die opening (Figure 8.8).

As demonstrated in Figures 8.5-8.18, the thin-sliced model with periodic boundary condition produces the same powder flow and segregation behaviours as the fully-3D model. On the other hand, the thin-sliced model involves a smaller computational domain with fewer particles compared to the fully-3D model, so that it is less computationally intensive using the thin-sliced model. As a result, the thin-sliced model with periodic boundaries rather than the fully-3D model will be adopted in the subsequent simulations.

8.6. Parametric study

As discussed above, the difference in particle size in a granular mixture can lead to segregation during die filling. It is expected that this segregation behaviour may be determined by a number of parameters, such as shoe velocity, particle size ratio, initial fines mass fraction, surface energy (for cohesive powders), the initial height of powder bed and so on. Therefore, in this section the effects of these parameters on the segregation during die filling are explored using the thin-sliced model.

8.6.1. The effect of shoe velocity

The shoe moving at different velocities results in different powder flow patterns during die filling, as discussed in Chapter 3. Therefore, the shoe velocity can also have an impact on the segregation behaviour by influencing the powder flow pattern. The horizontal and vertical concentration distributions of fines in the die after die filling for various shoe velocities v_s with initial fines mass fraction x_f = 10%, particle size ratio d_c/d_f =4 and initial height of powder bed $H \approx 7$ mm are plotted in Figure 8.19 and Figure 8.20, respectively. In the horizontal direction, a lower segregation tendency is observed for die filling with a stationary shoe (v_s =0). During die filling with a moving shoe, the leading side (left hand side) of the die is filled by the fines-depleted powder from the top region of the flow stream, while the trailing side (right hand side) of the die is filled by the fines-rich powder from the bottom region (see Figures 8.7 and 8.8). Therefore, more significant segregation with a lower concentration of fines on the leading side and a higher concentration on the trailing side is obtained for die filling with a moving shoe. As shoe velocity increases, the powder mass covers and passes the die opening more rapidly, so that less time is allowed for the fines-depleted powder to flow into the die from the top region and the

chance for the percolation of fines through the flow stream is also reduced. As a result, the extent of segregation decreases as shoe velocity increases for die filling with a moving shoe.

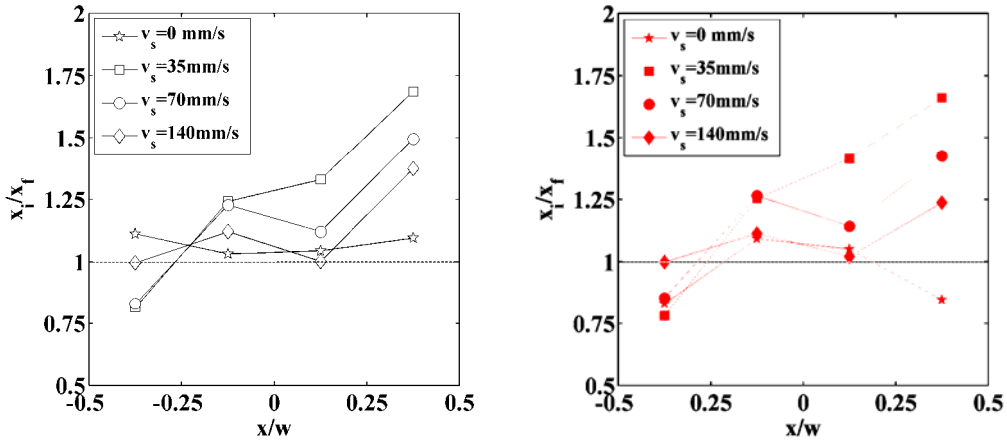

(a) In a vacuum (b) In air

Figure 8.19 Horizontal concentration distributions of fines in the die after die filling (a) in a vacuum and (b) in air for various shoe velocities, v_s , with x_f = 10%, d_c/d_f =4 and $H \approx 7$ mm.

In the vertical direction, as shown in Figure 8.20, the concentration of fines is higher at the bottom and lower at the top for die filling with a stationary shoe (v_s =0). For die filling with a moving shoe, higher concentrations of fines are observed not only at the bottom but also at the top of the die, and the concentration of fines in the upper region decreases as shoe velocity increases. As discussed in Section 8.4.2, for die filling with a moving shoe, the deposition of fine particles into the upper region of the die is promoted due to the effect of shearing between the moving powder in the shoe and the static powder in the die at the late stage of die filling. This causes a higher concentration of fines at the top of the die for die filling with a moving shoe. As the shoe velocity increases, less time is allowed for the shoe to stay over the die opening, and the chance for the fines to be filled into the voids in the top layer of the deposited

powder bed in the die is reduced. Thus, the concentration of fines at the top of the die decreases as the shoe velocity increases for die filling with a moving shoe.

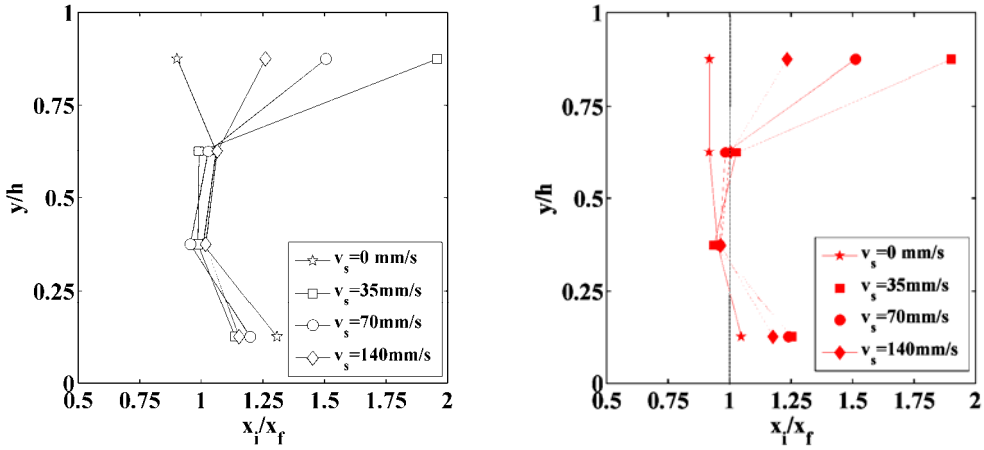

(a) In a vacuum (b) In air

Figure 8.20 Vertical concentration distributions of fines in the die after die filling (a) in a vacuum and (b) in air for various shoe velocities, v_s , with x_f = 10%, d_c/d_f =4 and $H \approx 7$ mm.

8.6.2. The effect of particle size ratio

The difference in particle size induces segregation, and the extent of this segregation is dependent on the particle size ratio. Previous studies showed that the extent of segregation increases with particle size ratio in hopper discharge (Samadani et al., 1999; Ketterhagen et al., 2008). For die filling, the dependence of segregation on the particle size ratio is discussed in the following.

Horizontal concentration distributions of fines in the die after die filling with a stationary shoe (v_s =0) for various particle size ratios, d_c/d_f , with x_f = 10% and $H \approx 7$ mm are plotted in Figure 8.21. For die filling in a vacuum, the concentration profile in the die is relatively uniform with d_c/d_f =2 and 3. However, as size ratio increases to d_c/d_f =4 and 5, segregation becomes more prevalent with higher fines mass fraction

close to the die walls. For die filling in the presence of air, segregation with lower fines mass fraction close to die walls occurs for each size ratio. An increase in the fines mass fraction in the centre of the die is observed as size ratio increases.

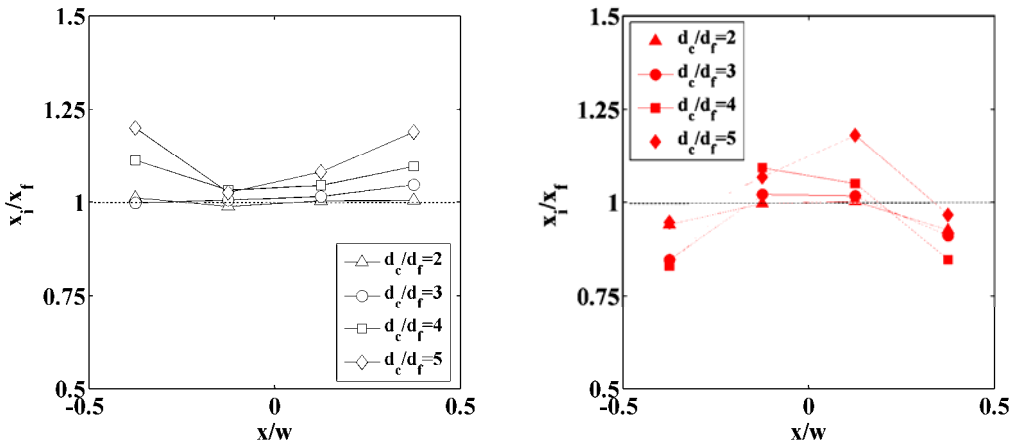

(a) In a vacuum (b) In air

Figure 8.21 Horizontal concentration distributions of fines in the die after die filling (a) in a vacuum and (b) in air for various size ratios, d_c/d_f , with v_s =0, x_f = 10%, and $H \approx 7$ mm.

Figure 8.22 shows the corresponding vertical concentration distributions. In a vacuum, little segregation occurs for d_c/d_f =2 and 3. As the size ratio increases, the fines mass fraction increases significantly at the bottom while it decreases at the top of the die. In the presence of air, little segregation occurs for d_c/d_f =2, 3 and 4. Segregation with a higher fines mass fraction at the bottom of die is observed for the largest size ratio considered (i.e., d_c/d_f =5). However, the extent of this segregation is obviously reduced due to the effect of air compared to that in a vacuum.

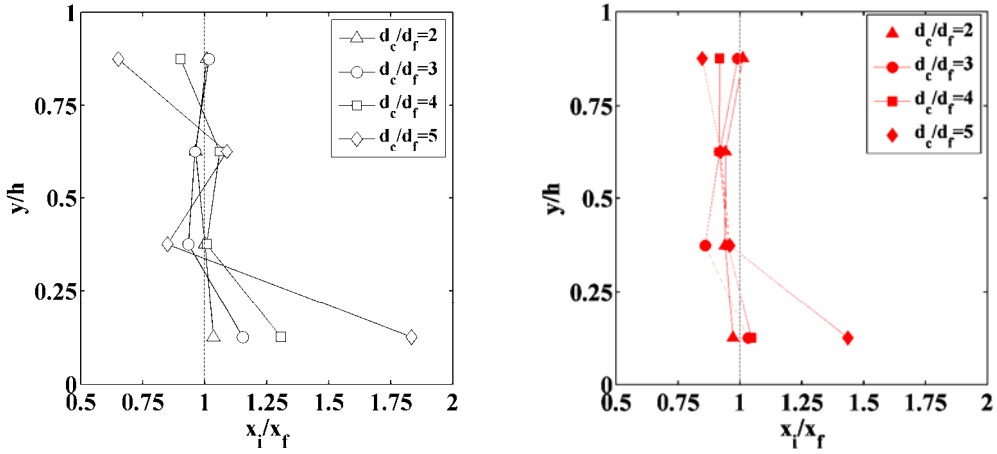

(a) In a vacuum (b) In air

Figure 8.22 Vertical concentration distributions of fines in the die after die filling (a) in a vacuum and (b) in air for various size ratios, d_c/d_f , with v_s =0, x_f = 10%, and $H \approx$ 7 mm.

The horizontal and vertical concentration distributions of fines in the die after die filling with a moving shoe (v_s =70 mm/s) for various size ratios, d_c/d_f , with x_f = 10% and $H \approx 7$ mm are shown in Figures 8.23 and 8.24, respectively. In the horizontal direction, segregation occurs with a lower concentration of fines on the leading side and a higher value on the trailing side for each size ratio. As size ratio increases, the fines mass fraction on the leading side decreases while the fines mass fraction on the trailing side increases, therefore leading to an increase in the extent of segregation. In the vertical direction, as shown in Figure 8.24, an excess of fines is obtained at the bottom for the relatively large size ratios d_c/d_f = 4 and 5, and in the upper region of the die, a higher concentration of fines is observed for each size ratio. In general, the fines mass fractions at the bottom and at the top increase as size ratio increases. As a result, the extent of segregation in the vertical direction also increases as size ratio increases.

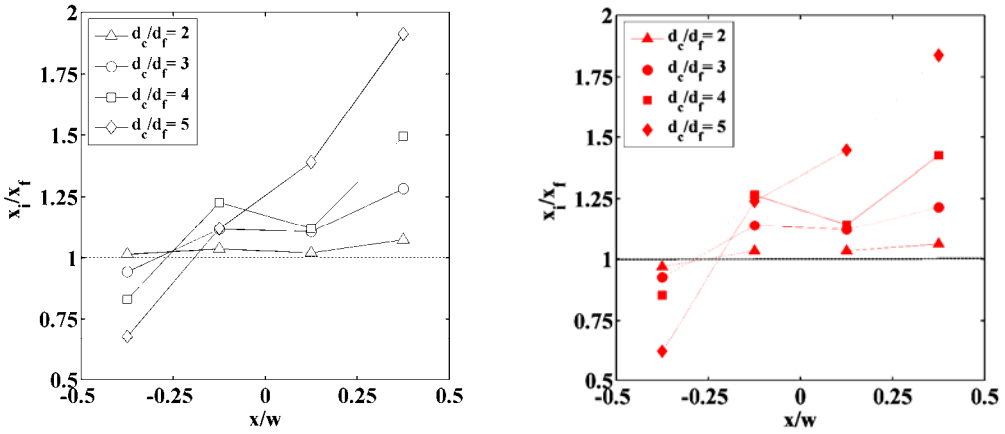

(a) In a vacuum (b) In air

Figure 8.23 Horizontal concentration distributions of fines in the die after die filling (a) in a vacuum and (b) in air for various size ratios, d_c/d_f , with v_s =70 mm/s, x_f = 10%, and $H \approx 7$ mm.

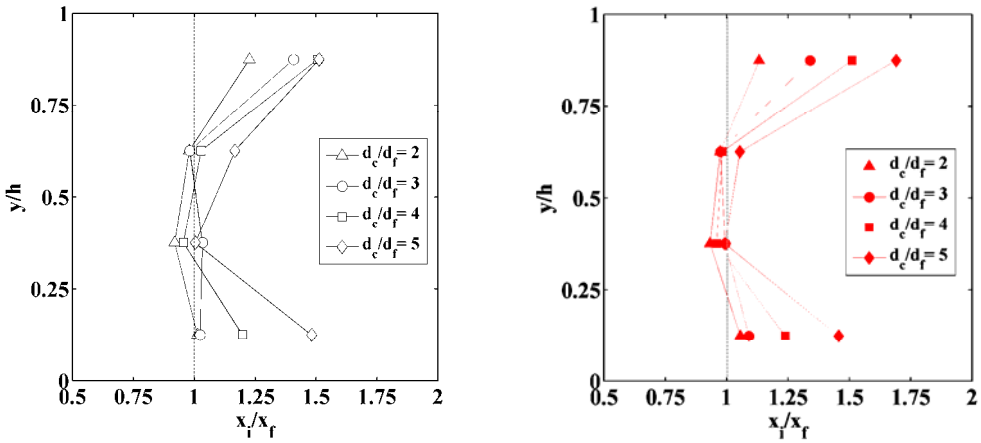

(a) In a vacuum (b) In air

Figure 8.24 Vertical concentration distributions of fines in the die after die filling (a) in a vacuum and (b) in air for various size ratios, d_c/d_f , with v_s =70 mm/s, x_f = 10%, and $H \approx 7$ mm.

In conclusion, the extent of segregation increases with particle size ratio d_c/d_f during die filling. As size ratio increases, the void space between the coarse particles increases compared to the size of fine particles. This facilitates the fine particles to percolate through the matrix of coarse particles and therefore the segregation induced by size difference is promoted.

8.6.3. The effect of initial fines mass fraction

The segregation of a binary mixture of different sized particles also depends on the initial fines mass fraction x_f, as reported by Ketterhagen et al. (2008). Arteaga and Tüzün (1990) indicated that as the fines mass fraction increases, the coarse particles tend to be surrounded by the fines and the structure of the particle system transfers from 'coarses-ontinuous' to 'fines-continuous'. Assuming that the segregation would be suppressed when the surfaces of coarse particles are completely covered by the fine particles, they proposed a limiting fines mass fraction, x_f^L, which is a function of the size ratio d_c/d_f:

$$x_f^L = \frac{4}{4 + d_c/d_f} \tag{8.1}$$

Segregation by the percolation mechanism only occurs when the initial fines mass fraction is less than this limiting value. In this study, a range of initial fines mass fractions, $5\% \le x_f \le 50\%$, were used with a fixed size ratio, $d_c/d_f = 4$, for which the limiting fines mass fraction x_f^L equals to 50% according to Eq. (8.1).

Figure 8.25 shows the horizontal concentration distributions of fines in the die after die filling with a stationary shoe ($v_s = 0$) for various initial fines mass fractions, x_f, with $d_c/d_f = 4$ and $H \approx 7$ mm. In a vacuum, the concentration profile of fines is uniform and the fines mass fractions are equal to the initial average value (i.e. $x_i/x_f = 1$) for $x_f = 50\%$, the largest initial fines mass fraction considered. While for $x_f = 5\%$, 10% and 20%, the horizontal segregation occurs with higher concentration of fines close to die walls. As the initial fines mass fraction increases, the extent of segregation decreases. For die filling in the presence of air, horizontal segregation occurs with a lower concentration of fines close to the die walls for each fines mass fraction.

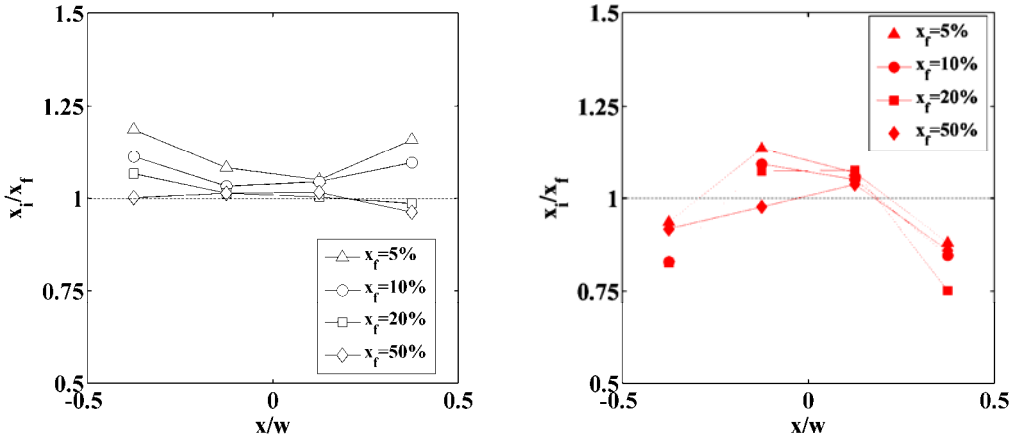

(a) In a vacuum (b) In air

Figure 8.25 Horizontal concentration distributions of fines in the die after die filling (a) in a vacuum and (b) in air for various initial fines mass fractions, x_f , with $v_s = 0$, $d_c/d_f = 4$ and $H \approx 7$ mm.

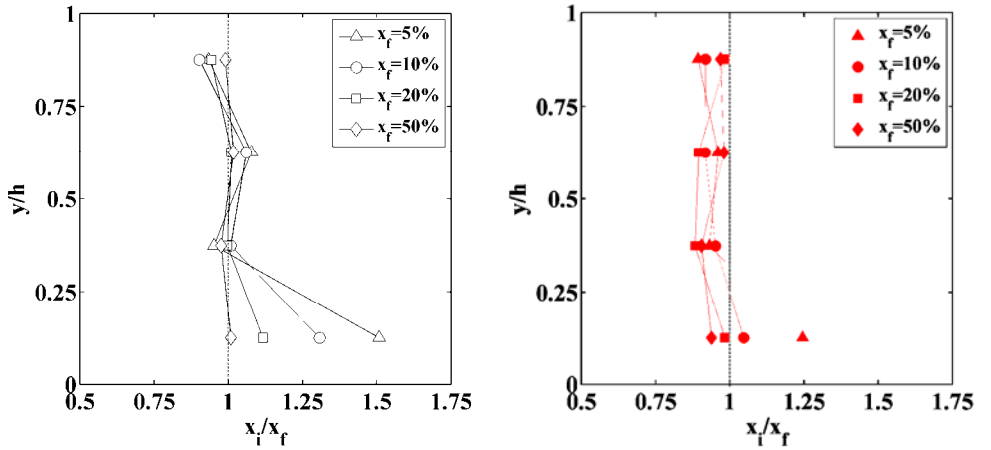

(a) In a vacuum (b) In air

Figure 8.26 Vertical concentration distributions of fines in the die after die filling (a) in a vacuum and (b) in air for various initial fines mass fractions, x_f , with $v_s = 0$, $d_c/d_f = 4$ and $H \approx 7$ mm.

The corresponding vertical concentration distributions of fines are shown in Figure 8.26. In a vacuum, no segregation occurs in the vertical direction and the concentration is identical to the initial fines mass fraction for x_f =50%. While for x_f =5%, 10% and 20%, segregation occurs with a higher concentration of fines at the bottom of die and the fines mass fraction at the bottom decreases as x_f increases. In the presence of air, the concentration profiles keep uniform for the higher initial fines

mass fractions x_f =20% and 50%, however, the overall fines mass fraction is lower than the initial average value (x_i/x_f <1) due to the resistance of air on the deposition of fine particles. Segregation occurs with a higher concentration of fines at the bottom for the lower initial fines mass fractions x_f =5% and 10%.

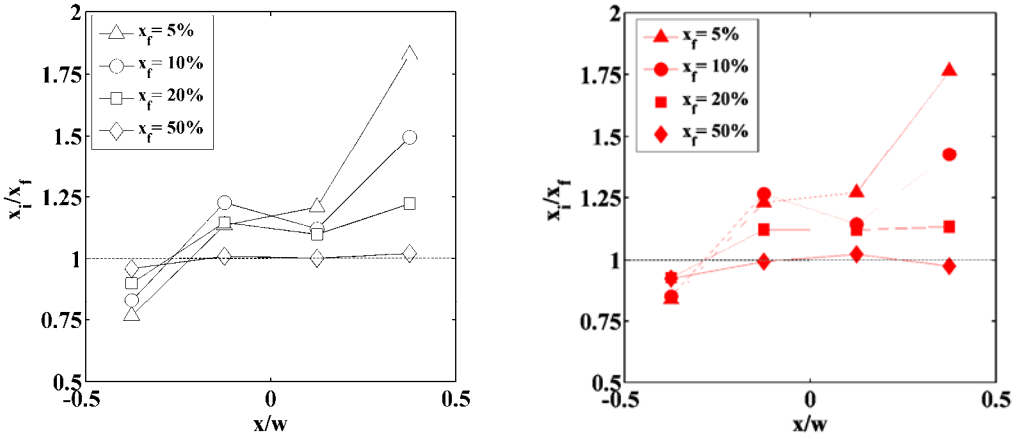

(a) In a vacuum (b) In air

Figure 8.27 Horizontal concentration distributions of fines in the die after die filling (a) in a vacuum and (b) in air for various initial fines mass fractions, x_f , with v_s = 70 mm/s, d_c/d_f = 4 and $H \approx 7$ mm.

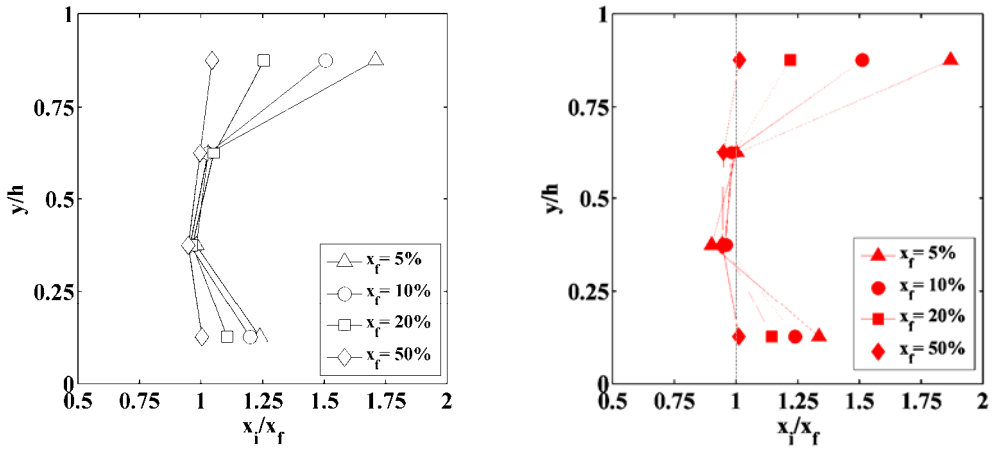

(a) In a vacuum (b) In air

Figure 8.28 Vertical concentration distributions of fines in the die after die filling (a) in a vacuum and (b) in air for various initial fines mass fractions, x_f , with v_s = 70 mm/s, d_c/d_f = 4 and $H \approx 7$ mm.

Figure 8.27 shows the horizontal concentration distributions of fines in the die after die filling with a moving shoe (v_s = 70) for various initial fines mass fractions, x_f, with

$d_c/d_f = 4$ and $H \approx 7$ mm. Significant segregation occurs in the horizontal direction with a lower concentration of fines on the leading side and a higher value on the trailing side for x_f =5%, 10% and 20%. As x_f increases, the extent of the segregation decreases. Only mild segregation occurs for x_f=50%. The corresponding vertical concentration distributions of fines are shown in Figure 8.28. For lower values of x_f, prominent segregation also occurs in the vertical direction with higher concentrations of fines at both the lower and the upper regions of the die. The extent of this segregation also decreases as x_f increases. Also, only slight segregation occurs for x_f=50%.

In conclusion, the initial fines mass fraction plays a crucial role on the segregation of binary mixture of different sized particles during die filling. The limiting fines mass fraction determined by Eq. (8.1) is also applicable to the prediction of the feasibility of size-induced segregation during die filling, except for die filling with a stationary shoe in air, in which the presence of air has a significant impact on segregation (see Figures 8.25b and 8.26b). The segregation due to size difference occurs only when the initial fines mass fraction is less than the limiting value, and the extent of this segregation decreases as the initial fines mass fraction increases.

8.6.4. The effect of cohesion

Cohesive binary granular mixtures were also used in the die filling process. The frictional elastic contact law for adhesive particles is provided in Section 2.3.2.2. The surface energy γ is prescribed by assuming the 'pull-off' force F_c is equal to k times the weight of a fine particle, i.e.

$$F_c = 3\pi\gamma R^* = k \cdot m_s g \tag{8.2}$$

then,

$$\gamma = k \cdot \frac{m_s g}{3\pi R^*} \tag{8.3}$$

In which, m_s is the mass of a single fine particle and R^* is defined in Eq. (2.7). Thus, different surface energies γ can be specified to obtain different values of k according to Eq. (8.3). If k equals zero (i.e., $\gamma = 0$), the powder is non-cohesive.

Figure 8.29 shows the die filling process with a stationary shoe and a cohesive binary mixture (k =100) in a vacuum and in air. During die filling in a vacuum, agglomerates of particles are formed due to the effect of cohesion and the particles are deposited into the die chunk by chunk. Therefore, an intermittent powder flow process is resulted. This is in broad agreement with the experimental observations by Sinka et al. (2004). In addition, the particles on the ledges of the die are too 'sticky' to flow down during this die filling (Figure 8.29a). When air is present, as shown in Figure 8.29b, the particles also flow into the die chunk by chunk. However, the filling process is terminated when a stable bridge is eventually created above the die opening. Consequently, the die is not completely filled. To examine the reproducibility of this die filling process, a binary mixture of a different configuration was also used. Figure 8.30 shows the final states for die filling in a vacuum and in air with a binary mixture, which consists of the same particles as used in Figure 8.29 but has a different spatial distribution of particles. For this die filling, the final state of particles in a vacuum is similar to that in Figure 8.29a. However, no bridge is created in the presence of air. Thus, the die filling process with a cohesive powder is dependent on the initial

configuration of the particle system in the shoe, and it is possible that a 'particle bridge' is formed over the die opening leading to an incomplete filling.

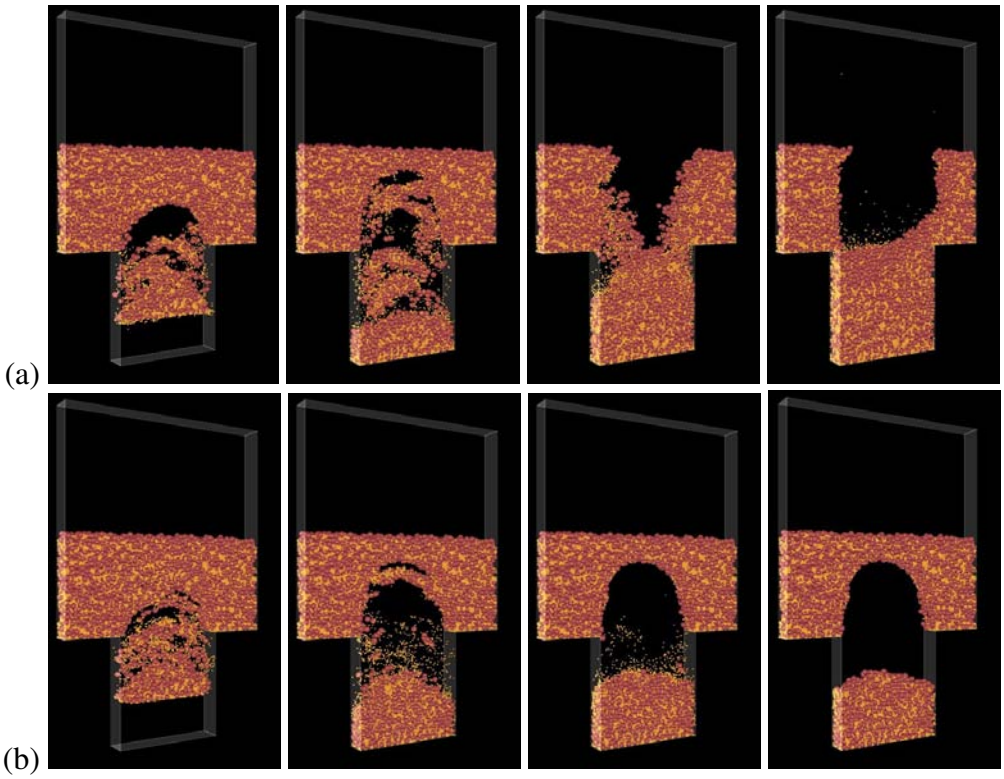

Figure 8.29 Die filling process with a cohesive binary mixture (k =100) and a stationary shoe (a) in a vacuum (top row) and (b) in air (bottom row). The labels indicate the elapsed time of filling process.

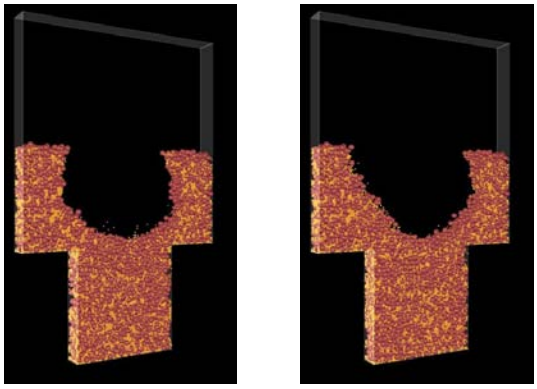

Figure 8.30 Final states for die filling (a) in a vacuum and (b) in air with an initial configuration of particle system different from that used in Figure 8.29.

Figure 8.31 shows a comparison of die filling processes in air with a non-cohesive binary mixture and a cohesive binary mixture (k =100). The shoe was translated over the die at a constant velocity of 140 mm/s. During die filling with a non-cohesive powder, due to the inertia of particles and the friction between the particles and the base of shoe, some particles flow backwards relatively to the shoe and a nose-shaped flow stream is formed in the front of powder bed (Figure 8.31a). During die filling with a cohesive powder, the cohesive forces prevent the relative movements of particles so that the change of the shape of powder bed in the shoe is limited at the early stage (see the first snapshot in Figure 8.31b). The powder flow process is smooth during die filling with a non-cohesive powder (Figure 8.31a). However, the cohesive powder cascades as chunks of agglomerates along the top free surface. Due to the effect of cohesion, the flowability of powder is reduced and the angle of repose is increased. As a result, a smaller amount of particles are filled into the die and a steeper slope is created in the shoe after die filling with a cohesive powder compared to with a non-cohesive powder.

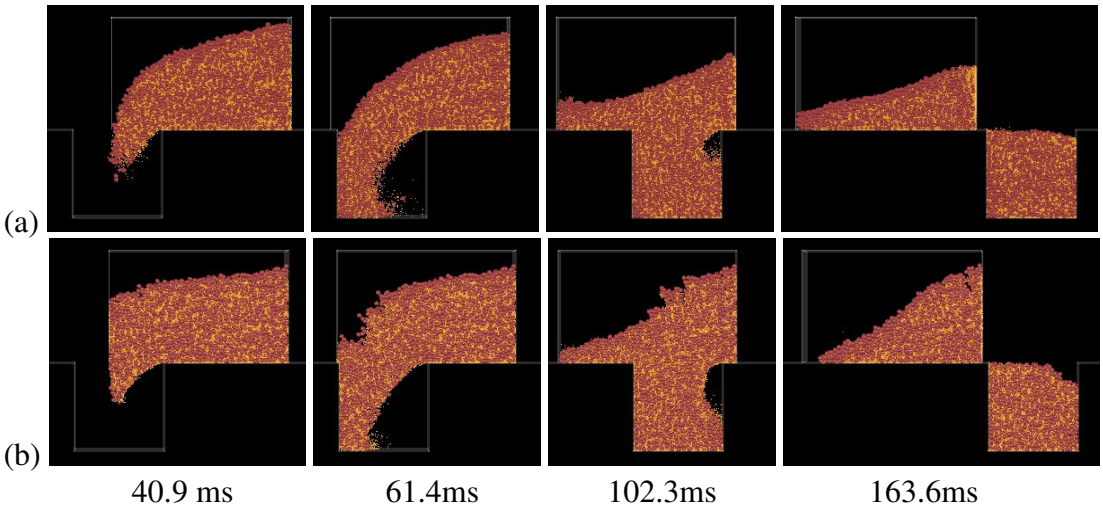

Figure 8.31 Comparison of die filling processes in air with (a) a non-cohesive binary mixture (top row) and (b) a cohesive binary mixture with k =100 (bottom row). A shoe moving at a constant velocity of 140 mm/s was employed. The labels indicate the elapsed time of the filling process.

The effect of cohesion on segregation during die filling is also investigated. Figure 8.32 shows the horizontal and vertical concentration distributions in the die after die filling in air for various surface energies with a stationary shoe (v_s = 0), x_f = 10%, d_c/d_f = 4 and $H \approx 7$ mm. For k =100, the concentration distributions of the final states shown in Figure 8.30 are plotted, as the die cavity was completely filled both in a vacuum and in air. In the horizontal direction, segregation occurs with a lower concentration of fines close to die walls and a higher value in the centre for die filling with a non-cohesive powder (k =0) and the low surface energy powders (k =2 and 10). However, little segregation occurs in the horizontal direction for die filling with a powder of high surface energy (k =100). During die filling with a non-cohesive powder and the powders of low surface energies, the continuous central flow stream causes the air to flow aside and be entrapped close to the die walls (see Figure 8.6). The entrapped air impedes the fine particles from flowing to the regions close to die walls, leading to a lower concentration of fines in those regions. When a high surface energy powder (e.g., k =100) is used, the particles flow down chunk by chunk. The air can escape through the space between the agglomerates, and no air pockets are generated close to the die walls. As a result, the air has a little effect on the concentration profile in the horizontal direction.

For the vertical concentration distribution, segregation also occurs with a higher concentration of fines at the bottom during die filling with cohesive powders. As the surface energy increases (i.e., k increases), the extent of the vertical segregation tends to increase. For die filling with a non-cohesive powder, the flow stream is continuous and the entrapped air needs to escape by going through the bulk of powder. During this process, the air flow hinders the deposition of fine particles. Therefore, the

segregation due to the percolation mechanism is reduced in the presence of air. For die filling with a cohesive powder of high surface energy (e.g., k =100), the intermittent powder flow allows the air to escape through the space between the agglomerates rather than through the powder bulk. This weakens the effect of air. On the other hand, the particles stick together within the agglomerates due to the effect of cohesion so that the relative movements between particles in the same agglomerate are restrained. As a result, the segregation initially existing in the shoe (Figure 8.9b) persists and transfers to the die for die filling with a cohesive powder of high surface energy (Figure 8.32b).

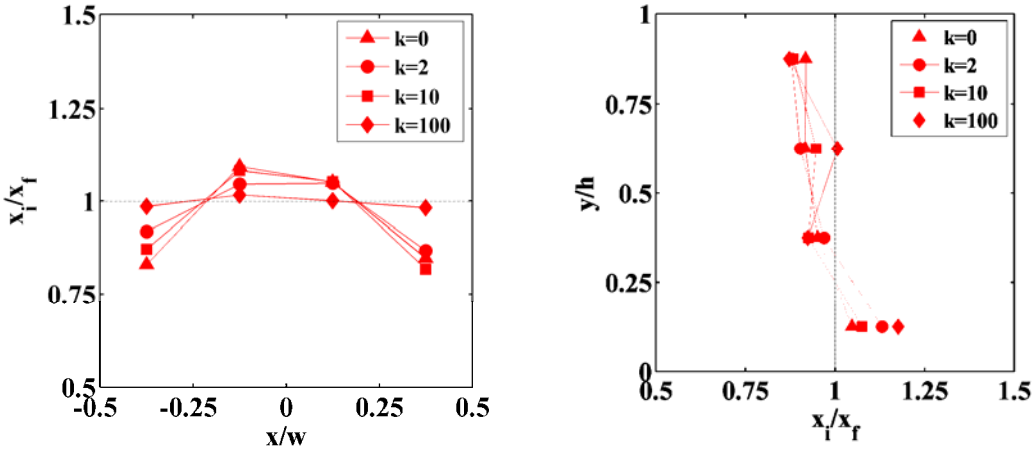

(a) Horizontal distribution (b) Vertical distribution

Figure 8.32 (a) Horizontal and (b) vertical concentration distributions in the die after die filling in air for various surface energies with a stationary shoe (v_s = 0), x_f = 10%, d_c/d_f = 4 and $H \approx 7$ mm.

Figure 8.33 shows the horizontal and vertical concentration distributions in the die after die filling in air for various surface energies with a moving shoe (v_s = 140 mm/s), x_f = 10%, d_c/d_f = 4 and $H \approx 7$ mm. For the horizontal concentration distribution, a lower concentration of fines is observed on the leading side (i.e., left hand side) of the die for k =0. During die filling with a non-cohesive powder (k =0), the coarses-rich powder can be delivered into the leading side of the die over the top free surface (see

Figure 8.31a), resulting in a lower concentration of fines on that side. While during die filling with a cohesive powder, the coarses-rich powder on the top surface can not flow into the die and the leading side of the die is filled by the fines-rich powder from the lower region of the shoe (see Figure 8.31b).

For the vertical concentration distribution, as shown in Figure 8.33b, it is observed that the concentration profiles with cohesion (k =2, 10 and 100) are more uniform than that without cohesion (k =0). This could be due to that the presence of cohesion inhibits the percolation of fines into the die, causing a lower concentration of fines in the top layer of the die compared to without cohesion.

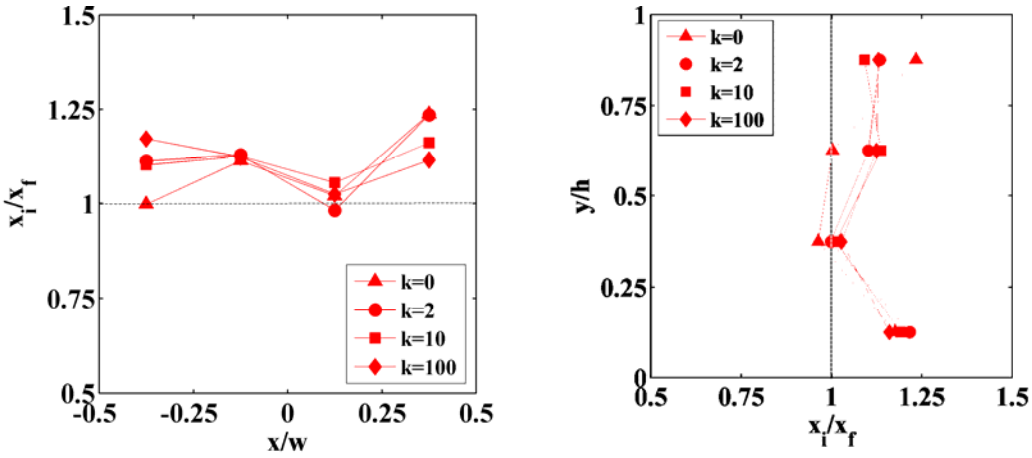

(a) Horizontal distribution (b) Vertical distribution

Figure 8.33 (a) Horizontal and (b) vertical concentration distributions in the die after die filling in air for various surface energies with v_s = 140 mm/s, x_f = 10%, d_c/d_f = 4 and $H \approx 7$ mm.

8.6.5. The effect of the initial height of powder bed

To examine the effect of initial height of powder bed, deep powder beds of height $H \approx$ 14 mm are employed in die filling with a stationary shoe and a moving shoe. Figure 8.34 shows the die filling processes with a deep powder bed (H≈14 mm) and a stationary shoe in a vacuum and in air. The powder flow patterns with a deep powder

bed are very similar to those with a shallow powder bed in a vacuum (Figure 8.5) and in air (Figure 8.6). As shown in Figures 8.5 and 8.6, a prominent V-shaped concave profile is formed on the top surface during die filling with a shallow powder bed. However, no such V-shaped profile is observed for die filling with a deep powder bed (Figure 8.34). During die filling with a deep powder bed, the movement of the particles in the top region is slightly affected by the stagnant zones below and they flow down nearly at the same pace. Therefore, the top free surface remains flat, as in the initial state. Due to the absence of the V-shaped profile, segregation with an excess of coarse particles in the centre of the shoe, which can be observed in die filling with a shallow powder bed in a vacuum (see Figure 8.5), does not occur during die filling with a deep powder bed.

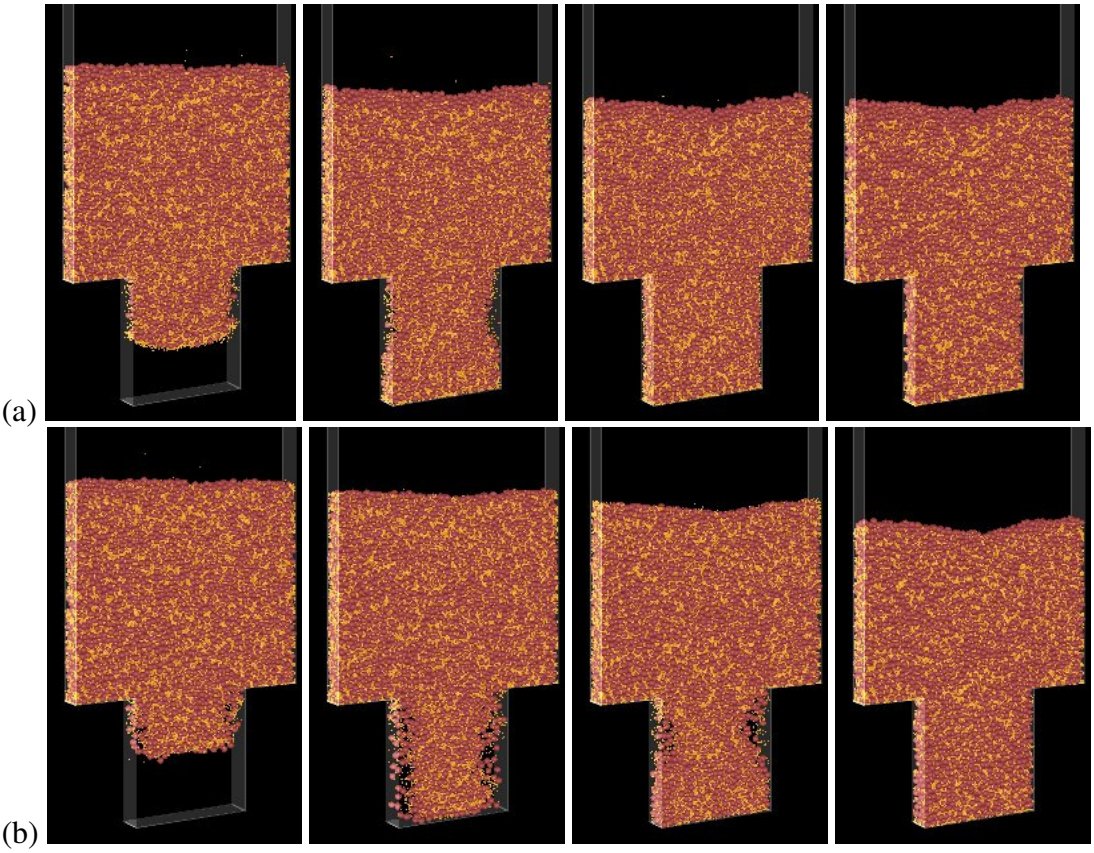

Figure 8.34 Die filling processes with a deep powder bed (H ≈14 mm) and a stationary shoe (a) in a vacuum (top row) and (b) in air (bottom row). The labels indicate the elapsed time of filling process.

Die filling with a deep powder bed (H≈14 mm) and a moving shoe (v_s =70mm/s) is also investigated. For this case, the powder flow patterns are similar in a vacuum and in air. Thus, only the die filling process in air is shown in Figure 8.35. During die filling with a deep powder bed, a layer of coarse particles is formed on the top surface. The coarse particles flow more easily over the top of fine particles during surface flow, so that an excess of coarse particles is eventually obtained at the bottom of the slope. However, compared with the die filling with a shallow powder bed (Figures 8.7 and 8.8), the coarses-rich powder flow stream can no longer flow into the die from the top free surface during die filling with a deep powder bed, and the die is filled only by the powder from the lower region of the shoe.

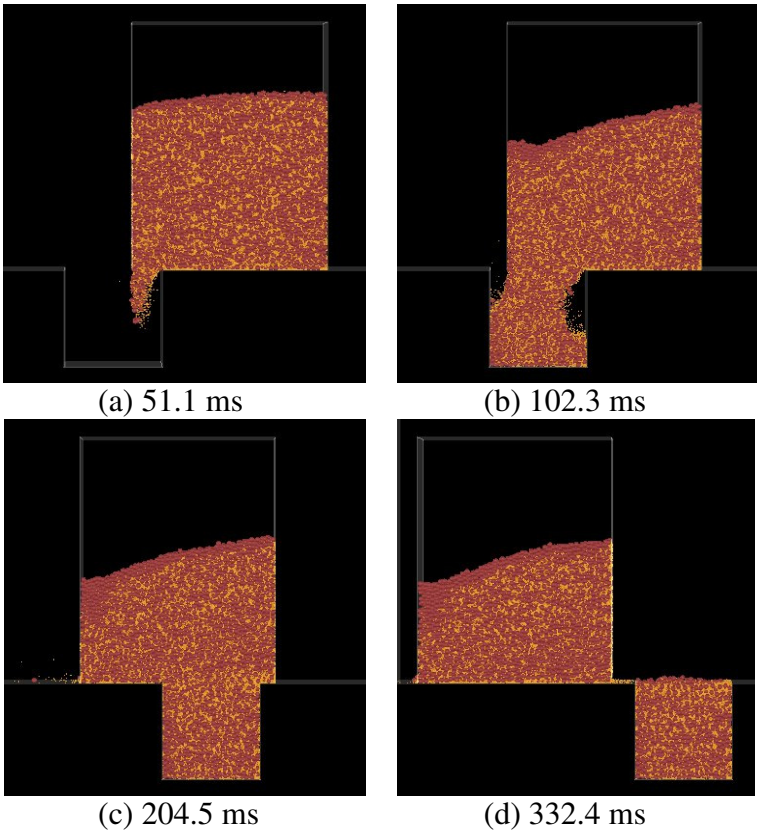

(a) 51.1 ms (b) 102.3 ms

(c) 204.5 ms (d) 332.4 ms

Figure 8.35 Die filling process with a deep powder bed (H≈14 mm) and a moving shoe (v_s =70mm/s) in air. The labels indicate the elapsed time of filling process in millisecond (ms).

Figure 8.36 shows the horizontal concentration distributions of fines in the die for die filling with different heights of powder bed, H. A stationary shoe ($v_s = 0$) and a binary mixture of x_f =10% and $d_c/d_f = 4$ were employed in this die filling. In a vacuum, the concentration of fines is always higher than the initial average value (i.e., $x_i/x_f > 1$) along the horizontal direction for each bed height, H. For the shallow powder bed ($H\approx$ 7mm), the concentration of fines is slightly lower in the central region due to the formation of a coarses-rich region in the centre of the shoe (see Figure 8.5). While with the deep powder bed ($H\approx$ 14mm), the concentration profile becomes a bit more uniform. In the presence of air, segregation with a lower concentration of fines close to die walls and a higher value in the centre occurs for each bed height, H.

The corresponding concentration distributions of fines in the vertical direction are shown in Figure 8. 37. In a vacuum, a higher concentration of fines is obtained at the bottom due to the percolation mechanism for each bed height, H. While, a lower concentration of fines is obtained at the top of the die for die filling with a shallow powder bed ($H\approx$ 7mm), in which the top of the die can be filled by the coarses-rich powder from the centre of the shoe (Figure 8.5). For die filling in air, the vertical segregation tendency due to the percolation of fines is reduced by the reverse flow of the entrapped air.

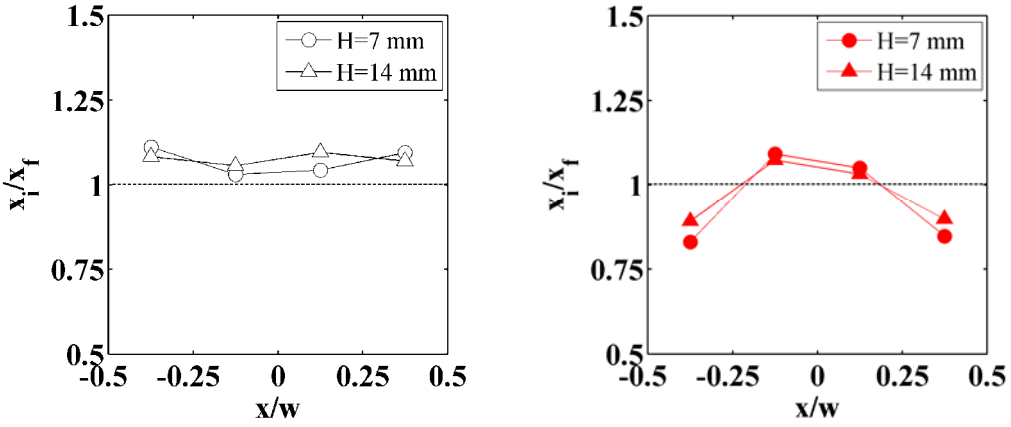

(a) In a vacuum (b) In air

Figure 8.36 Horizontal concentration distributions of fines in the die for die filling (a) in a vacuum and (b) in air with different heights of powder bed, *H*. (v_s = 0, x_f =10% and d_c/d_f = 4)

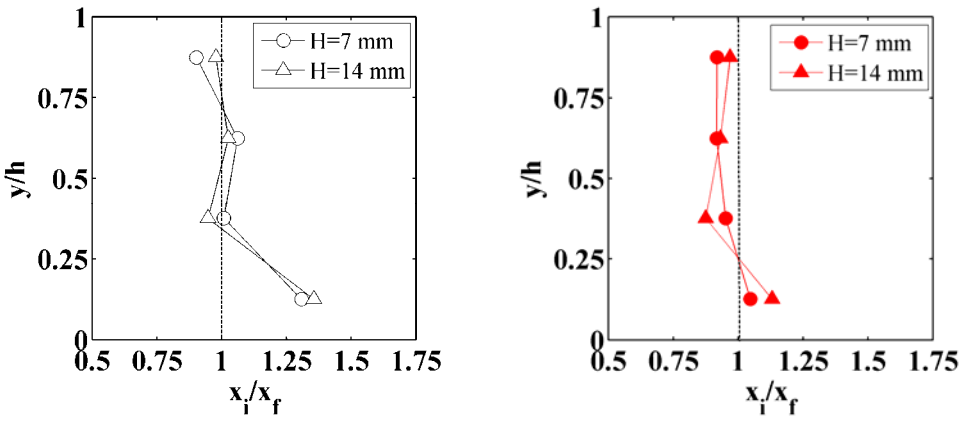

(a) In a vacuum (b) In air

Figure 8.37 Vertical concentration distributions of fines in the die for die filling (a) in a vacuum and (b) in air with different heights of powder bed, *H*. (v_s = 0, x_f =10% and d_c/d_f = 4)

Figure 8.38 shows the horizontal concentration distributions of fines in the die for die filling with different heights of powder bed, *H*. A moving shoe at a velocity of 70 mm/s and a binary mixture of x_f =10% and d_c/d_f = 4 were used in this die filling. A depletion of fines is obtained on the leading side (left hand side) of the die for die filling with a shallow powder bed (*H*≈7 mm). However, this does not occur for die filling with a deep powder bed (*H*≈14 mm). This is attributed to the fact that the

coarses-rich powder at the top of the powder mass can not flow into the die and the leading side of the die is filled by the fines-rich powder from the lower region of the shoe for die filling with a deep powder bed (see Figure 8.35). An excess of fines is obtained on the trailing side (right hand side) of the die for both cases. This is because the trailing side of the die cavity is always filled by the fines-rich powder from the lower region of the shoe whether with a shallow or deep powder bed.

The corresponding vertical concentration distributions of fines are plotted in Figure 8.39. Segregation with a higher concentration of fines at the bottom and an even higher value at the top occurs for both cases. It is observed that the concentration of fines with a shallow powder bed (H≈7 mm) is generally lower than that with a deep powder bed (H≈14 mm) except in the bottom layer of the die. This is because during die filling with a shallow bed, the die cavity is filled by both the fines-rich powder from the lower region of the shoe and the coarses-rich powder from the top region of the shoe (Figures 8.7 and 8.8), while during die filling with a deep bed, the die cavity is filled only by the fines-rich powder from the lower region of the shoe (Figure 8.35).

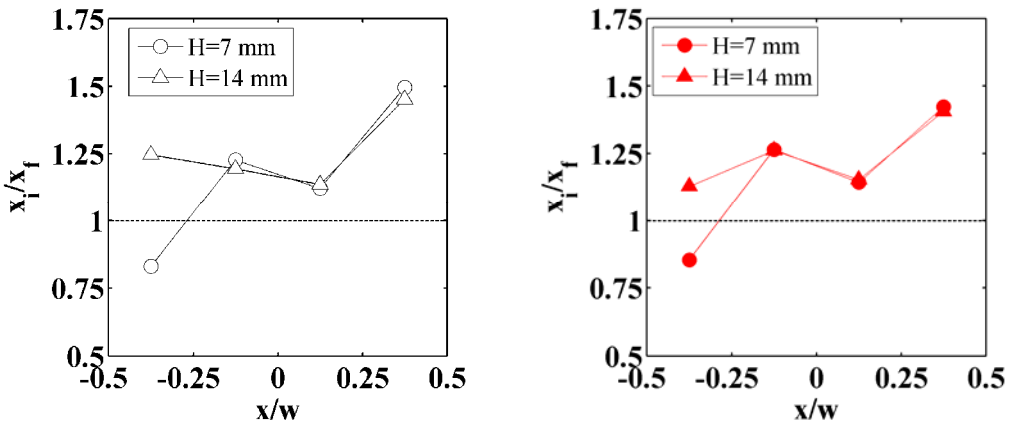

(a) In a vacuum (b) In air

Figure 8.38 Horizontal concentration distributions of fines in the die for die filling (a) in a vacuum and (b) in air with different heights of powder bed, H. (v_s = 70 mm/s, x_f =10% and d_c/d_f = 4)

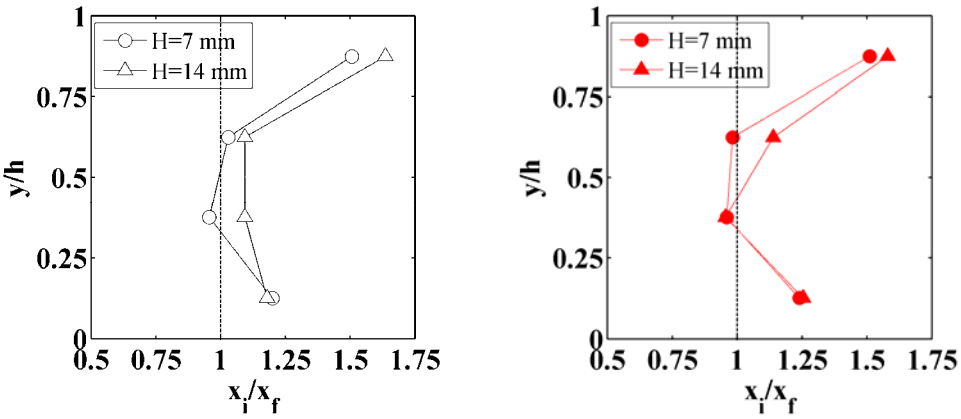

(a) In a vacuum (b) In air

Figure 8.39 Vertical concentration distributions of fines in the die for die filling (a) in a vacuum and (b) in air with different heights of powder bed, H. (v_s = 70 mm/s, x_f =10% and $d_c/d_f = 4$)

8.7. Summary

A thin-sliced model and a fully-3D model were employed to simulate die filling with binary mixtures of particles of the same density but different sizes in a vacuum and in air. It is found that segregation due to the size difference occurs during die filling, including the powder flow from the shoe and powder packing in the die. At the early stage of the filling process, fines-rich powder is delivered into the die from the bottom of the shoe, and thereafter the fines mass fraction in the discharged samples decreases until the die cavity is almost completely filled, when the fines are easier to be filled into the limited void space in the die than the coarse particles, therefore a sharp increase in fines mass fraction is observed at the final stage of die filling.

Different segregation patterns are obtained in the die for die filling with a stationary shoe and a moving shoe. For die filling with a stationary shoe, in the width direction (i.e., x-direction), a lower concentration of fines is obtained in the centre of the die in

a vacuum, while the concentration of fines is found to be lower in regions close to die walls if air is present. This is because the deposition of fine particles is hindered in those regions by the entrapped air. In the depth direction (y-direction), the vertical segregation occurs with a high concentration of fines at the bottom of the die for die filling in a vacuum, due to the percolation of fines through the voids in the matrix of coarse particles. The extent of this segregation is reduced when air is present, illustrating that the presence of air can suppress the size-induced segregation in the vertical direction by preventing the percolation of fine particles. The concentration distribution is found to be uniform in the thickness direction (z-direction) for fully-3D die filling, and the presence of air reduces the overall concentration of fines in the die.

For die filling with a moving shoe, the leading side of the die (referring to the motion of the shoe) is filled by the coarses-rich powder from the top surface of the flow stream, while the trailing side is filled by the fines-rich powder from the lower region of the shoe. Therefore, segregation occurs with a lower concentration of fines on the leading side and a higher value on the trailing side in the width direction of the die. In the depth direction, segregation also occurs with the concentration of fines higher at the bottom due to the percolation mechanism and even higher at the top of the die, which is due to the fact that the percolation of fines into the upper region of the die is promoted by the shearing between the moving powder bed in the shoe and the static powder bed in the die. The uniform concentration distribution in the thickness direction is also observed for the fully-3D die filling process with a moving shoe. The effect of air on the segregation is negligible when nose-flow dominates the filling process and the air can escape from the die before the die opening is completely covered by the powder mass.

It is also found that the powder flow patterns and segregation tendencies during die filling predicted by the thin-sliced model with the periodic boundaries are in good agreement with those predicted using the fully-3D model. This demonstrates the thin-sliced model, which significantly reduces the computational time by only modelling a small portion of the domain, is capable of capturing the essential behaviour during die filling.

Using the thin-sliced model, the effects of shoe velocity, particle size ratio, initial fines mass fraction, surface energy (for cohesive powders) and the initial height of powder bed on the segregation behaviour during die filling are investigated. It is found that the extent of segregation can be reduced through using a high shoe velocity, maintaining a small particle size ratio and keeping a large mass fraction of fine particles. Cohesion has a significant impact on powder flow pattern, by which the segregation behaviour is also affected. Increasing the initial height of the powder bed in the shoe can improve the uniformity of the horizontal concentration distribution, but it also brings in an excess of fines in the die.

CHAPTER 9: CONCLUDING REMARKS

9.1. Introduction

In this study, a coupled DEM/CFD approach is used to investigate die filling in a vacuum and in air. The results have shown that this approach is capable of modelling powder flow, mixing and segregation during die filling and can be effectively used to explore the effect of air. Based on this study, some important conclusions are summarised in this chapter.

9.2. Powder flow behaviour during die filling

The powder flow behaviour obtained from the simulations are generally in good agreement with the previous experimental results (Wu et al., 2003a and c; Wu and Cocks, 2004 and 2006; Schneider et al., 2005 and 2007). For die filling with a stationary shoe in a vacuum, the powder is deposited into the die smoothly and rapidly, and the dimensionless mass flow rate M^* is found to be constant with a value of 0.58, which is consistent with the Beverloo constant determined experimentally (Seville et al., 1997). In the presence of air, powder flow becomes slower and more chaotic due to the interaction of air and particles. The flow characteristics in air depend on the particle size and density. Two distinct regimes have been identified: (i) an air-sensitive regime with generally smaller and lighter particles, in which the presence of air has a significant impact on powder flow behaviour and the dimensionless mass flow rate increases as the particle size or density increases; (ii) an air-inert regime, in which the particle size and density are sufficiently large that the effect of air flow

becomes negligible and the dimensionless mass flow rate is essentially identical to that for the die filling in a vacuum. In addition, it is also found that the powder flow behaviour can be influenced by particle size distribution and cohesion.

For die filling with a moving shoe, different powder flow patterns identified from experimental observations are also observed: nose-flow, which dominates the die filling process at a low shoe velocity, and bulk-flow, which dominates when the shoe translates at a high velocity. There exists a critical shoe velocity above which incomplete filling occurs. The higher the critical shoe velocity is, the better the powder flowability for a given die filling system. For die filling with small and light particles, the average mass flow rate and critical shoe velocity are significantly reduced by the presence of air. For die filling with large and heavy particles, the effect of air is negligible.. The maximum value of the average mass flow rate for die filling with a moving shoe is achieved at the critical shoe velocity, which is consistent with the analysis of Wu (2008). When incomplete filling occurs (i.e., above the critical shoe velocity), the fill ratio decreases as shoe velocity increases and it follows a power law relationship with the shoe velocity (i.e., Eq. (3.27)). The powers α in Eq. (3.37) determined from the simulations are consistent with those obtained experimentally.

9.3. Competing flow during die filling

Competing flow occurs during die filling with bi-column or bi-layer mixtures, which comprise of identical sized particles but of different densities. During die filling with a bi-column mixture, the heavy particles prevent the light ones flowing into the die by

pushing them due to the difference in inertia. In the presence of air, it is easier for the entrapped air to penetrate the powder bed of light particles which are more sensitive to the air. Therefore, even fewer light particles are deposited into the die in air compared to in a vacuum. The number fraction of light particles in the die (NFLP) increases as the density difference decreases. The NFLP depends only on the particle density ratio for die filling in a vacuum but, for die filling in air, the NFLP depends not only on the particle density ratio but also on the absolute values of particle densities.

For die filling with a bi-layer mixture, the presence of air also prevents the light particles (i.e. air-sensitive particles) flowing into the die and therefore fewer light particles are deposited into the die in air compared to in a vacuum. As the shoe velocity increases, the powder mass covers the die opening more rapidly so that it becomes more difficult for the particles in the top layer of the powder bed to flow into the die. As a result, the number fraction of the component particles in the die, which were initially located at the top of the mixture, is reduced when the shoe moves faster.

9.4. Thin-sliced model versus fully-3D model

It is noted that the powder flow patterns and segregation tendencies in die filling predicted by the thin-sliced model with the periodic boundaries are in good agreement with those predicted by the fully-3D model. This demonstrates the thin-sliced model, which can dramatically reduce the computational expense by only modelling a small

portion of the domain, is capable to simulate the die filling process considered instead of the fully-3D model.

9.5. Segregation during die filling

Powders generally consist of particles of different physical properties, such as particle size and density. The difference in particle properties can cause segregation. Both density-induced and size-induced segregation during die filling are examined.

9.5.1. Density-induced segregation

The presence of air could have an impact on the segregation of particles of different densities due to the difference in air sensitivity. In addition, the density-induced segregation is also influenced by shoe velocity and density ratio. For die filling with a stationary shoe, the entrapped air resists the deposition of the air-sensitive particles (i.e. light particles), so that vertical segregation is induced with a lower concentration of light particles at the bottom of the die. As the density ratio (ρ_h / ρ_l) increases, the degree of segregation during die filling in air initially increases due to the increasing difference in falling acceleration from the effect of air drag; and then remains nearly constant or even decreases due to the formation of the denser powder flow stream that suppresses the segregation.

For die filling with a moving shoe, the degree of segregation generally decreases as the shoe velocity increases with the transition of die filling from nose-flow dominated to bulk-flow dominated. During nose-flow dominated die filling, segregation occurs with a depletion of light particles not only at the bottom of the die but also at the leading side of the die (referring to the direction of shoe motion). When nose-flow

occurs, the air can escape from the die before the die opening is completely covered by the powder mass, so that the influence of air on the powder flow and segregation behaviour is limited for nose-flow dominated die filling. During the bulk-flow dominated die filling, the air can be entrapped in the die by the fast-moving powder mass in the shoe, and the entrapped air could lead to an incomplete filling of the die or the outflow of a light particles-rich stream from the trailing side of the die. Consequently, the presence of air could have an impact on the segregation behaviour during the bulk-flow dominated die filling. It is also found that the degree of this segregation increases as the density ratio increases due to the increasing difference in particle inertia, which causes the light particles gaining higher post-collisional velocities to segregate from the heavy ones.

9.5.2. Size-induced segregation

Segregation due to the size difference is observed to occur during the entire die filling process, including the powder flow from the shoe and powder packing in the die. At the early stage of the filling process, fines-rich powder is delivered into the die from the bottom of the shoe, and thereafter the fines mass fraction in the discharged samples decreases. When the die cavity is almost completely filled, the fines can more easily fill the limited void space left in the die than the coarse particles, therefore a sudden increase in fines mass fraction is observed at the final stage of die filling.

Different segregation patterns are obtained in the die for die filling with a stationary shoe and a moving shoe. For die filling with a stationary shoe, vertical segregation occurs with a high concentration of fines at the bottom of the die due to the percolation of fines through the voids in the matrix of coarse particles. The presence

of air can reduce this segregation tendency by preventing the percolation of fine particles. For die filling with a moving shoe, horizontal segregation occurs with a lower concentration of fines on the leading side and an excess of fines on the trailing side of the die. In the vertical direction, the concentration of fines is higher at the bottom due to the percolation mechanism and even higher at the top of the die, which is due to the fact that the percolation of fines into the top layer of the die is promoted by the shearing between the moving powder bed in the shoe and the static powder bed in the die at the late stage of die filling.

A relatively lower segregation tendency is obtained for die filling with a stationary shoe. For die filling with a moving shoe, the degree of segregation decreases as shoe velocity increases. During die filling at a higher shoe velocity, the powder bed can sooner cover and pass the die opening, so that less time is allowed for the fines-depleted powder to flow into the die from the top region and the chance for the percolation of fines through the flow stream is also reduced. As particle size ratio (d_c/d_f) increases, it becomes easier for the fines to pass through the enlarged voids in the matrix of coarse particles, so that it is not a surprise that the segregation tendency is increased. As the initial fines mass fraction increases, more coarse particles become surrounded by the fine ones and the micro-structure of the granular system transits from the coarses-continuous to the fines-continuous, so that the percolation mechanism is suppressed. As a result, the segregation tendency can be reduced by increasing the fines mass fraction. Cohesion has a significant impact on the powder flow pattern, by which the segregation behaviour is also affected. Increasing the initial height of powder bed in the shoe can improve the uniformity of the horizontal concentration distribution, but it also brings in an excess of fines in the die.

9.6. Suction filling

The mass flow rate and critical shoe velocity can be significantly improved with suction filling compared to with gravity filling, due to the effect of air pressure gradient caused by the downward movement of the punch. A high punch velocity could enhance the effect of suction. However, the punch can not move too fast, otherwise turbulence occurs and influences powder flowability and composition uniformity (Sinka and Cocks, 2009). Moreover, in suction filling no nose flow occurs and the powder flows into the die very smoothly without severe collision and rebound, therefore the segregation induced by the particle density difference can be suppressed.

9.7. Recommendations for optimising die filling

From this study, some recommendations can be made in order to optimise die filling process in terms of productivity and uniformity:

- The entrapment of air in the die should be avoided. The ideal method to eliminate the effect of air is to conduct die filling in a vacuum, but generally it is not practical to create vacuum condition for die filling in industries. However, some approaches could be adopted to facilitate the evacuation of air, for example, installing a pipe in the shoe through which the air can escape (Sawayama and Seki, 1999).
- Suction filling is a very promising approach to improve the efficiency of die filling. However, a proper punch velocity should be adopted to perform the suction in case the powder flow is hindered by the slow-moving punch or turbulence takes place at high punch velocity.

- The segregation tendency due to the difference in particle density can be suppressed by reducing density difference and promoting bulk-flow. The latter can be achieved by using a stationary shoe or a moving shoe with a high shoe velocity. In addition, the utilization of suction filling can also reduce the degree of density-induced segregation.
- The degree of segregation due to the difference in particle size can be reduced through using a high shoe velocity, maintaining a small particle size ratio (d_c/d_f) and keeping a large mass fraction of fine particles.
- After a shoe moves across a die, significant density-induced or size-induced segregation also occurs inside the shoe with light or large particles congregating on the top surface (see Chapters 5 and 8). Therefore, caution must be taken if this shoe needs to successively pass over and feed a series of dies.

9.8. Limitations and future work

Although some interesting results are obtained from this work, there are still some limitations. In our DEM modelling, all the particles are spherical. However, the particle shapes in reality are usually very complex and irregular. Therefore, the irregularity of particle shape is not considered in this study. In real pharmaceutical, powder metallurgy and ceramic industries, millions even billions of particles are involved in the die filling process. But due to the limitation of computing capacity, we have simulated die filling only at a small scale (millimetres) with up to 300,000 particles. Running on the SGI work station, the largest simulation considered in our study took more than two months to complete. Compared to the time scale in die filling experiments (say seconds), the simulation is much more time-consuming.

Therefore, in the future work the irregular particles should be used in the DEM modelling. Wu and Cocks (2006) used 2D polygonal particles and Bierwisch et al. (2009) employed 3D complex grains consisting of agglomerates of spheres in the die filling simulations. However, the real particle shapes are far more irregular. On the other hand, the interparticle contact model of the irregular shaped particles is much more complicated than that of the spheres, so that the computational cost should be significantly increased with the irregular particles. In addition, if the irregular particles are used, the new air-particle interaction model should be developed in order to consider the effect of air drag.

Running a program in less time is a big issue in computer science and computational engineering. In recent years, parallel computing has shown a great potential to achieve this goal, therefore developing a parallelized DEM program is necessary in order to reduce the computing time and increase the number of particles used in the simulation.

In this study, die filling with rectangular shaped die was simulated. In future, die filling with cylindrical shaped die and more complex shaped dies should also be explored considering the various die geometries used in the real die filling. In this study, a shoe just moved across a single die. In future, we will simulate the successive passages of a shoe over a series of dies, as occurs in industry (e.g., pharmaceutical tableting).

Although it has been shown that our numerical results are in good agreement with experimental observations (see Chapter 3), it is still worth performing a thorough

experimental validations. In particular, die filling experiments on density-induced and size-induced segregations need to be conducted in order to validate the simulations presented in this study.

REFERENCES

Anderson, T.B., Jackson, R., 1967. A fluid mechanical description of fluidized beds. Equations of motion. Industrial and Engineering Chemistry Fundamentals 6, 527–539.

Arastoopour, H., 2001. Numerical simulation and experimental analysis of gas/solid flow systems. Powder Technology 119, 59–67.

Arteaga, P., Tüzün, U., 1990. Flow of binary mixtures of equal-density granules in hoppers—size segregation, flowing density and discharge rates. Chemical Engineering Science. 45 (1), 205-223.

Baxter, J., Abou-Chakra, H., Tuzun, U., Lamptey, B.M., 2000. A DEM simulation and experimental strategy for solving fine powder flow problems. Chemical Engineering Research and Design 78 (A7), 1019–1025.

Baxter, J., Tüzün, U., Burnell, J., Heyes, D.M., 1997. Granular dynamics simulations of two-dimensional heap formation. Physical Review E 55, 3546–3554.

Baxter, J., Tüzün, U., Heyes, D., Hayati, I., Fredlund, P., 1998. Stratification in poured granular heaps. Nature, 391, p.136.

Beverloo, W.A., Leniger, H.A., van de Velde, J., 1961. The flow of granular solids through orifices, Chemical Engineering Science 15, 260-269.

Bierwisch, C., Kraft, T., Riedel, H., Moseler, M., 2007. Predicting density distributions in die filling. Proceedings of European Powder Metallurgy 2007, vol.3, October 15-17, 2007. Toulouse, France, pp. 305-310.

Bierwisch, C., Kraft, T., Riedel, H., Moseler, M., 2009. Three-dimensional discrete element models for the granular statics and dynamics of powders in cavity filling. Journal of the Mechanics and Physics of Solids 57, 10-31.

Bocchini, G.F., 1987. Influence of small die width on filling and compacting densities. Powder Metallurgy, 30 (4), 261-266.

Brown, R.L., Richards, J.C., 1965. Kinematics of the flow of dry powders and bulk solids. Rheologica Acta 4, 153-165.

Burtally, N., King, P.J., Swift, M. R., 2002. Spontaneous air-driven separation in vertically vibrated fine granular mixtures. Science, 295, 1877-1879.

Choi, H.G., Joseph, D.D., 2001. Fluidization by lift of 300 circular particles in plane Poiseuille flow by direct numerical simulation. Journal of Fluid Mechanics 438, 101–128.

Chung, Y.C., Ooi, J.Y., 2008. Influence of discrete element model parameters on bulk behavior of a granular solid under confined compression. Particulate Science and Technology 26, 83–96.

Cizeau, P., Makse, H.A., Stanley, H.E., 1999. Mechanisms of granular spontaneous stratification and segregation in two-dimensional silos. Physical Review E, 59 (4), 4408-4421.

Cocks, A.C.F., Dihoru, L., Lawrence, T., 2001. Proc. PM2001, Nice, France, EPMA, 255-260.

Cook, B.K., Noble, D.R., Williams, J.R., 2004. A direct simulation method for particle–fluid systems. Engineering Computations 21, 151–168.

Coube, O., Cocks, A.C.F., Wu, C.-Y., 2005. Experimental and numerical study of die filling, powder transfer and die compaction. Powder Metallurgy 48, 68-76.

Crowe, C.T., Sommerfeld, M., Tsuji, Y., 1998. Multiphase Flow with Droplets and Particles. CRC Press, Boca Raton, FL.

Cundall, P.A., 1988. In M. Satake, J.T. Jenkins (Eds.), Micromechanics of Granular Materials, Amstedam, Elsevier, 113-123.

Cundall, P.A., Strack, O.D.L., 1979. A discrete numerical model for granular assemblies. Geotechnique 29, 47–65.

David, C.T., Garcia-Rojo, R., Herrmann, H.J., Luding, S., 2007. Powder flow testing with 2D and 3D biaxial and triaxial simulations. Particle and Particle Systems Characterization 24, 29–33.

Davidson, J.F., Nedderman, R.M., 1973. The hour-glass theory of hopper flow. Trans. Inst. Chem. Engrs. 51, 29-35.

de Silva, S., Dyrøy, A., Enstad, G.G., 2000. Segregation mechanisms and their quantification using segregation testers, in: A.D. Rosato, D.L. Blackmore (Eds.), IUTAM Symposium on Segregation in Granular Flows, Kluwer Academic Publishers, Boston, p.p. 11-29.

Demetry, C., Souto, F.S., Ryden, B.C., Roy, J.M., 1998. Tactile sensing of density uniformity in powder beds after die filling. Powder Technology 99, 119-124.

Derjaguin, B.V., Muller, V.M., Toporov, Y.P., 1975. Effect of contact deformation on the adhesion of particles. Journal of Colloid Interface Science 53, 314–326.

Di Felice, R., 1994. The voidage function for fluid–particle interaction systems. International Journal of Multiphase Flow 20, 153–159.

Di Renzo, A., Di Maio, F.P., 2004. Comparison of contact-force models for the simulation of collisions in DEM-based granular flow codes. Chemical Engineering Science 59, 525–541.

Drahun, J.A., Bridgwater, J., 1983. The mechanisms of free surface segregation. Powder Technology 36, 39-53.

Dury, C.M., Knecht, R., Ristow, G.H., 1998. Size segregation of granular materials in a 3D rotating drum. High-Performance Computing and Networking 1401, 860–862.

Ergun, S., 1952. Fluid flow through packed columns. Chemical Engineering and Processing 48, 89–94.

Fazekas, S., Kertesz, J., Wolf, D.E., 2005. Piling and avalanches of magnetized particles. Physical Review E 71, 061303.

Ganesh Palappan, K., Sai, P.S.T., 2008a. Studies on segregation of binary mixture of solids in a continuous fast fluidized bed: Part I. Effect of particles density. Chemical Engineering Journal 138, 358-366.

Ganesh Palappan, K., Sai, P.S.T., 2008b. Studies on segregation of binary mixture of solids in a continuous fast fluidized bed: Part II. Effect of particles size. Chemical Engineering Journal 139, 330-338.

Ge, W., Li, J.H., 2001. Macro-scale pseudo-particle modelling for particle–fluid systems. Chinese Science Bulletin 46, 1503–1507.

Ge, W., Li, J.H., 2003. Macro-scale phenomena reproduced in microscopic systems-pseudo-particle modeling of fluidization. Chemical Engineering Science 58, 1565–1585.

Gidaspow, D., 1994. Multiphase Flow and Fluidization. Academic Press, San Diego.

Glowinski, R., Pan, T.W., Hesla, T.I., Joseph, D.D., Periaux, J., 2000. A distributed Lagrange multiplier/fictitious domain method for the simulation of flow around moving rigid bodies: application to particulate flow. Computer Methods in Applied Mechanics and Engineering 184, 241–267.

Gui, N., Fan, J.R., Luo, K., 2008. DEM–LES study of 3-D bubbling fluidized bed with immersed tubes. Chemical Engineering Science 63, 3654-3663.

Guo, Y., Kafui, K.D., Thornton, C., Wu, C.-Y, 2007. A numerical study of die filling using a coupled discrete element method and computational fluid dynamics.

Proceedings of European Powder Metallurgy 2007, vol.3, October 15-17, 2007. Toulouse, France, pp. 317-322.

Guo, Y., Kafui, K.D., Thornton, C., Wu, C.-Y, 2008. 2D simulation of density-induced segregation during die filling in the presence of air. Proceedings of International Symposium/RCUK-China Summer School on Discrete Element Methods and Numerical Modelling of Discontinuum Mechanics, September 24-30, 2008. Beijing, China, pp. 268-277.

Guo, Y., Wu, C.-Y., Kafui, K.D., Thornton, C., 2009a. Numerical analysis of density-induced segregation during die filling, Powder Technology 197, 111-119.

Guo, Y., Kafui, K.D., Wu, C.-Y., Thornton, C., Seville, J.P.K., 2009b. A coupled DEM/CFD analysis of the effect of air on powder flow during die filling, AIChE Journal 55, 49-62.

Harmens, A., 1963. Flow of granular materials through horizontal apertures. Chemical Engineering Science 18, 297.

Hartl, J., Ooi, J.Y., 2008. Experiments and simulations of direct shear tests: porosity, contact friction and bulk friction. Granular Matter 10, 263–271.

Hashimoto, Y., Murakami, M., Seki, Y., 2002. 'Whizz' solutions agitate for a better-filled die. Metal Powder Report 57(12), 26-29.

Haskins, J.J., Jandeska, W.F., 1998. Powder flow and die filling studies using computed tomography. Int. Conf. on Powder Metallurgy and Particulate Materials, Las Vegas, NV, USA, 31 May-4 June 1999, 10.77-10.87.

Hertz, H., 1882. Über die Berührung fester elastischer Körper. Journal fur die reine und angewandte Mathematik 92, 156–171.

Hjortsberg, E., Bergquist, B., 2002. Filling induced density variations in metal powder, Powder Metallurgy 45(2), 146-153.

Hong, C.W., 1998. From long-range interaction to solid-body contact between colloidal surfaces during forming. Journal of the European Ceramic Society 18, 2159–2167.

Hu, H.H., 1996. Direct simulation of flows of solid–liquid mixtures. International Journal of Multiphase Flow 22, 335–352.

Jackson, S., Sinka, I.C., Cocks, A.C.F., 2007. The effect of suction during die fill on a rotary tablet press. European Journal of Pharmaceutics and Biopharmaceutics 65, 253-256.

Johnson, K.L., 1985. Contact Mechanics. Cambridge University Press, Cambridge.

Johnson K.L., Kendall K., Roberts A.D., 1971. Surface energy and the contact of elastic solids. Proc. Royal Society of London A 324, 301-313.

Johnson, R.W., 1998. The handbook of fluid dynamics, CRC Press, pp.18_2-18_3.

Kafui, K.D., Thornton, C., Adams, M.J., 2002. Discrete particle–continuum fluid modelling of gas-solid fluidised beds, Chemical Engineering Science, 57, 2395-2410.

Ketterhagen, W.R., Curtis, J.S., Wassgren, C.R., Kong, A., Narayan, P.J., Hancock, B.C., 2007. Granular segregation in discharging cylindrical hoppers: A discrete element and experimental study, Chemical Engineering Science, 62, 6423-6439.

Ketterhagen, W.R., Curtis, J.S., Wassgren, C.R., Hancock, B.C., 2008. Modeling granular segregation in flow from quasi-three-dimensional, wedge-shaped hoppers, Powder Technology, 179, 126-143.

Khakhar, D.V., McCarthy, J. J., Ottino, J.M., 1999. Mixing and segregation of granular materials in chute flows. Chaos, 9(3), 594-610.

Kohring, G.A., Melin, S., Puhl, H., Tillemans, H.J., Vermohlen, W., 1995. Computer-simulations of critical, nonstationary granular flow—through a hopper. Computer Methods in Applied Mechanics and Engineering 124, 273–281.

Kondoh, M., Takemoto, S., Urata, I., 1998. Development of uniform powder filling method-aeration powder filling, Proceedings of 1998 World Congress on Powder Metallurgy. Granada, Spain, 85-90.

Kong, C.M., Lannutti, J.J., 2000a. Localized densification during the compaction of alumina granules: the Stage I-II transition. Journal of the American Ceramic Society 83, 685–690.

Kuang, S.B., Chu, K.W., Yu, A.B., Zou, Z.S., Feng, Y.Q., 2008. Computational investigation of horizontal slug flow in pneumatic conveying. Industrial & Engineering Chemistry Research 47, 470–480.

Kuipers, J.A.M., van Swaaij, W.P.M., 1997. Application of computational fluid dynamics to chemical reaction engineering. Reviews in Chemical Engineering 13, 1–118.

Kuo, H.P., Knight, P.C., Parker, D.J., Tsuji, Y., Adams, M.J., Seville, J.P.K., 2002. The influence of DEM simulation parameters on the particle behaviour in a V-mixer. Chemical Engineering Science 57, 3621–3638.

Langston, P.A., Tüzün, U., Heyes, D.M., 1994. Continuous potential discrete particle simulations of stress and velocity-fields in hoppers—transition from fluid to granular flow. Chemical Engineering Science 49, 1259–1275.

Langston, P.A., Tüzün, U., Heyes, D.M., 1995. Discrete element simulation of granular flow in 2D and 3D hoppers—dependence of discharge rate and wall stress on particle interactions. Chemical Engineering Science 50, 967–987.

Langston, P.A., Nikitidis, M.S., Tuzun, U., Heyes, D.M., Spyrou, N.M., 1997. Microstructural simulation and imaging of granular flows in two- and three-dimensional hoppers. Powder Technology 94, 59–72.

Langston, P.A., Al-Awamleh, M.A., Fraige, F.Y., Asmar, B.N., 2004. Distinct element modelling of non-spherical frictionless particle flow. Chemical Engineering Science 59, 425–435.

Lawrence, L.R., Beddow, J.K., 1968a. Powder segregation during die filling, Powder Technology, 2, 253-259.

Lawrence, L.R., Beddow, J.K., 1968b. Some effects of vibration upon powder segregation during die filling, Powder Technology, 2, 125-130.

Lee, J., 1997. Time-dependent behavior of granular material in a vibrating box. Physica A 238, 129–148.

Lemieux, A., Leonard, G., Doucet, J., Leclaire, L.A., Viens, F., Chaouki, J., Bertrand, F., 2008. Large-scale numerical investigation of solids mixing in a V-blender using the discrete element method. Powder Technology 181, 205–216.

Li, J.F., Chen, C.S., Yu, B.Y., Wei, W.C.J., 2006. Simulation of colloidal particle packing for photonic bandgap crystals. Journal of the American Ceramic Society 89, 1257 –1265.

Li, J., Kuipers, J.A.M., 2002. Effect of pressure on gas–solid flow behavior in dense gas-fluidized beds: a discrete particle simulation study. Powder Technology 127, 173-184.

Li, J., Kuipers, J.A.M., 2003. Gas-particle interactions in dense gas-fluidized beds. Chemical Engineering Science 58, 711-718.

Li, J., Kuipers, J.A.M., 2007. Effect of competition between particle–particle and gas-particle interactions on flow patterns in dense gas-fluidized beds. Chemical Engineering Science 62, 3429–3442.

Li, Y., Zhang, J.P., Fan, L.S., 1999. Numerical simulation of gas–liquid–solid fluidization systems using a combined CFD-VOF-DPM method, bubble wake behavior. Chemical Engineering Science 54, 5101–5107.

Lim, E.W.C., Wang, C.H., Yu, A.B., 2006. Discrete element simulation for pneumatic conveying of granular material. A.I.Ch.E. Journal 52, 496–509.

Luding, S., 1997. Stress distribution in static two-dimensional granular model media in the absence of friction. Physical Review E 55, 4720–4729.

MacCormarck, R. W., 1971. Numerical solution of the interaction of a shock wave with a laminar boundary-layer. Proceedings of the second international conference numerical methods fluid dynamics, Lecture Notes in Physics 8, 151–163. New York: Springer.

Makse, H.A., Havlin, S., King, P.R., Stanley, H.E., 1997. Spontaneous stratification in granular mixtures. Nature, 386, 379-382.

Martin, C.L., Bouvard, D., Delette, G., 2006. Discrete element simulations of the compaction of aggregated ceramic powders. Journal of the American Ceramic Society 89, 3379–3387.

Matuttis, H.G., Luding, S., Herrmann, H.J., 2000. Discrete element simulations of dense packings and heaps made of spherical and non-spherical particles. Powder Technology 109, 278–292.

Meakin, P., 1990. A simple two-dimensional model for particle segregation. Physica A, 163, 733-746.

Mehrotra, A., Chaudhuri, B., Faqih, A., Tomassone, M.S., Muzzio, F.J., 2009. A modeling approach for understanding effects of powder flow properties on tablet weight variability. Powder Technology 188, 295-300.

Mindlin, R. D., Deresiewicz, H., 1953. Elastic spheres in contact under varying oblique forces. Journal of Applied Mechanics, 20, 327-344.

Motazedian, F., Cocks, A.C.F., Sinka, I.C., 2007. The influence of airflow on gravity and suction filling. Proceedings of International Conference on Powder Metallurgy & Particulate Materials, vol.1, Denver, CO(US), 20070513-16.

Ng, T.T., 1999. Fabric study of granular materials after compaction. Journal of Engineering Mechanics—ASCE 125, 1390–1394.

Ng, T.T., 2005. Behavior of gravity deposited granular material under different stress paths. Canadian Geotechnical Journal 42, 1644–1655.

Olivieri, G., Marzocchella, A., Salatino, P., 2004. Segregation of fluidized binary mixtures of granular solids. AIChE Journal, 50 (12), 3095-3106.

Pan, T.W., Joseph, D.D., Bai, R., Glowinski, R., Sarin, V., 2002. Fluidization of 1204 spheres: simulation and experiment. Journal of Fluid Mechanics 451, 169–191.

Portillo, P.M., Muzzio, F.J., Ierapetritou, M.G., 2007. Hybrid DEM-compartment modeling approach for granular mixing. A.I.Ch.E. Journal 53 (1), 119–128.

Potic, B., Kersten, S.R.A., Ye, M., van der Hoef, M.A., Kuipers, J.A.M., van Swaaij, W.P.M., 2005. Fluidization with hot compressed water in microreactors. Chemical Engineering Science 60, 5982–5990.

Prigonzhin, L., 1993. A variational problem of bulk solids mechanics and free-surface segregation. Chemical Engineering Science, 48 (21), 3647-3656.

Pudasaini, S.P., Mohring, J., 2002. Mathematical model and experimental validation of free surface size segregation for polydisperse granular materials. Granular Matter, 4, 45-56.

Rice, E.R., Tengzelius, J., 1986. Die filling characteristics of metal powders, Powder Metallurgy 29(3), 183-194.

Richardson, J.F., 1971. Incipient fluidization and particulate systems. In: Davidson, J.F., Harrison, D. (Eds.), Fluidization. Academic Press, New York.

Rhodes, M.J., 1998. Introduction to particle technology. John Wiley& Sons Ltd, Chichester, England.

Rock, M., Morgeneyer, M., Schwedes, J., Brendel, L., Wolf, D.E., Kadau, D., 2008. Visualization of shear motions of cohesive powders in the true biaxial shear tester. Particulate Science and Technology 26, 43–54.

Rosato, A.D., Lan, Y.D., Richman, M.W., 2008. On the calculation of self-diffusion in vertically agitated granular beds. Powder Technology 182, 228–231.

Savkoor, A.R., Briggs, G.A.D., 1977. The effect of tangential force on the contact of elastic solids in adhesion. Proceedings of the Royal Society of London A, 356, 103-114.

Samadani, A., Pradhan, A., Kudrolli, A., 1999. Size segregation of granular matter in silo discharges, Physical Review E, 60(6), 7203-7209.

Sawayama, T., Seki, Y., 1999. The effect of filling conditions on die filling. Advances in Powder Metallurgy & Particulate Materials 1(2), 61-72.

Schneider, L.C.R., Cocks, A.C.F., Apostolopoulos, A., 2005. Comparison of filling behaviour of metallic, ceramic, hardmetal and magnetic powders. Powder Metallurgy 48, 77-84.

Schneider, L.C.R., Sinka, I.C., Cocks, A.C.F., 2007. Characterisation of the flow behaviour of pharmaceutical powders using a model die-shoe filling system. Powder Technology 173, 59-71.

Seville, J.P.K., Tüzün, U., Clift, R., 1997. Processing of Particulate Solids, Blackie Academic and Professional, London, pp. 330-348.

Sinka, I.C., Cocks, A.C.F., 2009. Evaluating the flow behaviour of powders for die fill performance. Powder Metallurgy 52, 8-11.

Sinka, I.C., Motazedian, F., Cocks, A.C.F., Pitt, K.G., 2009. The effect of processing parameters on pharmaceutical tablet properties. Powder Technology 189, 276-284.

Sinka, I.C., Schneider, L.C.R., Cocks, A.C.F., 2004. Measurement of the flow properties of powders with special reference to die fill, International Journal of Pharmaceutics 280, 27-38.

Smith, L., Baxter, J., Tüzün, U., Heyes, D.M., 2001. Granular dynamics simulations of heap formation: effects of feed rate on segregation patterns in binary granular heap. Journal of Engineering Mechanics—ASCE 127, 1000–1006.

Standish, N., 1985a. Studies of size segregation in filling and emptying a hopper. Powder Technology, 45, 43-56.

Standish, N., 1985b. Comparison of stop-start and continuous sampling methods of studying segregation of materials discharging from a hopper. Chemical Engineering Science, 40 (11), 2152-2153.

Thornton, C., 1991. Interparticle sliding in the presence of adhesion. Journal of Physics D: Applied Physics 24, 1942-1946.

Thornton, C., 1997. Coefficient of restitution for collinear collisions of elastic-perfectly plastic spheres. ASME Journal of Applied Mechanics 64(2), 383-386.

Thornton, C., 2000. Numerical simulations of deviatoric shear deformation of granular media. Géotechnique 50, 43-53.

Thornton, C., Barnes, D. J., 1986. Computer simulated deformation of compact granular assemblies. Acta Mechanica 64, 45-61.

Thornton, C., Ciomocos, M.T., Adams, M.J., 2004. Numerical simulation of diametrical compression tests on agglomerates. Powder Technology 140, 258–267.

Thornton, C., Ning, Z., 1998. A theoretical model for the stick/bounce behaviour of adhesive, elastic-plastic spheres. Powder Technology 99, 154-162.

Thornton, C., Randall, W., 1988. In M. Satake, J.T. Jenkins (Eds.), Micromechanics of Granular Materials, Amstedam, Elsevier, 133-142.

Thornton C, Yin KK. Impact of elastic spheres with and without adhesion. Powder Technology. 1991; 65: 153-165.

Thornton, C., Zhang, L., 2003. Numerical Simulations of the direct shear test. Chemical Engineering and Technology 26, 153–156.

Thornton, C., Zhang, L., 2006. A numerical examination of shear banding and simple shear non-coaxial flow rules. Philosophical Magazine 86, 3425–3452.

Tsuji, Y., Kawaguchi, T., Tanaka, T., 1993. Discrete particle simulation of two-dimensional fluidized bed. Powder Technology 77, 79-87.

Tsuji, T., Yabumoto, K., Tanaka, T., 2008. Spontaneous structures in three-dimensional bubbling gas-fluidized bed by parallel DEM–CFD coupling simulation. Powder Technology 184, 132–140.

Tüzün, U., Arteaga, P., 1992. A Microstructural model of flowing ternary mixtures of equal-density granules in Hoppers. Chemical Engineering Science, 47 (7), 1619-1634.

Tüzün, U., Baxter, J., Heyes, D.M., 2004. Analysis of the evolution of granular stress-strain and voidage states based on DEM simulations. Philosophical Transactions of the Royal Society of London Series A—Mathematical Physical and Engineering Sciences 362, 1931–1951.

Urata, I., Takemoto, S., Kondoh, M., 1998. PM98: World congress on powder metallurgy, Shrewsbury, EPMA, 91-96.

Vu-Quoc, L., Zhang, X., 1999. An accurate and efficient tangential force-displacement model for elastic frictional contact in particle-flow simulations. Mechanics of Materials 31, 235-269.

Vu-Quoc, L., Zhang, X., Lesburg, L., 2001. Normal and tangential force–displacement relations for frictional elasto-plastic contact of spheres. International Journal of Solids and Structures 38, 6455-6489.

Vu-Quoc, L., Zhang, X., Walton, O.R., 2000. A 3-D discrete-element method for dry granular flows of ellipsoidal particles. Computer Methods in Applied Mechanics and Engineering 187, 483-528.

Walton, O.R., 1993. Numerical simulation of inclined chute flows of monodisperse inelastic, frictional spheres. Mechanics of Materials 16, 239–247.

Walton, O.R., Braun, R.L., 1986. Viscosity, granular-temperature, and stress calculations for shearing assemblies of inelastic, frictional disks. Journal of Rheology 30, 949–980.

Wen, C.Y., Yu, Y.H., 1966. Mechanics of fluidization. A.I.Ch.E. Series 62, 100–111.

Williams, J.R., Rege, N., 1997. The development of circulation cell structures in granular materials undergoing compression. Powder Technology 90, 187–194.

Wu, C.-Y., 2008. DEM simulations of die filling during pharmaceutical tabletting. Particuology 6, 412-418.

Wu, C.-Y., Cocks, A.C.F., 2004. Flow behaviour of powders during die filling, Powder Metallurgy, 47, 127-136.

Wu, C.Y., Cocks, A.C.F. 2006. Numerical and experimental investigations of the flow of powder into a confined space, Mechanics of Materials, 38(4), 304-324.

Wu, C.-Y., Cocks, A.C.F., Gillia, O.T., 2003a. Die filling and powder transfer. International journal of powder metallurgy 39, 51-64.

Wu, C.-Y., Cocks, A.C.F., Gillia, O.T., Thompson, D.A., 2003b. Experimental and numerical investigations of powder transfer. Powder Technology 138, 216-228.

Wu, C.-Y., Dihoru, L., Cocks, A.C.F., 2003c. The flow of powder into simple and stepped dies. Powder Technology 134, 24-39.

Xiang, J.S., McGlinchey, D., 2004. Numerical simulation of particle motion in dense phase pneumatic conveying. Granular Matter 6, 167–172.

Xie, X., Puri, V.M., 2006. Uniformity of powder die filling using a feed shoe: A review. Particulate Science and Technology 24(4), 411-426.

Xie, X., Puri, V.M., 2007a. Simultaneous deposition of powder in three parallel-oriented cylindrical dies. Particulate Science and Technology 25, 247-259.

Xie, X., Puri, V.M., 2007b. Powder deposition in three parallel-oriented dies of different shapes. Particulate Science and Technology 25, 507-518.

Xie, X., Puri, V.M., 2008. Modeling of simultaneous deposition of powder in three parallel-oriented cylindrical dies. Particulate Science and Technology 26, 563-573.

Xiong, Y.Q., Zhang, M.Y., Yuan, Z.L., 2005. Three-dimensional numerical simulation method for gas–solid injector. Powder Technology 160, 180–189.

Xu, B.H., Yu, A.B., 1998. Comments on the paper "Numerical simulation of the gas–solid flow in a fluidized bed by combining discrete particle method with computational fluid dynamics"-Reply. Chemical Engineering Science 53, 2646–2647.

Xu, B.H., Yu, A.B., Chew, S.J., Zulli, P., 2000. Numerical simulation of the gas–solid flow in a bed with lateral gas blasting. Powder Technology 109, 13–26.

Yang, F., Kafui, K.D., Thornton, C., Seville, J.P.K., 2007. A DEM study of Geldart Group A particle bed fluidisation behaviour across the regimes. Proc. 12th Int. Conf. on Fluidization, May 13-17, 2007. Vancouver, Canada, 679-686.

Yang, R.Y., Zou, R.P., Yu, A.B., 2000. Computer simulation of the packing of fine particles. Physical Review E 62, 3900–3908.

Yang, R.Y., Zou, R.P., Yu, A.B., 2003. A simulation study of the packing of wet particles. A.I.Ch.E. Journal 49, 1656–1666.

Yang, R.Y., Zou, R.P., Yu, A.B., Choi, S.K., 2008. Characterization of interparticle forces in the packing of cohesive fine particles. Physical Review E 78, 031302.

Yin, K.K., 1992. Numerical modelling of agglomerate degradation. Ph. D dissertation, Aston University, pp.56-57.

Yu, A.B., Xu, B.H., 2003. Particle-scale modelling of gas–solid flow in fluidisation. Journal of Chemical Technology and Biotechnology 78, 111–121.

Yuu, S., Umekage, T., Johno, Y., 2000. Numerical simulation of air and particle motions in bubbling fluidized bed of small particles. Powder Technology 110, 158–168.

Zahrah, T.F., Rowland, R., Gasbarre Jr., G., 2001. Fluidized fill shoe for uniform die filling. Key Engineering Materials 189-191, 288-295.

Zeilstra, C., van der Hoef, M.A., Kuipers, J.A.M., 2006. Simulation study of air-induced segregation of equal-sized bronze and glass particles. Physical Review E, 74, 010302(R).

Zeilstra, C., van der Hoef, M.A., Kuipers, J.A.M., 2008. Simulation of density segregation in vibrated beds. Physical Review E, 77, 031309.

Zhang, J.P., Fan, L.S., Zhu, C., Pfeffer, R., Qi, D.W., 1999b. Dynamic behaviour of collision of elastic spheres in viscous fluids. Powder Technology 106, 98–109.

Zhang, L., Thornton, C., 2007. A numerical examination of the direct shear test. Geotechnique 57, 343–354.

Zhu, H.P., Zhou, Z.Y., Yang, R.Y., Yu, A.B., 2007. Discrete particle simulation of particulate systems: Theoretical developments. Chemical Engineering Science 62, 3378 – 3396.

Zhu, H.P., Zhou, Z.Y., Yang, R.Y., Yu, A.B., 2008. Discrete particle simulation of particulate systems: A review of major applications and findings. Chemical Engineering Science 63, 5728-5770.

Zhou, Y.C., Wright, B.D., Yang, R.Y., Xu, B.H., Yu, A.B., 1999. Rolling friction in the dynamic simulation of sandpile formation. Physica A 269, 536–553.

Zhou, Y.C., Xu, B.H., Zou, R.P., Yu, A.B., Zulli, P., 2003. Stress distribution in a sandpile formed on a deflected base. Advanced Powder Technology 14, 401–410.

Zigan, S., Thorpe, R.B., Tüzün, U., Enstad, G. G., 2007. Air current segregation of alumina powder. Particle & Particle Systems Characterization, 24, 124-135.

Zigan, S., Thorpe, R.B., Tüzün, U., Enstad, G.G., Battistin, F., 2008. Theoretical and experimental testing of a scaling rule for air current segregation of alumina powder in cylindrical silos, Powder Technology, 183, 133-145.

APPENDIX A: DEFINITIONS OF SOME PARAMETERS USED IN CHAPTER 8

As shown in Figure A.1, the transient mass of particles discharged from the shoe into the die at time instant t_{i-1} is $m(t_{i-1})$. In a period Δt, i.e. at time instant t_i, the transient mass of the particles in the die becomes $m(t_i)$, which can be written as

$$m(t_i) = m(t_{i-1}) + \Delta m_i \tag{A.1}$$

where Δm_i is the incremental mass of the particles discharged from the shoe during Δt, and it can be expressed as a sum of the incremental mass of fine particles Δm_i^{f} and the incremental mass of coarse particles Δm_i^{c}, i.e.

$$\Delta m_i = \Delta m_i^{\mathrm{f}} + \Delta m_i^{\mathrm{c}} \tag{A.2}$$

The fines mass fraction in Δm_i is then defined as

$$\mathrm{x}_i^{\mathrm{s}} = \Delta m_i^{\mathrm{f}} / \Delta m_i \tag{A.3}$$

The transient fines mass fraction in the die at time instant t_i, $\mathrm{x}^{\mathrm{d}}(t_i)$, can be defined as

$$\mathrm{x}^{\mathrm{d}}(t_i) = m^{\mathrm{f}}(t_i) / m(t_i) \tag{A.4}$$

In which, $m^{\mathrm{f}}(t_i)$ is the transient mass of fine particles in the die at t_i.

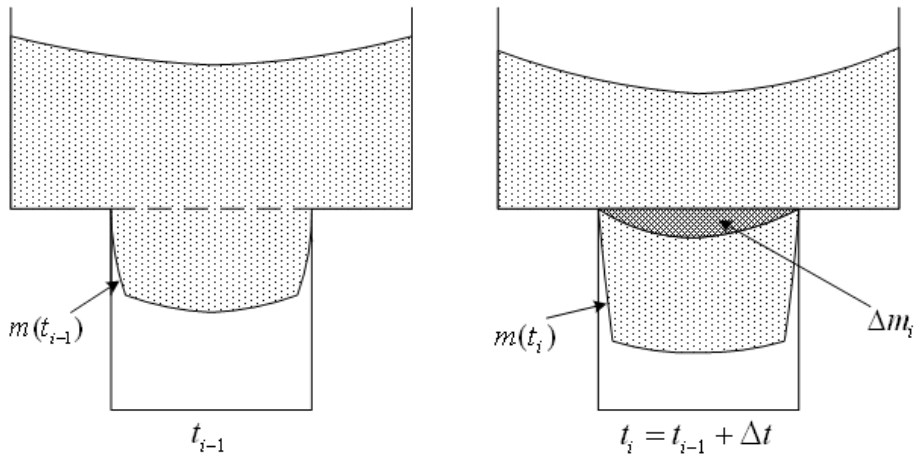

Figure A.1 Schematic illustration of some parameters.

APPENDIX B: INPUT FILES OF PROGRAM

In order to perform simulations, the program needs to read parameters from the input files, in which the properties of particles and walls are defined and the operating parameters are specified. Examples of input files for the die filling simulations are presented below.

B.1. Specification for the particle system

```
* Define the computational domain
start  0.0455  0.0234  0.00065  2520  15000  12  log

*Give a name to the job
Numerical model for die filling

*Switch on 2D mode for 2D simulations (the default is for 3D mode)
2-D

* specify particle properties (two types of particles are defined)
dia    0.000130     1
dia    0.000130     2

ymd       8.7e9     1
ymd       8.7e9     2

prat       0.30     1
prat       0.30     2

dens        400     1
dens      7.8e3     2

fric       0.30     1
fric       0.30     2

* specify wall properties
ymd     210e9       3
```

```
prat        0.29       3
dens       7.9e3       3
fric        0.30       3

* Specify a very large yield stress to make sure that only elastic deformations occur
yie   1.9306e30        1
yie   1.9306e30        2
yie   1.9306e30        3

*Specifiy 5% ball-ball and 10% ball-wall damping
damp    0.05    0.5    1    0     1
damp    0.10    0.5    1    0     0

*Specify the gravitational acceleration
grav       0.0      -9.81        0.0

*Generate a die cavity
dwall  fp(0.0200 0.0020  0.000325 0.0200 0.0090 0.000325) vel(0.0 0.0 0.0) mat(3)
dwall  fp(0.0270 0.0020  0.000325 0.0270 0.0090 0.000325) vel(0.0 0.0 0.0) mat(3)
dwall  fp(0.0200 0.0020  0.000325 0.0270 0.0020 0.000325) vel(0.0 0.0 0.0) mat(3)

*Generate platforms to carry shoe
dwall  fp(0.0010 0.0090  0.000325 0.0200 0.0090 0.000325) vel(0.0 0.0 0.0) mat(3)
dwall  fp(0.0270 0.0090  0.000325 0.0440 0.0090 0.000325) vel(0.0 0.0 0.0) mat(3)

*Generate a cover to avoid the particles flowing out of the domain
dwall  fp(0.0010 0.0090  0.000325 0.0010 0.0220 0.000325) vel(0.0 0.0 0.0) mat(3)
dwall  fp(0.0440 0.0090  0.000325 0.0440 0.0220 0.000325) vel(0.0 0.0 0.0) mat(3)
dwall  fp(0.0010 0.0220  0.000325 0.0440 0.0220 0.000325) vel(0.0 0.0 0.0) mat(3)

*Generate a shoe
dwall  fp(0.0290 0.0090  0.000325 0.0290 0.0210 0.000325) vel(0.0 0.0 0.0) mat(3)
dwall  fp(0.0430 0.0090  0.000325 0.0430 0.0210 0.000325) vel(0.0 0.0 0.0) mat(3)
dwall  fp(0.0290 0.0210  0.000325 0.0430 0.0210 0.000325) vel(0.0 0.0 0.0) mat(3)

* Specify 'agglomerate' regions for generating particles
agglom cub 1 0.0290 0.0430 0.0090 0.0210 0.0 0.00065
agglom cub 2 0.0290 0.0430 0.0090 0.0210 0.0 0.00065

*Randomly generate particles in the specified regions
rgenerate 3000 1 1 1
rgenerate 3000 2 2 2
```

*Specify a fraction (0~1) to determine time step
frac 0.5

*Show animations
anim on 1000
layers 500
plot axes wal cir

* Run cycles until the particles system reaches a static state with negligible kinetic
*energy.
cyc 50000
cyc 50000
……

* Save file
save GEN

B.2. Define fluid field mesh

*The following content is included in the file 'flowdata'.

Hydrodynamics model	PGF
X fluid cells in bed	82
Y fluid cells in bed	1
Z fluid cells in bed	38
Bed x-origin, xb0	0.0020
Bed y-origin, yb0	0.000075
Bed z-origin, zb0	0.0020
Bed x-dimension, xbed (m)	0.0410
Bed y-dimension, ybed (m)	0.0005
Bed z-dimension, zbed (m)	0.0190
Maximum Newton method iterates, itm_new	1000
Maximum ICG Method Iterates,itm_icg	1000
Relative error Newton iterates, eps_new	1.0e-6
Relative error ICG iterates, eps_icg	1.0e-12
Left boundary cell-flag, hxl	3
Right boundary cell-flag, hxh	3

Back boundary cell-flag, hyl	3
Front boundary cell-flag, hyh	3
Bottom boundary cell-flag, hzl	4
Top boundary cell-flag, hzh	6
Fluid temperature, TK (K)	293.0
Fluid shear viscosity, Mhu_gas (kg/ms)	1.8e-5
Fluid bulk viscosity, Labda_gas (kg/ms)	0.0
Average gas molar mass, M_gas (kg/mol)	2.88e-2
Initial x-fluid velocity (m/s)	0.0
Initial y-fluid velocity (m/s)	0.0
Initial z-fluid velocity (m/s)	0.0
Initial fluid pressure (pa)	101325.0
Left boundary fluid velocity (m/s)	0.0
Right boundary fluid velocity (m/s)	0.0
Back boundary fluid velocity (m/s)	0.0
Front boundary fluid velocity (m/s)	0.0
Bottom boundary fluid velocity (m/s)	0.0
Top boundary fluid velocity (m/s)	0.0
Left boundary fluid pressure (Pa)	101325.0
Right boundary fluid pressure (Pa)	101325.0
Back boundary fluid pressure (Pa)	101325.0
Front boundary fluid pressure (Pa)	101325.0
Bottom boundary fluid pressure (Pa)	101325.0
Top boundary fluid pressure (Pa)	101325.0
Number of obstacles, nobs	0
X fluid cells in die start from	37
X fluid cells in die end to	50
Y fluid cells in die start from	1
Y fluid cells in die end to	1
Z fluid cells in die start from	1
Z fluid cells in die end to	14
Suction filling? (YES/NO)	YES
Punch velocity (m/s)	-0.15
Wall number of punch	3

B.3. Simulate die filling process

**Restart the saved file generated from A.1*
restart GEN

**Name the job*
Die filling in the presence of air

**Specify fraction for time step*
frac 0.5

**Introduce air, i.e., read the parameters of air from the input file 'flowdata'*
gas

**Animation*
anim on 1000
plot axes wal cir fvel

**Move the shoe by specifying a horizontal velocity to the shoe walls*
awall 9 fp(0.028999 0.009080 0.000325 0.028999 0.0180 0.000325) vel(-0.070 0.0 0.0) mat(3)
awall 10 fp(0.043001 0.009080 0.000325 0.043001 0.0180 0.000325) vel(-0.070 0.0 0.0) mat(3)
awall 11 fp(0.028999 0.018000 0.000325 0.043001 0.0180 0.000325) vel(-0.070 0.0 0.0) mat(3)

**Move the punch if it is suction filling*
awall 3 fp(0.02000 0.0089999 0.000325 0.02700 0.0089999 0.000325) vel(0.0 -0.15 0.0) mat(3)

**Run cycles until the filling process is complete*
cyc 50000
pri mas zda cel bal
save df_50k
cyc 50000
pri mas zda cel bal
save df_100k
……

stop